Investigations of the reactivity of selected P_n ligand complexes

Dissertation

zur Erlangung des

DOKTORGRADES DER NATURWISSENSCHAFTEN

(Dr. rer. nat.)

der Naturwissenschaftlichen Fakultät IV – Chemie und Pharmazie

der Universität Regensburg

vorgelegt von

Eric Mädl

aus Kelheim

Regensburg 2016

Investigations of the reactivity of selected P_n ligand complexes

Dissertation

zur Erlangung des

DOKTORGRADES DER NATURWISSENSCHAFTEN

(Dr. rer. nat.)

der Naturwissenschaftlichen Fakultät IV – Chemie und Pharmazie

der Universität Regensburg

vorgelegt von

Eric Mädl

aus Kelheim

Regensburg 2016

Diese Arbeit wurde angeleitet von Prof. Dr. Manfred Scheer.

Promotionsgesuch eingereicht am:	23.02.2016
Tag der mündlichen Prüfung:	24.03.2016

Vorsitzender:	Prof. Dr. Arnd Vogler
Prüfungsausschuss:	Prof. Dr. Manfred Scheer
	Prof. Dr. Henri Brunner
	Prof. Dr. Frank-Michael Matysik

Universität Regensburg

Eidesstattliche Erklärung

Ich erkläre hiermit an Eides statt, dass ich die vorliegende Arbeit ohne unzulässige Hilfe Dritter und ohne Benutzung anderer als der angegebenen Hilfsmittel angefertigt habe; die aus anderen Quellen direkt oder indirekt übernommenen Daten und Konzepte sind unter Angabe des Literaturzitats gekennzeichnet.

_____

Mädl Eric

This thesis was elaborated within the period from November 2011 till February 2016 in the Institut of Inorganic Chemistry at the University of Regensburg, under the supervision of Prof. Dr. Manfred Scheer.

Parts of this thesis are already published:

- E. Mädl, M. V. Butovskii, G. Balázs, E. V. Peresypkina, A. V. Virovets, M. Seidl, M. Scheer, *Angew. Chem. Int. Ed.* **2014**, *53*, 7643-7646.
- E. Mädl, G. Balázs, E. V. Peresypkina, M. Scheer, *Angew. Chem . Int. Ed.* **2016**, *online*, DOI: 10.1002/anie.201601775.

Dedicated to my parents

Preface:

Some of the herein reported results are already published or close to being published. Therefore, if possible, a license number is given at the beginning of a chapter. This thesis is structured in such a manner that every chapter stands as an own paper, ready for publishing and therefore the numbering for compounds, figures and tables starts anew. Furthermore, some chapters may therefore contain the work of other people, which may already be discussed in their thesis. At the beginning of each chapter it is thus mentioned as detailed as possible which work was performed by the author of this thesis (Eric Mädl) or others, to avoid the accusation of plagiarism. Unfortunately, a strict separation of results is sometimes not possible. On the first page of each chapter the 'table of content' (TOC)/'graphical abstract' is depicted, in the case of unpublished results a suggestion is given instead. All graphics regarding the graphical abstract were made by the author of this thesis.

Table of Contents

1. Introduction

1.1 Phosphorus – red, black and white

Phosphorus is part of many aspect of our human organism. From the building blocks in our DNA, forming the well-known double helices, our bones or teeth, or in adenosine triphosphate, which is responsible for our intracellular energy transfer. For plants it is essential for the cell development and thus it is one of the key elements in fertilizer, beside nitrogen and potassium, helping us to sustain our food supply in big scales. Phosphorus is one of the fundaments of life as we know it and since its discovery as an element in 1669 it has come a long way in research. Hennig Brand, a german apothecary and alchemist, had great ambitions when he tried 1669 to create the philosopher's stone, by evaporating urine and working up the dry residue under exclusion of air. The chemiluminescence that is observed when white phosphorus gets in contact with air gave phosphorus its name, derived from the Greek, meaning "light-bearer". But white phosphorus is just one of many modifications of phosphorus, which can be found as white, red and black modifications. Respectively, the thermodynamic stability increases at room temperature in this order.[1] Since the rate of transformation is extremely slow under normal conditions, all mentioned modification can be isolated and easily handled in their metastable state.

Commercially available red phosphorus is amorphous and is obtained by heating up white phosphorus or by irradiation with UV light. In 1947 Roth *et al*. proposed polymorphism for red phosphorus by performing differential thermal analysis, X-ray analysis and optical microscopy examinations. As a result five types of red phosphorus (type I – V) were postulated.[2] The amorphous red phosphorus was classified as "type I", whereas the "type IV" modification of red phosphorus is known as fibrous phosphorus. Its name derives from its ductile property of splitting into fine fibers, by applying mechanical pressure. In 2005 it could also be characterized by X-ray structure analysis.[3] The fibrous phosphorus forms similar phosphorus cages like the Hittorf's allotrope (Figure 1, *vide infra*), but the arrangement of the phosphorus tubes differs slightly, by forming parallel double tubes. The "type V" modification is known as the violet modification (Hittorf's allotrope) and is synthesized by heating up red phosphorus to 550 °C. Its crystal structure could be determined in 1966 (Figure 1),[4] consisting of P_8 and P_9 moieties which are connected by a P_2 group to form infinite tubes. Different tubes are hereby connected via the P_9 units to form a complicated layer lattice structure. The crystal structures of the "type II" and "type III" modifications are still unknown, due to the difficulty of growing crystals suitable for single crystal X-ray diffraction.[5]

The black modification is obtained under high pressure at 200 °C from white phosphorus and consists of double layers of interlinked six membered rings of phosphorus atoms, exhibiting semiconductor

attributes. In 2004, phosphorus nanorods were synthesized by the group of Arno Pfitzner, at the University of Regensburg.[6] In this allotrope the P_{12} units form polymers in two modifications, resulting in nanorods with a diameter of 0.37 nm to 0.47 nm.

White phosphorus itself consists of a P_4 tetrahedron and exhibits high ring strain energies, explaining its high reactivity.[7] At room temperature it exists in the cubic α-form, the hexagonal β-form is obtained at temperatures lower than −76.9 °C. Calculations of the P-P bond length in the P_4 tetrahedron (2.194 Å), which was also determined by X-ray structure analysis (P-P: 2.209 (5) Å),[8] serve as a benchmark for a P-P single bond length.[9] White phosphorus is until today − besides all its other modifications − of special interest, by representing a source of discrete P_4 tetrahedrons and its property to be activated easily by nucleophiles[10] or transition metals.[11]

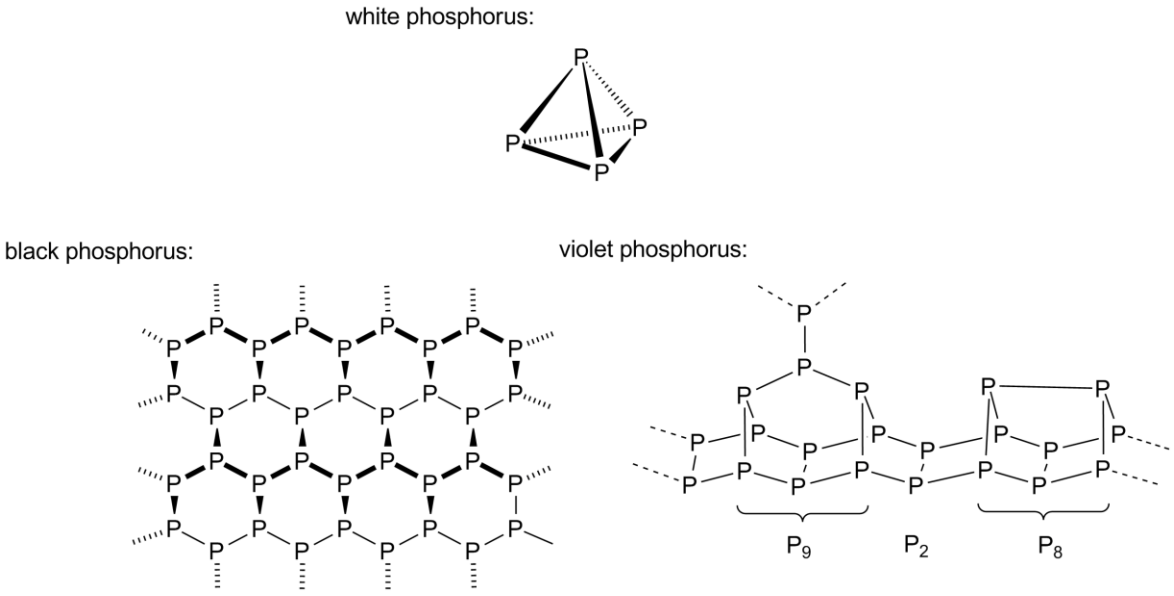

Figure 1. Modifications of phosphorus.

1.2 Milestones of the discovery of P_n ligand complexes containing a *cyclo*-P_n ring

In 1971 A. P. Ginsberg and W. E. Lindsell set one of the foundation stones for a new field of chemistry, by discovering the first P_n ligand complex, exhibiting a P_4 unit coordinating side-on to a rhodium fragment.[12] Sacconi *et al.* contributed by coordinating an intact P_4 tetrahedron end-on to a nickel triphos fragment (triphos = 1,1,1-tris(diphenylphosphino-methyl)ethane; Figure 2).[13]

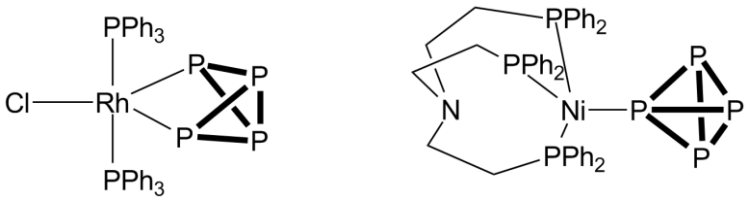

Figure 2. The first steps of P_n ligand chemistry; left: the ruthenium complex discovered by A. P. Ginsberg and W. E. Lindsell; right: the complex containing an end-on coordinated P_4 tetrahedron, discovered by Sacconi *et al.*

The group of Sacconi also obtained the first *cyclo*-P_3 ligand in 1978, which was coordinated in a terminal fashion to a transition metal in the compound [(triphos)Co(η^3-P_3)].[14] Furthermore, they also isolated the first triple-decker compound containing a *cyclo*-P_3 middle deck for nickel and cobalt in the same and the following year, respectively.[15] It took chemists about 20 more years to synthesize the first compounds featuring terminal P_4 or P_5 rings as ligands for transition metals.[16] Both P_n ligand complexes were discovered by the group of Scherer, the P_4 ring in the complex [Cp*Nb(CO)$_2$(η^4-P_4)], the *cyclo*-P_5 ligand in [Cp*Fe(η^5-P_5)] (**1**), which was named after its organic equivalent ferrocene as pentaphosphaferrocene. Since in this thesis **1** was mainly used as a starting material, a more detailed view of this molecule and its reactivity will be given in the next chapter.

The benzene analog P_6 ring could be stabilized for the first time in the triple-decker complex [(Cp*Mo)$_2$(μ,$\eta^{6:6}$-P_6)] and was published again by the group of Scherer.[17] Although bigger, "naked" P_n ligands are known, those complexes do not exhibit a planar ring system anymore. For a long time the group of Scherer was the record holder for the largest substituent free P_n ligand, by synthesizing the complex [(Cp'''Co)$_3$P$_{12}$][18] via thermolysis of [Cp'''Co(CO)$_2$] with white phosphorus at 190 °C. Our group could set up a new record by discovering a complex containing a "naked" P_{24} ligand, which is coordinating to Cr(CO)$_4$ and CoCp''' fragments.[19]

Until today a great variety of complexes, containing a substituent free ("naked") *cyclo*-P_n ring were synthesized, featuring P_n ligands with a ring sizes from n = 3 to n = 6 (Figure 3).

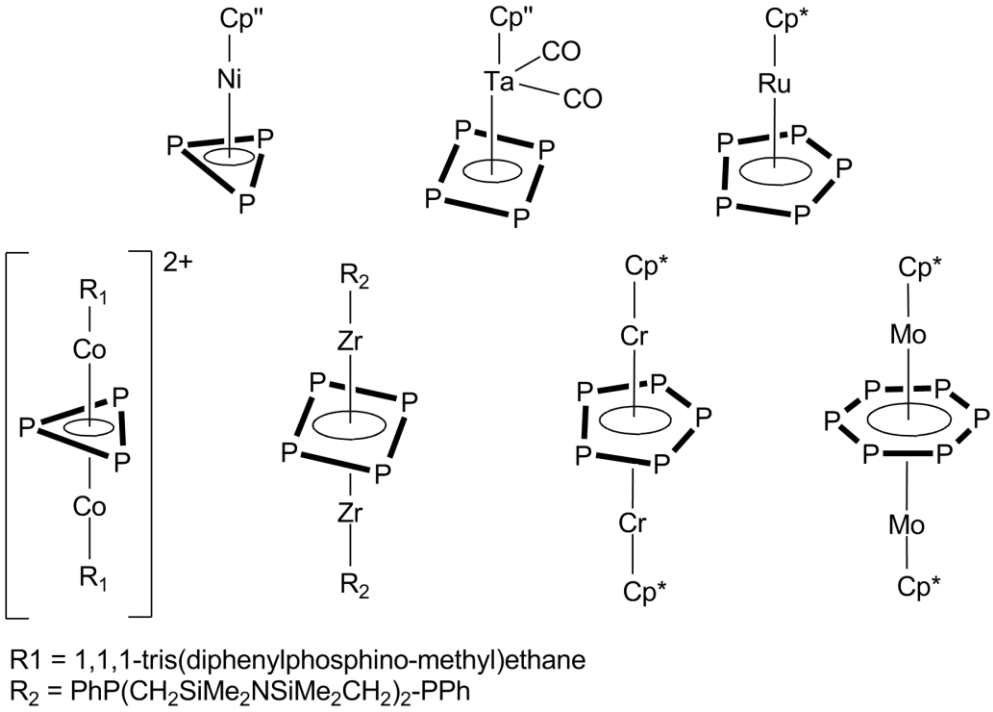

Figure 3. A selection of P_n ligand complexes. Authors from top left to top right: Scherer *et al.*,[20] Scherer *et al.*,[21] Scherer *et al.*;[22] authors from bottom left to bottom right: L. Sacconi *et al.*,[23] M. D. Fryzuk,[24] Scherer *et al.*,[25] Scherer *et al.*[17]

1.3 Theoretical examinations of the *cyclo*-P_5^- ligand and decaphosphaferrocene

Before Scherer *et al.* isolated the pentaphosphaferrocene in 1987 calculations were carried out, predicting, that the *cyclo*-P_5^- anion should be stable enough to be isolated under proper experimental conditions.[26] Every phosphorus atom in the *cyclo*-P_5^- ring contributes one electron to the π-system, resulting in a six π-electron donor ligand. Ab initio calculations show very high aromatic character of this ring system, with similar values compared to the Cp^- ligand.[27] In addition, the aromaticity of phospholes $(P_n(CH_2)_{4-n}P)^-$ (with n = 0 – 4) increase the more phosphorus atoms are present in the anionic ring system.[27b] However, the relative aromaticity of the *cylco*-P_5 ligand decreases drastically in the coordination sphere of iron, to 50.5 % in [CpFe(η^5-P_5)] and 51.1 % in [Fe(η^5-P_5)$_2$].[28] Furthermore, the *cyclo*-P_5 ligand introduces basicity on the transition metal center. Natural Population Analysis (NPA) shows, by exchanging one or two Cp ligands from [$FeCp_2$] with a P_5 ligand NPA charges for the iron atom drop from 0.28 in ferrocene, to −0.28 in **1** and −0.91 in [Fe(η^5-P_5)$_2$].[28] Similar values were obtained for the analogue ruthenium and osmium containing compounds.

The next logical step, after the discovery of the pentaphosphaferrocene would be the synthesis of the decaphosphaferrocene, a sandwich complex in which the iron atom is coordinated by two *cyclo*-P_5 rings. Carbon free sandwich complexes, which are formed of two *cyclo*-P_5 rings are not known until today, except for one compound. In 2002 [Ti(η^5-P_5)$_2$]$^{2-}$ has been isolated successfully, by reacting a highly reduced titanium complex with white phosphorus (Scheme 1).[29]

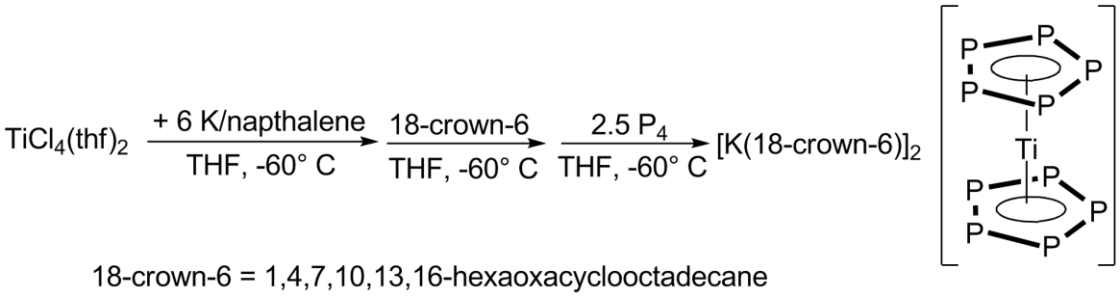

Scheme 1. Synthesis of decaphosphatitanocene.

Although the iron analogue decaphosphaferrocene was reported by Baudler *et al*. by reacting NaP_5 with $FeCl_2$, the conclusion of its formation was only based on IR studies.[30] Nevertheless calculations were carried out, showing that the bond dissociation energy of [Fe(η^5-P_5)$_2$], which would yield one iron and two *cyclo*-P_5 ligands is 128.3 kcal/mol − similar to ferrocene (131.3 kcal/mol). This indicates, that [Fe(η^5-P_5)$_2$] should be stable enough to be isolated,[31] while the optimized structure of

decaphosphaferrocene shows an analogue sandwich complex with D_{5h} symmetrie. However, the Fe-(η^5-E_5) bonding energy in **1** is much stronger than in decaphosphaferrocene.[31] This might be one of the reasons why the pentaphosphaferrocene is obtained in good yields, but a suitable synthesis for decaphosphaferrocene still has to be developed.

1.4 Pentaphosphaferrocene

1.4.1 Its redox chemistry unveiled

Pentaphosphaferrocene [Cp*Fe(η^5-P_5)] (**1**) was the first complex featuring a terminal η^5-P_5 ring and was named after its isostructural and isoelectronic organic equivalent ferrocene. However, the last years revealed a huge difference in the redox behavior of both compounds. Ferrocene is well known for its reversible oxidation and thus it is also used in the cyclic voltammetry as an internal standard. Compound **1** was screened for its redox properties by Winter *et al.* in extensive cyclic voltammetry (CV) studies, suggesting two one electron reductions or oxidations and a subsequent dimerization, linking two pentaphosphaferrocene moieties together.[32] Our group was able to isolate the reduced and oxidized compounds $[(Cp^*Fe)_2(\mu,\eta^{4:4}\text{-}P_{10})]^{2-}$ (**2**) as well as $[(Cp^*Fe)_2(\mu,\eta^{5:5}\text{-}P_{10})]^{2+}$, respectively, in accordance with those CV studies and their structures were determined by X-ray structure measurements in 2013.[33] In **2** the pentaphosphaferrocene moieties are connected by a P-P single bond forming a P_{10} ligand. The former P_5 rings adopt an envelope conformation and coordinate to the Cp*Fe fragments in a $\eta^{4:4}$-fashion. In contrast, in the oxidized compound $[(Cp^*Fe)_2(\mu,\eta^{5:5}\text{-}P_{10})]^{2+}$ the coordination of the P_{10} ligand is best described with a $\eta^{5:5}$-coordination mode. Furthermore, the dianionic monomeric compound $[Cp^*Fe(\eta^4\text{-}P_5)]^{2-}$ (**3**) was isolated and characterized, by reacting **1** with K, which was not observed in the previous CV measurements (Scheme 2).

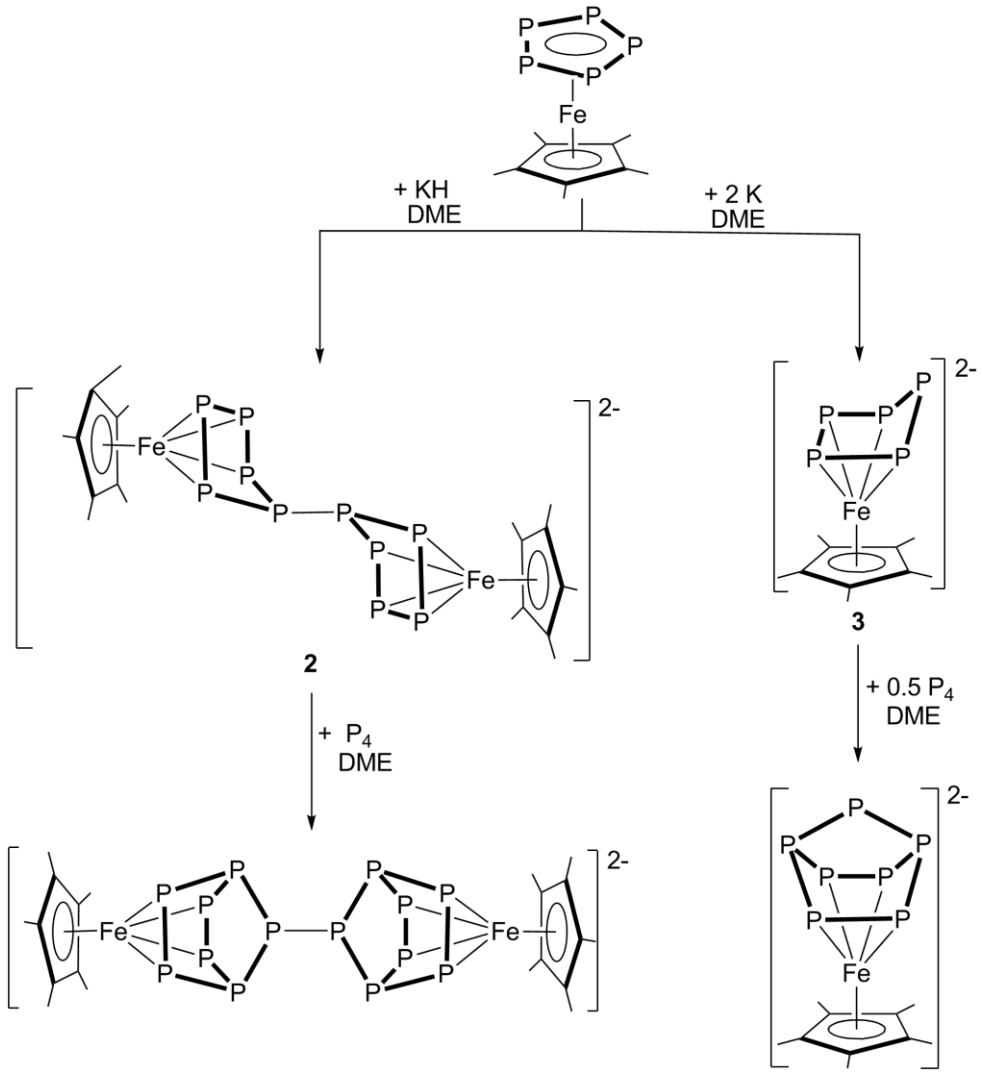

Scheme 2. Reduction of **1** and subsequent reactions with white phosphorus.

For both **2** and **3** reactivity studies were performed, activating white phosphorus. By adding the monomeric dianion **3** to P_4 a norbornene-like P_7 cage forms and compound $[Cp^*Fe(\eta^4\text{-}P_7)]^{2-}$ is isolated. If **2** is used instead a similar structural motif is observed, featuring a P_{14} ligand which consists of two P_7 norbornene-like units. The P_7 units are connected by a P-P single bond, yielding $[(Cp^*Fe)_2(\mu,\eta^{4:4}\text{-}P_{14})]^{2-}$ (Scheme 2).

In addition, prior studies are reported, reducing **1** in situ with K/naphthalene and adding $[(DIP)_2pyr)SmI(thf)_3]$ (DIP_2pyr = 2,5-bis-{N-(2,6-diispropylphenyl)iminomethyl}pyrrolyl).[34] A monomeric and a dimeric compound could be isolated, in which the samarium coordinates two or three phosphorus atoms of the *cyclo*-P_5 ring, respectively, forming a mixed 3d/4f element triple-decker complex (Scheme 3). The P_5 rings in both compounds show a structure analog to the uncoordinated, reduced species **3**, by exhibiting an enveloped conformation. By adding samarocene to **1** the same P_{10} framework is formed as observed in **2**, along the coordination of two samarocene fragments.[35]

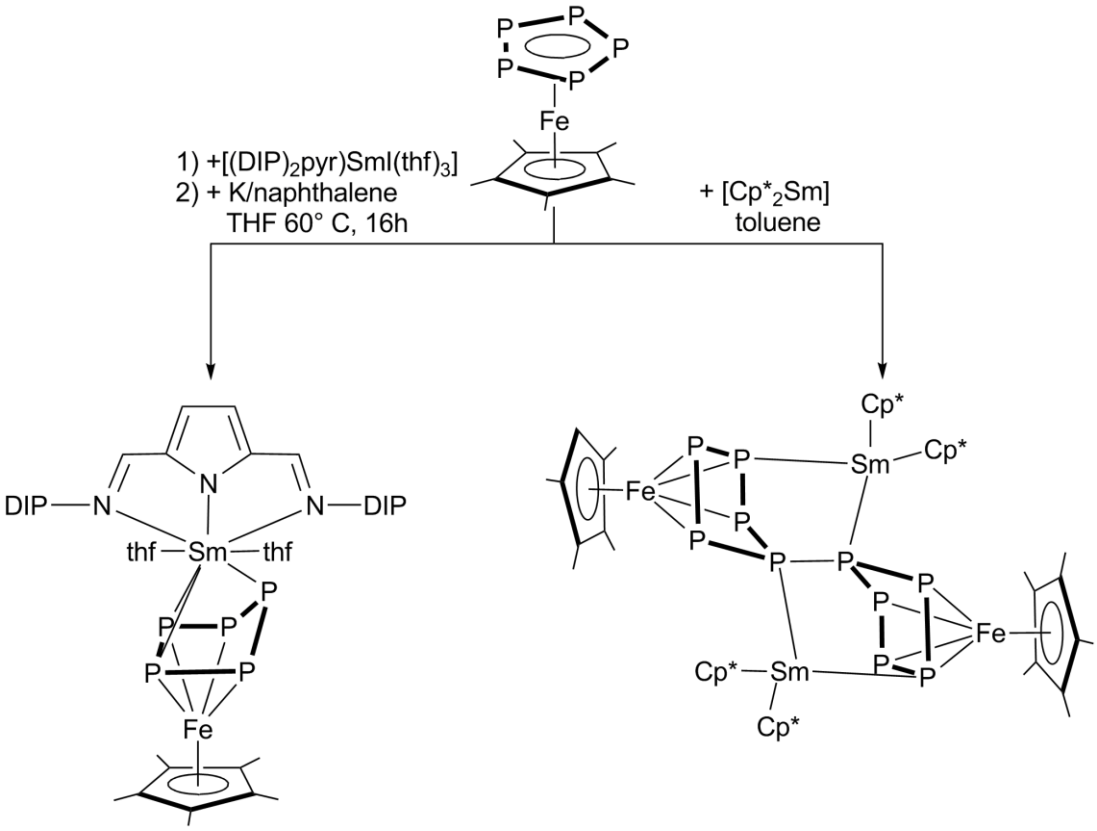

Scheme 3. Reduction of **1** with samarium containing complexes.

1.4.2 From coordination to supramolecular chemistry

In contrast to ferrocene, one of the most intensive studied reactivities of pentaphosphaferrocene is its coordination chemistry. Due to five accessible lone pairs of the P_5 ligand a broad range of products can be synthesized by coordination reactions. After the discovery of **1** first studies were performed, reacting pentaphosphaferrocene with 16 VE-transition metal fragments. By using $[Cr(CO)_5(thf)]$ a coordination of two of the five phosphorus atoms of the P_5 ring are achieved. By using the sterically less demanding fragment $[CpMn(CO)_2(thf)]$ up to four phosphorus atoms are coordinated. In both cases the planar structure of the P_5 ring stays intact.[36] Since then the coordination chemistry has expanded drastically, especially due to the usage of salts containing the weakly coordinating anion $[Al\{OC(CF_3)_3\}_4]^-$. A manifold variety of coordination polymers were obtained this way, for example by reacting **1** with the Ag(I) salt $Ag[Al\{OC(CF_3)_3\}_4]$ or with group 13 element cations such as Tl, In and Ga as their corresponding $[Al\{OC(CF_3)_3\}_4]^-$ salts (Scheme 4)[37]

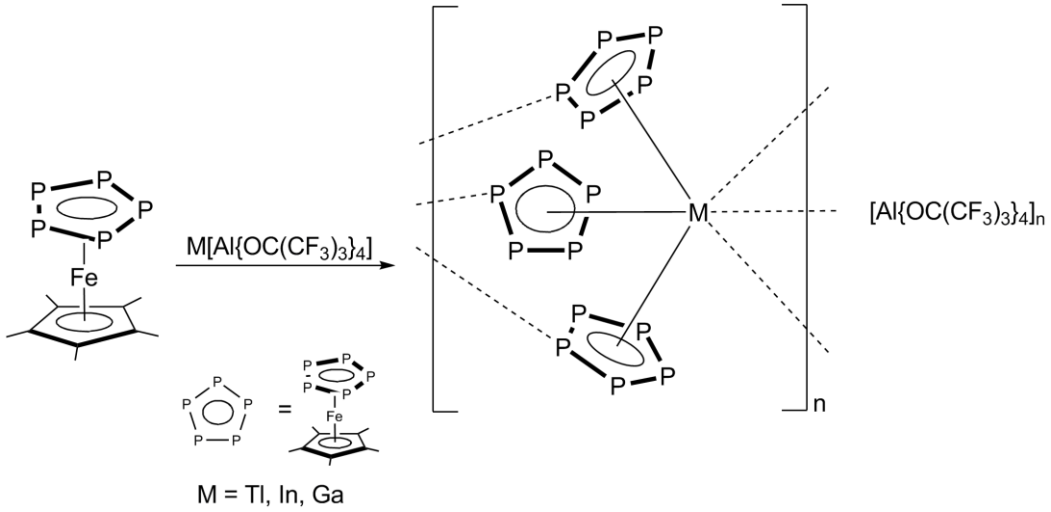

Scheme 4. Coordination polymers from the reaction of **1** with $M[Al\{OC(CF_3)_3\}_4]$ (M = Tl, In, Ga).

The coordination of Cu(I) halides yields polymeric systems, after layering **1** with CuX (X = Cl, Br, I). The structure of these polymer chains can be altered drastically by using different stoichiometries (Scheme 5).[38]

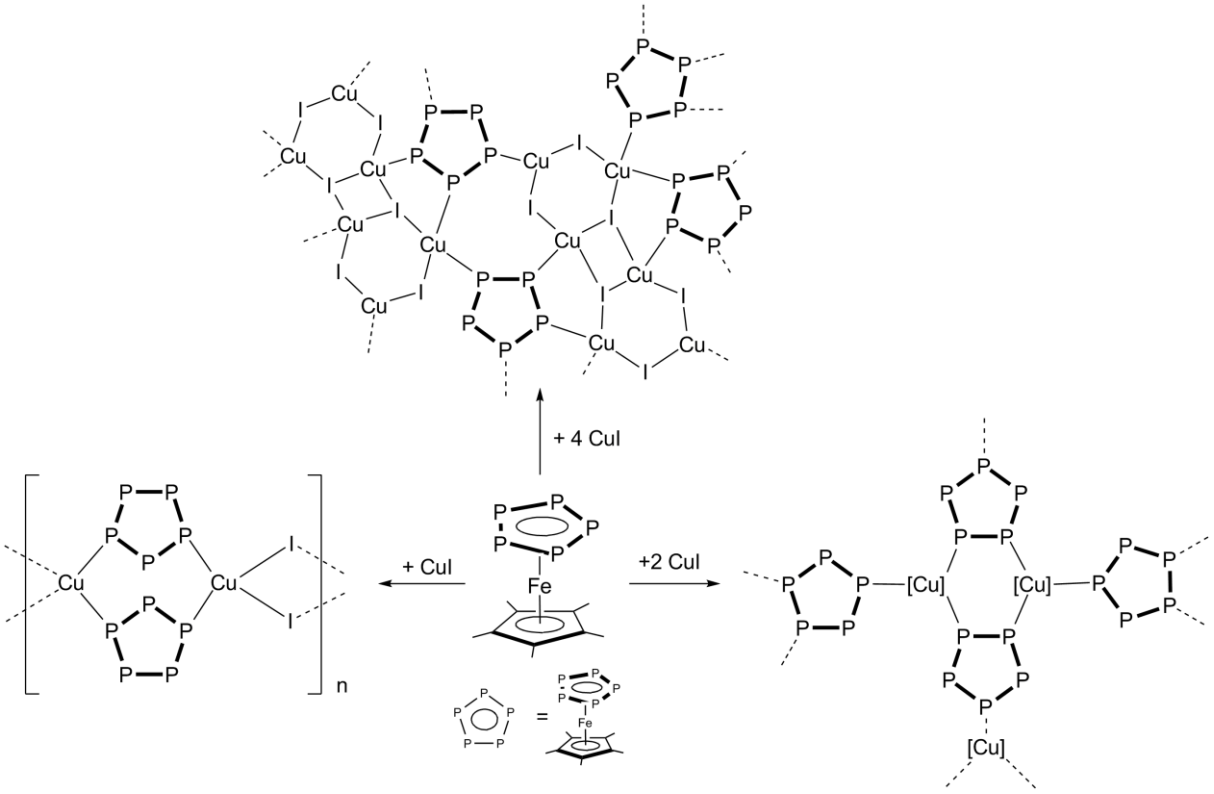

Scheme 5. Some of the different connectivity pattern that are obtained by reacting **1** with CuI in different stoichiometries.

In 2003 our working group succeeded in creating a supramolecular, fullerene-like nanocluster, by coordinating **1** to CuCl. It was the first of its kind and a milestone in the chemistry of pentaphosphaferrocene.[39] The cluster consists of a core of 90 inorganic core atoms, in which copper atoms are coordinating to each of the phosphorus atoms of the P_5 ring, forming P_4Cu_2 rings. As a result the structural motif is similar to the C_{60} fullerene. Most interestingly, molecules can be encapsulated in the core of such a cluster, if the reaction is carried out in the presence of a guest molecule, as it was performed with the C_{60} fullerene (Figure 4).[40] The fullerene is hereby surrounded by 13 pentaphosphaferrocenes, which are linked by 25 CuCl molecules.

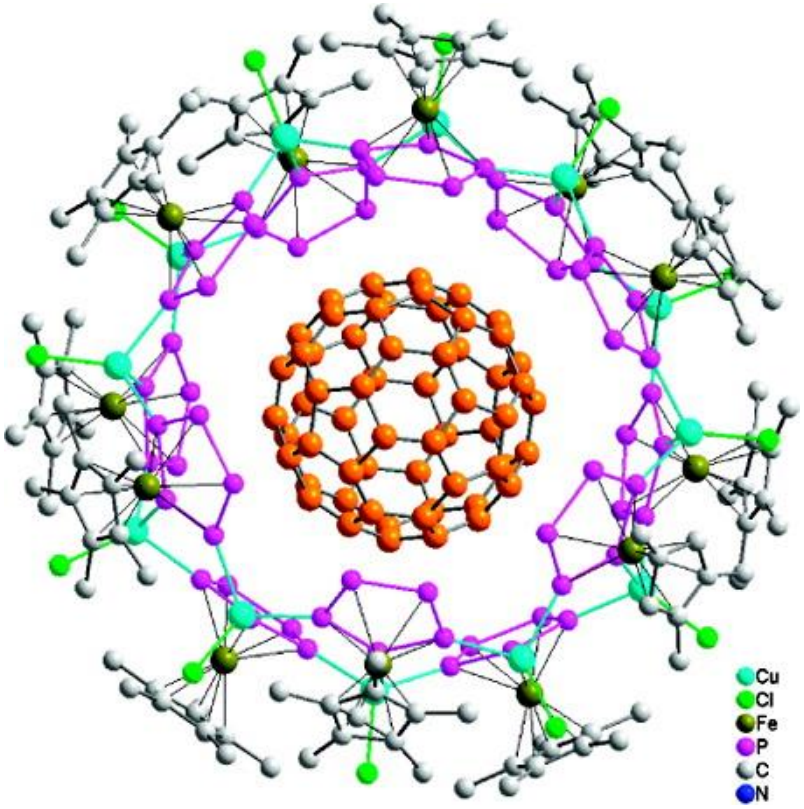

Figure 4. Partial view of the belt-like core of the supramolecular molecule surrounding the C_{60} molecule, that is obtained by reacting **1** with CuCl in presence of the C_{60} fullerene; the upper and lower part have been omitted, and the C atoms of C_{60} are highlighted in orange. Reprinted with permission from (M. Scheer, A. Schindler, R. Merkle, B. P. Johnson, M. Linseis, R. Winter, C. E. Anson, A. V. Virovets, *J. Am. Chem. Soc.* **2007**, *129*, 13386-13387). Copyright (2007) American Chemical Society.

The possibility to fine tune the building block [Cp*Fe(η^5-P_5)] by exchanging the Cp* ligand with a more sterically demanding one gives access to new unprecedented structural motifs and an enhanced solubility of the final products. If the five methyl groups in the Cp* are e.g. replaced with benzyl substituents in the Cp^{BN} ligand (Cp^{BN} = pentabenzylcyclopentadienyl), the compound [Cp^{BN}Fe(η^5-P_5)] yields together with CuI a spherical molecule beyond the fullerene topology, which lacks the formation of six-membered rings in the scaffold.[41] Furthermore, the shape of these supramolecular cluster can be tuned by varying the stoichiometry of CuI and [Cp^{BN}Fe(η^5-P_5)].[42]

1.4.3 Ring opening reactions and triple-decker complexes

Both in the redox reactions of pentaphosphaferrocene and its coordination chemistry the P_5 ring always stays intact, although in some case the former planar P_5 ligand adopts adopts an enveloped conformation. The fact, that the P_5 ring in the coordination sphere of the Cp*Fe fragment exhibits an extraordinary stability and a thermodynamical minimum is represented by its synthesis. It forms in good yields in a thermolytical reaction of $[Cp^*Fe(CO)_2]_2$ and white phosphorus at 190 °C. Nevertheless, in the past reactivity studies have shown that an opening of the P_5 ring is possible. If **1** is stirred at 190 °C for about 10 h with $[Cp''Ta(CO)_4]$ one P-P bond breaks and a Cp"Ta-fragment is inserted.[43] By reducing the reaction time to 6 h also cubane structural motifs could be obtained (Scheme 6).[44]

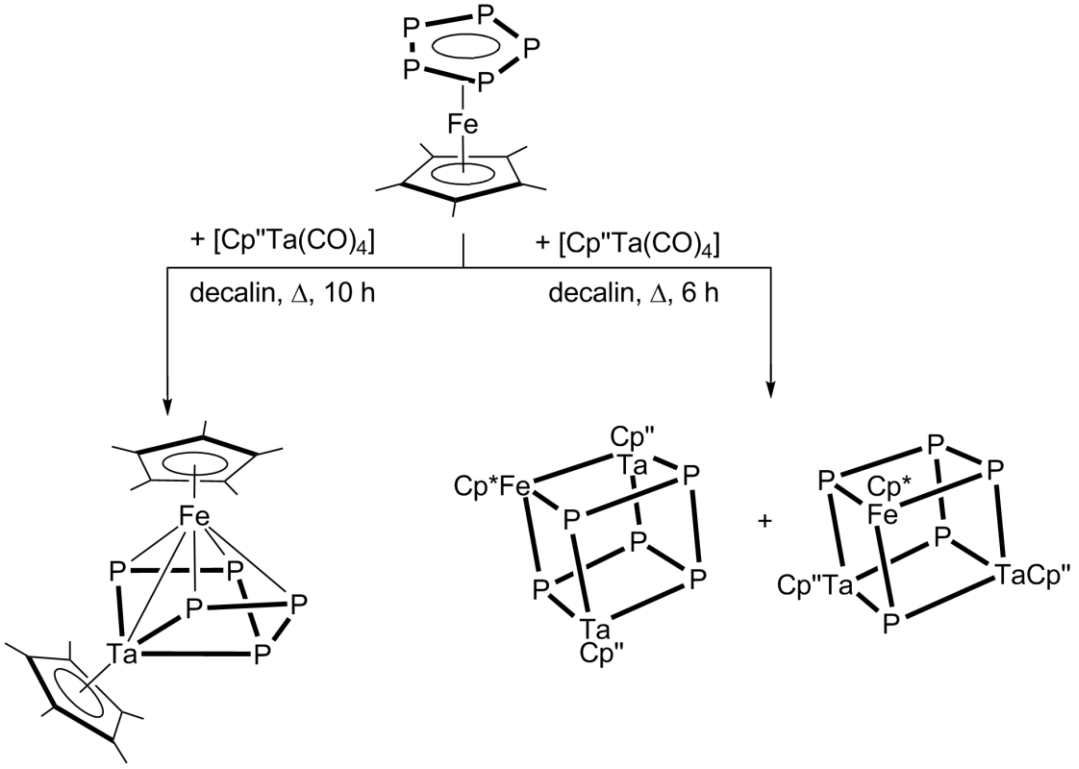

Scheme 6. Reactions of **1** with $[Cp''Ta(CO)_4]$.

If $[Cp''Ru(CO)_2]_2$ is used instead of $[Cp''Ta(CO)_4]$, one Ru-atom is inserted along the formation of other byproducts,[45] by using $[Cp^RCo(CO)_2]$ (Cp^R = Cp', Cp") similar ring opening reactions take place.[46] But even at a moderate temperature and the usage of $[Cp^*Ir(CO)]_2$ an insertion is observed.[43]

In contrast, under mild conditions and by the adding unsaturated fragments to **1**, such as the $[CpFe]^+$ fragment, a coordination of the P_5 ring is observed, forming a triple-decker complex

[(CpFe)(Cp*Fe)(μ,η$^{5:5}$-P_5)] as reported by Scherer *et al.*[36] The P_5 ring in these structural motifs is planar and intact, as proven by X-ray structure analysis. The group of Kudinov expanded this area of chemistry with both the formation of the analogue mixed triple-decker [(Cp*Fe)(RuCp*)(μ,η$^{5:5}$-P_5)]$^+$, by reacting **1** directly with $[Cp^*RuCl_2]_2$ in the presence of $TlBF_4$ and by replacing one Cp* ligand with carboranes.[47] All triple-decker complexes obtained this way are positively charged and although the compound [(Cp*Fe)$_2$(μ,η$^{5:5}$-P_5)]$^+$ shows both one reversible oxidation and one reversible reduction,[47c] their analogous neutral complexes have not been isolated so far. However, neutral triple-decker compounds with a P_5 middle deck are known for chromium or for manganese (Figure 5).[25,48] It was only possible to isolate the latter due the stabilization of highly sterically demanding cyclopentadienyl ligands. Also a mixed triple-decker complex with iron, molybdenum and a P_5 middle deck has been discovered,[49] but beside those mentioned complexes no other compounds with the same [(R_1M_1)(R_2M_2)(μ,η$^{5:5}$-P_5)] structural motif are known.

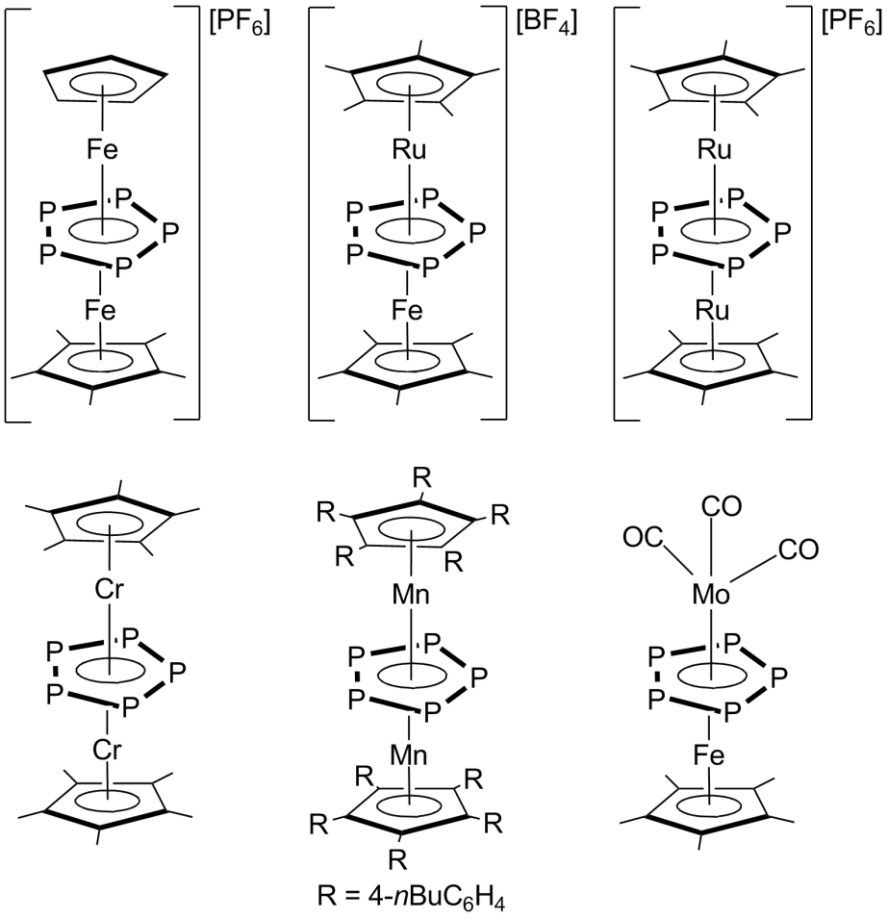

Figure 5. Examples of structural motifs of triple-decker compounds exhibiting a *cyclo*-P_5 ring.

1.5 References

[1] A. F. Hollemann, E. Wiberg, N. Wiberg, *Lehrbuch der Anorganischen Chemie, Vol. 102*, Walter de Gruyter & Co., **2007**.

[2] W. L. Roth, T. W. DeWitt, A. J. Smith, *J. Am. Chem. Soc.* **1947**, *69*, 2881-2885.

[3] M. Ruck, D. Hoppe, B. Wahl, P. Simon, Y. Wang, G. Seifert, *Angew. Chem. Int. Ed.* **2005**, *44*, 7616-7619.

[4] a) H. Thurn, H. Krebs, *Angew. Chem. Int. Ed.* **1966**, *5*, 1047-1048; b) H. Thurn, H. Krebs, *Acta Crystallogr. Sect. B: Struct. Sci.* **1969**, *25*, 125-135.

[5] R. A. L. Winchester, M. Whitby, M. S. P. Shaffer, *Angew. Chem. Int. Ed.* **2009**, *48*, 3616-3621.

[6] A. Pfitzner, M. F. Bräu, J. Zweck, G. Brunklaus, H. Eckert, *Angew. Chem. Int. Ed.* **2004**, *43*, 4228-4231.

[7] W. W. Schoeller, V. Staemmler, P. Rademacher, E. Niecke, *Inorg. Chem.* **1986**, *25*, 4382-4385.

[8] a) A. Simon, H. Borrmann, J. Horakh, *Chem. Ber.* **1997**, *130*, 1235-1240; b) A. Simon, H. Borrmann, H. Craubner, *Phosphorus, Sulfur Relat. Elem.* **1987**, *30*, 507-510.

[9] M. Häser, O. Treutler, *J. Chem. Phys* **1995**, *102*, 3703-3711.

[10] R. Riedel, H.-D. Hausen, E. Fluck, *Angew. Chem. Int. Ed.* **1985**, *24*, 1056-1057.

[11] M. Scheer, G. Balázs, A. Seitz, *Chem. Rev.* **2010**, *110*, 4236-4256.

[12] A. P. Ginsberg, W. E. Lindsell, *J. Am. Chem. Soc.* **1971**, *93*, 2082-2084.

[13] M. D. Vaira, L. Sacconi, *Angew. Chem. Int. Ed.* **1982**, *21*, 330-342.

[14] M. Di Vaira, C. A. Ghilardi, S. Midollini, L. Sacconi, *J. Am. Chem. Soc.* **1978**, *100*, 2550-2551.

[15] M. Di Vaira, S. Midollini, L. Sacconi, *J. Am. Chem. Soc.* **1979**, *101*, 1757-1763.

[16] a) O. J. Scherer, J. Vondung, G. Wolmershäuser, *Angew. Chem. Int. Ed.* **1989**, *28*, 1355-1357; b) J. Scherer, T. Brück, *Angew. Chem. Int. Ed.* **1987**, *99*, 59.

[17] O. J. Scherer, H. Sitzmann, G. Wolmershäuser, *Angew. Chem. Int. Ed.* **1985**, *24*, 351-353.

[18] O. J. Scherer, G. Berg, G. Wolmershäuser, *Chem. Ber.* **1996**, *129*, 53-58.

[19] F. Dielmann, M. Sierka, A. V. Virovets, M. Scheer, *Angew. Chem. Int. Ed.* **2010**, *49*, 6860-6864.

[20] O. J. Scherer, T. Dave, J. Braun, G. Wolmershäuser, *J. Organomet. Chem.* **1988**, *350*, C20-C24.

[21] O. J. Scherer, R. Winter, G. Wolmershäuser, *Z. Anorg. Allg. Chem.* **1993**, *619*, 827-835.

[22] O. J. Scherer, T. Brück, G. Wolmershäuser, *Chem. Ber.* **1988**, *121*, 935-938.

[23] C. Bianchini, M. D. Vaira, A. Meli, L. Sacconi, *Inorg. Chem.* **1981**, *20*, 1169-1173.

[24] W. W. Seidel, O. T. Summerscales, B. O. Patrick, M. D. Fryzuk, *Angew. Chem.* **2009**, *121*, 121-123.

[25] O. J. Scherer, J. Schwalb, G. Wolmershäuser, W. Kaim, R. Gross, *Angew. Chem. Int. Ed.* **1986**, *25*, 363-364.

[26] N. C. Baird, *Can. J. Chem.* **1984**, *62*, 341-347.

[27] a) E. J. P. Malar, *J. Org. Chem.* **1992**, *57*, 3694-3698; b) A. Dransfeld, L. Nyulászi, P. v. R. Schleyer, *Inorg. Chem.* **1998**, *37*, 4413-4420.

[28] E. J. Padma Malar, *Eur. J. Inorg. Chem.* **2004**, *2004*, 2723-2732.

[29] E. Urne˙žius, W. W. Brennessel, C. J. Cramer, J. E. Ellis, P. v. R. Schleyer, *Science* **2002**, *295*, 832-834.

[30] M. Baudler, S. Akpapoglou, D. Ouzounis, F. Wasgestian, B. Meinigke, H. Budzikiewicz, H. Münster, *Angew. Chem. Int. Ed.* **1988**, *27*, 280-281.

[31] J. Frunzke, M. Lein, G. Frenking, *Organometallics* **2002**, *21*, 3351-3359.

[32] R. F. Winter, W. E. Geiger, *Organometallics* **1999**, *18*, 1827-1833.

[33] M. V. Butovskiy, G. Balázs, M. Bodensteiner, E. V. Peresypkina, A. V. Virovets, J. Sutter, M. Scheer, *Angew. Chem. Int. Ed.* **2013**, *52*, 2972-2976.

[34] T. Li, J. Wiecko, N. A. Pushkarevsky, M. T. Gamer, R. Köppe, S. N. Konchenko, M. Scheer, P. W. Roesky, *Angew. Chem. Int. Ed.* **2011**, *50*, 9491-9495.
[35] T. Li, M. T. Gamer, M. Scheer, S. N. Konchenko, P. W. Roesky, *Chem. Commun.* **2013**, *49*, 2183-2185.
[36] O. J. Scherer, T. Brück, G. Wolmershäuser, *Chem. Ber.* **1989**, *122*, 2049-2054.
[37] a) M. Scheer, L. J. Gregoriades, A. V. Virovets, W. Kunz, R. Neueder, I. Krossing, *Angew. Chem. Int. Ed.* **2006**, *45*, 5689-5693; b) M. Fleischmann, S. Welsch, H. Krauss, M. Schmidt, M. Bodensteiner, E. V. Peresypkina, M. Sierka, C. Gröger, M. Scheer, *Chem. Eur. J.* **2014**, *20*, 3759-3768.
[38] F. Dielmann, A. Schindler, S. Scheuermayer, J. Bai, R. Merkle, M. Zabel, A. V. Virovets, E. V. Peresypkina, G. Brunklaus , H. Eckert, M. Scheer, *Chem. Eur. J.* **2012**, *18*, 1168-1179.
[39] J. Bai, A. V. Virovets, M. Scheer, *Science* **2003**, *300*, 781-783.
[40] M. Scheer, A. Schindler, R. Merkle, B. P. Johnson, M. Linseis, R. Winter, C. E. Anson, A. V. Virovets, *J. Am. Chem. Soc.* **2007**, *129*, 13386-13387.
[41] F. Dielmann, C. Heindl, F. Hastreiter, E. V. Peresypkina, A. V. Virovets, R. M. Gschwind, M. Scheer, *Angew. Chem. Int. Ed.* **2014**, *53*, 13605-13608.
[42] F. Dielmann, M. Fleischmann, C. Heindl, E. V. Peresypkina, A. V. Virovets, R. M. Gschwind, M. Scheer, *Chem. Eur. J.* **2015**, *21*, 6208-6214.
[43] M. Detzel, T. Mohr, O. J. Scherer, G. Wolmershäuser, *Angew. Chem.* **1994**, *106*, 1142-1144.
[44] O. J. Scherer, T. Mohr, G. Wolmershäuser, *J. Organomet. Chem.* **1997**, *529*, 379-385.
[45] B. Koch, O. J. Scherer, G. Wolmershäuser, *Z. Anorg. Allg. Chem.* **2000**, *626*, 1797-1802.
[46] O. J. Scherer, S. Weigel, G. Wolmershäuser, *Chem. Eur. J.* **1998**, *4*, 1910-1916.
[47] a) D. A. Loginov, I. D. Baravi, O. I. Artyushin, Z. A. Starikova, P. V. Petrovskii, A. R. Kudinov, *Russ. Chem. Bull.* **2010**, *59*, 1312-1316; b) D. A. Loginov, M. M. Vinogradov, Z. A. Starikova, P. V. Petrovskii, J. Holub, A. R. Kudinov, *Collect. Czech. Chem. Commun.* **2010**, *75*, 981-993; c) Alexander R. Kudinov, Dmitry A. Loginov, Zoya A. Starikova, Pavel V. Petrovskii, M. Corsini, P. Zanello, *Eur. J. Inorg. Chem.* **2002**, *2002*, 3018-3027.
[48] S. Heinl, G. Balazs, M. Bodensteiner, M. Scheer, *Dalton Trans.* **2016**, 45, 1962-1966.
[49] B. Rink, O. J. Scherer, G. Heckmann, G. Wolmershauser, *Chem. Ber.* **1992**, *125*, 1011-1016.

2. Research objectives

In contrast to the coordination chemistry of pentaphosphaferrocene, which has been broadly investigated, the reactivity of [Cp*Fe(η^5-P_5)] towards nucleophiles was not studied. In the scope of my master thesis the reactivity of pentaphosphaferrocene [Cp*Fe(η^5-P_5)] towards the nucleophiles KOH, $LiNMe_2$ and $NaNH_2$ was explored, yielding anionic pentaphosphaferrocene derivatives. This reactivity has been neglected so far, and therefore the research objectives for this thesis are:

- Further investigation of the reactivity of [Cp*Fe(η^5-P_5)] towards different C, N, and P donating nucleophiles.
- Study of the reactivity of anionic pentaphosphaferrocene derivatives towards electrophiles.

Furthermore, is was of special interest, whether the nucleophilic addition as observed for [Cp*Fe(η^5-P_5)] can be transferred to other P_n ligand complexes. Compound [Cp'''Ni(η^3-P_3)], exhibiting a *cylco*-P_3 ligand seems a promising starting material, due to the ring strain of the P_3 ligand, which might lead after the nucleophilic attack to an aggregation of the phosphorus ligand and thus to the formation of larger phosphorus containing scaffolds. Therefore, the second part of this thesis is dedicated to these objectives:

- Investigation of the reactivity of [Cp'''Ni(η^3-P_3)] towards C, N and P donating nucleophiles.
- Study of the reactivity of [Cp'''Ni(η^3-P_3)] towards reducing agents.

3. Functionalization of a *cyclo*-P_5 ligand by main group nucleophiles

Eric Mädl, Mikhail V. Butovskii, Gábor Balázs, Eugenia V. Peresypkina, Alexander V. Virovets, Michael Seidl and Manfred Scheer*

The following text has been reprinted with the permission of ´John Wiley and Sons´, from: E. Mädl, M. V. Butovskii, G. Balázs, E. V. Peresypkina, A. V. Virovets, M. Seidl, M. Scheer, *Angew. Chem. Int. Ed.* **2014**, *53*, 7643-7646; license number: 3741280773540.

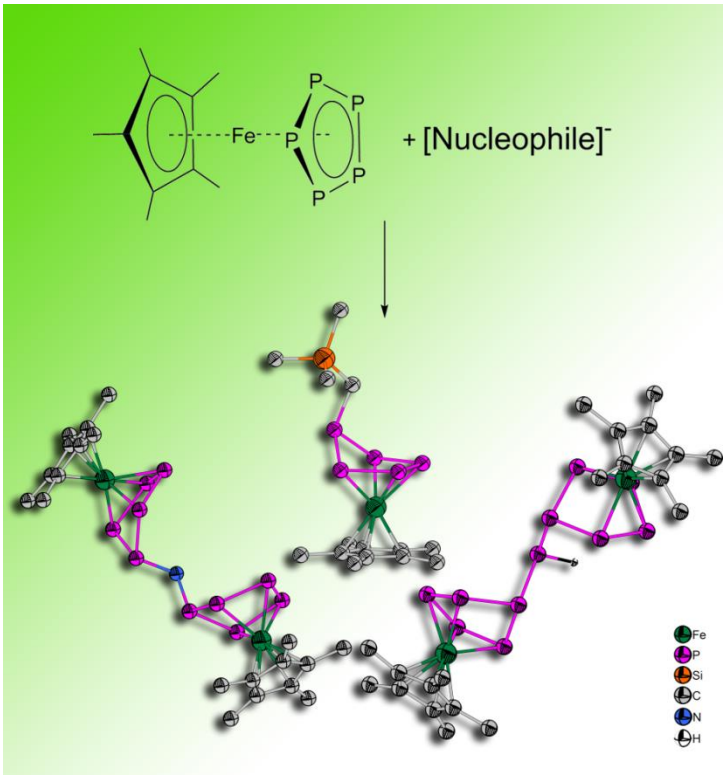

- Compounds **5** and **6** were synthesized by Eric Mädl. Compounds **3** and **4** were already synthesized and characterized in the master thesis of Eric Mädl. Compound **2** was synthesized and characterized by Mikhail. V. Butovskii.

- The chapter "discussion" was written by Eric Mädl, except for parts regarding calculations, which were written by Gabor Balázs. Details about X-ray structure analyses in the chapter "supporting information" were written by Eugenia V. Peresypkina and Alexander V. Virovets.

- DFT calculations were performed by Gabor Balázs. X-ray structure analyses and refinements were performed by Eugenia V. Peresypkina, Alexander V. Virovets and Michael Seidl.

- Figures were made by Eric Mädl, except figures regarding any calculations, which were made by Gabor Balázs.

3.1 Discussion

Abstract: *Unprecedented functionalized products with a η^4-P_5 ring are obtained by the reaction of [Cp*Fe(η^5-P_5)] (**1**) (Cp* = η^5-C_5Me_5) with different nucleophiles. With $LiCH_2SiMe_3$ and $LiNMe_2$, the monoanionic products [Cp*Fe(η^4-$P_5CH_2SiMe_3$)]$^-$ (**2**) and [Cp*Fe(η^4-P_5NMe_2)]$^-$ (**3**), respectively, are formed. The reaction of **1** with $NaNH_2$ leads to the formation of the trianionic compound [{Cp*Fe(η^4-P_5)}$_2$N]$^{3-}$ (**4**), whereas the reaction with $LiPH_2$ yields [Cp*Fe(η^4-P_5PH_2)]$^-$ (**5**) as the main product, with [(Cp*Fe)$_2$(μ,$\eta^{4:4}$-$P_{11}H$)]$^{2-}$ (**6**) as a byproduct. The calculated energy profile of the reactions provides a rationale for the formation of the different products.*

Ferrocene, the first organometallic sandwich complex, being discovered over 60 years ago,[1] has proven to be a versatile and significant compound in chemistry. Whereas in the beginning of the ferrocene chemistry, extensive reactivity studies were performed,[2] it is currently widely used for polymer chemistry,[3] for asymmetric catalysis,[4] or for medical applications.[5] One of the most striking reactions of ferrocene is its reaction with strong organometallic bases like organolithium compounds,[6,7] which lead to the deprotonation of the C_5H_5 unit and the formation of mono- and dilithioferrocenes. This demonstrates that the reactivity pattern of ferrocene is dominated by the C_5H_5 ligands. The most analogous polyphosphorus derivative is pentaphosphaferrocene [Cp*Fe(η^5-P_5)] (Cp* = η^5-C_5Me_5) (**1**).[8] We and others have been interested in the reactivity of **1**, and it has been shown that the *cylco*-P_5 unit can coordinate to transition metal carbonyls to give triple-decker complexes and other subsequent organometallic compounds containing distorted P_5 units,[9] and to copper(I) halides to give 1D and 2D polymers[10] or even spherical fullerene-like superballs.[11] The redox chemistry of **1** was initially investigated by Winter and Geiger,[12] and only recently were we able to isolate and characterize the dicationic species [(Cp*Fe)$_2$(μ,$\eta^{5:5}$-P_5)]$^{2+}$, as well as the dianionic species [(Cp*Fe)$_2$(μ,$\eta^{4:4}$-P_{10})]$^{2-}$ and [Cp*Fe(η^4-P_5)]$^{2-}$.[13] However, what is missing in the chemistry of **1** is reactivity towards main group nucleophiles to develop a better understanding of its reaction chemistry in comparison to its carbonaceous relative ferrocene. Density functional theory calculations on **1** show that the LUMO and LUMO+1 orbitals are mostly localized on the P atoms of the *cyclo*-P_5 ligand and the positive charge is also located there.[14] Therefore, it can be assumed that a nucleophilic attack can occur at the *cyclo*-P_5 ligand. Herein, we report the first reactivity of pentaphosphaferrocene towards main group nucleophiles leading to an unprecedented functionalization of the *cyclo*-P_5 ligand. With these first results, this molecule is now becoming a valuable starting material in organometallic based main group chemistry.

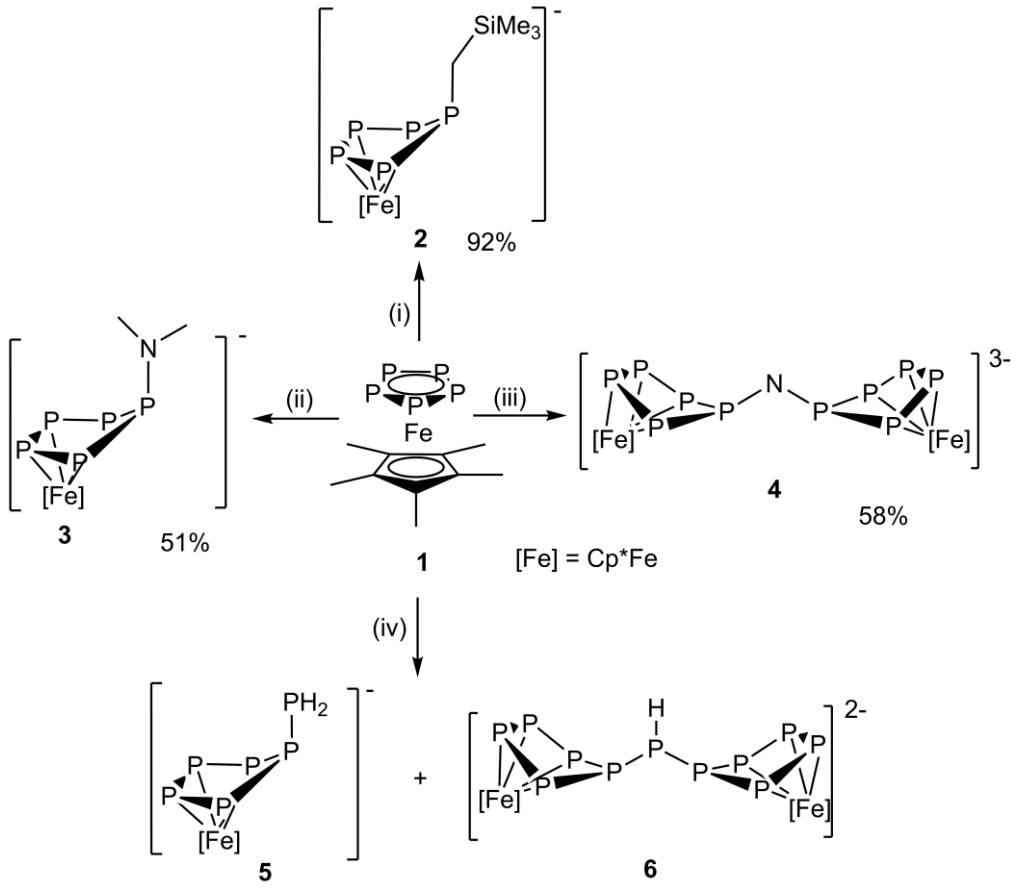

Scheme 1. Reactivity of **1** towards nucleophiles: (i) $LiCH_2SiMe_3$ in Et_2O, −35 °C → r.t.; (ii) $LiNMe_2$ in THF, −35 °C → r.t.; (iii) $NaNH_2$ in DME, r.t.; (iv) $LiPH_2$ in THF, −60 °C → r.t.

Mixing a green solution of **1** and $LiCH_2SiMe_3$ or $LiNMe_2$ in diethyl ether or THF at low temperatures resulted in immediate color change to dark brown to give, after work-up, [Li(Et_2O)][**2**] (92% yield) or [Li(thf)$_4$][**3**] (51% yield) (Scheme 1). The ^{31}P NMR spectra of **2** and **3** show an AMM'XX′ spin system with resonances centered at −56.0, 13.2, and 76.5 ppm and at –32.4, 23.9, and 119.7 ppm, respectively. Whereas for **2** crystals of suitable quality could be obtained, all attempts to get such crystals for [Li(thf)$_4$][**3**] failed, and its X-ray structure analysis was impeded by intrinsic disorder of the Cp* and η^4-{$P_5(NMe_2)$} groups over alternative positions prevented a satisfying determination of the structural parameters. However, the atom connectivity of **3** was unambiguously determined being similar to that one found for **2**. The X-ray structure analysis of [Li(Et_2O)][**2**], which represents a Li bridged dimer {[Li(Et_2O)$_2$][**2**]}$_2$ in the solid state, shows an η^4-P_5 ring of the former *cyclo*-P_5 unit in envelope conformation with the CH_2SiMe_3 group being attached to the phosphorus atom which is bent out plane from the η^4-P_5 ring (Figure 1). All P-P bonds show double bond character (2.1299(10) − 2.1623(8) Å), while the nearly planar P_4 unit is coordinating almost symmetrically to the Cp*Fe fragment. Beside **2** and the other products **3** − **6** of this publication and former reported oxidation/reduction products of **1**[13] only very few compounds are known containing *cyclo*-P_5 ligands in envelope conformation, coordinating in a η^4-manner to a transition metal. One of these rare

examples is the niobium complex $[Na(thf)_6][\{Ar(Np)N\}(\eta^4\text{-}P_5)Nb\{N(Np)Ar\}_2]$ (Np = $CH_2{}^tBu$; Ar = 3,5-$Me_2C_6H_3$) reported recently by Cummins *et al.* [15] The bond lengths of **2** are in the same range as in the mentioned compounds.

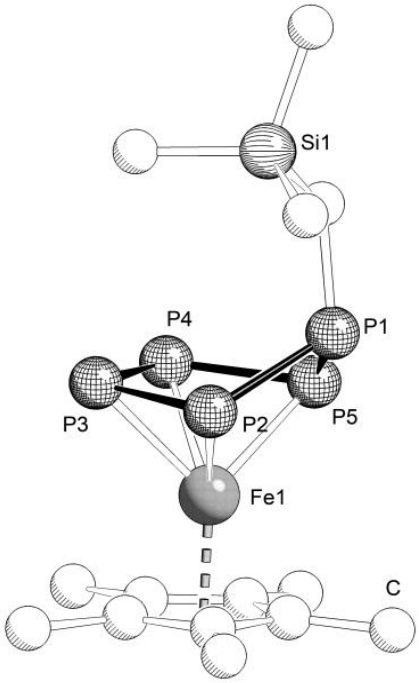

Figure 1. Molecular structure of the anion of $[Li(Et_2O)][\mathbf{2}]$. H atoms are omitted for clarity. Selected bond lengths [Å] and angles [°]: P1-P2 2.1663(9), P1-P5 2.1569(9), P2-P3 2.1466(10), P3-P4 2.1342(11), P4-P5 2.1535(9), P1-C1 1.843(3), Fe1-P2 2.3218(8), Fe1-P3 2.3350(8), Fe1-P4 2.3420(8), Fe1-P5 2.3040(7), P5-P1-P2 92.81(4), P3-P2-P1 106.53(4), P4-P3-P2 103.91(4), P3-P4-P5 102.90(4), P4-P5-P1 106.93(4).

By using the parent NH_2^- nucleophile, despite several attempts, we were not able to isolate a monoanionic compound. However, brown crystals of the trianion **4** could be isolated in 58% yield (Scheme 1).[16] The ^{31}P NMR spectrum of **4** shows an AA'XX'X"X"'YY'Y"Y"' spin system with three multiplets centered at −0.5, 13.8, and 149.6 ppm. The X-ray structure analysis of $[Na_3(dme)_5][\mathbf{4}]$ (Figure 3) reveals that two $[Cp^*FeP_5]$ fragments are linked by one nitrogen atom, resulting in the trianionic unit $[\{Cp^*Fe(\eta^4\text{-}P_5)\}_2N]^{3-}$. The P-P bonds are similar to those of **2**. The P-N bonds are in the expected range of a P-N single bond (P5-N1: 1.688(3) Å; P6-N1: 1.692(3) Å).

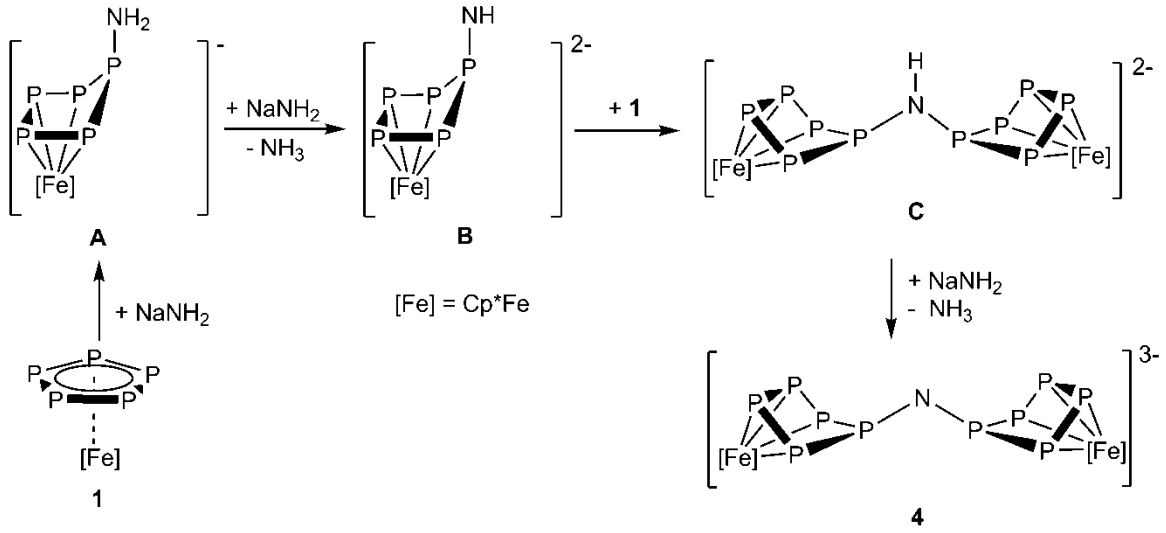

Scheme 2. Proposed pathway for the formation of **4**.

The formation of **4** can be rationalized as follows: The first step of the reaction is a nucleophilic attack of NH_2^- leading to the formation of **A** (Scheme 2). Because NH_2^- is also a strong base it can deprotonate **A** to give **B**, which reacts with a further molecule of **1** to form the dianionic species **C**. The subsequent deprotonation of **C** by NH_2^- gives the final product **4**. The formation of the intermediates **A** and **C** was monitored by ^{31}P NMR spectroscopy. When a ^{31}P NMR spectrum of the reaction mixture is recorded after 30 min, two sets of signals are observed for $[Cp^*Fe(\eta^4\text{-}P_5)NH_2]^-$ (**A**) and $[\{Cp^*Fe(\eta^4\text{-}P_5)\}_2NH]^{2-}$ (**C**), respectively. Note that **4** has not formed at this stage yet and **1** is still present in the reaction mixture. After another three days, all sets of signals corresponding to **A** – **C** have disappeared and only the signals corresponding to **4** as well as some decomposition products are observed. The long reaction time is caused by the poor solubility of $NaNH_2$. According to DFT calculations, the reaction of **1** with NH_2^- and the deprotonation of **A** by NH_2^- are exothermic in solution by −190.1 kJ·mol^{-1} and −30.0 kJ·mol^{-1}, respectively. Both, the reaction of **B** with **1** and the deprotonation of **C** by NH_2^- are exothermic in solution by −134.5 kJ·mol^{-1} and −17.4 kJ·mol^{-1}, respectively (Figure 2). Although there is a large difference between the relative energies of **1** and **4**, intermediates **A** and **C** are detected by ^{31}P NMR spectroscopy because the solubility of $NaNH_2$ is very low, and there is not enough NH_2^- available in solution for further reaction.

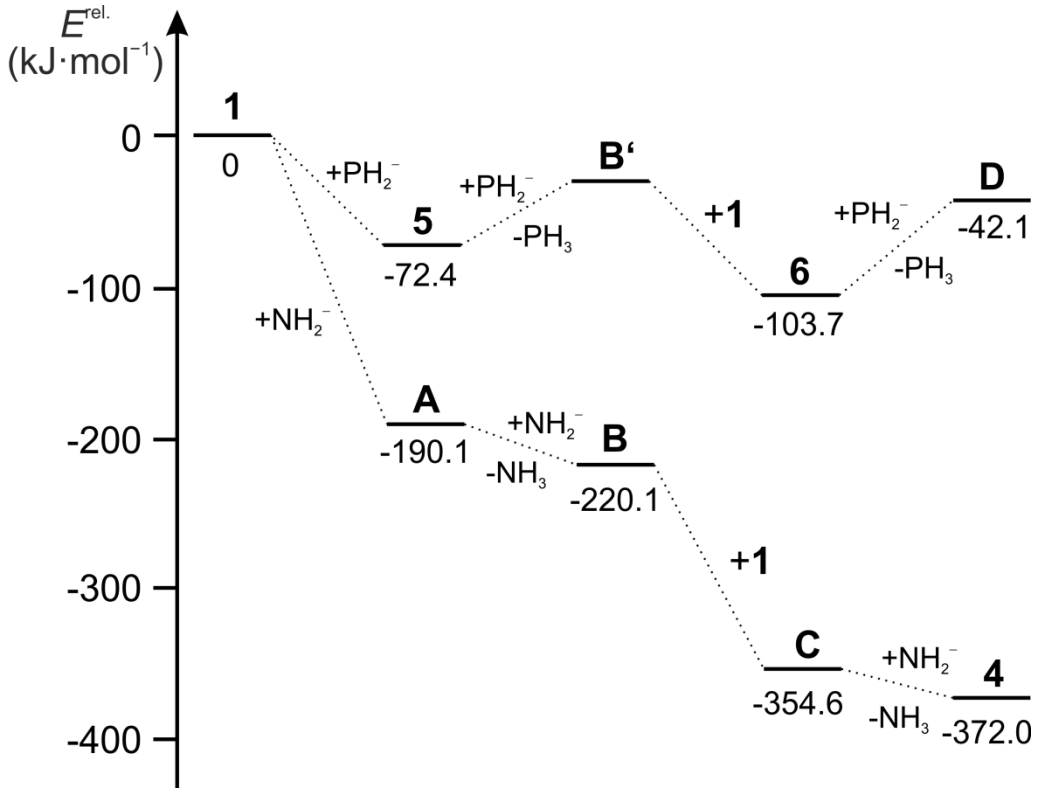

Figure 2. Energy profile of the formation of **4**, **5** and **6**, respectively.

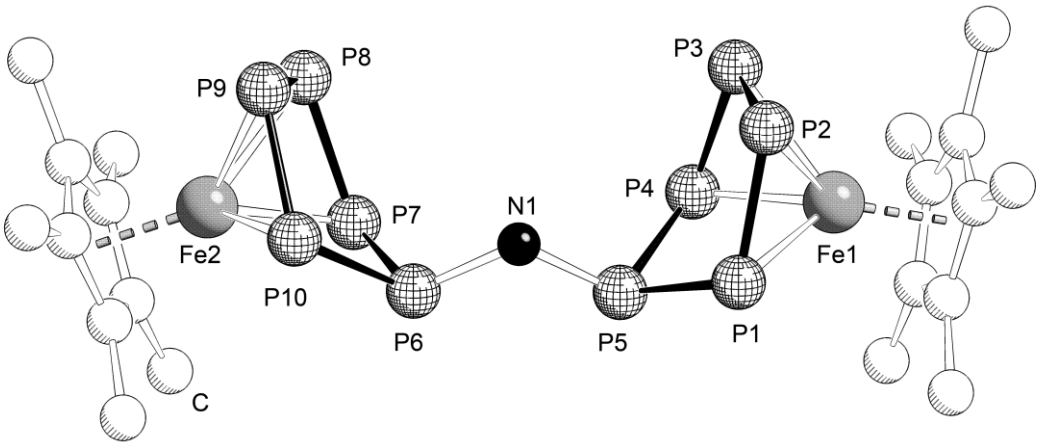

Figure 3. Molecular structure of the anion of $[Na_3(dme)_5][$**4**$]$. H atoms are omitted for clarity. Selected bond lengths [Å] and angles [°]:P1-P5 2.1700(13), P1-P2 2.1843(18), P2-P3 2.156(3), P3-P4 2.1411(19), P4-P5 2.1785(14), P6-P10 2.1614(13), P6-P7 2.1837(14), P7-P8 2.1593(18), P8-P9 2.136(2), P9-P10 2.1611(17), P1-Fe1 2.3026(11), P2-Fe1 2.2988(12), P3-Fe1 2.3157(13), P4-Fe1 2.3237(12), P5-P1-P2 106.80(6), P3-P2-P1 102.49(6), P4-P3-P2 102.51(6), P3-P4-P5 108.21(7), N1-P5-P1 110.77(11), N1-P5-P4 112.00(11), P5-N1-P6 116.77(17).

The proposed reaction pathway is also based on the autometalation ability of $LiP(SiMe_3)_2$ which we studied a time ago.[17] Therefore, we selected $LiPH_2$ as a nucleophilic reagent, and an excess of **1** was reacted with $LiPH_2$ in THF at −60 °C. An immediate color change from green to deep red was observed. The ^{31}P NMR spectrum of the reaction mixture show the formation of **5** as the main product with some unassigned impurities (Scheme 1). All attempts to isolate $[Li(thf)_x][\mathbf{5}]$ as a pure crystalline solid failed, but it can be precipitated with *n*-hexane as a solid in a 76% purity (determined by ^{31}P NMR). The identity of **5** was confirmed by $^{31}P\{^1H\}$ NMR spectroscopy in which an AMXX'YY' spin system was observed with signals centered at −114.9, −40.5, 20.3, and 50.0 ppm. The presence of the PH_2 unit was unambiguously proven by ^{31}P NMR spectroscopy and is attributed to the signal at −114.9 ppm. The other multiplets were assigned by ^{31}P, ^{31}P COSY experiments. Furthermore, the simulated coupling constants for **5** are very similar to those found for **2**, **3**, and **4**. However, from a concentrated solution in THF, crystals of **6**, suitable for single crystal X-ray diffraction, were obtained. Since **6** was only isolated by few crystals, unfortunately, it could not be characterized further. All attempts to synthesize **6** directly and in higher yields failed. Note, that all reported products **2 − 6** are extremely sensitive towards air and especially moisture.

DFT calculations show that the relative energy profile of the reaction of **1** with PH_2^- differs considerably from that of the reaction of **1** with NH_2^- (Figure 2). While the formation of **5** is exothermic by −72.4 kJ·mol^{-1}, deprotonation of **5** to $[Cp^*Fe(\eta^4\text{-}P_5PH)]^{2-}$ (**B'**) is endothermic by 39.7 kJ·mol^{-1}. Hence, the latter reaction is hampered, which allows the isolation of **5**. Furthermore, the deprotonation of **6** to the trianionic species $[(Cp^*Fe)_2(\mu,\eta^{4:4}\text{–}P_{11})]^{3-}$ (**D**) is also endothermic by 61.6 kJ·mol^{-1}. These data clearly explain why in the reaction of **1** with NH_2^- **4** is obtained as final product, whereas for the reaction of **1** with PH_2^- **5** is obtained as the main product.

The structure of $[Li_2(dme)_6][\mathbf{6}]$ was determined by single crystal X-ray diffraction (Figure 4). In **6** two $[Cp^*Fe(\eta^4\text{-}P_5)]$ fragments are linked together by a PH unit with P-P distances corresponding to single bonds (P5-P6: 2.2043(15) Å, P6-P7: 2.155(15) Å). The P-P bond lengths within the $\eta^4\text{-}P_5$ unit are comparable with those found in **2**, with the exception of the P9-P10 bond which is 2.096 Å, slightly shorter than the corresponding bond length in **2** (P3-P4 2.1342(11)). The hydrogen atom attached to the atom P6 could be located from residual electron density map and refined with fixed thermal parameters.

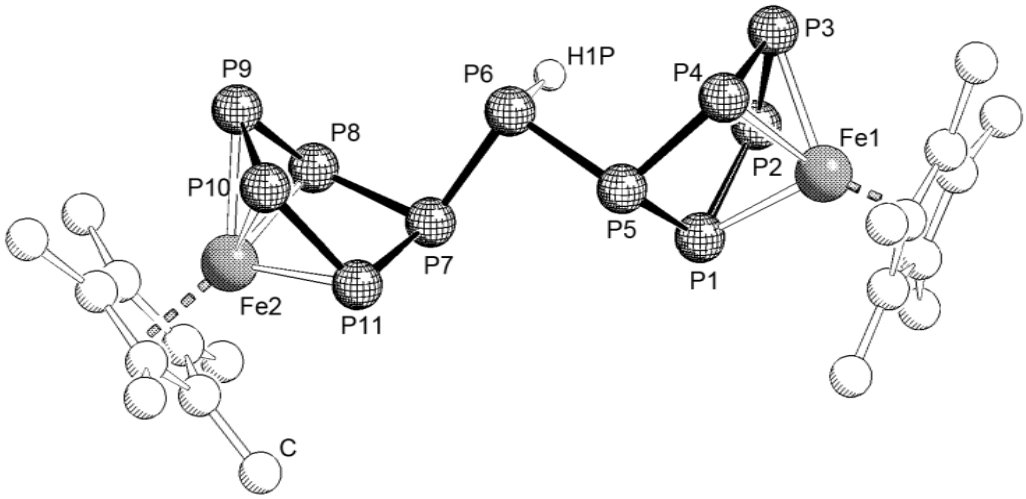

Figure 4. Molecular structure of the anion of $[Li_2(dme)_6]$[**6**]. Li atoms, coordinated DME, and H atoms are omitted for clarity. Selected bond lengths [Å] and angles [°]: P1-P2 2.1537(15), P1-P5 2.1669(14), P2-P3 2.1327(15), P3-P4 2.1467(14), P4-P5 2.1700(13), P5-P6 2.2055(14), P6-H1P 1.38(5), P6-P7 2.2161(15), P7-P8 2.1348(18), P7-P11 2.165(2), P8-P9 2.118(2), P9-P10 2.094(3), P10-P11 2.155(3), P1-Fe1 2.3172(10), P2-Fe1 2.3325(10), P3-Fe1 2.3289(10), P4-Fe1 2.3248(10), P2-P1-P5 107.57(5), P3-P2-P1 103.63(5), P2-P3-P4 103.83(5), P3-P4-P5 107.77(5), P1-P5-P4 93.29(5), P1-P5-P6 108.94(6), P5-P6-P7 98.10(6).

We have shown, that pentaphosphaferrocene is a reactive molecule, not only useful in coordination chemistry with transition metals but also reactive with different main group nucleophiles. In this respect, it shows some similarities with its all-carbon relative ferrocene. However, in its reactivity **1** differs by undergoing transformations of the aromatic *cyclo*-P_5 ligand and forming unprecedented compounds with a η^4-P_5 structural pattern. Moreover, if H-containing nucleophiles are used, an aggregation of pentaphosphaferrocene molecules can yield di- and trianionic derivatives revealing the ability of **1** to form novel aggregated and P-rich species. With these novel reactivity patterns pentaphosphaferrocene becomes a valuable organometallic building block and opens a new chapter for its use in main group chemistry.

References:

[1] T. J. Kealy, P. L. Pauson, *Nature* **1951**, *168*, 1039-1040.

[2] a) R. B. Woodward, M. Rosenblum, M. C. Whiting, *J. Am. Chem. Soc.* **1952**, *74*, 3458; b) R. A. Benkeser, D. Goggin, G. Schroll, *J. Am. Chem. Soc.* **1954**, *76*, 4025.

[3] N. J. Long, K. Kowalski, in *Ferrocenes*, John Wiley & Sons, Ltd, **2008**, pp. 393-446.

[4] R. Gómez Arrayás, J. Adrio, J. C. Carretero, *Angew. Chem. Int. Ed.* **2006**, *45*, 7674-7715.

[5] M. F. R. Fouda, M. M. Abd-Elzaher, R. A. Abdelsamaia, A. A. Labib, *Appl. Organomet. Chem.* **2007**, *21*, 613-625.

[6] M. D. Rausch, D. J. Ciappenelli, *J. Organomet. Chem.* **1967**, *10*, 127.

[7] F. Rebiere, O. Samuel, H. B. Kagan, *Tetrahedron Lett.* **1990**, *31*, 3121-3124.

[8] J. Scherer, T. Brück, *Angew. Chem.* **1987**, *99*, 59*; Angew. Chem. Int. Ed.* **1987**, *99*, 59.

[9] O. J. Scherer, T. Brück, G. Wolmershäuser, *Chem. Ber.* **1989**, *122*, 2049-2054.

[10] a) J. Bai, A. V. Virovets, M. Scheer, *Angew. Chem. Int. Ed.* **2002**, *41*, 1737-1740; b) M. Scheer, L. J. Gregoriades, A. V. Virovets, W. Kunz, R. Neueder, I. Krossing, *Angew. Chem. Int. Ed.* **2006**, *45*, 5689-5693.

[11] a) J. Bai, A. V. Virovets, M. Scheer, *Science* **2003**, *300*, 781-783; b) T. Li, J. Wiecko, N. A. Pushkarevsky, M. T. Gamer, R. Köppe, S. N. Konchenko, M. Scheer, P. W. Roesky, *Angew. Chem. Int. Ed.* **2011**, *50*, 9491-9495; c) M. Scheer, J. Bai, B. P. Johnson, R. Merkle, A. V. Virovets, C. E. Anson, *Eur. J. Inorg. Chem.* **2005**, *2005*, 4023-4026; d) M. Scheer, A. Schindler, J. Bai, B. P. Johnson, R. Merkle, R. Winter, A. V. Virovets, E. V. Peresypkina, V. A. Blatov, M. Sierka, H. Eckert, *Chem. Eur. J.* **2010**, *16*, 2092-2107; e) M. Scheer, A. Schindler, C. Gröger, A. V. Virovets, E. V. Peresypkina, *Angew. Chem.* **2009**, *121*, 5148-5151; *Angew. Chem. Int. Ed.* **2009**, *48*, 5046 – 5049; f) M. Scheer, A. Schindler, R. Merkle, B. P. Johnson, M. Linseis, R. Winter, C. E. Anson, A. V. Virovets, *J. Am. Chem. Soc.* **2007**, *129*, 13386-13387; g) S. Welsch, C. Gröger, M. Sierka, M. Scheer, *Angew. Chem.* **2011**, *123*, 1471-1474; *Angew. Chem. Int. Ed.* **2011**, *50*, 1435–1438.

[12] R. F. Winter, W. E. Geiger, *Organometallics* **1999**, *18*, 1827-1833.

[13] M. V. Butovskiy, G. Balázs, M. Bodensteiner, E. V. Peresypkina, A. V. Virovets, J. Sutter, M. Scheer, *Angew. Chem. Int. Ed.* **2013**, *52*, 2972-2976.

[14] a) E. J. P. Malar, *Eur. J. Inorg. Chem.* **2004**, 2723–2732; b) H. Krauss, G. Balazs, M. Bodensteiner, M. Scheer, *Chem. Sci.* **2010**, *1*, 337-342.

[15] D. Tofan, B. M. Cossairt, C. C. Cummins, *Inorg. Chem.* **2011**, *50*, 12349-12358.

[16] Due to the limited solubility of $NaNH_2$ in DME this reaction proceeds slowly, even at ambient temperature.

[17] a) M. Scheer, St. Gremler, E. Herrmann, U. Grünhagen, M. Dargatz, E. Kleinpeter, *Z. Anorg. Allg. Chem.* **1991**, *600*, 203 – 210; b) M. Scheer, St. Gremler, E. Herrmann, P. G. Jones, *J. Organomet. Chem.* **1991**, *414*, 337 – 349; c) M. Scheer, St. Gremler, E. Herrmann, M. Dargatz, H.-D. Schädler, *Z. Anorg. Allg. Chem.* **1993**, *619*, 1047 – 1052.

3.2 Supporting Information

Supporting information of the manuscript entitled:

Functionalization of the *cyclo*-P_5 ligand in pentaphosphaferrocene by main group nucleophiles

Eric Mädl, Mikhail V. Butovskii, Gábor Balázs, Eugenia V. Peresypkina, Alexander V. Virovets, Michael Seidl and Manfred Scheer*

Contents

3.2.1 Experimental details: complex syntheses and characterization

General Procedures: All manipulations were performed with rigorous exclusion of oxygen and moisture in Schlenk-type glassware on a dual manifold Schlenk line in argon atmosphere or in Ar filled glove box with a high-capacity recirculator (<0.1ppm O_2). THF, toluene, hexane, and DME were distilled from sodium benzophenoneketyl. Deuterated solvents were degassed, dried and distilled prior to use. The complex [Cp*Fe(η^5-P_5)][1] (**1**), was prepared according to its published procedure. NMR spectra were recorded on a Bruker Avance 300 MHz and Bruker Avance 400 MHz spectrometers. Chemical shifts were measured at ambient temperature and are given in ppm; they are referenced to TMS for ^{1}H and ^{13}C, and 85% H_3PO_4 for ^{31}P as external standard. Elemental analyses (CHN) were determined using in-house facility.

Synthesis of [Li(Et_2O)][2]: To a solution of ((trimethylsilyl)methyl)lithium (68 mg, 0.723 mmol) in Et_2O (5 mL) at −35 °C was added a solution of **1** (250 mg, 0.723 mmol) in Et_2O (15 mL). Immediate color change was observed. The solution was slowly warmed up to ambient temperature and volume of the reaction mixture was reduced to ca. 15 mL and layered with *n*-hexane (20 mL). Black crystals

of {[Li(Et_2O)][**2**]}$_2$ (342 mg, 92 % yield were formed after 2 days at 0 °C. $C_{18}H_{36}FeLiOP_5Si$ (514.22): calcd. C 42.04, H 7.06; found C 41.77, H 6.51. ^{1}H NMR (400.13 MHz, THF-d_8): δ [ppm] = −0.64 (t, 2H, *CH*$_2$SiMe$_3$), −0.15 (s, 9H, CH$_2$*SiMe*$_3$), 1.48 (C$_5$(C*H*$_3$)$_5$). ^{13}C{^{1}H} NMR (100.62 MHz, THF-d_8): δ = 0.82 (CH$_2$*SiMe*$_3$), 11.77 (s, C$_5$(*C*H$_3$)$_5$), 32.14 (dm, J_{PC} = 69.86 Hz, *CH*$_2$SiMe$_3$), 85.80 (*s, C*$_5$(C*H*$_3$)$_5$) ppm. ^{31}P{^{1}H} NMR (161.97 MHz, THF-d_8): δ = −56.02 (m, 2P, P^X/ $P^{X'}$), 13.18 (m, 2P, P^M/ $P^{M'}$), 76.51 (m, 1P, P_A). For coupling constants see Table S1.

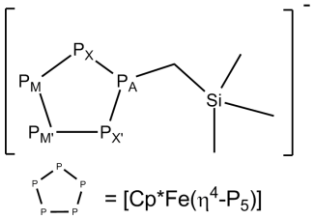

Figure S1. Spin system of [Li(Et_2O)][**2**].

Synthesis of [Li(thf)$_{2.5}$][3]: To a solution of **1** (176 mg, 0.51 mmol) in 5 mL THF a solution of $LiNMe_2$ (26 mg, 0.51 mmol) was added at −35 °C. The color of the solution turned immediately from green to brown. The reaction mixture was stirred over 20 hours, the solvent was concentrated to 3 mL and finally layered with *n*-hexane. After 4 days on room temperature light brown square shaped crystals of [Li(thf)$_{2.5}$][**2**] (150 mg, 51 %) were formed. $C_{22}H_{41}FeLiNO_{2.5}P_5$ (577.22): calcd. C 45.78, H 7.16, N 2.43; found C 45.01, H 6.95, N 2.62. ^{1}H NMR (400.13 MHz, THF-d_8): δ [ppm] = 1.32 (s, 6H, NMe_2), 1.42 (s, 15H, C$_5$(C*H*$_3$)$_5$). ^{13}C{^{1}H} NMR (100.62 MHz, THF-d_8): δ [ppm] = 11.9 (s, C$_5$(*C*H$_3$)$_5$), 40.9 (s, NMe_2), 84.9 (s, *C*$_5$(CH$_3$)$_5$). ^{31}P NMR (161.97 MHz, THF-d_8): δ [ppm] = −32.4 (m, 2P, P^Y/$P^{Y'}$), 23.9 (m, 2P, P^X/$P^{X'}$), 119.7 (m, 1P, P^A). For coupling constants see Table S2.

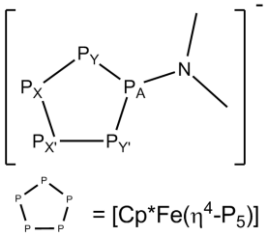

Figure S2. Spin system of [Li(thf)$_{2.5}$][**3**].

Synthesis of [Na$_3$(dme)$_5$][4]: To a mixture of **1** (118 mg, 0.34 mmol) and $NaNH_2$ (20 mg, 0.51 mmol) 20 mL DME was added. The reaction mixture turned immediately brown and was stirred for 2 days, the solvent was concentrated to 3 mL and layered with *n*-hexane. After 7 days on room temperature long brown needles of [Na(dme)$_3${Na(dme)}$_2$][**4**] could be isolated. $Na_3C_{40}H_{80}Fe_2P_{10}NO_{10}$ (1225.46): calcd. C 39.14, H 6.73, N 1.14; found C 39.02, H 6.37, N 1.28. ^{1}H NMR (400.13 MHz, THF-d_8): δ [ppm] = 3.2 (s, 15H C$_5$(CH$_3$)$_5$). ^{13}C{^{1}H} NMR (100.62 MHz, THF-d_8): δ [ppm] = 10.7 (s, C$_5$(*C*H$_3$)$_5$),

86.2 (s, $C_5(CH_3)_5$). ^{31}P NMR (161.97 MHz, THF-d_8): δ [ppm] = −0.5 (m, 4P, P^Y/ $P^{Y'}$/ $P^{Y''}$/ $P^{Y'''}$), 13.8 (m, 4P, P^X/ $P^{X'}$/$P^{X''}$/$P^{X'''}$), 149.6 (m, 2P, P^A/ $P^{A'}$). For coupling constants see Table S3.

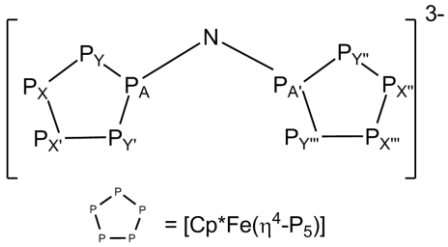

Figure S3. Spin system of $[Na_3(dme)_5]$[**4**].

Synthesis of $[Li(thf)_x]$[5]: To a solution of **1** (120 mg, 0.35 mmol) in 15 mL DME a suspension of [{Li(dme)}PH_2] (38 mg, 0.29 mmol) was added at −60 °C. The color of the solution turned immediately burgundy. The solution was slowly warmed up to ambient temperature during the night and the reaction mixture was reduced to 2 mL. After three months at −80 °C very few crystals of $[Li_2(dme)_6]$[**6**] could be obtained for a single crystal measurement. ^{1}H NMR (400.13 MHz, THF-d_8): δ [ppm] = 1.6 (dquint, PH_2; partly superimposed by the signal of the $C_5(CH_3)_5$ group), 1.48 (s, 15H, $C_5(CH_3)_5$). ^{13}C{^{1}H} NMR (100.62 MHz, THF-d_8): δ [ppm] = 11.61 (s, $C_5(CH_3)_5$), 86.2 (s, $C_5(CH_3)_5$). ^{31}P NMR (161.97 MHz, THF-d_8): δ [ppm] = −115.85 (dt, 1P, P^Y), −41.59 (m, 2P, P^X/ $P^{X'}$), 18.57 (m, 2P, P^M/ $P^{M'}$), 39.35 (m, 1P, P^A). For coupling constants see Table S5.

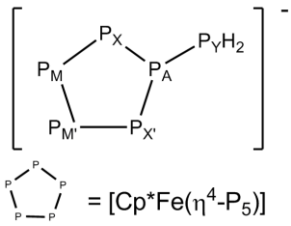

Figure S4. Spin system of $[Li(thf)_x]$[**5**].

3.2.2 Experimental and simulated NMR spectra and ortep-like plots

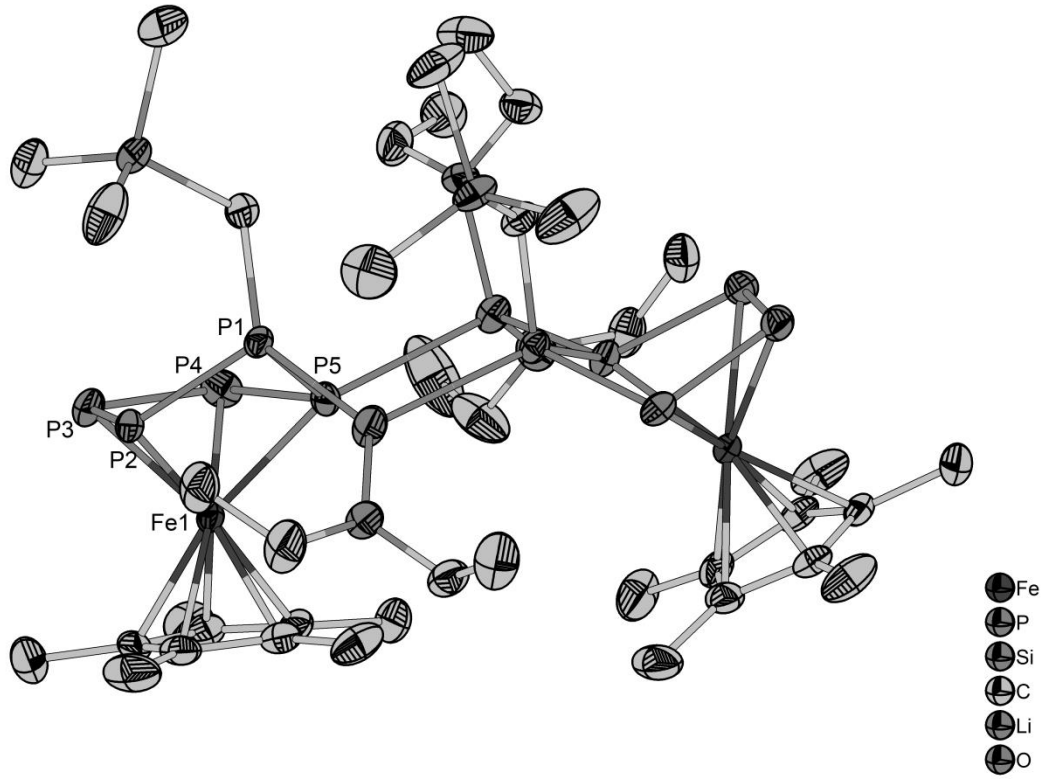

Figure S5. Molecular structure of the compound $\{[Li(Et_2O)][\mathbf{2}]\}_2$. H atoms are omitted for clarity. Ellipsoids are depicted at 50% probability. Selected bond lengths [Å] and angles [°]: P1-P2 2.1663(9), P1-P5 2.1569(9), P1-C1 1.843(3), P2-P3 2.1466(10), P3-P4 2.1342(11), P4-P5 2.1535(9), Fe1-P2 2.3218(8), Fe1-P3 2.3350(8), Fe1-P4 2.3420(8), Fe1-P5 2.3040(7), P5-P1-P2 92.81(4), P3-P2-P1 106.53(4), P3-P4-P5 102.90(4), P4-P5-P1 106.93(4).

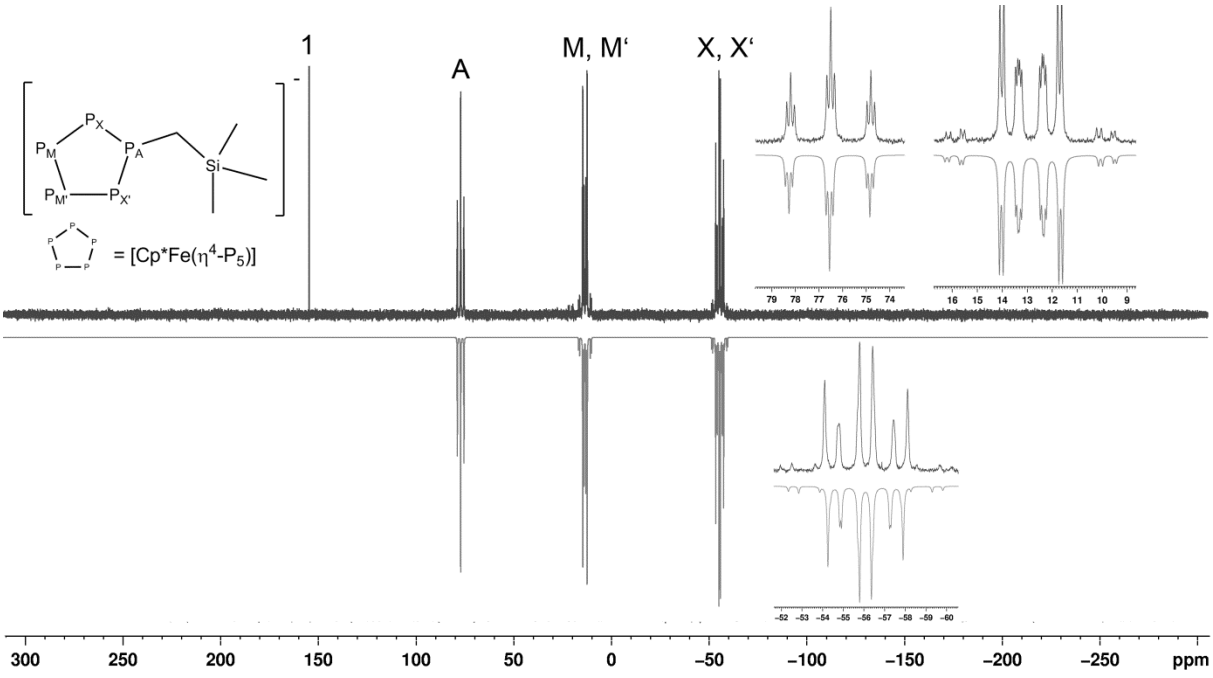

Figure S6. Experimental (top) and simulated (bottom) ^{31}P NMR (161.97 MHz, THF-d_8) spectrum of [Li(Et_2O)][**2**].

Table S1. ^{31}P NMR chemical shifts and coupling constants of [Li(Et_2O)][**2**] obtained from the simulation.

	J (Hz)			*δ* (ppm)	
$^2J_{P_A\text{-}P_M}$	−23.5	$^1J_{P_M\text{-}P_X}$	382.6	$P_{X,X'}$	−56.0
$^2J_{P_A\text{-}P_{M'}}$	−29.1	$^2J_{P_M\text{-}P_{X'}}$	−8.8	$P_{M,M'}$	13.2
$^1J_{P_A\text{-}P_X}$	275.1	$^2J_{P_{M'}\text{-}P_X}$	−5.5	P_A	76.5
$^1J_{P_A\text{-}P_{X'}}$	275.3	$^1J_{P_{M'}\text{-}P_{X'}}$	381.0		
$^1J_{P_M\text{-}P_{M'}}$	409.7	$^2J_{P_{X'}\text{-}P_X}$	−53.2		

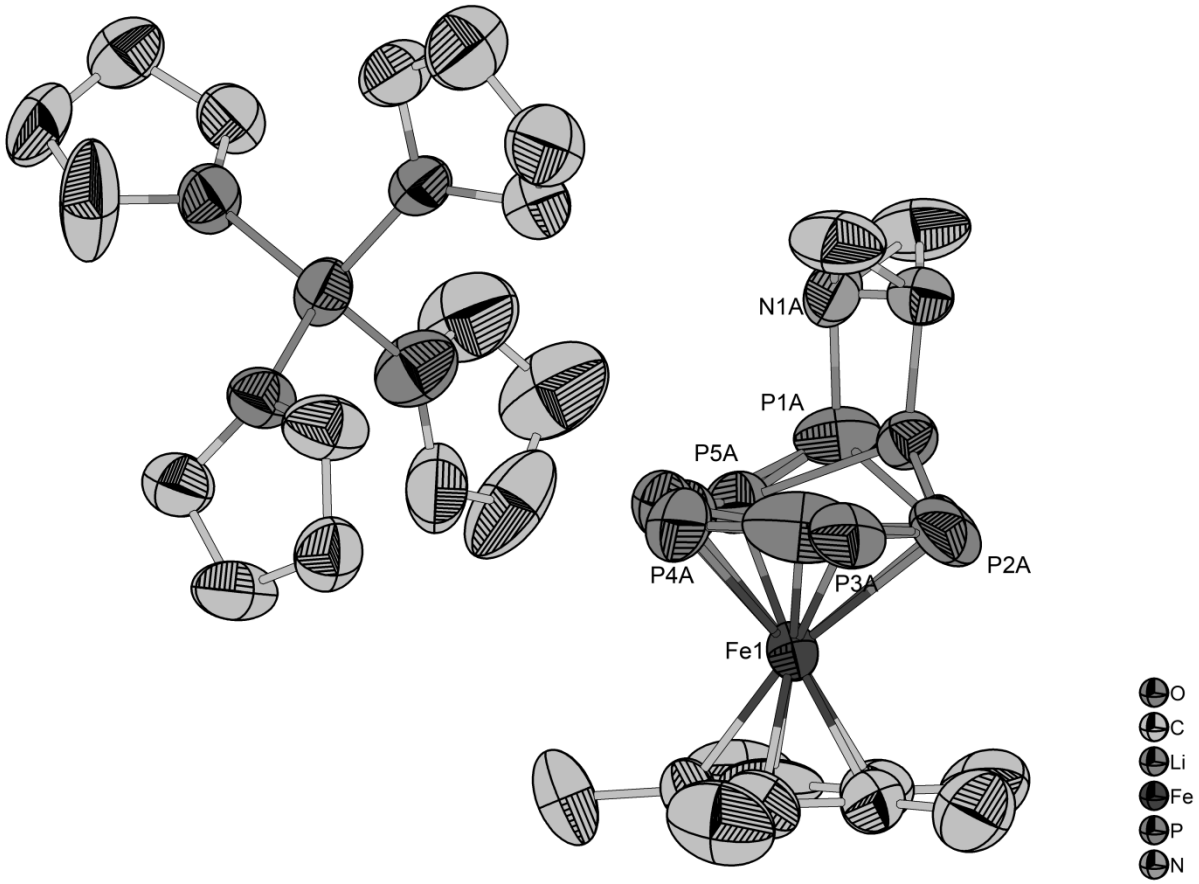

Figure S7. Molecular structure of the compound $[Li(thf)_4][\mathbf{3}]$. H atoms are omitted for clarity. The P_5 and the NMe_2 units are disordered over two positions with 50% occupancy. Selected bond lengths [Å] and angles [°]: P1A-P2A 2.201(10), P1A P5A 2.123(9), P1A-N1A 1.701(15), P2A-P3A 2.175(14), P3A-P4A 2.091(13), P4A-P5A 2.117(10), Fe1-P2A 2.289(8), Fe1-P3A 2.333(11), Fe1-P4A 2.319(7), Fe1-P5A 2.287(6), P2A-P1A-P5A 94.1(3), P2A-P1A-N1A 115.7(6), P5A-P1A-N1A 111.8(6), P1A-P2A-P3A 108.3(4), P2A-P3A-P4A 103.2(5), P3A-P4A-P5A 105.9(5), P1A-P5A-P4A 109.8(4).

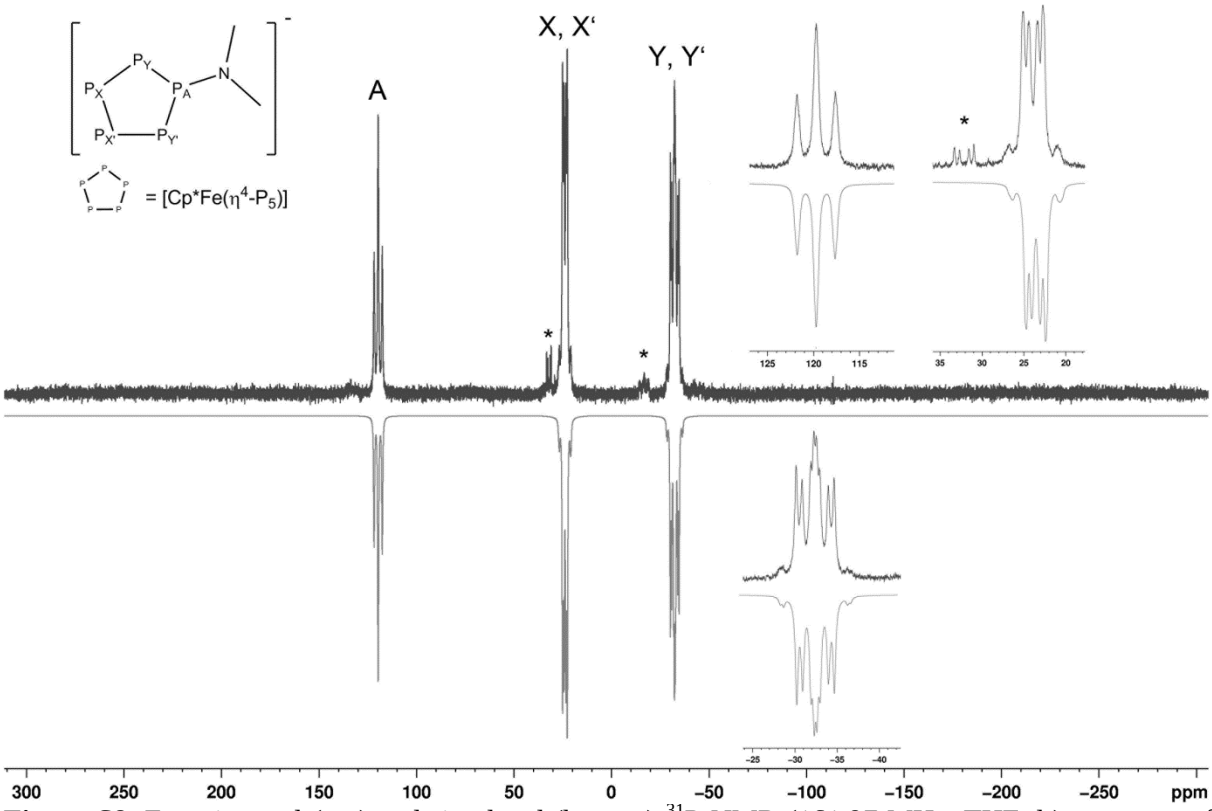

Figure S8. Experimental (top) and simulated (bottom) ^{31}P NMR (161.97 MHz, THF-d_8) spectrum of [Li(thf)$_{2.5}$][**3**]. Impurities are marked with *.

Table S2. ^{31}P NMR chemical shifts and coupling constants of [Li(thf)$_{2.5}$][**3**] obtained from the simulation.

J (Hz)		δ (ppm)	
$^2J_{PA\text{-}PX} = {}^2J_{PA\text{-}PX'}$	33.2	P_A	119.7
$^1J_{PA\text{-}PY} = {}^1J_{PA\text{-}PY'}$	339.0	$P_{X,X'}$	−32.4
$^1J_{PX\text{-}PY} = {}^1J_{PX'\text{-}PY'}$	392.0	$P_{Y,Y'}$	23.9
$^2J_{PX\text{-}PY'} = {}^2J_{PX'\text{-}PY}$	0.1		
$^1J_{PX\text{-}PX'}$	403.2		
$^2J_{PY\text{-}PY'}$	38.5		

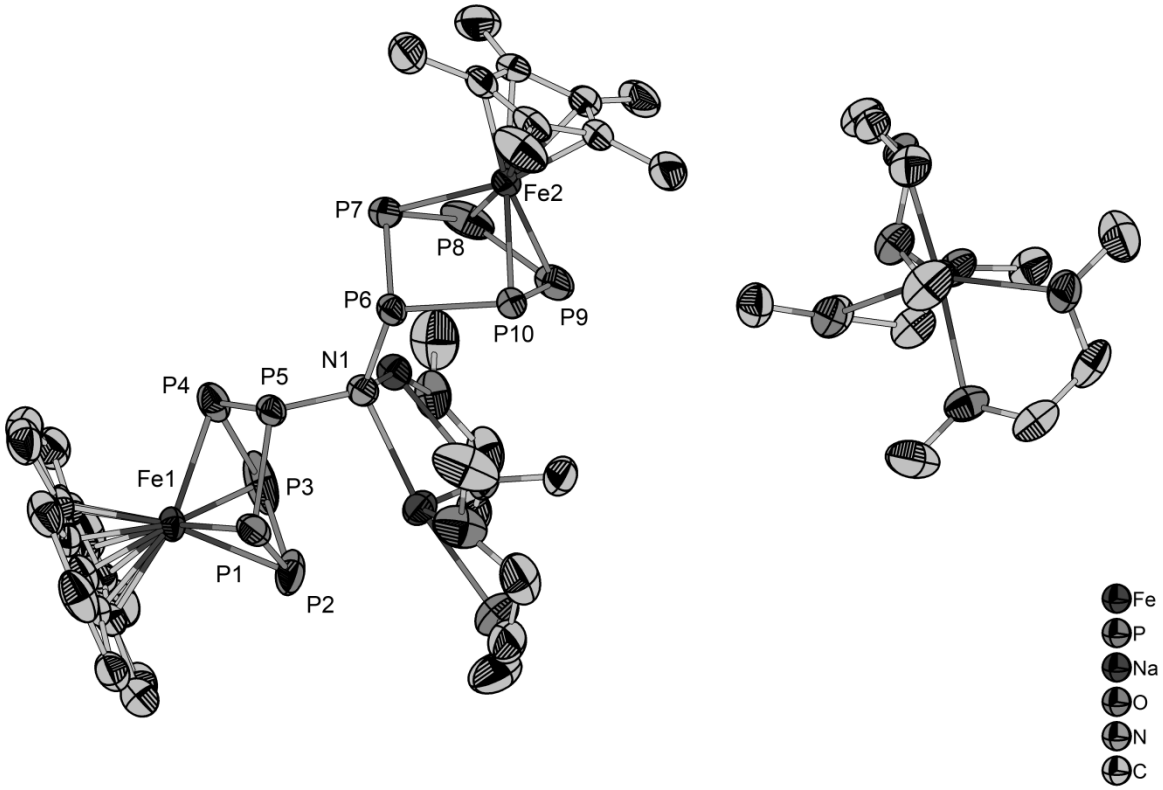

Figure S9. Molecular structure of the compound $[Na(dme)_3\{Na(dme)\}_2]$[**4**]. H atoms are omitted for clarity. Selected bond lengths [Å] and angles [°]: P1-P5 2.1700(13), P1-P2 2.1843(18), P2-P3 2.156(3), P3-P4 2.1411(19), P4-P5 2.1785(14), P6-P10 2.1614(13), P6-P7 2.1837(14), P7-P8 2.1593(18), P8-P9 2.136(2), P9-P10 2.1611(17), P1-Fe1 2.3026(11), P2-Fe1 2.2988(12), P3-Fe1 2.3157(13), P4-Fe1 2.3237(12), P5-P1-P2 106.80(6), P3-P2-P1 102.49(6), P4-P3-P2 102.51(6), P3-P4-P5 108.21(7), N1-P5-P1 110.77(11), N1-P5-P4 112.00(11), P5-N1-P6 116.77(17).

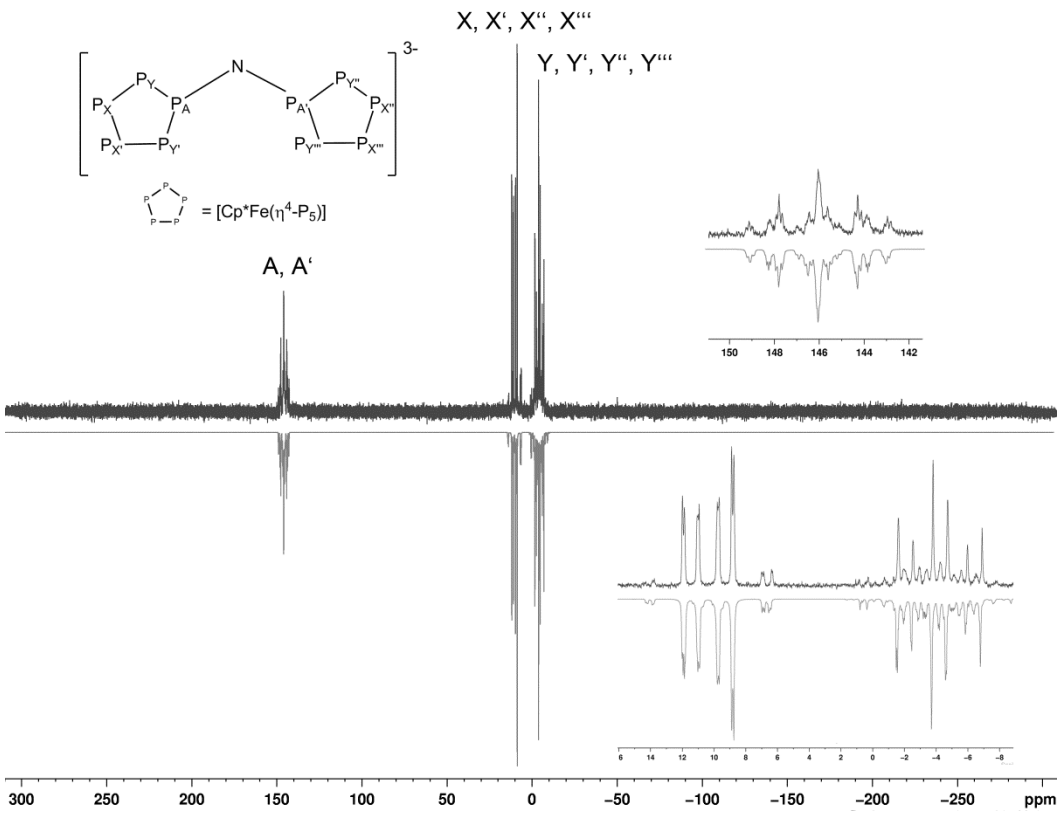

Figure S10. Experimental (top) and simulated (bottom) ^{31}P NMR (161.97 MHz, THF-d_8) spectrum of $[Na_3(dme)_5]$[**4**].

Table S3. ^{31}P NMR chemical shifts and coupling constants of $[Na_3(dme)_5]$[**4**] obtained from the simulation.

J (Hz)				δ (ppm)	
$^2J_{PA\text{-}PX} = {}^2J_{PA',\text{-}PX''}$	13.2	$^2J_{PX'\text{-}PY} = {}^2J_{PX''',\text{-}PY''}$	−12.1	A, A’	146.0
$^2J_{PA\text{-}PX'} = {}^2J_{PA',\text{-}PX'''}$	16.8	$^2J_{PA\text{-}PA'}$	−156.5	X, X’’	10.1
$^1J_{PA\text{-}PY} = {}^1J_{PA',\text{-}PY''}$	277.1	$^3J_{PY\text{-}PA'} = {}^3J_{PY'',\text{-}PA}$	−2.0	X’, X’’’	10.3
$^1J_{PA\text{-}PY'} = {}^1J_{PA',\text{-}PY'''}$	269.4	$^3J_{PY'\text{-}PA'} = {}^3J_{PY''',\text{-}PA}$	−4.0	Y, Y’’	−4.1
$^1J_{PX\text{-}PY} = {}^1J_{PX'',\text{-}PY''}$	384.1	$^4J_{PX\text{-}PA'} = {}^4J_{PX'',\text{-}PA}$	−2.0	Y’, Y’’’	−4.0
$^1J_{PX'\text{-}PY'} = {}^1J_{PX''',\text{-}PY'''}$	359.2	$^4J_{PX'\text{-}PA'} = {}^4J_{PX''',\text{-}PA}$	4.0		
$^1J_{PX\text{-}PX'} = {}^1J_{PX'',\text{-}PX'''}$	382.8	$^4J_{PY\text{-}PY''} = {}^4J_{PY',\text{-}PY'''}$	0.3		
$^2J_{PX\text{-}PY'} = {}^2J_{PX'',\text{-}PY'''}$	16.2	$^2J_{PY\text{-}PY'} = {}^2J_{PY'',\text{-}PY'''}$	30.1		
$^4J_{PY'\text{-}PY''} = {}^4J_{PY\text{-}PY'''}$	5.6	$^5J_{PY'\text{-}PX''} = {}^5J_{PY\text{-}PX'''}$	−0.6		
$^5J_{PY'\text{-}PX'''} = {}^5J_{PY\text{-}PX''}$	−0.37	$^4J_{PY\text{-}PY'''} = {}^4J_{PY'\text{-}PY''}$	2.0		

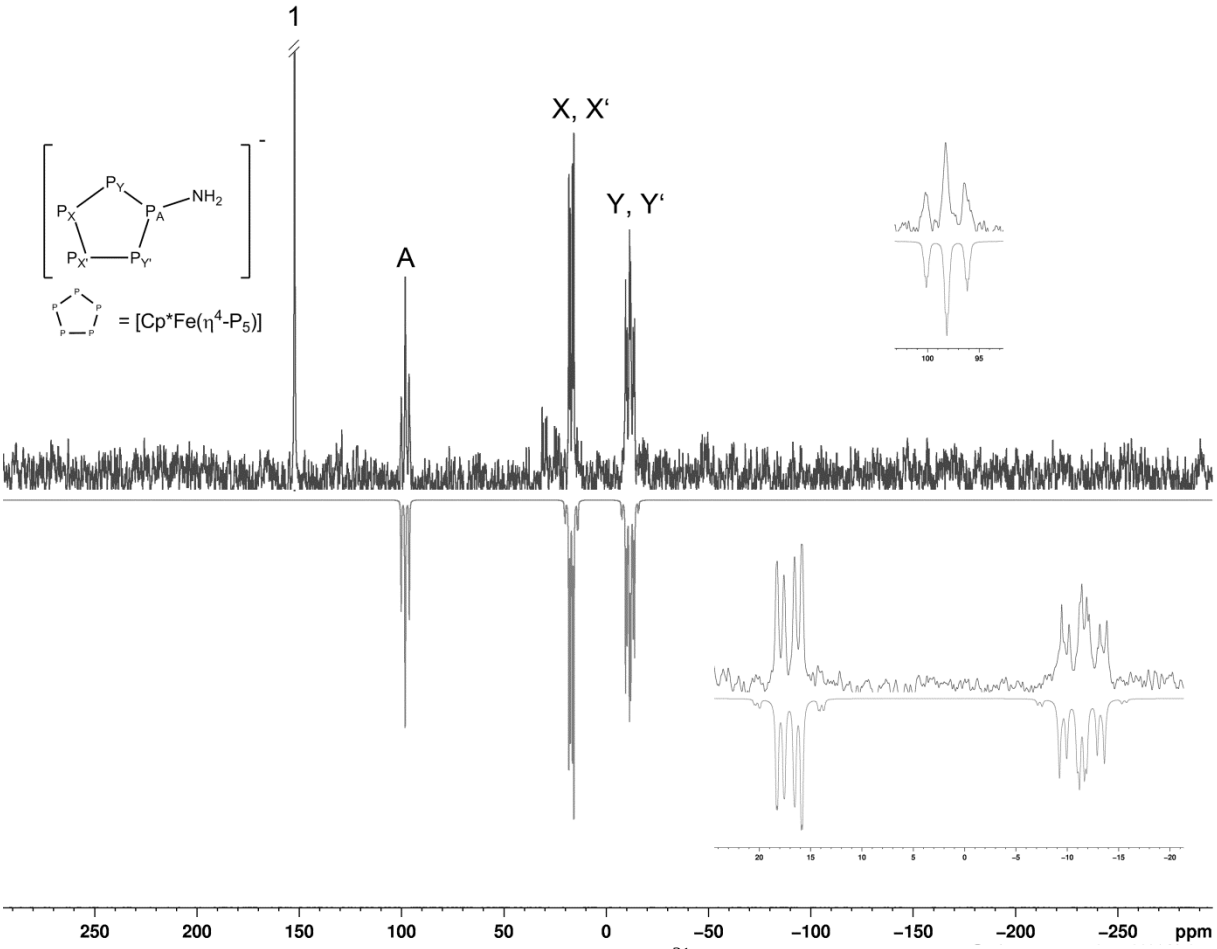

Figure S11. Experimental (top) and simulated (bottom) ^{31}P NMR (161.97 MHz, THF-d_8) spectrum of [Na(dme)$_x$)][**A**].

Table S4. ^{31}P NMR chemical shifts and coupling constants of [Na(dme)$_x$)][**A**] obtained from the simulation. The $^2J_{PH}$ coupling is not resolved in the experimental spectrum (leads only to line broadening).

J (Hz)		δ (ppm)	
$^1J_{P_A\text{-}P_Y} = {}^1J_{P_A\text{-}P_Y}$	319.4	A	98.3
$^2J_{P_A\text{-}P_X} = {}^2J_{P_A\text{-}P_{X'}}$	−24.0	X, X’	17.0
$^1J_{P_X\text{-}P_Y} = {}^1J_{P_{X'}\text{-}P_{Y'}}$	402.0	Y, Y’	−11.6
$^1J_{P_X\text{-}P_{X'}}$	428.3		
$^2J_{P_Y\text{-}P_{Y'}}$	−41.4		
$^2J_{P_Y\text{-}P_{X'}} = {}^2J_{P_{Y'}\text{-}P_X}$	−7.7		

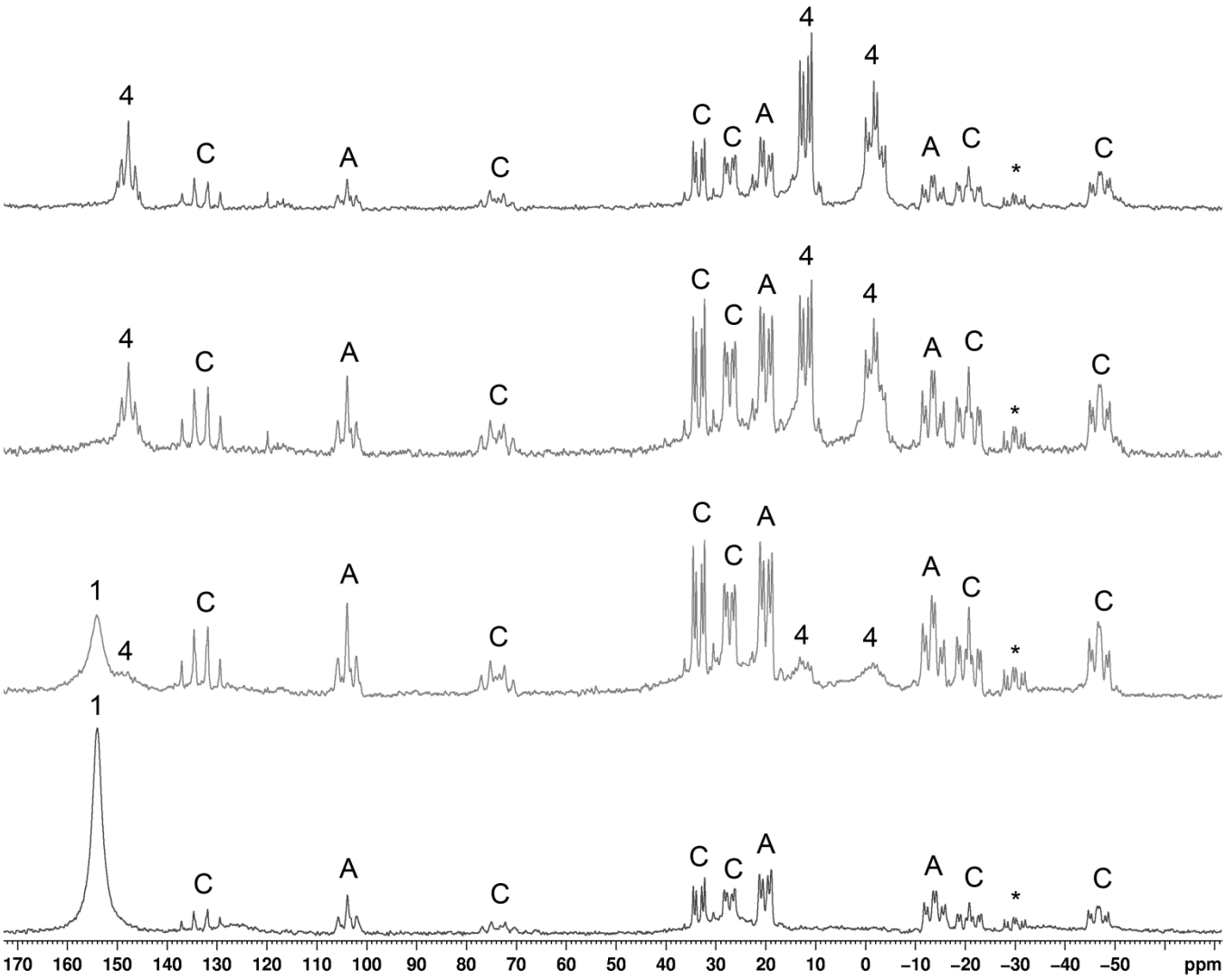

Figure S12. Experimental ^{31}P NMR (161.97 MHz, THF-d_8) spectrum of the reaction of **1** with $NaNH_2$ after 30 minutes (bottom), 3h, 7h and 12h (top).

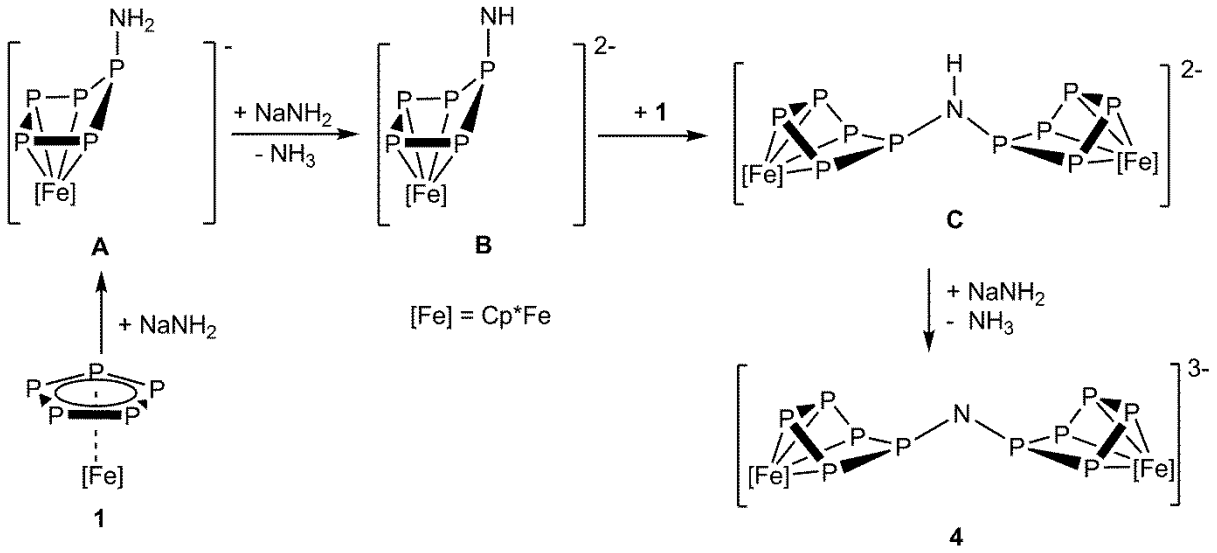

Figure S13. Proposed formation pathway for **4**.

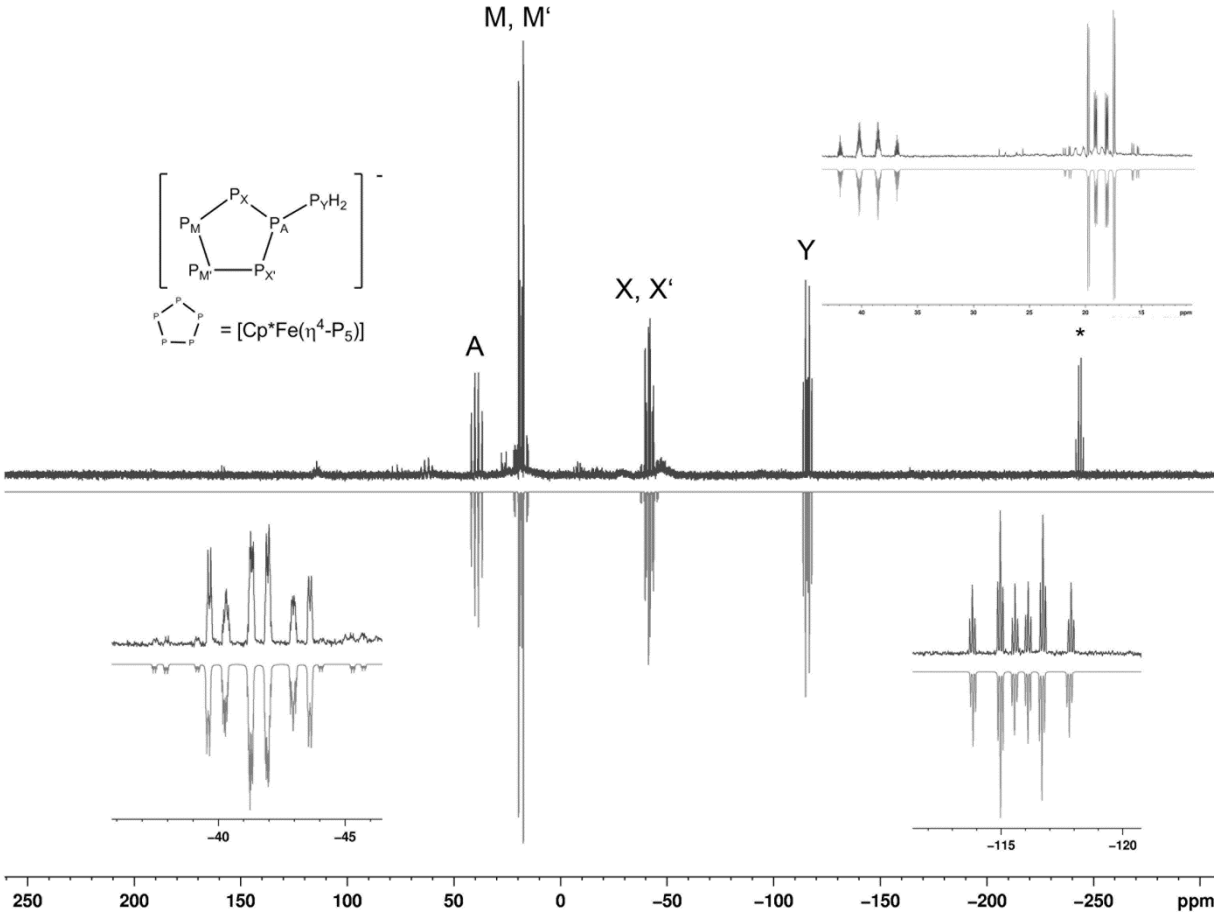

Figure S14. Experimental (top) and simulated (bottom) ^{31}P NMR (161.97 MHz, THF-d_8) spectrum of $[Li(thf)_x][\mathbf{5}]$. * = PH_3

Table S5. ^{31}P NMR chemical shifts and coupling constants of $[Li(thf)_x][\mathbf{5}]$, obtained from the simulation.

	J (Hz)				δ (ppm)
$^1J_{P_A\text{-}P_X} = {}^1J_{P_A\text{-}P_{X'}}$	269.8	$^2J_{P_X\text{-}P_{X'}}$	41.6	A	39.4
$^1J_{P_A\text{-}P_Y}$	282.0	$^3J_{P_M\text{-}P_Y} = {}^3J_{P_{M'}\text{-}P_Y}$	−2.0	M, M’	18.6
$^2J_{P_A\text{-}P_M} = {}^2J_{P_A\text{-}P_{M'}}$	−22.7	$^2J_{P_X\text{-}P_Y} = {}^2J_{P_{X'}\text{-}P_Y}$	−16.9	X, X’	−41.6
$^1J_{P_M\text{-}P_{M'}}$	409.0	$^1J_{P_Y\text{-}H}$	186.2	Y	−115.8
$^1J_{P_X\text{-}P_M} = {}^1J_{P_{X'}\text{-}P_{M'}}$	383.8	$^2J_{P_A\text{-}H}$	10.6		
$^2J_{P_X\text{-}P_{M'}} = {}^2J_{P_{X'}\text{-}P_M}$	−11.4	$^3J_{P_X\text{-}H} = {}^3J_{P_{X'}\text{-}H}$	5.7		

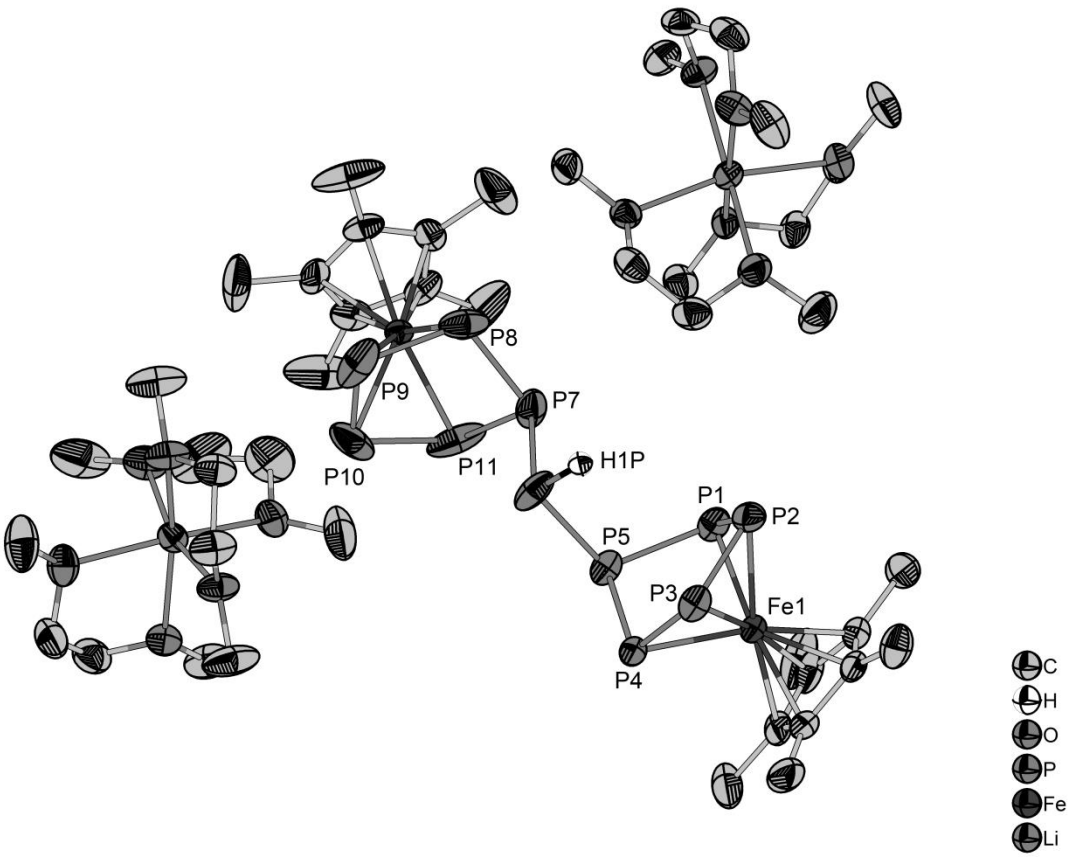

Figure S15. Molecular structure of the compound $[\{Li(dme)_3\}_2][\mathbf{6}]$. All H atoms, except H1P, are omitted for clarity. Selected bond lengths [Å] and angles [°]: P1-P2 2.1537(15), P1-P5 2.1669(14), P2-P3 2.1327(15), P3-P4 2.1467(14), P4-P5 2.1700(13), P5-P6 2.2055(14), P6-H1P 1.38(5), P6-P7 2.2161(15), P7-P8 2.1348(18), P7-P11 2.165(2), P8-P9 2.118(2), P9-P10 2.094(3), P10-P11 2.155(3),

P1-Fe1 2.3172(10), P2-Fe1 2.3325(10), P3-Fe1 2.3289(10), P4-Fe1 2.3248(10), P2-P1-P5 107.57(5), P3-P2-P1 103.63(5), P2-P3-P4 103.83(5), P3-P4-P5 107.77(5), P1-P5-P4 93.29(5), P1-P5-P6 108.94(6), P5-P6-P7 98.10(6).

3.2.3 Details on X-ray structure determinations

The diffraction data were collected on a Gemini R-Ultra or SuperNova CCD diffractometers (Agilent Technologies) with CuK_α radiation (λ = 1.54178Å) using ω scans of 1° frames at 123 K. The structures were solved by direct method with SIR-97 ([Li(thf)$_4$][**3**]),[2] SHELXS[3] ([Li(Et$_2$O)$_2$Li(Et$_2$O)][**2**]$_2$, [Na(dme)$_3${Na(dme)}$_2$][**4**] and [{Li(dme)$_3$}$_2$][**6**]) programs and refined by full-matrix least-squares method against $|F|^2$ in anisotropic approximation using SHELXTL program.[4] Absorption corrections were applied empirically using SCALE3 program implemented to *CrysAlis PRO* Software for [Li(thf)$_4$][**3**] or analytically using a multifaceted crystal model for [Li(Et$_2$O)$_2$Li(Et$_2$O)][**2**]$_2$, [Na(dme)$_3${Na(dme)}$_2$][**4**] and [{Li(dme)$_3$}$_2$][**6**].[5] All non-hydrogen atoms were refined in anisotropic approximation. Hydrogen atoms were refined in calculated positions using riding on pivot atom model.

In case of [Li(thf)$_4$][**3**] a strong tendency to disorder involving almost all atoms (P_5 cycle, THF molecules and Cp* ligands) takes place. We failed to resolve it despite acceptable residuals, and the bond distances and bond angles cannot therefore be trusted. Here we report only atomic connectivity.

The crystal of [Na(dme)$_3${Na(dme)}$_2$][**4**] was measured to give resolution limit of 0.87 Å of because of weak diffraction capability. One of Cp* fragments is disordered over two close positions (re-orientation) with relative weight of 0.55/0.45. SIMU restraints are used to refine minor component in anisotropic approximation.

The crystal of [{Na(dme)$_3$}$_2$][**6**] appeared to be a pseudo-merohedric twin with twin law of (1 0 1, 0 -1 0, 0 0 -1) and ratio of the components refined to 0.713/0.287. The hydrogen atom on the bridging P was localized from electron density map and refined with U_{iso} fixed at 0.05.

CCDC-989571 ([Li(Et$_2$O)$_2$Li(Et$_2$O)][**2**]$_2$), -989572 ([Na(dme)$_3${Na(dme)}$_2$][**4**]), -989573 ([{Li(dme)$_3$}$_2$][**6**]) contain the supplementary crystallographic data for this publication. These data can be obtained free of charge at www.ccdc.cam.ac.uk/conts/retrieving.html (or from the Cambridge Crystallographic Data Centre, 12 Union Road, Cambridge CB2 1EZ, UK; Fax: + 44-1223-336-033; e-mail: deposit@ccdc.cam.ac.uk).

Table S6. Crystal data, data collection parameters and convergence results for $[Li(Et_2O)_2Li(Et_2O)][\mathbf{2}]_2$, $[Li(thf)_4][\mathbf{3}]$.

Compound	$[Li(Et_2O)_2Li(Et_2O)][\mathbf{2}]_2$	$[Li(thf)_4][\mathbf{3}]$
Crystal data		
Chemical formula	$C_{40}H_{82}Fe_2Li_2O_3P_{10}Si_2$	$C_{28}H_{53}FeLiNO_4P_5$
M_r	1102.52	678.31
Crystal system, space group	Orthorhombic, *Pbca*	Orthorhombic, $Pna2_1$
Temperature (K)	123	123
a, *b*, *c* (Å)	18.3762(6), 21.2112(7), 29.8732(10)	17.0520(4), 10.5317(5), 19.6728(4)
β (°)	90	90
V (Å^3)	11644.0 (7)	3533.0(2)
Z	8	4
F(000)	4656	1436
Radiation type	Cu *K*α	Cu *K*α
μ (mm^{-1})	7.24	5.81
Crystal shape, colour	Prism, brown	Rod, red
Crystal size (mm)	0.56 × 0.34 × 0.06	0.47 × 0.03 × 0.03
Data collection		
Diffractometer	Xcalibur, Ruby, Gemini ultra diffractometer	SuperNova, Single source at offset, Atlas diffractometer
Absorption correction	Analytical *CrysAlis PRO*, Oxford Diffraction Ltd., Version 1.171.33.55 (release 05-01-2010 CrysAlis171 .NET) (compiled Jan 5 2010,16:28:46) Analytical numeric absorption correction using a multifaceted crystal model based on expressions derived by R.C. Clark & J.S. Reid.	Multi-scan *CrysAlis PRO*, Agilent Technologies, Version 1.171.34.49 (release 20-01-2011 CrysAlis171 .NET) (compiled Jan 20 2011,15:58:25) Empirical absorption correction using spherical harmonics, implemented in SCALE3 ABSPACK scaling algorithm.
T_{min}, T_{max}	0.147, 0.706	0.475, 1.000
No. of measured, independent and observed [$I > 2\sigma(I)$] reflections	30897, 11409, 8862	7531, 4383, 3824
R_{int}	0.049	0.037
Range of *h*, *k*, *l*	*h* = -22→22, *k* = -26→12, *l* = -37→34	*h* = -20→14, , *k* = -9→12, *l* = -23→14
Refinement		
$R[F^2 > 2\sigma(F^2)]$, $wR(F^2)$, *S*	0.041, 0.106, 0.95	0.068, 0.192, 1.065
No. of reflections	11409	4383
No. of parameters	554	421
No. of restraints	0	31
H-atom treatment	H-atom parameters constrained	H-atom parameters constrained
$\Delta\rangle_{max}$, $\Delta\rangle_{min}$ (e Å^{-3})	0.67, -0.64	0.62, -0.53
Weighting scheme	$w = 1/[\sigma^2(F_o^2) + (0.0700P)^2]$ where $P = (F_o^2 + 2F_c^2)/3$	$w = 1/[\sigma^2(F_o^2) + (0.1328P)^2 + 0.5584P]$, where $P = (F_o^2 + 2F_c^2)/3$
Flack parameter	-	0.004(8)

Table S7. Crystal data, data collection parameters, and convergence results for $[Na(dme)_3\{Na(dme)\}_2]$[**4**] and $[\{Li(dme)_3\}_2]$[**6**].

Compound	$[Na(dme)_3\{Na(dme)\}_2]$[**4**]	$[\{Li(dme)_3\}_2]$[**6**]
Crystal data		
Chemical formula	$C_{40}H_{80}Fe_2NNa_3O_{10}P_{10}$	$C_{44}H_{91}Fe_2Li_2O_{12}P_{11}$
M_r	1225.42	1278.42
Crystal system, space group	Monoclinic, $P2_1/n$	Monoclinic, $P2_1/c$
Temperature (K)	123	123
a, b, c (Å)	13.1865(2), 29.5462(4), 16.0638(2)	26.2355(6), 13.4578(2), 19.9238(4)
β (°)	104.812(2)	112.273(2)
V (Å^3)	6050.66(15)	6509.7(2)
Z	4	4
F(000)	2568	2696
Radiation type	Cu $K\alpha$	Cu $K\alpha$
μ (mm^{-1})	6.95	6.53
Crystal shape, colour	Block, brown	Plate, brown
Crystal size (mm)	0.57 × 0.21 × 0.14	0.2417 × 0.1860 × 0.0332
Data collection		
Diffractometer	Xcalibur, Ruby, Gemini ultra diffractometer	SuperNova, Single source at offset, Atlas diffractometer
Absorption correction	Analytical *CrysAlis PRO*, Agilent Technologies, Version 1.171.36.21 (release 14-08-2012 CrysAlis171 .NET) (compiled Sep 14 2012, 17:21:16) Analytical numeric absorption correction using a multifaceted crystal model based on expressions derived by R.C. Clark & J.S. Reid.	Analytical *CrysAlis PRO*, Agilent Technologies, Version 1.171.36.28 (release 01-02-2013 CrysAlis171 .NET) (compiled Feb 1 2013, 16:14:44) Analytical numeric absorption correction using a multifaceted crystal model based on expressions derived by R.C. Clark & J.S. Reid.
T_{min}, T_{max}	0.150, 0.483	0.932, 0.987
No. of measured, independent and observed [$I > 2\sigma(I)$] reflections	17746, 9484, 8547	61622, 12875, 12014
R_{int}	0.036	0.059
Range of h, k, l	h = -13→14, k = -33→27, l = -18→18	h = -32→31, k = -16→14, l = -24→24
Refinement		
$R[F^2 > 2\sigma(F^2)]$, $wR(F^2)$, S	0.054, 0.144, 1.031	0.049, 0.137, 1.091
No. of reflections	9484	12875
No. of parameters	709	666
No. of restraints	30	0
H-atom treatment	H-atom parameters constrained	H-atom parameters constrained
$\Delta\rangle_{max}$, $\Delta\rangle_{min}$ (e Å^{-3})	1.41, -1.12	1.85, -0.71
Weighting scheme	$w = 1/[\sigma^2(F_o^2) + (0.0796P)^2 + 5.5396P]$, where $P = (F_o^2 + 2F_c^2)/3$	$w = 1/[\sigma^2(F_o^2) + (0.1000P)^2 + 0.7538P]$, where $P = (F_o^2 + 2F_c^2)/3$
Flack parameter	-	-

3.2.4 Details on DFT calculations

All calculations were carried out using the TURBOMOLE program package package.[6] The geometries were optimized using the RI-[7]BP86[8] functional together with the def2-TZVP[9] basis set for Fe, P, and N atoms and def2-SV(P) basis sets for C and H atoms. For the geometry optimizations the Multipole Accelerated Resolution of Identity (MARI-J)[10] approximation was used. Through the geometry optimization steps, the solvent effects have been incorporated according to the COSMO[11] formalism as implemented in TURBOMOLE using the dielectric constant of THF (ε = 7.25). The final energy of the molecules has been determined by single point calculations without using the RI formalism. For the calculations of the relative energies of different transformations the values of the total energy (SCF energy) plus the energy for the outlying charge correction (OC) has been used.

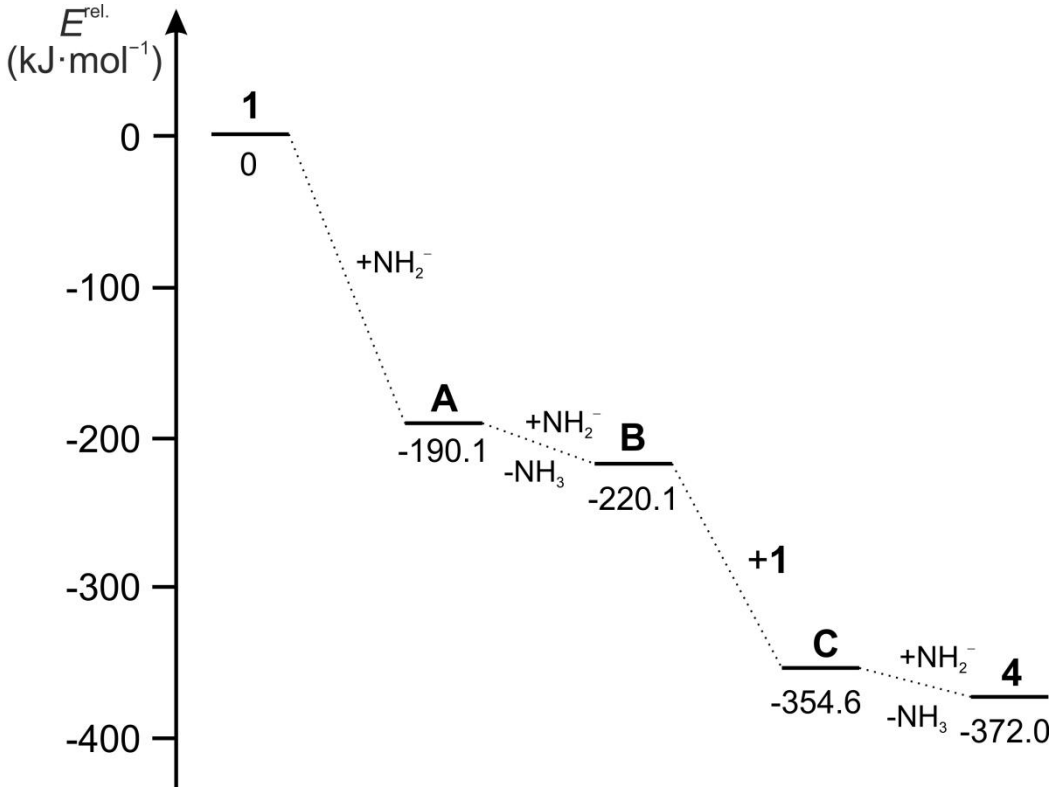

Figure S16. Energy profile of the reaction of [Cp*Fe(η^5-P_5)] with NH_2^-.

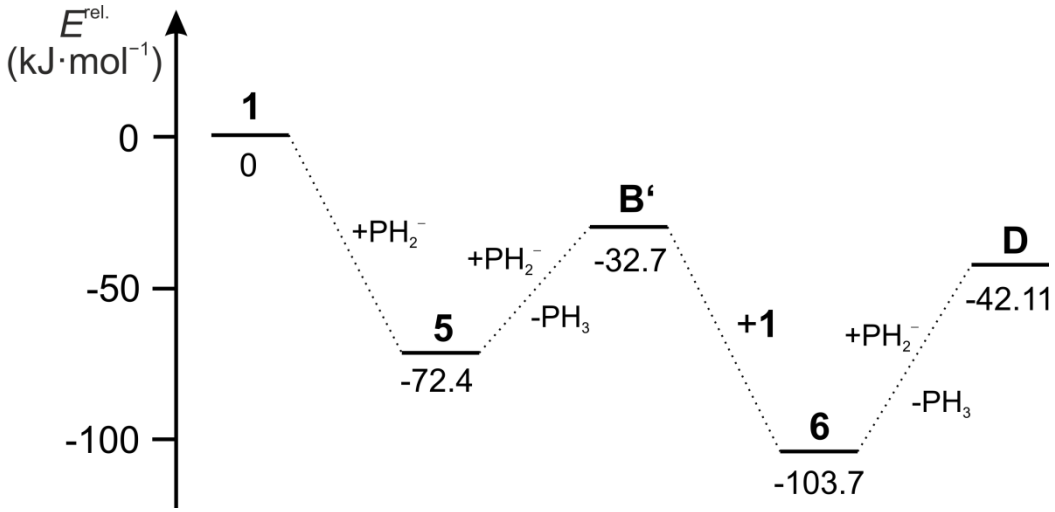

Figure S17. Energy profile of the reaction of [Cp*Fe(η^5-P_5)] with PH_2^-.

Table S8. Calculated reaction enthalpies at the BP86/def2-SV(P) (for C and H) and def2-TZVP (for P, N, Fe) level of theory.

Transformation	Rel. Energie (kJ·mol^{-1})
[Cp*Fe(η^5-P_5)] + NH_2^- = [Cp*Fe(η^4-P_5)NH_2]$^-$	−190,14
[Cp*Fe(η^4-P_5NH_2)]$^-$ + NH_2^- = [Cp*Fe(η^4-P_5)NH]$^{2-}$ + NH_3	−29,97
[Cp*Fe(η^4-P_5NH)]$^{2-}$ + [Cp*Fe(η^5-P_5)] = [{Cp*Fe(η^4-P_5)}$_2$NH]$^{2-}$	−134,53
[{Cp*Fe(η^4-P_5)}$_2$NH]$^{2-}$ + NH_2^- = [{Cp*Fe(η^4-P_5)}$_2$N]$^{3-}$ + NH_3	−17,39
2 [Cp*Fe(η^5-P_5)] + 3 NH_2^- = [{Cp*Fe(η^4-P_5)}$_2$N]$^{3-}$ + 2 NH_3	−372,03
2 [Cp*Fe(η^4-P_5NH_2)]$^-$ = [(Cp*Fe)$_2$(μ,$\eta^{4:4}$-P_{10})]$^{2-}$ + H_2NNH_2	528,69
2 [Cp*Fe(η^4-P_5NH_2)]$^-$ = [{Cp*Fe(η^4-P_5)}$_2$NH]$^{2-}$ + NH_3	25,64

Table S9. Calculated reaction enthalpies at the BP86/def2-SV(P) (for C and H) and def2-TZVP (for P, N, Fe) level of theory.

Transformation	Rel. Energie (kJ·mol^{-1})
[Cp*Fe(η^5-P_5)] + PH_2^- = [Cp*Fe(η^4-P_5)PH_2]$^-$	−72,43
[Cp*Fe(η^4-P_5PH_2)]$^-$ + PH_2^- = [Cp*Fe(η^4-P_5)PH]$^{2-}$ + PH_3	39,74
[Cp*Fe(η^4-P_5PH)]$^{2-}$ + [Cp*Fe(η^5-P_5)] = [(Cp*Fe)$_2$(μ,$\eta^{4:4}$-$P_{11}H$)]$^{2-}$	−71,01
[(Cp*Fe)$_2$(μ,$\eta^{4:4}$-$P_{11}H$)]$^{2-}$ + PH_2^- = [(Cp*Fe)$_2$(μ,$\eta^{4:4}$-P_{11})]$^{3-}$ + PH_3	61,60
2 [Cp*Fe(η^5-P_5)] + 3 PH_2^- = [(Cp*Fe)$_2$(μ,$\eta^{4:4}$-P_{11})]$^{3-}$ + 2 PH_3	−42,11
2 [Cp*Fe(η^4-P_5PH_2)]$^-$ = [(Cp*Fe)$_2$(μ,$\eta^{4:4}$-P_{10})]$^{2-}$ + H_2PPH_2	62,05
2 [Cp*Fe(η^4-P_5PH_2)]$^-$ = [(Cp*Fe)$_2$(μ,$\eta^{4:4}$-$P_{11}H$)]$^{2-}$ + PH_3	41,15

Tables regarding the cartesian coordinates of all performed calculations can be found on the DVD-Rom, which is attached in the back of this work.

3.2.5 References

[1] O. J. Scherer, T. Brück, *Angew. Chem. Int. Ed. Engl.* **1987**, *26*, 59-59.

[2] A. Altomare, M. C. Burla, M. Camalli, G. L. Cascarano, C. Giacovazzo, A. Guagliardi, A. G. G. Moliterni, G. Polidori and R. Spagna. *J. Appl. Cryst.* **1999**, *32*, 115-119.

[3] Bruker, SHELXTL. Version 6.22. **2003** Bruker AXS Inc. Madison, WI, USA.

[4] Bruker, SHELXTL. Version 6.22. **2003** Bruker AXS Inc. Madison, WI, USA.

[5] Clark, R. C. & Reid, *J. S. Acta Cryst* **1995**, *A51*, 887-897.

[6] a) R. Ahlrichs, M. Bär, M. Häser, H. Horn, C. Kölmel, *Chem. Phys. Lett.***1989**, *162*, 165–169; b) O. Treutler, R. Ahlrichs, *J. Chem. Phys.***1995**, *102*, 346–354.

[7] a) K. Eichkorn, O. Treutler, H. Oehm, M. Häser, R. Ahlrichs, *Chem. Phys. Lett.***1995**, *242*, 652–660; b) K. Eichkorn, F. Weigend, O. Treutler, R. Ahlrichs, *Theor. Chem. Acc.***1997**, *97*, 119.

[8] a) P. A. M. Dirac, *Proc. Royal Soc. A*, **1929**, *123*, 714-733. b) J. C. Slater, *Phys. Rev.***1951**, *81*, 385-390. c) S. H. Vosko, L. Wilk, M. Nusair, *Can. J. Phys.* **1980**, *58*, 1200-1211. d). A. D. Becke, *Phys. Rev. A*, **1988**, *38*, 3098. e) J. P. Perdew, *Phys. Rev. B* **1986**, *33*, 8822-8824.

[9] a) A. Schäfer, C. Huber, R. Ahlrichs, *J. Chem. Phys.* **1994**, *100*, 5829; b) K. Eichkorn, F. Weigend, O. Treutler, R. Ahlrichs, *Theor. Chem. Acc.***1997**, *97*, 119.

[10] M. Sierka, A. Hogekamp, R. Ahlrichs, *J. Chem. Phys.***2003**, *118*, 9136.

[11] A. Klamt, G. Schüürmann*J. Chem. Soc. Perkin Trans. 2*, **1993**, 799–805.

3.3 Reaction of [Cp*Fe(η^5-P_5)] with LiNH*t*Bu

The following chapter should be neglected for the publication of the previous chapter titled "Functionalization of a cyclo-P_5 ligand by main group nucleophiles". Therefore, this chapter is excluded and added at the end of the previous one.

The previous chapter revealed the formation of the trianionic complex [{Cp*Fe(η^4-P_5)}$_2$N]$^{3-}$ (**4**) in the reaction of **1** with $NaNH_2$, in which two pentaphosphaferrocene moieties are bridged by one nitrogen atom. The reaction pathway in this reaction is described by an autometalation process. The question arises, whether similar dianionic compounds of the type [{Cp*Fe(η^4-P_5)}$_2$NR]$^{2-}$ can be synthesized in an analog reaction, if one proton of the $NaNH_2$ is exchanged by an organic group. Therefore, the reaction of pentaphosphaferrocene with LiNH*t*Bu was performed. However, this reaction leads exclusively to the anionic complex [Cp*Fe(η^4-P_5NH*t*Bu)]$^-$ (**7**) and the formation of [{Cp*Fe(η^4-P_5)}$_2$N*t*Bu]$^{2-}$ was not observed (Scheme 3). In the ^{31}P NMR spectrum of the isolated compound **7** an AMM´XX´ spin system is monitored, with three signals centered at −17.2, 13.0 and 99.8 ppm. The heavy atom framework of [Li(thf)$_4$thf][**7**] was determined by X-ray structure analysis and shows a structural motif similar to the previously discussed compounds [Cp*Fe(η^4-$P_5CH_2SiMe_3$)]$^-$ (**2**) and [Cp*Fe(η^4-P_5NMe_2)] (**3**), exhibiting and enveloped η^4-P_5 ring.

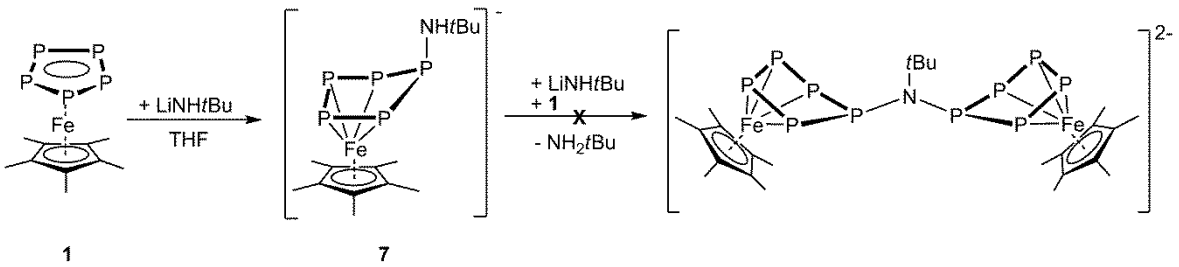

Scheme 3. Reactivity of **1** towards LiNH*t*Bu.

Further reactions were performed in order to remove the proton of **2** and to yield the dianionic compound [Cp*Fe(η^4-P_5N*t*Bu)]$^{2-}$. However, after the addition of LDA or DBU to **7** no reaction is observed in the ^{31}P NMR spectrum. By adding KH to **7** a decomposition occurs, forming the anionic complex [(Cp*Fe)$_2$($\eta^{4:4}$-P_{10})]$^{2-}$, which is usually obtained in the reduction of **1** by KH.[1] The addition of the N-heterocyclic carbene 1,3-bis-(2,6-diisoproylphenyl)imidazole-2-ylidene to **7** leads again to a

decomposition, yielding unidentifiable products. Therefore it has to be stated, if one proton from $NaNH_2$ is replaced by an organic group no autometallation process is observed anymore and compounds of the type $[\{Cp^*Fe(\eta^4\text{-}P_5)\}_2NR]^{2-}$ cannot be obtained this way.

References:

[1] M. V. Butovskiy, G. Balázs, M. Bodensteiner, E. V. Peresypkina, A. V. Virovets, J. Sutter, M. Scheer, *Angew. Chem. Int. Ed.* **2013**, *52*, 2972-2976.

Experimental Part

Synthesis of [Li(thf)$_4$thf][Cp*Fe(η^4-P$_5$)NH*t*Bu]: 0.1 g (0.3 mmol) of **1** are solved in THF at room temperature and 23 mg (0.3 mmol) of LiNH*t*Bu in THF are slowly added. An immediate color change to brown is observed. The solution is stirred for 3 days, the solvent reduced (10 mL) and layered with *n*-hexane (30 mL). The solution is stored at 4 °C and 59 mg (38%) of crystalline [Li(thf)$_4$thf][Cp*Fe(η^4-P$_5$)NH*t*Bu] is isolated. $C_{20}H_{37}FeLiNO_{1.5}P_5$ (533.10): calcd. C 45.05, H 6.99, N 2.63; found C 45.39, H 8.81, N 2.45. ^{1}H NMR (400.13 MHz, C_6D_6): δ [ppm] = −0.05 (q, 1H, NH), 0.83 (s, 9H, *t*Bu), 1.45 (s, 15H, Cp*). $^{13}C\{^1H\}$ NMR (100.62 MHz, C_6D_6): δ = 11.95 (s, $C_5(CH_3)_5$), 32.91 (s, $C(CH_3)_3$), 51.70 (s, $C(CH_3)_3$), 85.29 (s, $C_5(CH_3)_5$). ^{31}P NMR (161.97 MHz, C_6D_6): δ = −17.19 (m, 2P, P_5), 12.99 (m, 2P, P_5), 99.82 (tt, 1P, P_5).

Due to the insufficient quality of the single crystal X-ray measurement only the heavy atom framework of **7** was determined and therefore only the cell parameters for [Li(thf)$_4$thf][Cp*Fe(η^4-P$_5$)NH*t*Bu] are given below.

Table 1. Cell parameters of [Li(thf)$_4$thf][**7**].

Chemical formula	$C_{124}H_{228}Fe_4Li_4N_4O_{18}P_{20}$
Formula weight	2933.65
Temperature/K	123(2)
Crystal system	orthorhombic
Space group	*Pnma*
a/Å	24.006(2)
b/Å	11.0863(13)
c/Å	16.4089(15)
α/°	90
β/°	90
γ/°	90
Volume/Å^3	4367.0(8)
Z	1

4. Subsequent functionalization of the *cyclo*-P_5 ligand in [Cp*Fe(η^5-P_5)]

Eric Mädl, Gábor Balázs, Eugenia Peresypkina and Manfred Scheer*

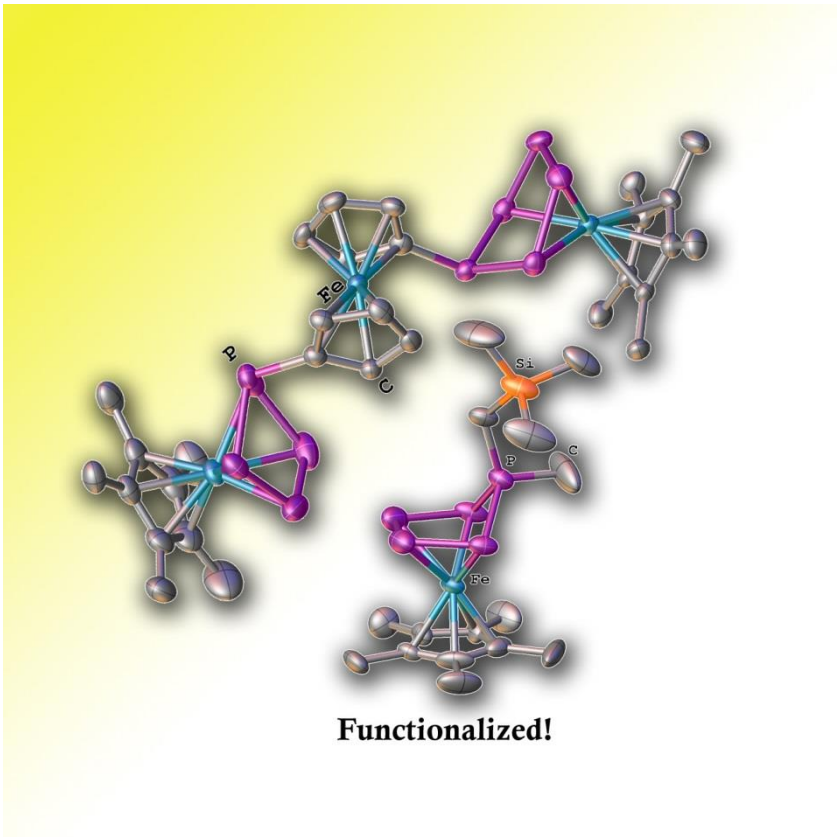

- All compounds were synthesized by Eric Mädl.
- The chapter "discussion" was written by Eric Mädl, except for parts regarding calculations, which were written by Gabor Balázs. Details about X-ray structure analyses in the chapter "supporting information" were written by Eugenia V. Peresypkina.
- DFT calculations were performed by Gabor Balázs. X-ray structure analyses and refinements were performed by Eric Mädl and Eugenia V. Peresypkina.
- Figures in the chapter "discussion" were made by Eric Mädl. Figures in the chapter "supporting information" regarding X-ray structure analyses were made by Eugenia V. Peresypkina.

4.1 Discussion

Abstract: *The reactions of [Cp*Fe(η^4-P_5R)]$^-$ (**1a**: R = CH_2SiMe_3; **1b**: R = NMe_2) with MeI yield the neutral compounds [Cp*Fe(η^4-$P_5MeCH_2SiMe_3$)] (**2a**) and [Cp*Fe(η^4-P_5MeNMe_2)] (**2b**), respectively. [Cp*Fe(η^5-P_5)] (**I**) was reacted with MeLi, giving [Cp*Fe(η^4-P_5Me)]$^-$ (**3**). Reactivity studies on the reduced pentaphosphaferrocene derivative [(Cp*Fe)$_2$(μ,$\eta^{4:4}$-P_{10})]$^{2-}$ (**II**) towards salt elimination were performed, yielding the dimethylated compound [Cp*Fe(η^4-P_5Me_2)] (**4**). Compound [{Cp*Fe(η^4-P_5)}$_2$$Cp_2Fe$]$^{2-}$ (**5**) was synthesized by reacting **I** with [Li_2(TMEDA)][Cp_2Fe]. Compounds **2a**, **2b**, Li[**3**], Li_2[**5**] were completely characterized by NMR spectroscopy and X-ray structure analysis.*

Due to the stability and the property of ferrocene to be functionalized multiple times by metalation, a large variety of ferrocene containing compounds are accessible.[1] The isolobal analog of ferrocene, pentaphosphaferrocene [Cp*Fe(η^5-P_5)] (**I**), was discovered by the Scherer group.[2] Although both molecules show similar structural motifs, ferrocene and pentaphosphaferrocene exhibit a different reactivity, due to the lone pairs located on the phosphorus atoms in **I**. Hence, pentaphosphaferrocene is essentially used in coordination chemistry, to give with transition metals access to polymers or even molecular spherical aggregates.[3] Compared to ferrocene, which is known for its reversible oxidation, **I** exhibits a more diverse redox chemistry.[4] Recently, the postulated oxidation and reduction products [(Cp*Fe)$_2$(μ,$\eta^{5:5}$-P_{10})]$^{2+}$ and [(Cp*Fe)$_2$(μ,$\eta^{4:4}$-P_{10})]$^{2-}$ (**II**) were synthesized, exhibiting a P_{10} ligand.[5] In addition, the strongly reduced compound [Cp*Fe(η^4-P_5)]$^{2-}$ was isolated. Furthermore, the reactivity of pentaphosphaferrocene towards nucleophiles was discovered and therefore a functionalization of the *cyclo*-P_5 ring was achieved, to give anionic compounds of the type [Cp*Fe(η^4-P_5R)]$^-$ (**1a**: R = NMe_2, **1b**: R = CH_2SiMe_3), containing an enveloped *cyclo*-P_5 ring.[6] However, the reactivity of **I** towards dianionic nucleophiles has to be investigated yet. It was of interest − as a next step in the transformation to organophosphorus ligands − to determine, whether **1a**/**1b** or **II** show any reactivity towards organic electrophiles, on which phosphorus atom of the *cyclo*-P_5 ring the substitution might occur and whether the P_{10} ligand in **II** will stay intact. Herein we report on the reactivity of **1a**/**1b** and **II** towards MeI and the reaction of **I** with the dianionic nucleophile [Li_2(TMEDA)][Cp_2Fe].

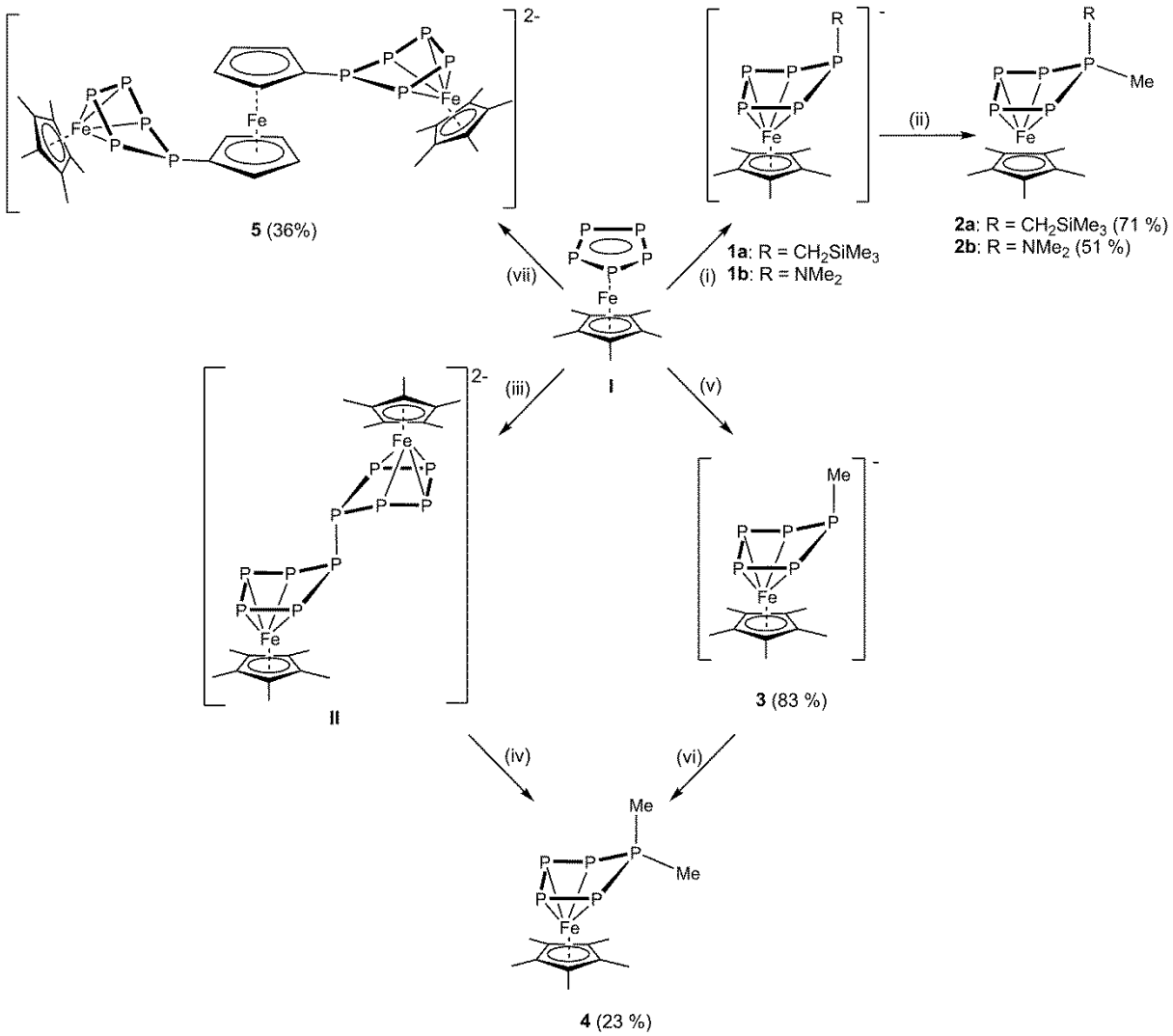

Scheme 1. Reaction of **I**: (i) $LiCH_2SiMe_3$ or $LiNMe_2$ in THF, r.t.; (iii) KH in DME, r.t.; (v) MeLi in DME, −60 °C → r.t.; (vii) $[Li_2(TMEDA)][Cp_2Fe]$ in DME, r.t.; reaction of **1a**/**1b**: (ii) MeI in THF, r.t.; reaction of **II**: (iv) 2 eq. MeI in DME, r.t.; reaction of **3**: (vi) MeI in DME, r.t.; yields are given in parenthesis.

If **1a**/**1b** is dissolved in THF and an equimolar amount of MeI is added a color change from brown to dark greenish is observed, accompanied by the formation of LiI. Compounds **2a**/**2b** are obtained in good crystalline yields from *n*-hexane (Scheme 1). Besides small amounts of **I** (< 5 %) the raw reaction solution shows the exclusive formation of **2a**/**2b**, as proven by ^{31}P NMR spectroscopy. The ^{31}P NMR spectra of the isolated compounds **2a** and **2b** show an AMM'XX' spin-system, with resonances centered at 132.9, 36.8 and −65.14 ppm and at 129.4, 37.0 and −97.8 ppm, respectively. Single crystal measurements of **2a** and **2b** reveal an envelope-like P_5 ring, similar to their starting materials **1a**/**1b** (Figure 1). All P-P bonds exhibit double bond character with a slightly longer average bond length in **2b** (average P-P bond length in **2a**: 2.1322 Å; in **2b**: 2.1414 Å), due to the donating effect of the NMe_2 group.

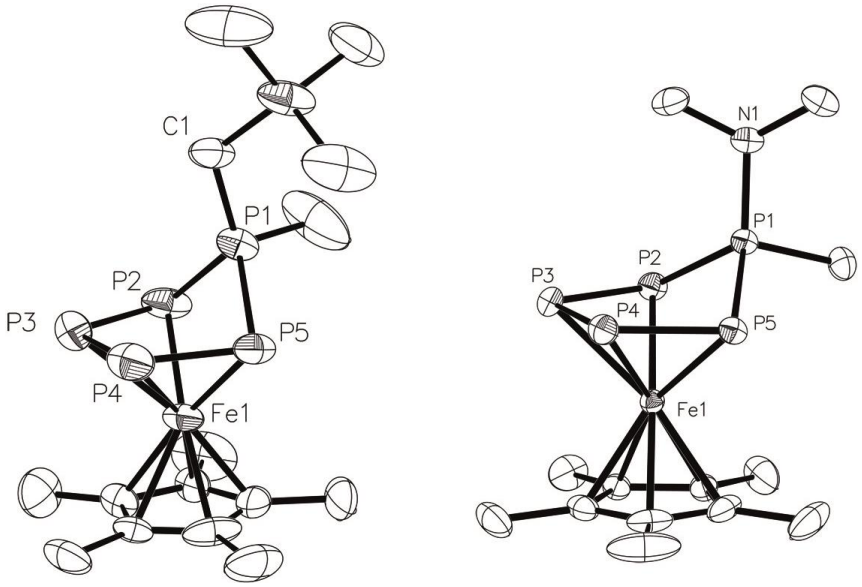

Figure 1. Molecular structure of **2a** (left) and **2b** (right). Ellipsoids are drawn at 50% probability level. H atoms bonded to carbon are omitted for clarity.

The methylated compounds exhibit a four times substituted phosphorus atom (P1). The phosphonium character of the P1 atom is reflected by the deep field shift of the corresponding ^{31}P NMR signal of about 53 ppm compared to **1a**. However, the P1-P5 and P1-P2 bonds both exhibit double bond character (Table 1). Natural Population Analysis (NPA) underlines the phosphonium character with a value of 0.89 for the P1 atom in **2a**. The other phosphorus atoms of the *cyclo*-P_5 ring exhibit values between −0.03 and −0.09. The value for iron atom is slightly negative (−0.26). In **2a**/**2b** the enveloped conformation is very distinct and therefore only a small interaction between the P1 atom the iron atom is suggested. The corresponding Wiberg bond index (WBI) of the P1-Fe1 bond amounts to 0.16, in contrast to the other phosphorus iron bonds with values between 0.52 and 0.64. Similar studies of the compound [Cp*Fe(η^5-P_3C_2tBu$_2$)], exhibiting a triphospholyl ligand, are reported.[7] Furthermore, for phosphacymantrenes or iron sandwich complexes an analog structural motif is known, featuring an enveloped five-membered monophospholyl ring that exhibits phosphonium character.[8]

Table 1. P-P bond lengths of the complexes **2a**, **2b**, **3** and **5**.

	P1-P2 (Å)	P1-P5 (Å)	P2-P3 (Å)	P3-P4 (Å)	P4-P5 (Å)
2a:	2.084(5)	2.165(3)	2.135(4)	2.143(4)	2.133(4)
2b:	2.1347(5)	2.1426(5)	2.1342(5)	2.1519(6)	2.1360(5)
3:	2.158(1)	2.1490(1)	2.1462(2)	2.118(2)	2.135(1)
5:	2.152(2)	2.170(2)	2.150(2)	2.126(2)	2.150(2)

If *t*BuCl is added to **1a** no reaction occurs, as proven by ^{31}P NMR spectroscopy. However, if a sterically less demanding organohalide, such as 2-iodopropane, is used, the ^{31}P NMR spectrum of the reaction mixture shows the formation of one main product with three multiplets centered at 154.8, 36.8 and −112.9 ppm, similar to **2a**. In contrast to the previously described clean methylation, the formation of [Cp*Fe(η^4-P_5(C_3H_7)CH_2SiMe_3)] (**2c**) is accompanied by a considerable amount of byproducts. Although **2c** could not be isolated as analytically pure compound, its formation could be determined by means of FD mass, with a peak at m/z = 467.06 (M^+, 100%).

To investigate if the *cyclo*-P_5 ring in **2a** can be functionalized even further, the reaction of **2a** with another equivalent of $LiCH_2SiMe_3$ was performed. In the ^{31}P NMR spectrum of this raw reaction mixture a new product, with three multiplets centered at 121.0, 28.1 and −122.9 ppm is determined in about 30% yield. However, the other 70% belong to unconsumed starting material **2a**. In the FD mass spectrum the molecule ion peak for **2a** at m/z = 448.1 (100 %), and a molecule ion peak at m/z = 520.1 (30 %) is detected. The latter indicates that the methyl group of **2a** has been displaced by another trismethylsilylmethanyl group during the reaction.

In addition, by reacting **I** with MeLi − yielding the compound [Cp*Fe(η^4-P_5Me)]$^-$ (**3**) − followed by a subsequent reaction with MeI, the dimethylated compound [Cp*Fe(η^4-P_5Me_2)] (**4**) was isolated. For the isolated compound **3** a triplet of triplets centered at 71.3 ppm and two multiplets centered at 13.7 and −71.5 ppm are determined in the ^{31}P NMR spectrum (Figure 2). The formation of **4** is accompanied by a small amount of unknown byproducts and **4** shows three multiplets centered at 117.4, 35.2 and −122.3 ppm in the ^{31}P NMR spectrum. In analogy to **2a**/**2b**, the disubstituted phosphorus atom in **4** is deep field shifted by about 46 ppm, in comparison to **3**. The structural motif of **3**, which could be determined by means of X-ray structure analysis, is similar to the starting materials **1a**/**1b** (Figure 3).[6] As expected, the *cyclo*-P_5 ring in **3** exhibits an enveloped conformation, with the methyl group occupying the *endo*-position and P-P bond lengths between 2.118(2) − 2.170(2) Å. **4** could not be crystallized so far, but in the FD mass the ion peak for **4** at m/z = 376.1 (MH^+, 60%; MH^+ − P, 100%) was detected.

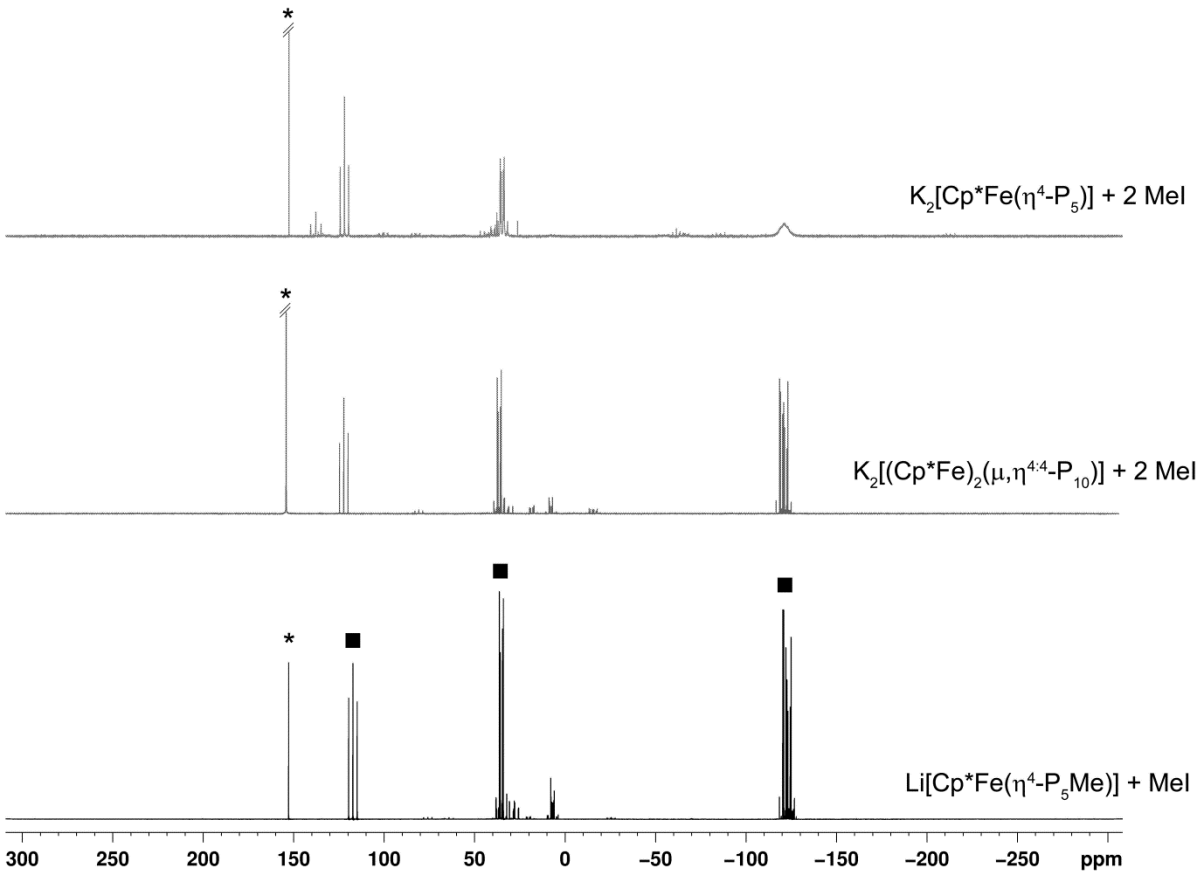

Figure 2. ^{31}P NMR (161.97 MHz, C_6D_6) spectra of the formation of the dimethylated, neutral compound [Cp*Fe(η^4-P_5Me_2)] (**4**) (marked with ■) by different reactions. Impurities of **I** are marked with *.

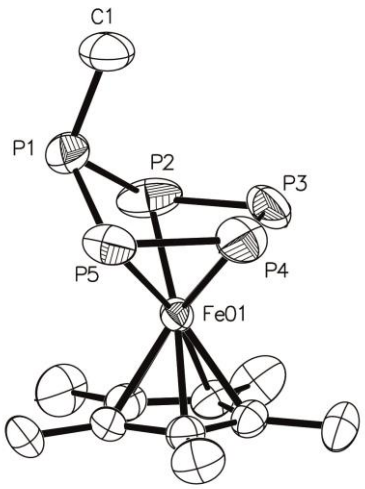

Figure 3. Molecular structure of the anionic part of [Li(dme)$_3$][**3**]. Ellipsoids are drawn at 50% probability level. H atoms bonded to carbon are omitted for clarity.

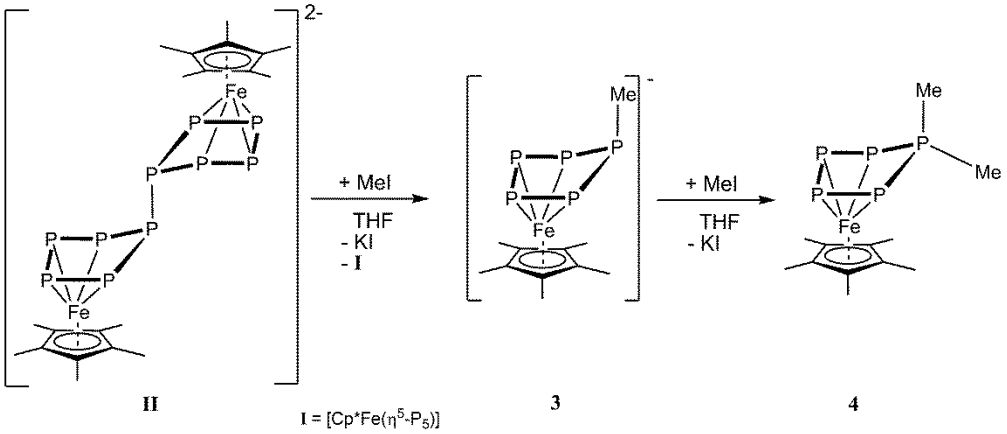

Scheme 2. Reaction pathway of the reaction of K_2[**II**] with MeI.

It was of interest, whether the anion $[(Cp^*Fe)_2(\mu,\eta^{4:4}\text{-}P_{10})]^{2-}$ (**II**) shows a reactivity analog to the synthesis of **2a**/**2b** and **4**. In particular, whether the P_{10} ligand will stay intact during reactions with organohalides. Therefore, **II** was reacted with two equivalents of MeI, leading to the dimethylated compound [Cp*Fe(η^4-P_5Me_2)] (**4**) (*vide supra*, Scheme 2). Besides the signals for **4** in about 28 % yield, the ^{31}P NMR spectrum of the reaction mixture shows the formation of **I** in about 72% yield. Only small impurities are monitored (Figure 2). The formation of such a large amount of pentaphosphaferrocene suggests a heterolytic bond cleavage of the P-P bond in **II**, which connects the two [Cp*Fe(η^4-P_5)] moieties.

Besides the functionalization of anionic pentaphosphaferrocene derivatives as discussed above, the first step to yield those anionic derivatives by nucleophilic addition has been discovered just recently. So far, only mono anionic nucleophiles were used in the reactions with pentaphosphaferrocene. By reacting **I** with $NaNH_2$ two pentaphosphaferrocene units are linked by one nitrogen atom, forming the trianionic compound $[\{Cp^*Fe(\eta^4\text{-}P_5)\}_2N]^{3-}$ due to an autometalation process.[6] To link two pentaphosphaferrocene moieties, without relying on autometalation processes, **I** is reacted with a dianionic nucleophile. For this purpose the dilithiated ferrocene $[Li_2(TMEDA)][Cp_2Fe]$ (TMEDA = tetramethyletylenediamine) was chosen. In $[Li_2(TMEDA)][Cp_2Fe]$ the negative charges are separated far enough from each other to leave sufficient space to connect two pentaphosphaferrocene moieties. In addition, the resulting compound is expected to exhibit interesting electro chemical properties, due to the bridging ferrocene unit. After adding $[Li_2(TMEDA)][Cp_2Fe]$ to two equivalents of **I** an immediate color change to brown is observed. After three days of stirring the ^{31}P NMR spectrum shows the exclusive formation of one product, with a triplet of triplets centered at 69.7 ppm and two multiplets centered at 18.7 ppm and −48.7. X-ray structure analysis reveals that two pentaphosphaferrocenes were coupled successfully by the dianionic nucleophile in $[\{Cp^*Fe(\eta^4\text{-}P_5)\}_2Cp_2Fe]^{2-}$ (**5**, Figure 4).

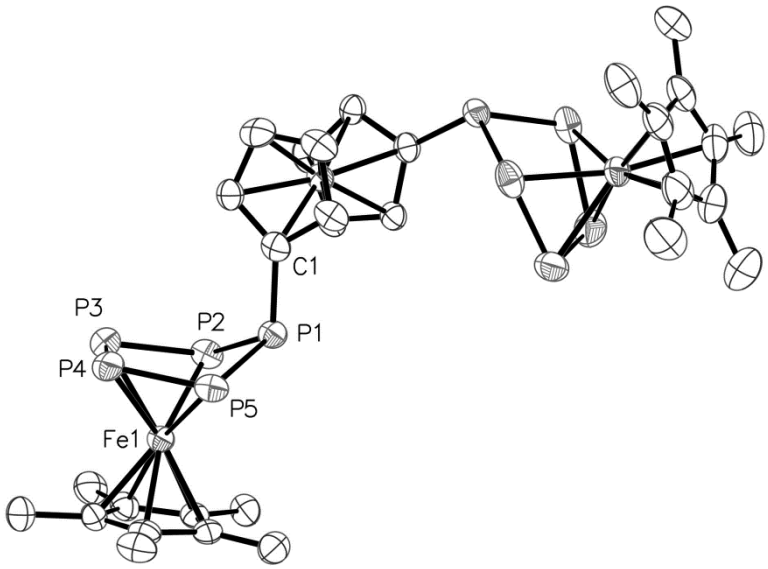

Figure 4. Molecular structure of the anionic part of $[Li(dme)_3]_2$[**5**]. Ellipsoids are drawn at 50% probability level. H atoms bond to carbon are omitted for clarity.

Contrary to the initial expectation, the cyclic voltammogram of **5** does not show a reversible oxidation, due to the ferrocene moiety. Instead two irreversible oxidations are observed at −0.93 V and at 0.11 V and one irreversible reduction at −2.2 V is recorded.[9] 1,1′-dibromoferrcocene was added to **5** to determine if another ferrocene unit can be added to the *cyclo*-P_5 ring. Unfortunately, the ^{31}P NMR spectrum proofs that no reaction occurs, which can be attributed to the steric demand of the second ferrocene unit.

In conclusion, the reported reactivity of the anionic pentaphosphaferrocene derivatives towards organic halides gives access to novel compounds [Cp*Fe(η^4-$P_5MeCH_2SiMe_3$)] (**2a**) and [Cp*Fe(η^4-P_5MeNMe_2)] (**2b**), featuring twofold functionalized *cyclo*-P_5 ligands. In regards to supramolecular chemistry these neutral compounds are intriguing new building blocks, which should lead to the formation of unprecedented scaffolds. If $K_2[(Cp^*Fe)_2(\mu,\eta^{4:4}\text{-}P_{10})]$ is reacted with MeI the P_{10} ligand is cleaved and the bisfunctionalized pentaphosphaferrocene derivative [Cp*Fe(η^4-P_5Me_2)] (**4**) is formed. This reactivity gives access to the synthesis of twofold functionalized pentaphosphaferrocene derivatives, without the prior use of nucleophiles. Furthermore, by reacting a dianionic nucleophile with [Cp*Fe(η^5-P_5)] (**I**) two P_5 units are connected successfully by a ferrocene unit, which should be considered as a discovery for synthesizing a broad range of chelate ligands, containing pentaphosphaferrocene moieties.

References:

[1] a) R. B. Woodward, M. Rosenblum, M. C. Whiting, *J. Am. Chem. Soc.* **1952**, *74*, 3458; b) R. A. Benkeser, D. Goggin, G. Schroll, *J. Am. Chem. Soc.* **1954**, *76*, 4025; c) F. Rebiere, O. Samuel, H. B. Kagan, *Tetrahedron Lett.* **1990**, *31*, 3121-3124; d) M. Rausch, M. Vogel, H. Rosenberg, *J. Org. Chem.* **1957**, *22*, 900-903.

[2] O. J. Scherer, T. Brück, *Angew. Chem. Int. Ed.* **1987**, *26*, 59-59.

[3] a) F. Dielmann, M. Fleischmann, C. Heindl, E. V. Peresypkina, A. V. Virovets, R. M. Gschwind, M. Scheer, *Chem. Eur. J.* **2015**, *21*, 6208-6214; b) F. Dielmann, C. Heindl, F. Hastreiter, E. V. Peresypkina, A. V. Virovets, R. M. Gschwind, M. Scheer, *Angew. Chem. Int. Ed.* **2014**, *53*, 13605-13608; c) M. Fleischmann, S. Welsch, H. Krauss, M. Schmidt, M. Bodensteiner, E. V. Peresypkina, M. Sierka, C. Gröger, M. Scheer, *Chem. Eur. J.* **2014**, *20*, 3759-3768; d) S. Welsch, L. J. Gregoriades, M. Sierka, M. Zabel, A. V. Virovets, M. Scheer, *Angew. Chem. Int. Ed.* **2007**, *46*, 9323-9326; e) F. Dielmann, A. Schindler, S. Scheuermayer, J. Bai, R. Merkle, M. Zabel, A. V. Virovets, E. V. Peresypkina, G. Brunklaus , H. Eckert, M. Scheer, *Chem. Eur. J.* **2012**, *18*, 1168-1179; f) J. Bai, A. V. Virovets, M. Scheer, *Angew. Chem. Int. Ed.* **2002**, *41*, 1737-1740.

[4] R. F. Winter, W. E. Geiger, *Organometallics* **1999**, *18*, 1827-1833.

[5] M. V. Butovskiy, G. Balázs, M. Bodensteiner, E. V. Peresypkina, A. V. Virovets, J. Sutter, M. Scheer, *Angew. Chem. Int. Ed.* **2013**, *52*, 2972-2976.

[6] E. Mädl, M. V. Butovskii, G. Balázs, E. V. Peresypkina, A. V. Virovets, M. Seidl, M. Scheer, *Angew. Chem. Int. Ed.* **2014**, *53*, 7643-7646.

[7] M. M. Al-Ktaifani, P. B. Hitchcock, J. F. Nixon, *J. Organomet. Chem.* **2008**, *693*, 611-618.

[8] a) B. Deschamps, P. Toullec, L. Ricard, F. Mathey, *J. Organomet. Chem.* **2001**, *634*, 131-135; b) B. Deschamps, J. Fischer, F. Mathey, A. Mitschler, L. Ricard, *Organometallics* **1982**, *1*, 312-316.

[9] referenced against ferrocene.

4.2 Supporting Information

Supporting information of the manuscript entitled:

Subsequent functionalization of the *cyclo*-P_5 ligand in [Cp*Fe(η^5-P_5)]

Eric Mädl, Gábor Balázs, Eugenia Peresypkina and Manfred Scheer*

Contents

General Procedures: All manipulations were performed with rigorous exclusion of oxygen and moisture in Schlenk-type glassware on a dual manifold Schlenk line in argon atmosphere or in Ar filled glove box with a high-capacity recirculator (<0.1ppm O_2). THF, toluene, hexane, and DME were distilled from sodium benzophenoneketyl. Deuterated solvents were degassed, dried and distilled prior to use. The complex [Cp*Fe(η^5-P_5)] (**I**), [Li][Cp*Fe(η^4-$P_5CH_2SiMe_3$)] (**1a**) and [Li][Cp*Fe(η^4-P_5NMe_2)] (**1b**) were prepared according to their published procedures.[1] NMR spectra were recorded on a Bruker Avance 300 MHz and Bruker Avance 400 MHz spectrometers. Chemical shifts were measured at ambient temperature and are given in ppm; they are referenced to TMS for ^{1}H and ^{13}C, and 85 % H_3PO_4 for ^{31}P as external standard. Elemental analyses (CHN) were determined using in-house facility.

4.2.1 Experimental details: complex syntheses and characterization

Synthesis of 2a: 686 mg (1.33 mmol) of **1a**·Et_2O was dissolved in 100 mL THF. 1.2 mL of MeI in Ether (1.11 mol/L; 1.33 mmol) was added under strong stirring at room temperature and the solution was stirred overnight. White precipitate (LiI) was observed on the glass wall. The solvent was removed, **2a** extracted with *n*-hexane and filtered through a frit. The solvent was removed. **2a** could be isolated in 71.0 % (426 mg) crystalline yield. Crystals suitable for X-ray analysis were obtained from a concentrated *n*-hexane solution at −30 °C. $C_{15}H_{29}FeP_5Si$ (448.01): calcd. C 40.20, H 6.52; found C 39.64, H 6.48. ^{1}H NMR (400.13 MHz, C_6D_6): δ [ppm] = 1.90 (s, 9 H, CH_2SiMe_3), 2.59 (d, 2 H, CH_2SiMe_3), 3.50 (s, 15 H, $C_{10}H_{15}$), 4.12 (m, 3 H, P-*Me*). ^{13}C{^{1}H} NMR (100.62 MHz, C_6D_6): δ = −0.01 (CH_2SiMe_3), 9.31 (m, P-*Me*), 10.82 (s, $C_5(CH_3)_5$), 31.95 (d, $^1J_{PC}$ = 22.38 Hz CH_2SiMe_3), 88.72 (*s*, $C_5(CH_3)_5$). ^{31}P NMR (161.97 MHz, C_6D_6): δ = −96.76 (m, 2 P), 37.00 (m, 2 P), 129.42 (m, 1 P).

Synthesis of 2b: 168 mg (0.3 mmol) of **1b**·1.5 THF was dissolved in 50 mL THF. 0.3 mL of MeI in Ether (1.11 mol/L; 0.3 mmol) was added under strong stirring at room temperature and the solution was stirred overnight. White precipitate (LiI) was observed on the glass wall. The solvent was removed, **2b** extracted with hexane and filtered through a frit. The solvent was reduced to 5 mL and stored at −30 °C overnight. **2b** could be isolated in 51.5% (69 mg) crystalline yield.$C_{13}H_{24}FeP_5N$ (405.05): calcd. C 38.55, H 5.97, N 3.46; found C 38.14, H 6.03, N 4.43. ^{1}H NMR (400.13 MHz, C_6D_6): δ [ppm] = 1.48 (s, 3 H, NMe_2), 1.50 (s, 3 H, NMe_2), 1.61 (s, 15 H, $C_{10}H_{15}$), 1.79 (m, 3 H, P-*Me*). ^{13}C{^{1}H} NMR (100.62 MHz, C_6D_6): δ = 9.08 (broad, P-*Me*), 11.51 (s, $C_5(CH_3)_5$), 37.33 (s, NMe_2), 88.49 (*s*, $C_5(CH_3)_5$). ^{31}P NMR (161.97 MHz, C_6D_6): δ = −65.05 (m, 2 P), 37.68 (m, 2 P), 130.78 (tt, 1 P).

Synthesis of 2c: To a solution of 0.1 g (0.2 mmol) of **1a**·Et_2O in 15 mL THF, 0.02 mL (0.2 mmol) of C_3H_7I was added at room temperature. The solution was stirred for 12 h, the solvent removed and **2c** was extracted with *n*-hexane (15 mL). The hexane solution was filtered through a frit. The *n*-hexane solution could be purified further by column chromatography (Al_2O_3, 2x6 cm, *n*-hexane). One large green fraction was collected. However, the resulting solution still contained a large amount of byproducts and thus no yield is given, nor could the ^{1}H NMR signals be assigned. LIFDI-MS: 476.1 (M^+, 100%). ^{31}P NMR (161.97 MHz, C_6D_6): δ = −113.52 (m, 2 P), 33.11 (m, 2 P), 158.46 (tt, 1 P).

Synthesis of 3: To a solution of 0.15 g (0.4 mmol) of **I** in DME at −60 °C 0.27 mL (1.6 mol/L; 0.4 mmol) of MeLi in Et_2O was added and an immediate color change to brown could be observed. The solution was stirred for 4 hours, the solvent was reduced to 5 mL and layered with *n*-hexane (25 mL). [Li(dme)$_{2.7}$][**3**] could be isolated in 83 % crystalline yield (216 mg). $C_{21.8}H_{45}FeLiO_{5.4}P_5$ (611.24): calcd. C 42.84, H 7.08; found C 42.84, H 7.42. ^{1}H NMR (400.13 MHz, C_6D_6): δ [ppm] = 0.39 (sextet,

3 H, P-Me), 1.48 (s, 15 H, $C_{10}H_{15}$). $^{13}C\{^1H\}$ NMR (100.62 MHz, C_6D_6): δ = 11.77 (s, $C_5(CH_3)_5$), 26.97 (dt, $^1J_{PC}$ = 22.38 Hz, $^2J_{PC}$ = 2.0 Hz, CH_3), 85.88 ($C_5(CH_3)_5$). ^{31}P NMR (161.97 MHz, C_6D_6): δ = −71.45 (m, 2 P), 13.74 (m, 2 P), 71.30 (tt, 1 P).

Synthesis of 4: To a solution of 90 mg (0.15 mmol) of $[Li(dme)_{2.7}][\mathbf{3}]$ in DME 0.11 mL (0.14 mmol, 1.11 mol/L) of MeI in Et_2O was added at room temperature, and stirred overnight. The solvent was removed, **4** extracted with toluene and the toluene solution is filtered through a frit. The solvent is removed. **4** is obtained in 23 % yield (13 mg). LIFDI-MS: 376 (M^+, 100%); 361.0 ($M^+ - CH_3$, 40%), 346.0 ($M^+ - (CH_3)_2$, 20%), 315.0 ($M^+ - P(CH_3)_2$, 10%), 284.1 ($M^+ - P_2(CH_3)_2$, 15%), 253.1 ($M^+ - P_3(CH_3)_2$, 45%), 190.1 ($M^+ - P_5(CH_3)_2$, 35%). ^1H NMR (400.13 MHz, C_6D_6): δ [ppm] = 0.10 (d, 3 H, P-Me), 1.56 (m, 3H, P-Me), 1.60 (s, 15 H, $C_{10}H_{15}$). $^{13}C\{^1H\}$ NMR (100.62 MHz, C_6D_6): δ = 11.49 (s, $C_5(CH_3)_5$), 9.04 (m, P-*Me*), 27.89 (broad d, P-*Me*), 89.23 ($C_5(CH_3)_5$).). ^{31}P NMR (161.97 MHz, C_6D_6): δ = −112.09 (m, 2 P), 35.22 (m, 2 P), 117.29 (m, 1 P).

Synthesis of 5: To 0.2 g (0.6 mmol) of **I** in DME, 91 mg (0.3 mmol) of $[Li_2(TMEDA)][Cp_2Fe]$ are added at room temperature. A color change from green to brown is observed. After three days of stirring the solution is concentrated (10 mL) and layered with *n*-hexane (30 mL). After two days at room temperature 150 mg (36 %) of crystalline $[Li(dme)_3]_2[\mathbf{5}]$ is isolated. $C_{54}H_{98}Fe_3Li_2O_{12}P_{10}$ (1430.5): calcd. C 45.34, H 6.91; found C 45.01, H 6.48. ^1H NMR (400.13 MHz, C_6D_6): δ [ppm] = 1.47 (30 H, s, $C_{10}H_{15}$), 3.05 (s, 4 H, C_5H_4), 4.04 (s, 4 H, C_5H_4). $^{13}C\{^1H\}$ NMR (100.62 MHz, C_6D_6): δ = 11.83 (s, $C_5(CH_3)_5$), 69.89 (s, C_5H_4), 70.90 (s, C_5H_4), 85.87 (*s*, $C_5(CH_3)_5$). ^{31}P NMR (161.97 MHz, C_6D_6): δ = −48.71 (m, 2 P), 18.67 (m, 2 P), 69.71 (tt, 1 P).

4.2.2 Experimental and simulated NMR spectra

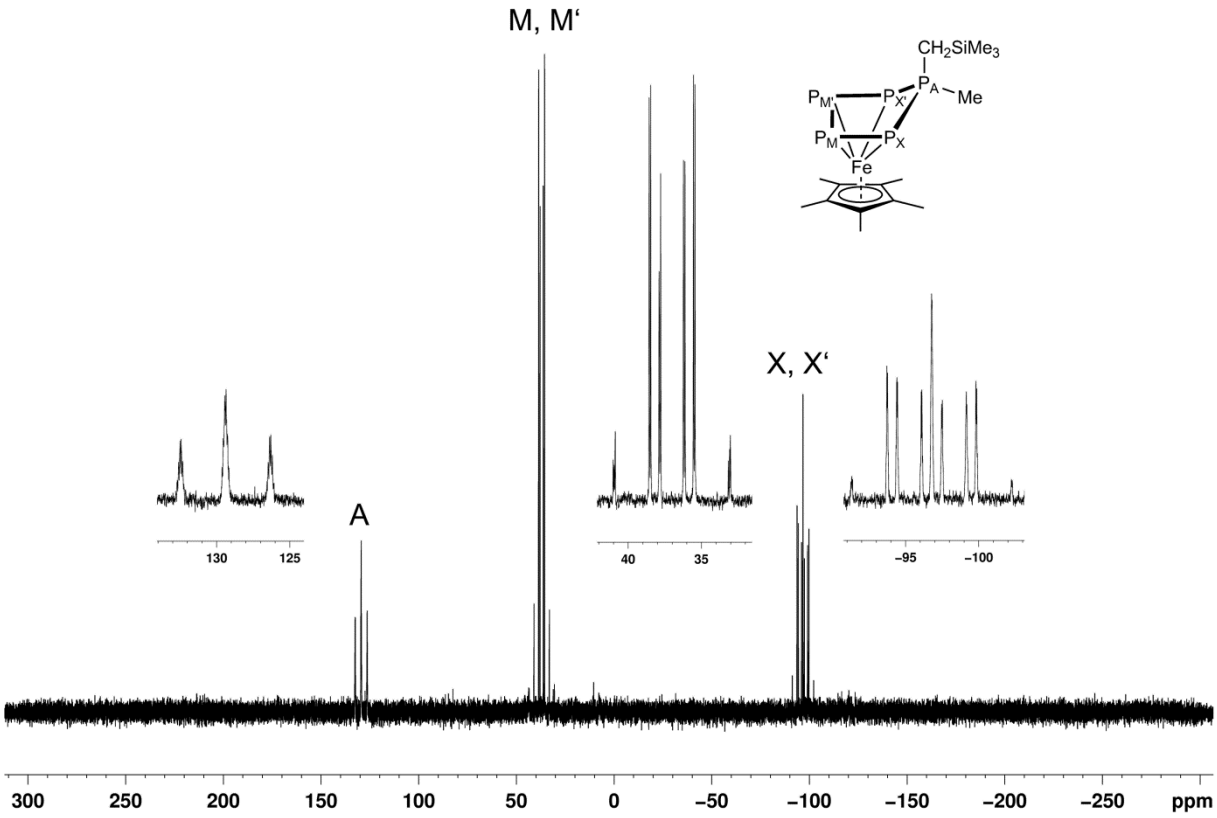

Figure S1. ^{31}P NMR (161.97 MHz, C_6D_6) spectrum of **2a**.

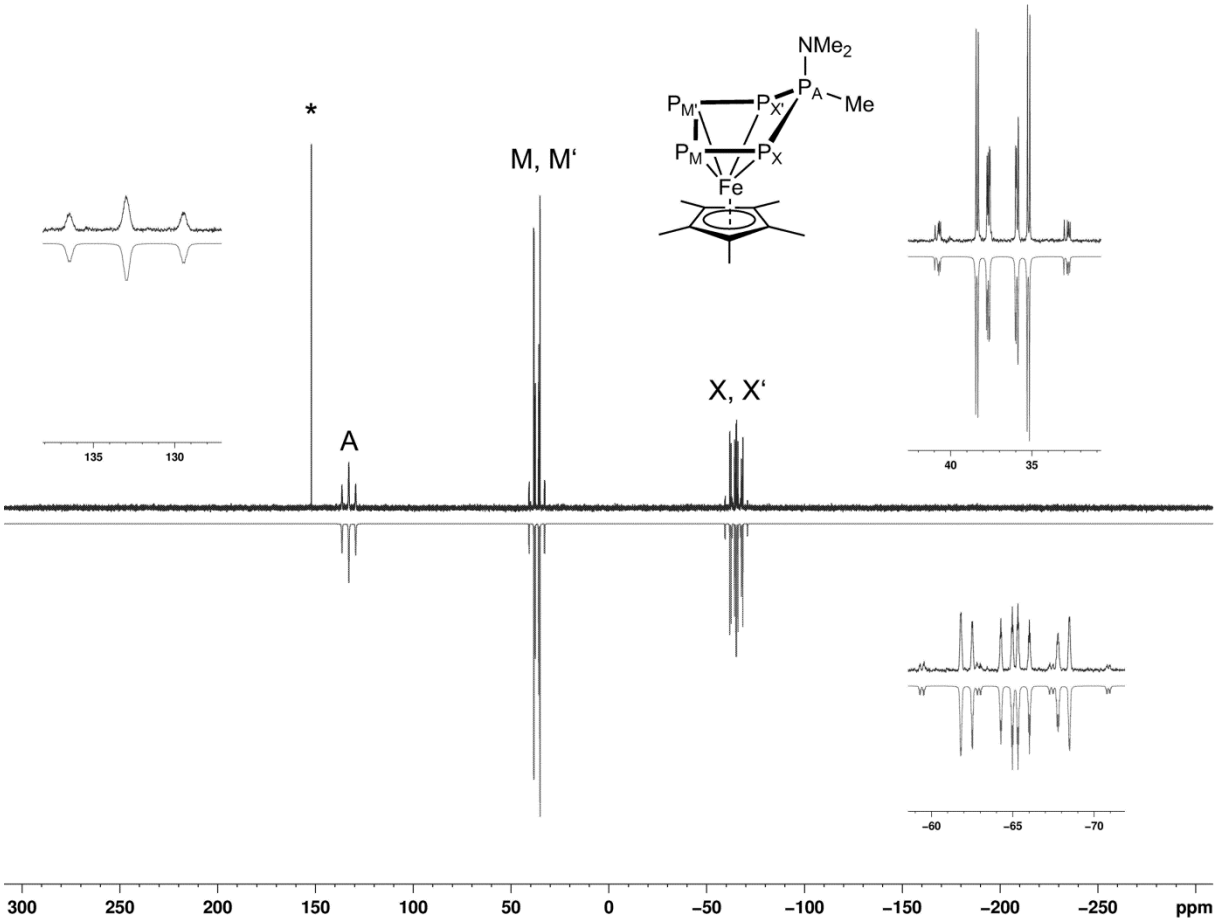

Figure S2. ^{31}P NMR (161.97 MHz, C_6D_6) spectrum of **2b**. Impurities of **1** are marked with *.

Table S1. ^{31}P NMR chemical shifts and coupling constants for **2b** obtained from the simulation.

J (Hz)				δ (ppm)	
$^1J_{P_A\text{-}P_X}$	426.58	$^1J_{P_M\text{-}P_X}$	423.61	A	132.93
$^1J_{P_A\text{-}P_{X'}}$	426.62	$^1J_{P_{M'}\text{-}P_{X'}}$	414.80	M, M’	36.77
$^2J_{P_A\text{-}P_M}$	17.27	$^2J_{P_M\text{-}P_{X'}}$	−29.94	X, X’	−65.10
$^2J_{P_A\text{-}P_{M'}}$	15.77	$^2J_{P_{M'}\text{-}P_X}$	−39.54		
$^1J_{P_M\text{-}P_{M'}}$	376.67	$^2J_{P_X\text{-}P_{X'}}$	15.35		

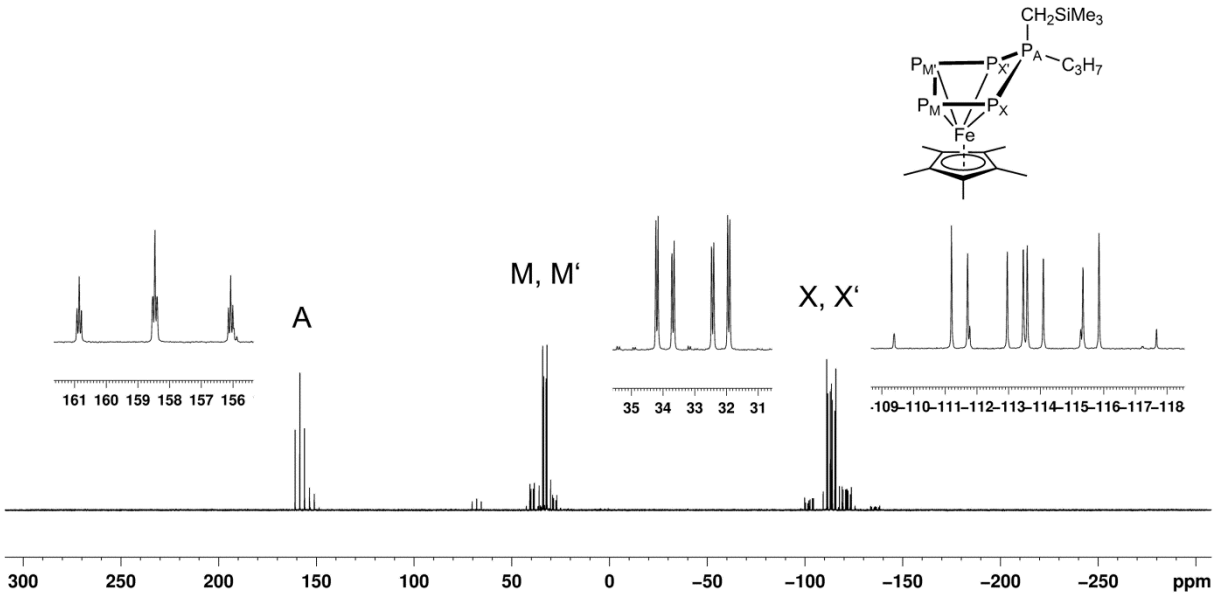

Figure S3. ^{31}P NMR (161.97 MHz, C_6D_6) spectrum of **2c**.

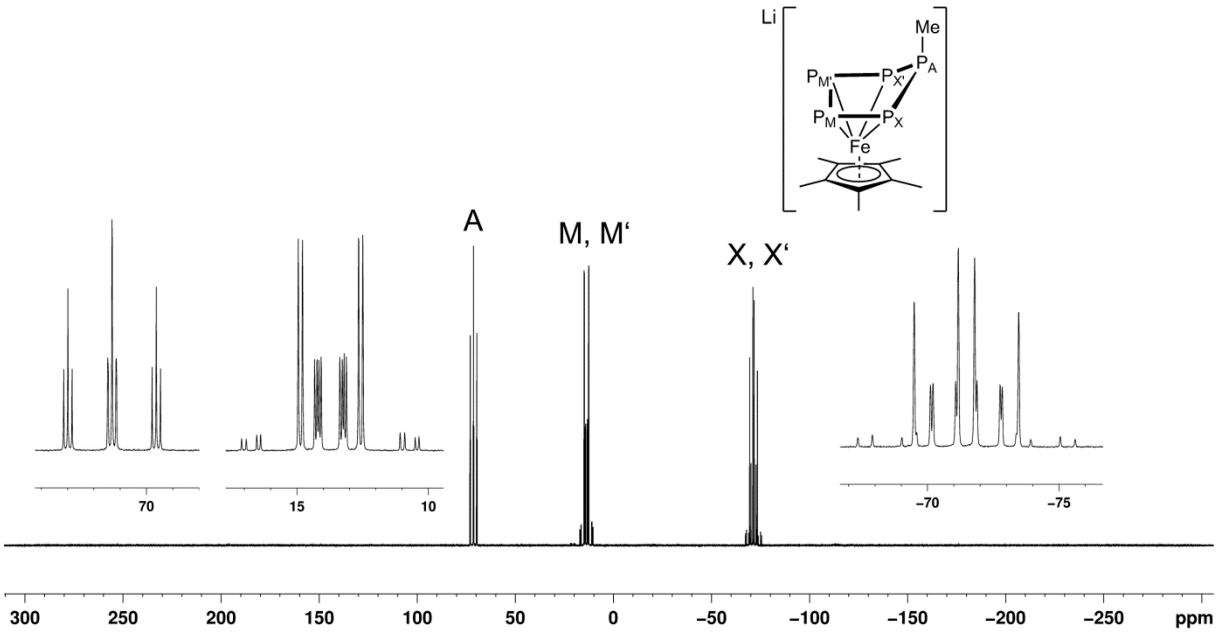

Figure S4. ^{31}P NMR (161.97 MHz, C_6D_6) spectrum of **3**.

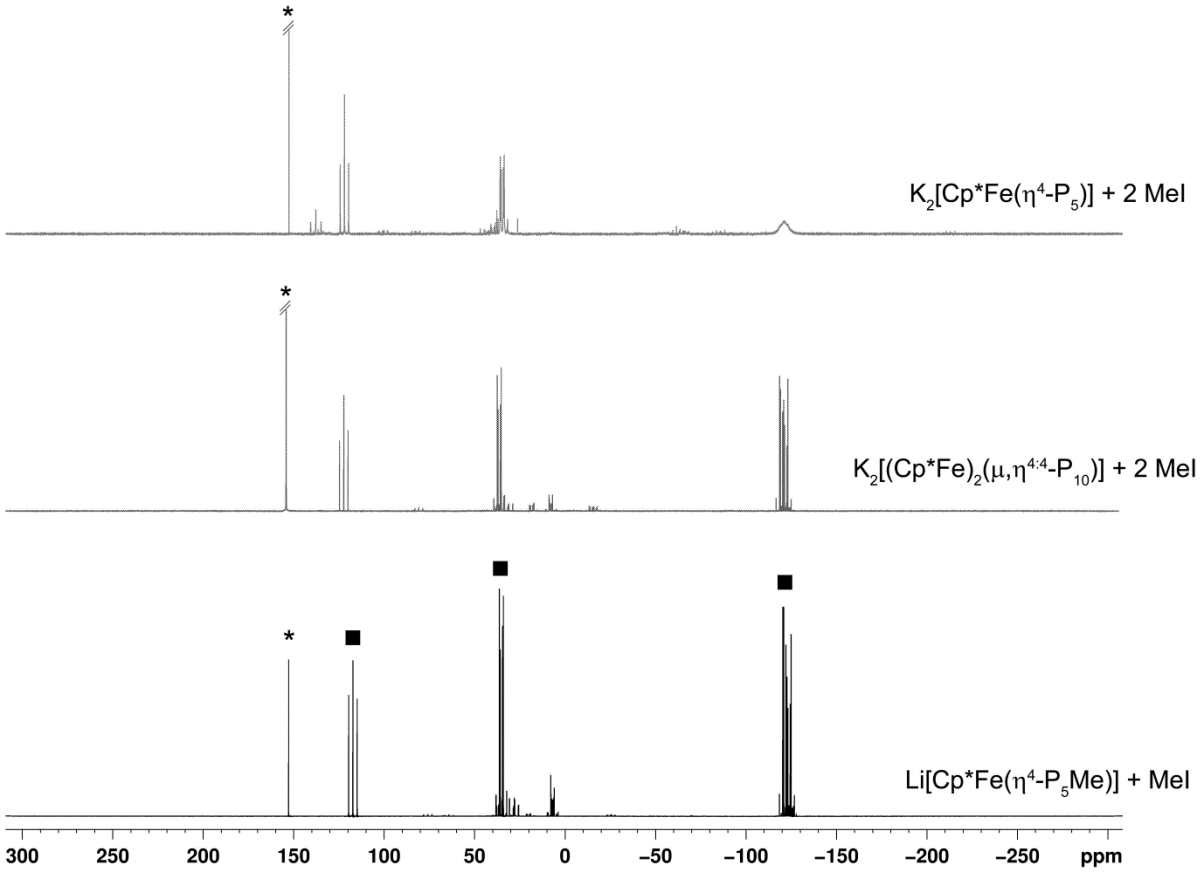

Figure S5. ^{31}P NMR (161.97 MHz, C_6D_6) spectra of the formation of the dimethylated, neutral compound [Cp*Fe(η^4-P_5Me_2)] (**4**) (marked with ■) in different reactions. Impurities of **I** are marked with *.

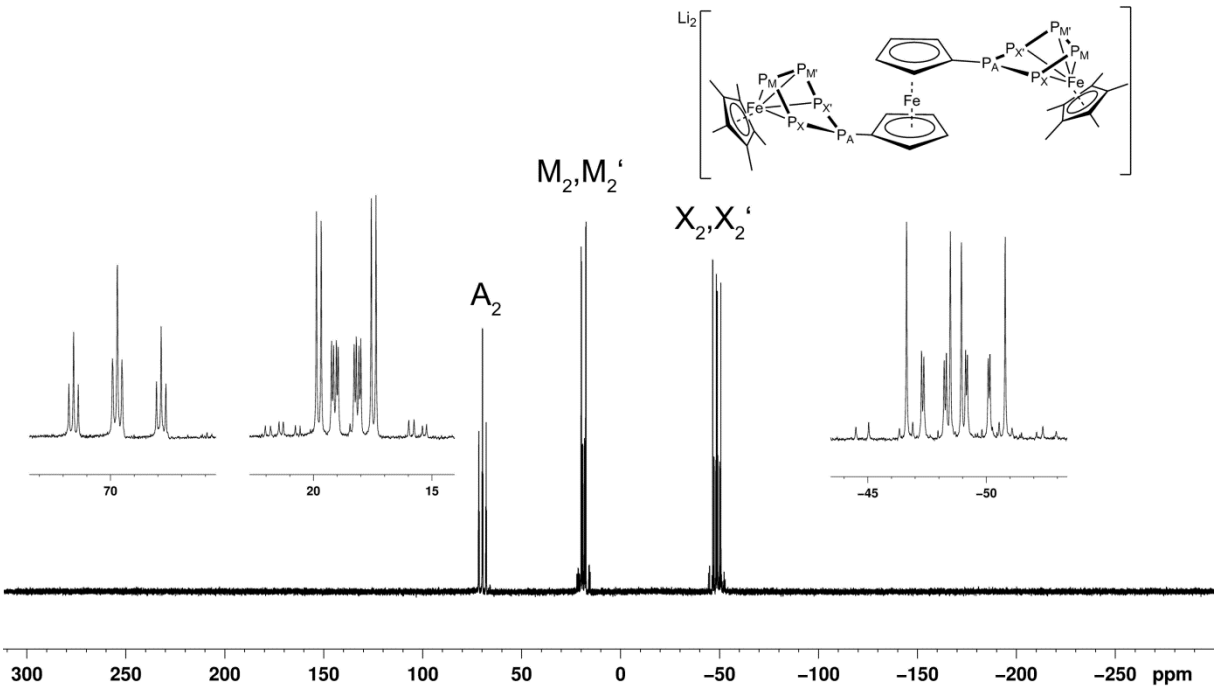

Figure S6. ^{31}P NMR (161.97 MHz, C_6D_6) spectrum of **5**.

4.2.3 Details on X-ray structure determinations and ortep-like plots

The diffraction data were collected on a Gemini R-Ultra diffractometer (**2a**, **3**) equipped with a Ruby detector or SuperNova diffractometers (Agilent Technologies) equipped with an Atlas (**2b**, **5**) CCD detector, and micro-focus SuperNova sourse (CuK_α radiation, λ = 1.54178 Å) using ω scans of 1° or 0.5 frames. The measurements were performed at 123K (**2a**, **2b**, **5**) or 203 K (**3**; at lower temperature a phase transition was observed). All structures were solved by direct methods with ShelXT[2] or Olex2[3] programs and refined by full-matrix least-squares method against $|F|^2$ in anisotropic approximation using SHELXTL or its multiprocessor version SHELX2013[2]. Absorption corrections were applied analytically using *CrysAlis PRO* Software[4] (Table S2). All non-hydrogen atoms were refined in anisotropic approximation. Hydrogen atoms were refined in calculated positions using riding on pivot atom model.

The structure **2a** is severely disordered over two positions (Figure S7b). The positions overlap almost completely so as only an iron and a silicon atoms are ordered. The disorder components were refined to give different ratios for Cp* group and {$P_5Me(CH_2SiMe_3)$} fragment equal to 0.65/0.35 and 0.69/0.31, respectively. The refinement of molecular occupancies was performed with displacement atomic parameters fixed at U_{iso} = 0.05. The resulting values were then fixed, and the displacement parameters were refined. We also tried to assume equal occupancies for both disordered fragments for the sake of model simplicity. However, the resulting model is characterised with worse quality factors. The atoms of the minor positions were refined in isotropic approximation.

According to CIFCheck, the structure of **2b** shows pseudo-B symmetry (with B-lattice extinction violations of I(mean) > 3.2σ(I)). To take it into account one needs to choose another unit cell, which is two times smaller in volume. The attempt to solve and refine the crystal structure in the smaller monoclinic unit cell (a=7.9306, b=29.8376, c=8.8657 Å, β=116.507°, V=1620.12 Å^3) and $P2_1/c$ space group gives R_1=0.0288 and wR_2 (all data) = 0.0803 with single molecular complex **2b** in the unit cell instead of two crystallographically unique molecules in larger unit cell (Table S1). In the smaller cell, a Cp* ligand becomes disordered while Cp*s of both independent molecules in larger cell are ordered. The disorder is refined as equal occupancies for both Cp* positions. The quality factors are somewhat worse for this model, and the displacement parameters are deformed. Therefore, the pseudo-B lattice is not correct, and is a sign for superstuctural ordering of molecules **2b** at low temperature that causes the lowering of the crystallographic symmetry.

The structure **3** comprises a molecular anion [Cp*Fe(η^5-P_5Me)]$^-$ (Figure S9) and a cation [Li(dme)$_3$]$^+$; the latter coordinates three DME molecules, of which two are disordered over two close positions with a ratio of 0.55/0.45 and 0.64/0.36. The oxygen and carbon atoms of minor positions are refined isotropically.

The compound **5** crystallizes in non-centrosymmetric space group *Pna*2_1. The structural model was derived as an inversion twin with very small twin batch of 3.2(4)%. This minor contribution has nevertheless improved the residual *R* factors and a Flack parameter.

The supplementary crystallographic data for this publication (Tables S2) can be obtained free of charge at www.ccdc.cam.ac.uk/conts/retrieving.html (or from the Cambridge Crystallographic Data Centre, 12 Union Road, Cambridge CB2 1EZ, UK; Fax: + 44-1223-336-033; e-mail: deposit@ccdc.cam.ac.uk). All drawings for **2a**, **2b**, **3** and **5** were made in Olex2[3].

Table S2. Crystal data, data collection parameters and convergence results for **2a**, **2b**, **3**, **5**.

	2a	**2b**	**3**	**5**
CCDC Code	CCDC-XXXXX	CCDC-XXXXX	CCDC-XXXXX	CCDC-XXXXX
Crystal data				
Chemical formula	$C_{15}H_{29}FeP_5Si$	$C_{13}H_{24}FeNP_5$	$C_{23}H_{48}FeLiO_6P_5$	$C_{54}H_{98}Fe_3Li_2O_{12}P_{10}$
M_r	448.17	405.03	638.25	1430.45
Crystal system, space group	Monoclinic, $P2_1/n$	Monoclinic, $P2_1/c$	Monoclinic, $P2_1/c$	Orthorhombic, $Pna2_1$
Temperature (K)	123	123	203	123
a, b, c (Å)	8.32648 (12), 9.12374 (11), 29.0199 (4)	14.3059 (2), 29.8376 (4), 8.8657 (1)	15.7568 (2), 13.1533 (2), 16.9675 (2)	18.00998 (16), 20.6076 (2), 19.7734 (2)
α, β, γ (°)	93.6816 (12)	97.175 (1)	102.508 (1)	7338.72 (13)
V (Å^3)	2200.05 (5)	3754.72 (8)	3433.12 (8)	4
Z	4	8	4	3008
F(000)	936	1680	1352	1.295
Radiation type	Cu $K\alpha$	Cu $K\alpha$	Cu $K\alpha$	Cu $K\alpha$
μ (mm^{-1})	9.41	10.36	5.97	7.02
Crystal shape and colour	Black plate	Black prism	Black truncated prism	Black prism
Crystal size (mm)	0.34 × 0.25 × 0.04	0.18 × 0.12 × 0.08	0.40 × 0.15 × 0.11	0.33 × 0.18 × 0.15
Data collection				
Diffractometer	Xcalibur, Atlas^{S2}, Gemini ultra diffractometer	SuperNova, Single source at offset, Atlas diffractometer	Xcalibur, Atlas^{S2}, Gemini ultra diffractometer	SuperNova, Single source at offset, Atlas diffractometer
Absorption correction	Multi-scan	Gaussian	Analytical	Analytical
T_{min}, T_{max}	0.131, 1.000	0.321, 0.563	0.240, 0.595	0.217, 0.469
No. of measured, independent and observed [> 2σ(I)] reflections	25018, 3882, 3568	19702, 7371, 6535	25941, 6042, 4741	50719, 12975, 12360
R_{int}	0.049	0.017	0.027	0.037
(sin θ/λ)$_{max}$ (Å^{-1})	0.596	0.624	0.596	0.622
Range of h, k, l	h = -9→8, k = -10→10, l = -34→34	h = -17→16, k = -37→31, l = -10→10	h = -18→18, k = -15→15, l = -20→20	h = -22→21, k = -25→25, l = -20→24
Refinement				
$R[F^2 > 2\sigma(F^2)]$, $wR(F^2)$, S	0.048, 0.130, 1.06	0.021, 0.055, 1.01	0.040, 0.112, 1.03	0.041, 0.112, 1.03
No. of reflections	3882	7371	6042	12975
No. of parameters	314	377	381	753
No. of restraints	6	0	0	1
H-atom treatment	H-atom parameters constrained	H-atom parameters constrained	H-atom parameters constrained	H-atom parameters constrained
$\Delta\rangle_{max}$, $\Delta\rangle_{min}$ (e Å^{-3})	0.71, -0.70	0.25, -0.32	0.88, -0.45	1.27, -0.45
Flack parameter	-	-	-	0.032 (4)

Computer programs: *CrysAlis PRO* 1.171.38.41 (Rigaku OD, 2015), *SHELXS2013* (Sheldrick, 2013), *SHELXL2013* (Sheldrick, 2013)

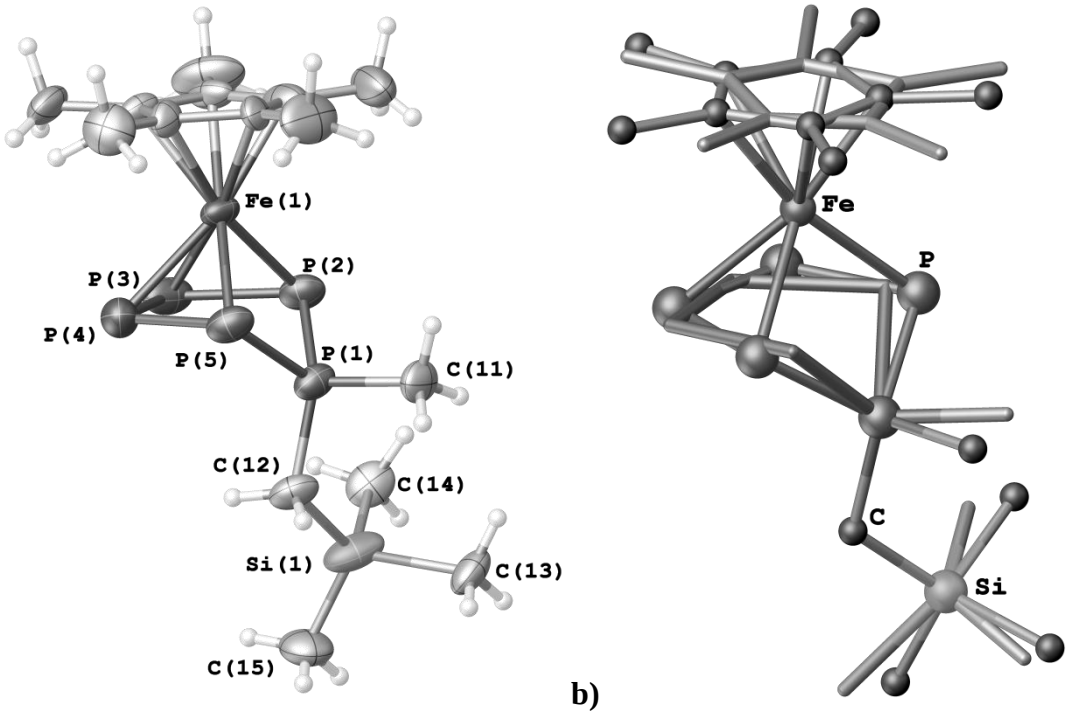

Figure S7. (a) Molecular structure (ellipsoids at 50% probability) and enumeration scheme for **2a**; (b) the model of the disorder (major component is shown in ball-and-stick model) in **2a**

Table S3. Selected geometric parameters (Å, º) for **2a**

P1—C11	1.788 (6)	Si1—C12	1.880 (4)
P1—C12	1.797 (4)	P1—C11A	1.893 (13)
P1—P2	2.084 (5)	P1—P2A	2.215 (7)
P2—P3	2.135 (4)	P2A—P3A	2.145 (6)
P3—P4	2.143 (4)	P3A—P4A	2.130 (6)
P4—P5	2.133 (4)	P4A—P5A	2.124 (6)
P1—P5	2.167 (3)	P1—P5A	2.110 (4)
Si1—C13	1.983 (8)	Si1—C13A	1.602 (16)
Si1—C14	1.926 (6)	Si1—C14A	1.818 (14)
Si1—C15	1.744 (7)	Si1—C15A	2.126 (15)

C11—P1—P2	111.2 (3)	C15—Si1—C13	109.9 (4)
C12—P1—P2	122.52 (19)	C12—Si1—C13	108.9 (3)
C12—P1—P5A*	124.44 (17)	C14—Si1—C13	103.4 (4)
C11A—P1—P5A	103.3 (4)	C13A—Si1—C15A	105.8 (7)
C11—P1—P5	108.5 (3)	C14A—Si1—C15A	101.1 (7)
C12—P1—P5	113.24 (15)	C12—Si1—C15A	94.6 (4)
P2—P1—P5	98.02 (15)	P1—C12—Si1	120.3 (2)
C12—P1—P2A	117.1 (2)	P1—P2—P3	98.82 (19)

C11A—P1—P2A	100.6 (5)	P2—P3—P4	104.98 (17)
P5A—P1—P2A	95.0 (2)	P5—P4—P3	103.97 (13)
C13A—Si1—C14A	127.3 (8)	P4—P5—P1	98.32 (14)
C13A—Si1—C12	115.5 (6)	P3A—P2A—P1	94.8 (3)
C15—Si1—C12	112.6 (3)	P4A—P3A—P2A	104.0 (2)
C14A—Si1—C12	106.3 (5)	P5A—P4A—P3A	104.69 (18)
C15—Si1—C14	110.7 (4)	P1—P5A—P4A	96.12 (18)
C12—Si1—C14	110.9 (2)		

* the letter ‘a’ denotes the minor component of the disordered molecule.

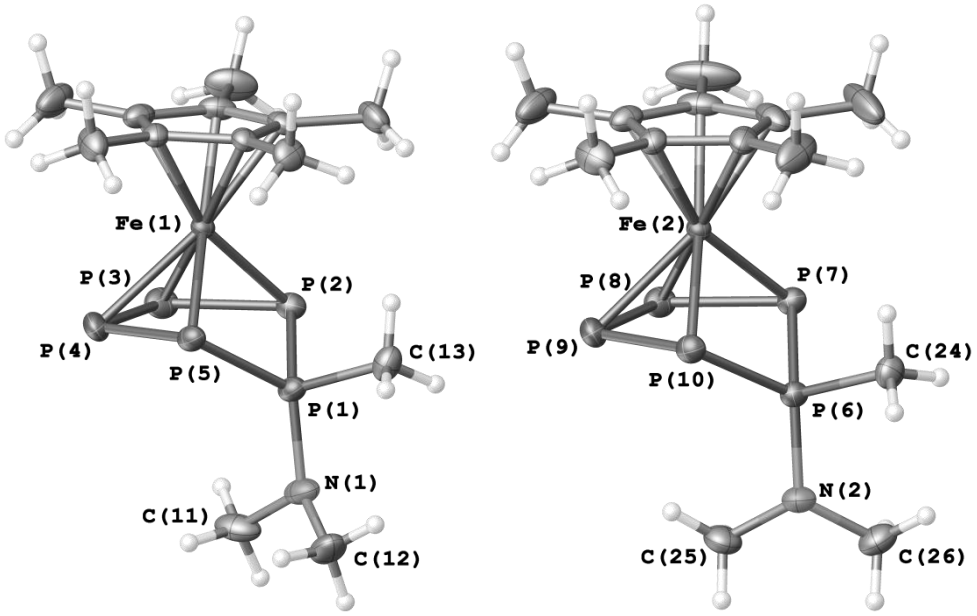

Figure S8. Molecular structure (ellipsoids at 50% probability) and enumeration scheme for two crystallographically unique molecules **2b**

Table S4. Selected geometric parameters (Å, º) for **2b**

Fe1—C2	2.0603 (13)	P1—N1	1.6779 (12)
Fe1—C1	2.0717 (12)	P1—C13	1.8168 (14)
Fe1—C3	2.0801 (14)	P1—P2	2.1347 (5)
Fe1—C5	2.0943 (12)	P1—P5	2.1426 (5)
Fe1—C4	2.1010 (13)	P2—P3	2.1342 (5)
Fe1—P5	2.3168 (4)	P3—P4	2.1519 (6)
Fe1—P3	2.3198 (4)	P4—P5	2.1360 (5)
Fe1—P2	2.3303 (4)	P6—N2	1.6766 (11)
Fe1—P4	2.3399 (4)	P6—C24	1.8164 (13)
Fe2—C14	2.0693 (13)	P6—P10	2.1385 (5)

Fe2—C15	2.0726 (14)	P6—P7	2.1448 (4)
Fe2—C16	2.0877 (14)	P7—P8	2.1338 (5)
Fe2—C18	2.0943 (13)	P8—P9	2.1511 (5)
Fe2—C17	2.1027 (14)	P9—P10	2.1387 (5)
Fe2—P10	2.3258 (4)	N1—C12	1.465 (2)
Fe2—P9	2.3288 (4)	N1—C11	1.466 (2)
Fe2—P7	2.3289 (4)	N2—C26	1.4638 (19)
Fe2—P8	2.3382 (4)	N2—C25	1.4702 (18)

N1—P1—C13	103.77 (7)	C24—P6—P7	105.45 (5)
N1—P1—P2	117.53 (5)	P10—P6—P7	99.619 (18)
C13—P1—P2	104.76 (5)	P8—P7—P6	101.011 (19)
N1—P1—P5	122.92 (5)	P7—P8—P9	105.449 (19)
C13—P1—P5	106.16 (5)	P10—P9—P8	104.97 (2)
P2—P1—P5	100.084 (19)	P6—P10—P9	101.506 (19)
P3—P2—P1	102.06 (2)	C12—N1—C11	112.28 (13)
P2—P3—P4	105.44 (2)	C12—N1—P1	120.27 (12)
P5—P4—P3	105.14 (2)	C11—N1—P1	115.83 (11)
P4—P5—P1	101.54 (2)	C26—N2—C25	112.46 (12)
N2—P6—C24	103.84 (6)	C26—N2—P6	120.93 (10)
N2—P6—P7	123.77 (4)	C25—N2—P6	116.79 (10)

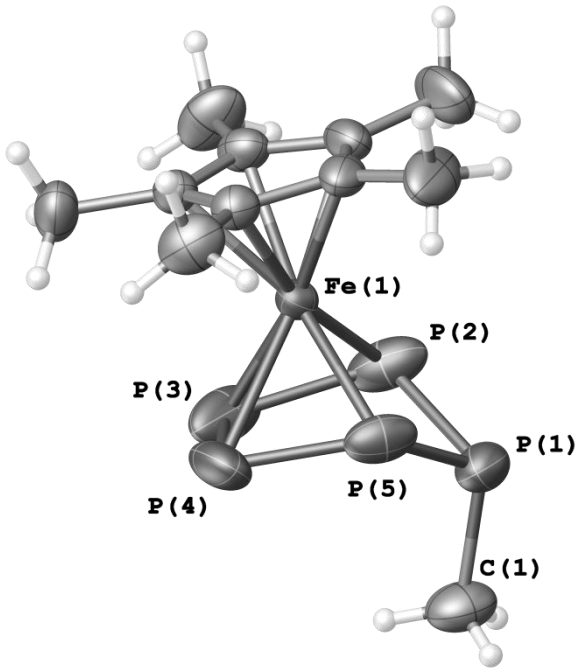

Figure S9. Molecular structure (ellipsoids at 50% probability) and enumeration scheme for the anion in **3**.

Table S5. Selected geometric parameters (Å, º) for **3**

Fe1—C14	2.065 (2)	Fe1—P4	2.3324 (8)
Fe1—C13	2.076 (2)	P1—C1	1.848 (3)
Fe1—C15	2.086 (2)	P1—P5	2.1490 (12)
Fe1—C12	2.091 (2)	P1—P2	2.1580 (12)
Fe1—C11	2.094 (2)	P2—P3	2.1461 (16)
Fe1—P2	2.3036 (9)	P3—P4	2.1182 (17)
Fe1—P3	2.3146 (8)	P4—P5	2.1351 (13)
Fe1—P5	2.3196 (8)		

C1—P1—P5	107.77 (12)	P4—P3—P2	103.56 (5)
C1—P1—P2	108.04 (12)	P3—P4—P5	102.94 (5)
P5—P1—P2	92.05 (4)	P4—P5—P1	106.61 (5)
P3—P2—P1	105.65 (5)		

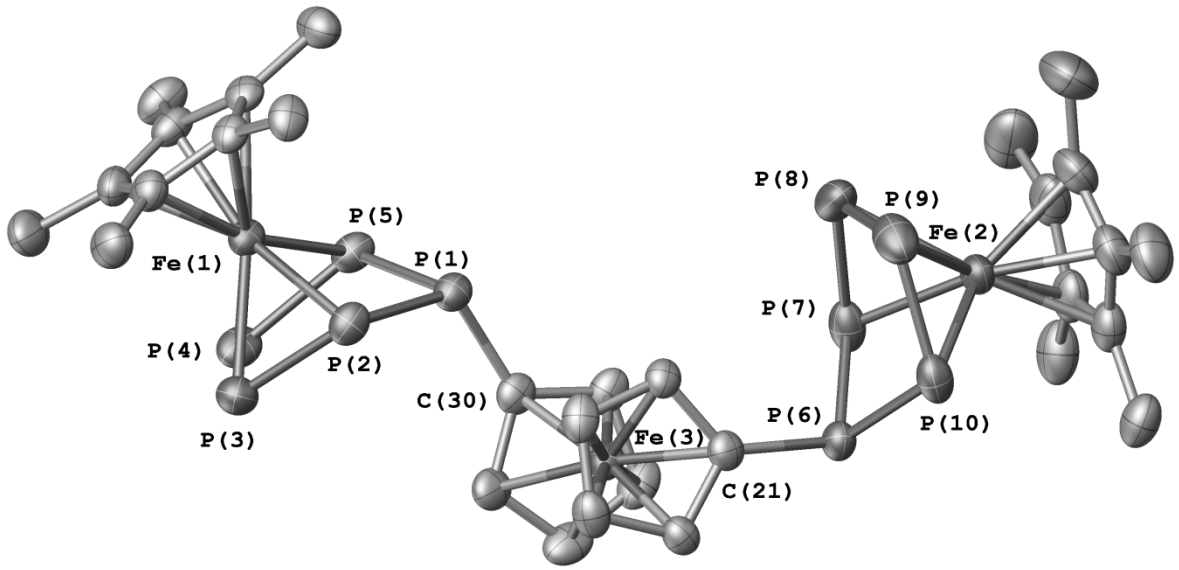

Figure S10. Molecular structure (ellipsoids at 50% probability) and enumeration scheme for the dianion in **5**

Table S6. Selected geometric parameters (Å, º) for **5**

Fe1—P4	2.3157 (15)	P1—P5	2.1700 (16)
Fe1—P5	2.3165 (15)	P2—P3	2.1502 (18)
Fe1—P2	2.3212 (13)	P3—P4	2.126 (2)
Fe1—P3	2.3250 (14)	P4—P5	2.1502 (19)

Fe2—P7	2.3142 (15)	P6—C21	1.820 (5)
Fe2—P10	2.3167 (15)	P6—P10	2.1572 (18)
Fe2—P8	2.3216 (16)	P6—P7	2.1630 (17)
Fe2—P9	2.322 (2)	P7—P8	2.154 (3)
P1—C30	1.808 (5)	P8—P9	2.149 (3)
P1—P2	2.1521 (18)	P9—P10	2.132 (2)

C30—P1—P2	111.36 (16)	C21—P6—P7	112.13 (15)
C30—P1—P5	111.72 (15)	P10—P6—P7	92.40 (7)
P2—P1—P5	93.67 (6)	P8—P7—P6	108.29 (9)
P3—P2—P1	109.66 (7)	P9—P8—P7	102.47 (8)
P4—P3—P2	103.79 (7)	P10—P9—P8	103.68 (9)
P3—P4—P5	103.83 (7)	P9—P10—P6	108.15 (8)
P4—P5—P1	109.41 (7)	P9—P10—Fe2	62.78 (7)
C21—P6—P10	110.31 (16)	P6—P10—Fe2	89.80 (6)

4.2.4 Details on DFT calculations

The DFT calculations on the complexes [Cp*Fe(η^4-$P_5CH_2SiMe_3$)]$^-$ (**1a**; labeling according to scheme 1 of the manuscript) and [Cp*Fe(η^4-$P_5MeCH_2SiMe_3$)] (**2a**) have been performed with the TURBOMOLE program package[5]. The geometry was optimized at the RI[6]-BP86[7]/def2-SVP[8] level followed by single point calculations at the BP86/def2-TZVPP[9,8b] level of theory. The Multipole Accelerated Resolution of Identity (MARI-J)[10] approximation was used in the geometry optimization steps.

Table S7. Selected Wiberg bond indexes (WBI) (numbering of atoms corresponds to Figure 1 in the manuscript).

	2a	**1a**
P1-P2	1.11	1.14
P1-P5	1.12	1.15
P2-P3	1.22	1.23
P3-P4	1.25	1.31
P4-P5	1.22	1.24
P1-Fe1	0.16	0.07
P2-Fe1	0.64	0.69
P3-Fe1	0.54	0.54
P4-Fe1	0.52	0.54
P5-Fe1	0.56	0.62

Table S8. Selected Natural atomic charges (numbering of atoms corresponds to Figure 1 in the manuscript).

	2a	**1a**
Fe1	-0.26	-0.24
P1	0.89	0.22
P2	-0.07	-0.13
P3	-0.03	-0.11
P4	-0.03	-0.11
P5	-0.09	-0.15

Tables regarding the cartesian coordinates of all performed calculations can be found on the DVD-Rom, which is attached in the back of this work.

4.2.5 References

[1] E. Mädl, M. V. Butovskii, G. Balázs, E. V. Peresypkina, A. V. Virovets, M. Seidl, M. Scheer, *Angew. Chem. Int. Ed.* **2014**, *53*, 7643-7646.
[2] G. M. Sheldrick. Acta Cryst. (2015). C71, 3-8.
[3] Dolomanov, O.V., Bourhis, L.J., Gildea, R.J, Howard, J.A.K. & Puschmann, H. (2009), J. Appl. Cryst. 42, 339-341.
[4] *CrysAlis PRO*, Agilent Technologies, Versions 1.171.36-38 and *CrysAlis PRO* 1.171.38.41 (Rigaku OD, 2015)
[5] a) F. Furche, R. Ahlrichs, C. Hättig, W. Klopper, M. Sierka, F. Weigend, *WIREs Comput. Mol. Sci.* **2014**, *4*, 91-100. b) R. Ahlrichs, M. Bär, M. Häser, H. Horn, C. Kölmel, *Chem. Phys. Lett.***1989**, *162*, 165–169; c) O. Treutler, R. Ahlrichs, *J. Chem. Phys.***1995**, *102*, 346–354.
[6] a) K. Eichkorn, O. Treutler, H. Oehm, M. Häser, R. Ahlrichs, *Chem. Phys. Lett.*1995, **242**, 652–660; b) K. Eichkorn, F. Weigend, O. Treutler, R. Ahlrichs, *Theor. Chem. Acc.*1997, **97**, 119.
[7] a) P. A. M. Dirac, *Proc. Royal Soc. A*, 1929, 123, 714-733. b) J. C. Slater, *Phys. Rev.*1951, 81, 385-390. c) S. H. Vosko, L. Wilk, M. Nusair, *Can. J. Phys.* 1980, 58, 1200-1211. d). A. D. Becke, *Phys. Rev. A*, 1988, 38, 3098. e) J. P. Perdew, *Phys. Rev. B* 1986, 33, 8822-8824.
[8] a) H. Horn, R. Ahlrichs, *J. Chem. Phys.* **1992**, *97*, 2571. b) F. Weigend, R. Ahlrichs, *Phys. Chem. Chem. Phys.* **2005**, *7*, 3297.
[9] F. Weigend, M. Häser, H. Patzelt, R. Ahlrichs *Chem. Phys. Letters* **1998**, *294*, 143.
[10] M. Sierka, A. Hogekamp, R. Ahlrichs, *J. Chem. Phys.*2003, 118, 9136.

5. Triple-decker sandwich complexes with a bent *cyclo*-P_5 middle deck

Eric Mädl, Eugenia Peresypkina, Alexey Y. Timoshkin, Fabian Dielmann and Manfred Scheer*

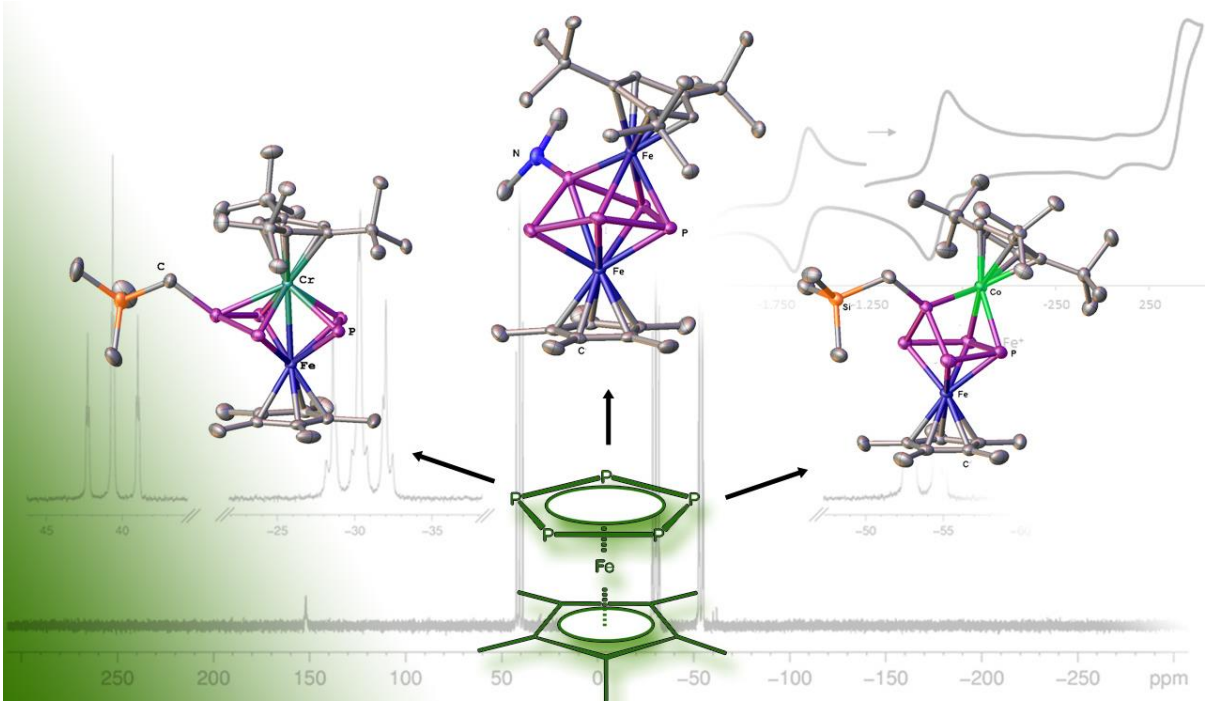

- All compounds were synthesized by Eric Mädl.
- The chapter "discussion" was written by Eric Mädl, except for parts regarding calculations, which were written by Alexey Timoshkin. Details about X-ray structure analyses in the chapter "supporting information" were written by Eugenia V. Peresypkina.
- DFT calculations were performed by Alexey Timoshkin. X-ray structure analyses and refinements were performed by Eric Mädl and Eugenia V. Peresypkina.
- Figures in the chapter "discussion" were made by Eric Mädl. Figures in the chapter "supporting information" regarding X-ray structure analysis were made by Eugenia V. Peresypkina. Figures in the chapter "supporting information" regarding calculations were made by Alexey Timoshkin.
- Compound **7** was already described by Fabian Dielmann. The analytical data of **7** regarding FD-mass and elemental analysis was adopted from his thesis.

5.1 Discussion

Abstract: *Reactions of* $[Cp^*Fe(\eta^4\text{-}P_5R)]^-$ (***1a***: *R =* CH_2SiMe_3; ***1b***: *R =* NMe_2) *with the transition metal dimers* $[Cp'''MX]_2$ *(M = Cr, Fe, Co, Ni; X = Cl, Br) leads via salt elimination to the triple-decker complexes* $[(Cp^*Fe)(Cp'''Co)(\mu,\eta^{4:3}\text{-}P_5CH_2SiMe_3)]$ (***2a***), $[(Cp^*Fe)(Cp'''Co)(\mu,\eta^{4:3}\text{-}P_5NMe_2)]$ (***2b***), $[(Cp^*Fe)(Cp'''Ni)(\mu,\eta^{4:3}\text{-}P_5NMe_2)]$ (***3***), $[(Cp^*Fe)(Cp'''Fe)(\mu,\eta^{4:4}\text{-}P_5NMe_2)]$ (***4***) *and* $[(Cp^*Fe)(Cp'''Cr)(\mu,\eta^{4:5}\text{-}P_5CH_2SiMe_3)]$ (***5***), *respectively. All compounds were characterized by multinuclear NMR spectroscopy and single crystal X-ray diffractions. The oxidation of* ***2a*** *with* $[Cp_2Fe][PF_6]$ *leads to the formation of the cationic complex* $[(Cp^*Fe)(Cp'''Co)(\mu,\eta^{5:4}\text{-}P_5CH_2SiMe_3)]^+$ (***6***), *which was crystallographically characterized. Moreover, in the reaction of* $K_2[(Cp^*Fe)_2(\mu,\eta^{4:4}\text{-}P_5)]$ *with* $[Cp'''MX]_2$ *(M = Fe, Co; X = Cl, Br) the neutral triple-decker complexes* $[(Cp^*Fe)(Cp'''M)(\mu,\eta^{5:4}\text{-}P_5)]$ (***7***: *M = Fe;* ***8***: *M = Co) were isolated and fully characterized. They exhibit an unsubstituted* cyclo-P_5 *middle deck. The electronic structure of the synthesized complexes was elucidated by DFT calculations.*

Ferrocene is one of the most frequently used organometallic reagents in chemistry, with a very broad field of application.[1] This 65 years old molecule[2] does not only show a fascinating chemistry in redox processes but particularly as a starting material for further reactions. Due to its ability to be metalated[3] or to undergo Friedel-Craft reactions[4] ferrocene is a valuable building block in organometallic synthesis. The isolobal analogue of ferrocene is pentaphosphaferrocene, for which the Cp* derivative $[Cp^*Fe(\eta^5\text{-}P_5)]$ (**I**) was first discovered in 1987.[5] The majority of reactivity studies of **I** is dedicated to the coordination chemistry towards Lewis acidic coordination moieties, forming 1D and 2D coordination polymers[6] or spherical supramolecular clusters.[7] In cothermolysis or cophotolysis reactions with organometallic reagents fragmentations and deformations of the *cyclo*-P_5 ring of **I** occurs.[8] A new direction of the reactivity of pentaphosphaferrocene was opened up when **I** was used in redox processes[9] and especially when it was converted by nucleophiles.[10] In the latter case a selective functionalization of the P_5 ring in **I** is achieved. As a result mono anionic complexes of the type $[Cp^*Fe(\eta^4\text{-}P_5R)]^-$ (R = CH_2SiMe_3, NMe_2, PH_2) were isolated which opened new perspectives in the chemistry of **I**. Having such monoanionic complexes in hand the question arises, whether by quenching these derivatives with electrophiles a reformation of the initial *cyclo*-P_5 ring does occur (by the retention of the former substitution) or does a rearrangement take place, to give products with novel structural motifs. Moreover, so far only few triple-decker complexes exhibiting a *cyclo*-P_5 middle deck are known. Starting from P_4 in thermolysis reactions the compounds $[(Cp^{BIG}Mn)_2(\mu,\eta^{5:5}\text{-}P_5)]$ (Cp^{BIG} = $C_5(4\text{-}n\text{Bu}C_6H_4)_5$) and $[(Cp^RCr)_2(\mu,\eta^{5:5}\text{-}P_5)]$ (Cp^R = Cp, Cp*) are obtained.[11] Starting from **I** some cationic triple-decker compounds $[(Cp^*M)(Cp^RM')(\eta^{5:5}\text{-}P_5)]^+$ (M, M' = Fe, Ru; Cp^R = Cp, Cp*), containing group 8 elements, have been reported.[12] Furthermore, mixed-

metal lanthanide-iron compounds with a *cyclo*-P_5 middle deck[9b] and triple-decker complexes consisting of **I** and a $[M(CO)_3]$ fragment (M = Cr, Mo, W) are known.[13] Herein we report of the synthesis of neutral complexes with a functionalized P_5 middle deck under mild conditions. By using different transition metal halides $[Cp'''MX]_2$ (M = Cr, Fe, Co, Ni; X = Cl, Br) a broad variety of different triple-decker complexes are easy accessible. Their bonding situation has been investigated by quantum chemical computations.

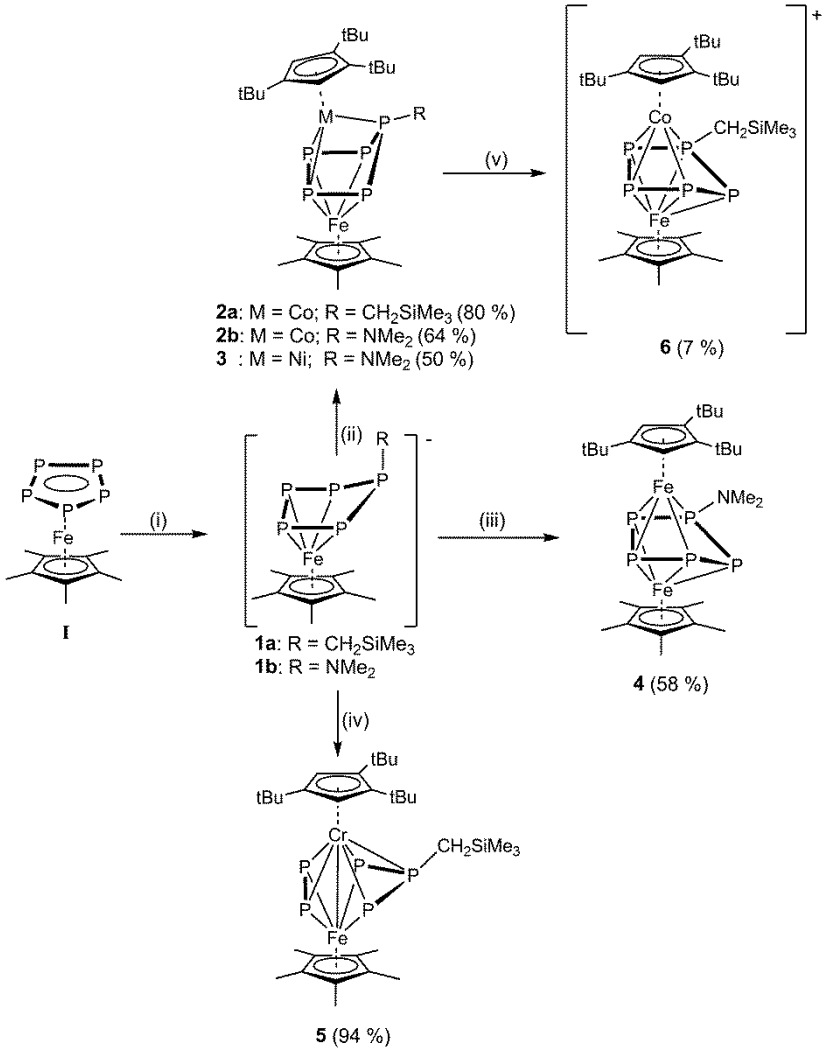

Scheme 1. Reactions of **I**: (i) $LiCH_2SiMe_3$ in Et_2O or $LiNMe_2$ in THF, r.t.; reaction of **1a**: (ii) $[Cp'''CoCl]_2$ in THF, r.t., (iv) $[Cp'''CrCl]_2$ in THF, r.t.; reaction of **1b**: (ii) $[Cp'''CoCl]_2$ or $[Cp'''NiBr]_2$ in THF, r.t.; (iii) $[Cp'''FeBr]_2$ in THF, r.t.; reaction of **2a**: (v) $[Cp_2Fe][PF_6]$ in THF, −50 °C → r.t; yields are given in parenthesis.

The reaction of **1a**/**1b** with the transition metal dimers $[Cp'''MX]_2$ (M = Cr, Fe, Co, Ni; X = Cl, Br) leads to the formation of the triple-decker complexes **2** – **5** which have been isolated in good yields (Scheme 1). Despite several efforts we were not able to synthesize the missing manganese containing

triple-decker complex in this series. In contrast to the diamagnetic compounds **3** – **5**, the obtained cobalt/iron triple-decker **2a**/**2b** are paramagnetic. The EPR spectra of **2a** and **2b** in toluene at 77 K show an isotropic signal for both compounds, centered at g_{iso} = 2.069 and 2.076, respectively, without hyperfine coupling. The determination of the effective magnetic moment of **2a** and **2b** in solution, by the Evans method, results in one unpaired electron (**2a**: μ_{eff} = 1.94 μ_B; **2b**: μ_{eff} = 1.62 μ_B). As DFT calculations on the B3LYP/def2-SVP level of theory show, the single-occupied molecular orbitals (SOMO) of **2a** and **2b** are very similar, indicating the minor influence of the substituent of the *cyclo*-P_5 ring on the properties of the SOMO.[14] All SOMOs are delocalized, but the analysis of the spin density reveals, that the metal center bonded to the Cp''' ligand exhibits the highest spin density. The calculated atomic spin densities of **2a**/**2b** show, that the Co atom possesses the highest positive spin density (circa 62 %), followed by the Fe atom (circa 19 %).

In the ^{31}P NMR spectrum of the isolated nickel/iron triple-decker complex **3** an AXX'ZZ' spin system is monitored, with one triplet of triplets centered at 40.6 ppm and two multiplets centered at −30.29 and −53.9 ppm. For the isolated iron/iron triple-decker complex **4** in the ^{1}H NMR spectrum only sharp signals are determined. However, in contrast to the triple-decker complex **3**, in the ^{31}P NMR spectrum of compound **4** one sharp signal at 73.8 ppm, one broad signal at −131.1 ppm and one very broad signal at −150.8 ppm are observed. By cooling down the sample to 193 K in the ^{31}P NMR spectrum five broad signals in a 1:1:1:1:1 integral ratio are monitored, centered at 65.8, 42.2, −104.5, −195.0 and −344.9 ppm, which reveal a dynamic process of the P_5 ring. The signals of the Cp''' ligand in the ^{1}H NMR spectrum at 193 K become very broad, showing that the free rotation of the cyclopentadienyl ligand is slowed down. When **1a** is reacted with $[Cp'''CrCl]_2$ in the ^{31}P NMR spectrum of the reaction solution a broad doublet of doublets at 281.11, one broad doublet at 9.5 ppm and a triplet of triplets at −66.7 ppm are determined for the chromium/iron triple-decker complex **5**. Also one set of signals of an unknown byproduct are observed (in about 13%), but **5** can be isolated and purified further by recrystallization. By cooling down the sample of **5** in the ^{31}P NMR spectrum at 253 K the signals become sharp and a fine structure is monitored.[14] The simulation of this spectrum reveals unusual coupling constants: The $^1J_{P\text{-}P}$ coupling (P2-P3) between the P_2 dumbbell and the P_3 allylic moiety is considerably small, with a coupling of only 22.65 Hz. This is consistent with the corresponding P-P distance which is elongated (*vide infra*). The $^2J_{P\text{-}P}$ coupling (P1-P3) is comparably larger with a value of about 100 Hz. Usually the absolute value of a $^1J_{P\text{-}P}$ coupling is significantly higher compared to a $^2J_{P\text{-}P}$ coupling, as it is observed in **3** or the starting materials **1a**/**1b**. This unusual behavior may originate from the orbital interaction between the phosphorus atoms via the metal centers (as it is seen in the HOMO-3,[14] which has contributions from the atomic orbitals of the P1, Cr and Fe atom, respectively and the orbital of the P3-P4 unit).

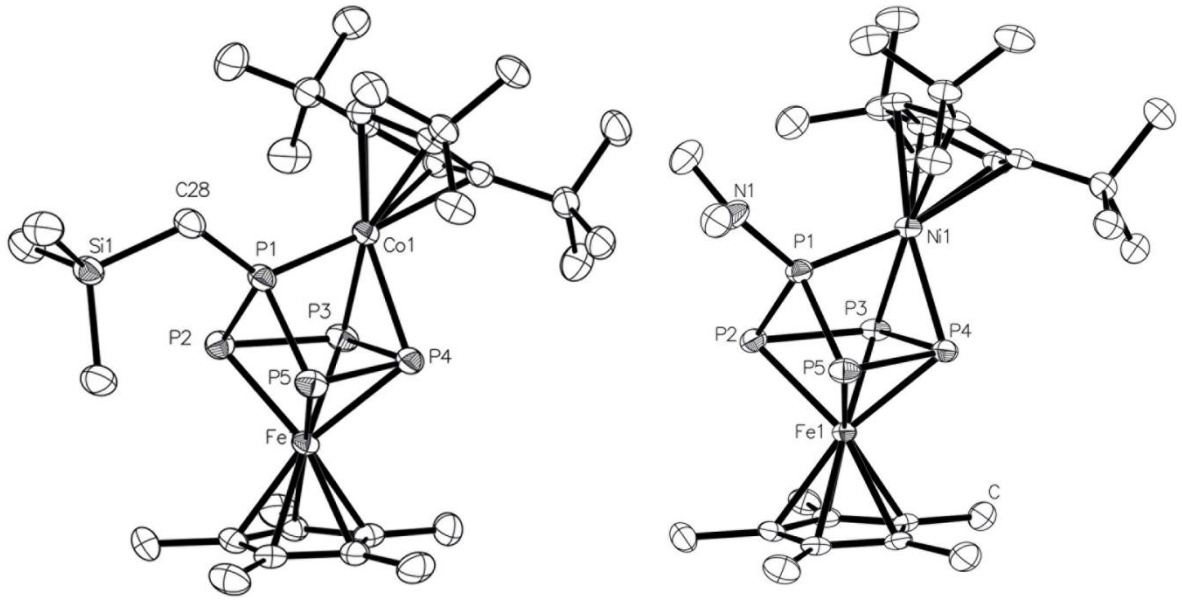

Figure 1. Molecular structure of **2a** (left) and **3** (right). Ellipsoids are drawn at 50% probability level. H atoms bonded to carbon are omitted for clarity.

Compounds **2** − **5** could all be characterized by X-ray structure analysis. The triple-decker complexes **2a**, **2b** and **3** exhibit a similar structural motif, in which the P_5 ligand adopts a $\eta^{4:3}$-coordination mode (Figure 1). Compared to **1a**/**1b**, in **2a**/**2b** and **3** the enveloped conformation of the P_5 unit becomes more distinct, with three of the five phosphorus atoms (P1, P3, P4; labeling according to Figure1) coordinating to the Cp''' metal fragment. The phosphorus atom, which doesn't lie in the η^4-P_4 plane still bears the organic rest. In **1a**/**1b** all P-P bonds of the P_5 ring exhibit double bond character. In the triple-decker sandwich complex **2a** the P-P bond lengths range from 2.1771(7) Å to 2.3530(7) Å. Compounds **2b** and **3** show similar values (**2b**: 2.1569(8) – 2.4132(8) Å; **3**: 2.1620(7) – 2.4739(7) Å; Table 1) . Particularly noticeable is the P-P bond (P3-P4) in the backbone of the P_5 ring of **2a**, **2b** and **3**. (P3-P4 bond length in **2a**: 2.3530(7) Å; **2b**: 2.4132(8) Å; **3**: 2.4738(7) Å). The corresponding Wiberg bond indexes (WBI) values for these bonds are 0.70, 0.67 and 0.51 for **2a**, **2b**, and **3**, respectively. The elongation of this P-P bond, by going from **2a** to **3**, is in line with the increased electron density in the P_5 moiety (compound **2a** features a CH_2SiMe_3 group, exhibiting a *+I* effect; compound **2b** features an NMe_2 group exhibiting *+M* effect; compound **3** contains one additional electron due the exchange of the cobalt with a nickel atom). Furthermore, in **2b** and **3** the NMe_2 group is planar with the sum of the angles around nitrogen of 360° (in **2a**: 359.99°; in **3**: 359.96°) and the N-P bond possesses double bond character (**2b**: 1.665(2); **3**: 1.671(2) Å), which represents the donating character of the NMe_2 group in these compounds. The WBI values for the Co1-P1 bond order in **2b** (0.67) decreases upon introduction of the more electronegative NMe_2 substituent on the P1 atom, compared to **2a** (0.75). The Mulliken charges in **2a** and **2b** are very similar, nevertheless.[14]

Table 1. Comparison of P-P bond lengths of the complexes **2a** – **8**; experimental values (top) and computed values (bottom).

	P1-P2 (Å)	P1-P5 (Å)	P2-P3 (Å)	P3-P4 (Å)	P4-P5 (Å)
2a: [(Cp*Fe)(Cp'''Co)(μ,$\eta^{4:3}$-$P_5CH_2SiMe_3$)]	2.1928(7)	2.1771(7)	2.1911(7)	2.3530(7)	2.1790(7)
computed	2.212	2.214	2.208	2.344	2.215
2b: [(Cp*Fe)(Cp'''Co)(μ,$\eta^{4:3}$-P_5NMe_2)]	2.1569(8)	2.2004(8)	2.1854(8)	2.4132(8)	2.1855(8)
computed	2.200	2.244	2.198	2.369	2.204
3: [(Cp*Fe)(Cp'''Ni)(μ,$\eta^{4:3}$-P_5NMe_2)]	2.1791(7)	2.1620(7)	2.1738(7)	2.4739(7)	2.1753(7)
computed	2.223	2.196	2.197	2.489	2.196
4: [(Cp*Fe)(Cp'''Fe)(μ,$\eta^{4:4}$-P_5NMe_2)]	2.2063(6)	2.0952(6)	2.3587(6)	2.1054(6)	2.3187(6)
computed	2.220	2.149	2.365	2.175	2.279
5: [(Cp*Fe)(Cp'''Cr)(μ,$\eta^{4:5}$-$P_5CH_2SiMe_3$)]	2.1558(7)	2.1549(6)	2.6328(7)	2.1040(7)	2.6258(7)
computed	2.195	2.198	2.670	2.108	2.682
6: [(Cp*Fe)(Cp'''Co)(μ,$\eta^{5:4}$-$P_5CH_2SiMe_3$)]$^+$	2.1089(5)	2.1986(5)	2.2811(5)	2.1045(5)	2.2715(5)
7: [(Cp*Fe)(Cp'''Co)(μ,$\eta^{5:4}$-P_5)]	2.148 (2)	2.142 (2)	2.236 (2)	2.121 (2)	2.242 (2)
computed	2.186	2.187	2.254	2.161	2.255
8: [(Cp*Fe)(Cp'''Fe)(μ,$\eta^{5:4}$-P_5)]	2.153(3)	2.141(3)	2.203(3)	2.126(3)	2.193(3)
computed	2.180	2.181	2.217	2.154	2.217

In comparison to **2a**, **2b** and **3**, in **4** the conformation of the P_5 ring changes (Figure 2). Due to a distortion of the phosphorus ring the Fe2-P5 bond (2.6313(5) Å) is elongated (remaining Fe-P bond lengths in **4**: 2.1362(5) – 2.4690(5) Å, Figure 2), thus the coordination of the P_5 ligand is best described with a $\eta^{4:4}$-coordination mode. Furthermore, the enveloped P_5 ring is bent towards the Cp*Fe fragment − instead towards the Cp'''M fragment, as observed in the former discussed triple−decker sandwich complexes. The phosphorus atom which bears the dimethylamine rest lies within a distorted η^4-P_4 plane. In comparison to **2a**, **2b** and **3** the P2-P3 (2.3587(6) Å) and P4-P5 (2.3187(6) Å) bonds are considerably longer in **4** (Table 1) and the P3-P4 bond exhibits double bond character in **4** (2.1054(6) Å). If the P_5 moiety is coordinating to the electron deficient Cp'''-chromium metal fragment a variety of structural changes are observed for **5**. The *cylco*-P_5 ring in **5** is broken into a P_2 dumbbell (P3-P4: 2.1040(7) Å; labeling according to Figure 2) and a P_3 fragment (P1-P5: 2.1549(6) Å; P1-P2: 2.1558(7) Å), while a Fe-Cr bond (2.6252(4) Å) is formed. The WBI of the P2-P3 and P4-P5 distances (0.22 each), reflects the P_2/P_3 separation of the former P_5 ring. Compared to the Cr-Fe bond length in [$CpFe(CO)_2Cr(CO)_3Cp$] (2.901(1) Å)[15] or in [(CpCr)(CpFe)($\eta^{4:4}$-oct)] (oct = cyclooctatetraen), (2.7261(8) Å),[16] the metal-metal bond in **5** is shortened. The WBI for the Cr-Fe

bond equals to 0.45, which is considerably larger in comparison to the M-M WBI of the previously discussed triple-decker compounds **2a** – **3** (0.12 − 0.14).

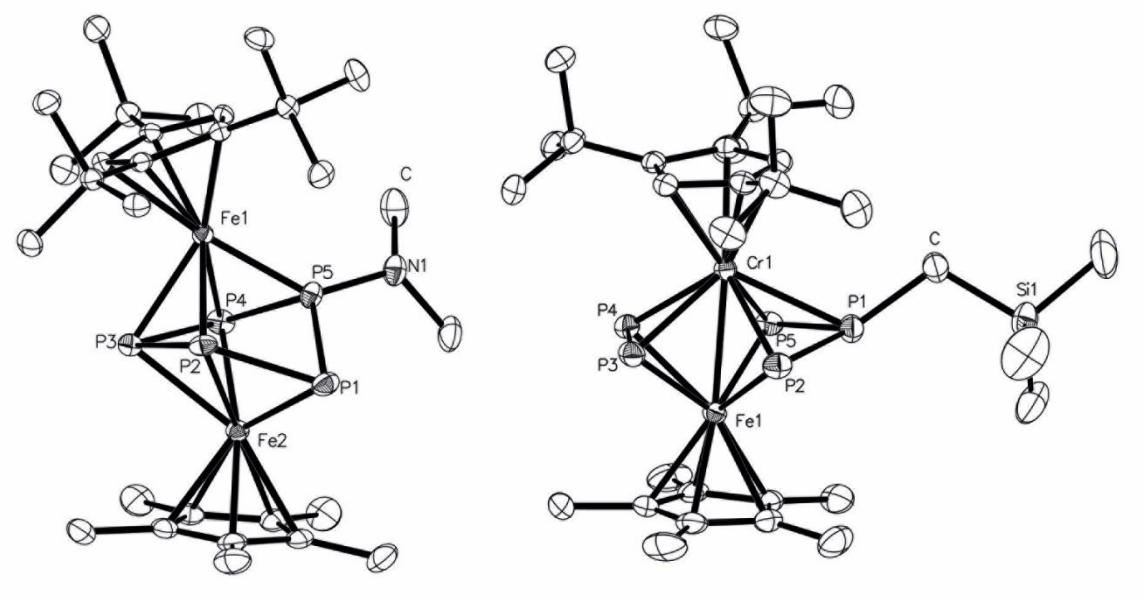

Figure 2. Molecular structure of **4** (left) and **5** (right). Ellipsoids are drawn at 50% probability level. H atoms bonded to carbon are omitted for clarity.

The iron/nickel and iron/iron containing complexes **3** and **4** are stable and formally only differ by one electron in comparison to the iron/cobalt containing triple-decker complexes **2a**/**2b**. Therefore the electrochemical properties of **2a/2b** were investigated. The cyclic voltammogram of **2a** in CH_2Cl_2 shows two oxidations and one reduction (Figure 3). The first oxidation occurs at a half potential of −0.79 V and exhibits reversible character ($\boldsymbol{i}_{p(reverse)}/\boldsymbol{i}_{p(forward)}$ = 0.82).[17] The second oxidation at 0.39 V is considered irreversible. At −1.67 V a reversible reduction is observed ($\boldsymbol{i}_{p(reverse)}/\boldsymbol{i}_{p(forward)}$ = 0.98).

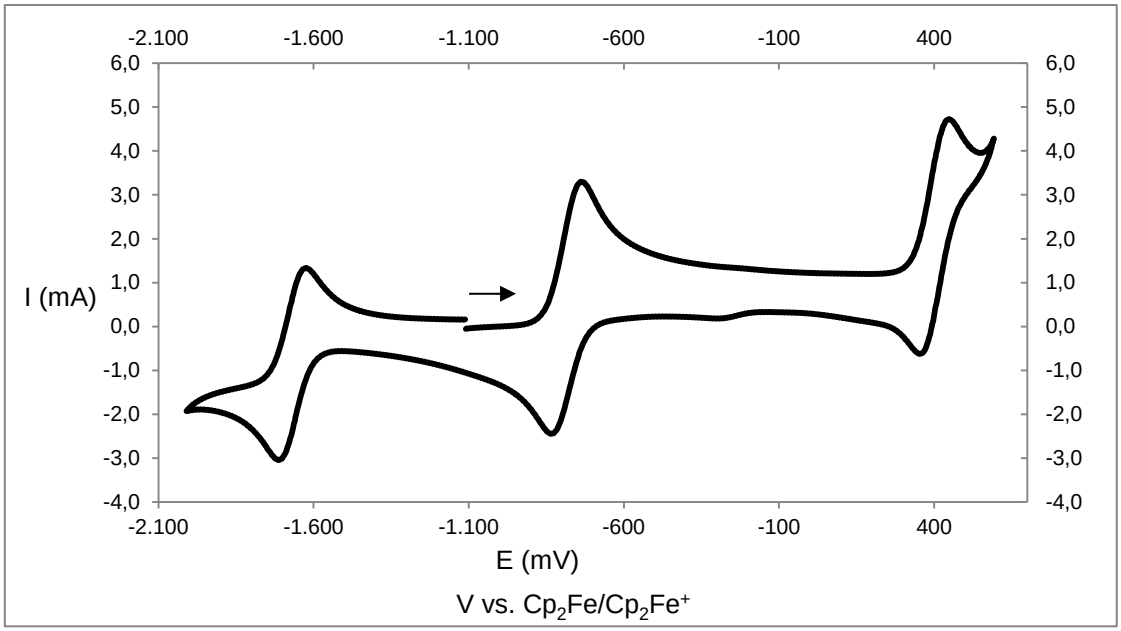

Figure 3. Cyclic voltammogram of **2a** recorded at a platinum disc electrode in CH_2Cl_2 at 100 mV/s and referenced against fc/fc$^+$; supporting electrolyte $[Bu_4N][PF_6]$ (0.1 mol/L).

The cyclic voltammogram of **2b** exhibits similar features, with one reversible oxidation at −0.88 V ($\boldsymbol{i}_{p(reverse)}/\boldsymbol{i}_{p(forward)}$ = 0.98) and a following irreversible one at 0.39 V.[17] A reversible reduction is observed at −1.61 V ($\boldsymbol{i}_{p(reverse)}/\boldsymbol{i}_{p(forward)}$ = 0.97). Based on these studies we choose the oxidizing agents $[Cp_2Fe][PF_6]$ for the chemical oxidization of **2a** , which has a half potential of −0.59 V against fc/fc$^+$ in MeCN.[18] Contrary to the expectation that $[(Cp^*Fe)(Cp'''Co)(\mu,\eta^{4:3}\text{-}P_5CH_2SiMe_3)]^+$ (**6**) should be diamagnetic in analogy to **4**, in the ^{31}P NMR spectrum of the reaction solution of **2a** with $[Cp_2Fe][PF_6]$ only signals of low intensity for some minor impurities are determined, as well as a septet centered at −140.4 ppm for the $[PF_6]^-$ ion. However, the EPR spectrum of **6** at 298 K shows an isotropic signal centered at g_{iso} = 2.013.[19] A few single crystal of [**6**][PF_6] could be obtained from a Et_2O solution. The X-ray structure analysis reveals that **6** is not just isoelectronical to the triple-decker complex $[(Cp^*Fe)(Cp'''Fe)(\mu,\eta^{5:4}\text{-}P_5NMe_2)]$ (**4**), but that **2a** also undergoes a structural rearrangement during the oxidation, resulting in **6** to be isostructural to **4** (Figure 4). The phosphorus atom, which bears the organic rest and was out of the η^4-P_4 plane in **2a**, swaps hereby position with an unsubstituted phosphorus atom from the η^4-P_4 plane. Unfortunately we were not able to isolate any reduced products, by using K or KH as reducing agents.

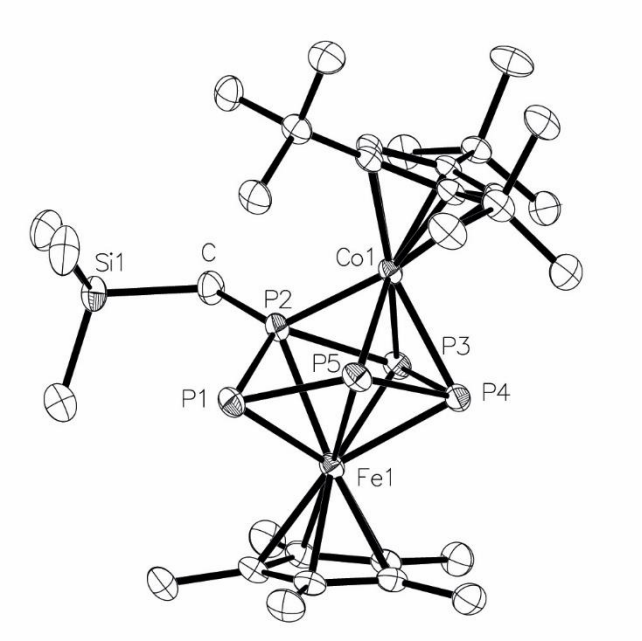

Figure 4. Molecular structure of cationic part of [**6**][PF_6]. Ellipsoids are drawn at 50% probability level. H atoms bonded to carbon are omitted for clarity.

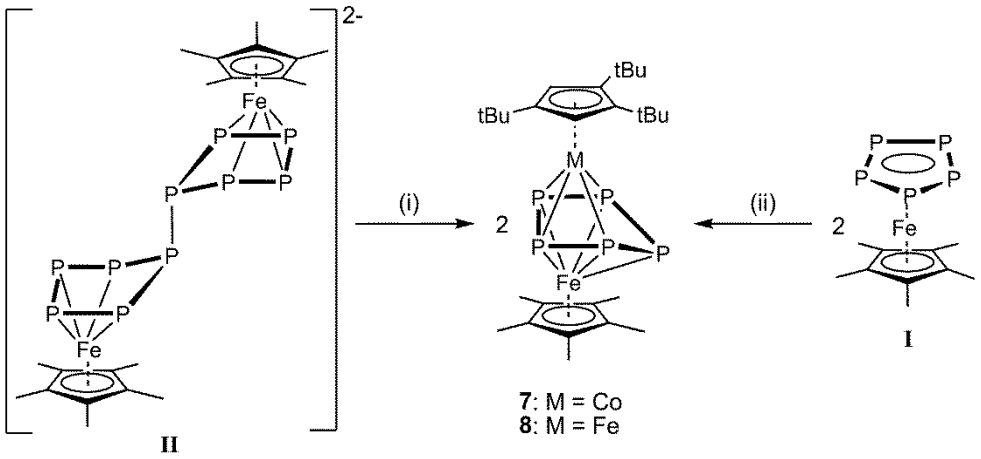

Scheme 2. Reaction of **II**: (i) $[Cp'''CoCl]_2$ or $[Cp'''FeBr]_2$ in THF, r.t.; reaction of **I**: (ii) $[(Cp'''Co)_2(\mu,\eta^{4:4}\text{-}C_6H_8)]$ in THF, r.t.

By reducing the pentaphosphaferrocene **I** with potassium hydride the dianionic compound $[(Cp^*Fe)_2(\mu,\eta^{4:4}\text{-}P_{10})]^{2-}$ (**II**) is accessible in high yields, exhibiting a P_{10} ligand.[9a] Bearing the previously shown salt eliminations in mind, the question arises, if a similar reactivity is observed by reacting **II** with [Cp'''MX] (M = Fe, Co; X = Cl, Br; Scheme 2). Considering the preformed P_{10} unit in **II** the coordination of two Cp'''M metal fragments would be expected. However, the P-P bond which links the two P_5 moieties breaks and the neutral and unsubstituted triple-decker complexes $[(Cp^*Fe)(Cp'''M)(\mu,\eta^{5:4}\text{-}P_5)]$ (**7**: M = Co; **8**: M = Fe) are obtained. The ^{31}P NMR spectrum of the isolated compound **7** shows only one very broad signal at −132.9 ppm at room temperature. By cooling down the sample to 213 K three sharp signals are observed at 289.0 (triplet), −206.5 (multiplet) and −249.7 (multiplet) ppm, respectively, with coupling patterns similar to those determined for **1a**/**1b**, which are characteristic for an enveloped *cyclo*-P_5 ligand. The dynamic of the phosphorus ring is hereby comparable with the previously discussed iron/iron triple-decker complex **4**. In addition, **7** could also be synthesized by reacting **I** with $[(Cp'''Co)_2(\mu,\eta^{4:4}\text{-}C_7H_8)]$. By adding **II** to $[Cp'''FeBr]_2$ the neutral triple-decker complex $[(Cp^*Fe)(Cp'''Fe)(\mu,\eta^{5:4}\text{-}P_5)]$ (**8**) is isolated. For the paramagnetic compound **8** the determination of the effective magnetic moment in solution by the Evans method results in roughly one unpaired electron (μ_{eff} = 1.0 μ_B). The EPR spectrum of **8** in C_6D_6 at 77 K shows an isotropic signal centered at g_{iso} = 2.047. No hyperfine coupling was observed in the EPR spectrum. The LIFDI mass spectrum of **7** and **8** shows the molecular ion peak at m/z = 638.2 and 635.1, respectively. The structure of these products could be determined by single crystal X-ray diffraction (Figure 5).

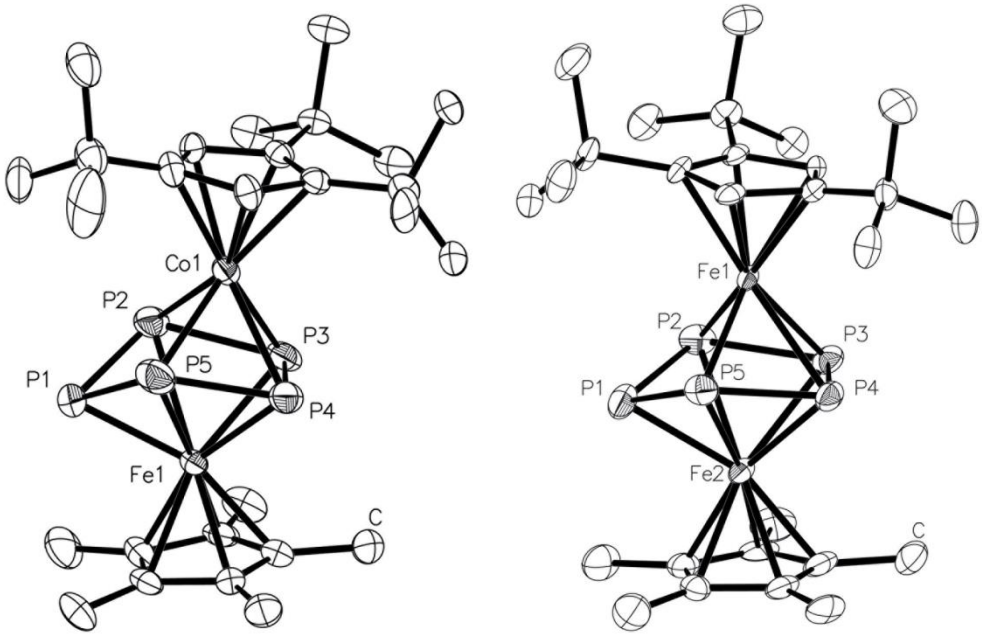

Figure 5. Molecular structure of **7** (left) and **8** (right). Ellipsoids are drawn at 50% probability level. H atoms bonded to carbon are omitted for clarity.

As proposed by the ^{31}P NMR spectrum of **7** at low temperature, the intact P_5 ring exhibits in both **7** and **8** an enveloped conformation. This is in contrast to the known cationic compounds $[(CpFe)(Cp^{+}Fe)(\mu,\eta^{5:5}\text{-}P_5)][PF_6]$ (Cp^{+} = ethyl-tetramethylcyclopentadienyl) and $[(CpFe)(Cp^{*}Ru)(\mu,\eta^{5:5}\text{-}P_5)][BF_4]$, which exhibit a planar *cyclo*-P_5 middle deck.[12a,20] In contrast to **2a**/**2b** the Cp''' Co fragment in **7** coordinates the P_5 ligand in a η^4-fashion and the *cyclo*-P_5 ring is bent towards the Cp* Fe fragment. Three P-P bond lengths exhibit double bond character (P1-P5 2.142(2) Å, P1-P2 2.148(2) Å, P3-P4 2.121(2) Å)[21] and two bonds are elongated (P2-P3 2.236(2) Å, P4-P5 2.242(2) Å). The P-P bond lengths in **8** (2.126(3) − 2.203(3) Å) exhibit values between a P-P single and a P-P double bond, featuring a structural motif similar to **7**.

In summary, we were able to introduce subsequent chemistry to the functionalized pentaphosphaferrocenes. By reacting them with transition metal halide dimers various neutral triple-decker sandwich complexes with a functionalized *cyclo*-P_5 middle deck were synthesized. Triple-decker compounds with an unsubstituted *cyclo*-P_5 middle deck could be obtained by using the reduced, dianionic compound $K_2[(Cp^{*}Fe)_2(\mu,\eta^{4:4}\text{-}P_{10})]$ as a starting material for similar reactions.

Acknowledgments

The authors want to thank Dr. M Walter, from the Technical University of Braunschweig, for providing samples of $[Cp'''MnI]_2$.

References:

[1] a) C. Ornelas, *New J. Chem.* **2011**, *35*, 1973-1985; b) R. Gómez Arrayás, J. Adrio, J. C. Carretero, *Angew. Chem. Int. Ed.* **2006**, *45*, 7674-7715; c) X. Zhai, H. Yu, L. Wang, Z. Deng, Z.-u. Abdin, R. Tong, X. Yang, Y. Chen, M. Saleem, *Appl. Organomet. Chem.* **2016**, *30*, 62-72.

[2] a) T. J. Kealy, P. L. Pauson, *Nature* **1951**, *168*, 1039-1040; b) S. A. Miller, J. A. Tebboth, J. F. Tremaine, *J. Chem. Soc.* **1952**, 632-635.

[3] a) M. Rausch, M. Vogel, H. Rosenberg, *J. Org. Chem.* **1957**, *22*, 900-903; b) R. A. Benkeser, D. Goggin, G. Schroll, *J. Am. Chem. Soc.* **1954**, *76*, 4025.

[4] a) G. P. Sollott, E. Howard, *J. Org. Chem.* **1962**, *27*, 4034-4040; b) G. D. Broadhead, J. M. Osgerby, P. L. Pauson, *J. Chem. Soc.* **1958**, 650-656.

[5] O. J. Scherer, T. Brück, *Angew. Chem. Int. Ed.* **1987**, *26*, 59-59.

[6] a) O. J. Scherer, J. Vondung, G. Wolmershäuser, *Angew. Chem. Int. Ed.* **1989**, *28*, 1355-1357; b) M. Fleischmann, S. Welsch, H. Krauss, M. Schmidt, M. Bodensteiner, E. V. Peresypkina, M. Sierka, C. Gröger, M. Scheer, *Chem. Eur. J.* **2014**, *20*, 3759-3768; c) S. Welsch, L. J. Gregoriades, M. Sierka, M. Zabel, A. V. Virovets, M. Scheer, *Angew. Chem. Int. Ed.* **2007**, *46*, 9323-9326; d) M. Scheer, L. J. Gregoriades, A. V. Virovets, W. Kunz, R. Neueder, I. Krossing, *Angew. Chem. Int. Ed.* **2006**, *45*, 5689-5693; e) J. Bai, A. V. Virovets, M. Scheer, *Angew. Chem. Int. Ed.* **2002**, *41*, 1737-1740.

[7] a) J. Bai, A. V. Virovets, M. Scheer, *Science* **2003**, *300*, 781-783; b) M. Scheer, J. Bai, B. P. Johnson, R. Merkle, A. V. Virovets, C. E. Anson, *Eur. J. Inorg. Chem.* **2005**, *2005*, 4023-4026; c) M. Scheer, A. Schindler, J. Bai, B. P. Johnson, R. Merkle, R. Winter, A. V. Virovets, E. V. Peresypkina, V. A. Blatov, M. Sierka, H. Eckert, *Chem. Eur. J.* **2010**, *16*, 2092-2107; d) M. Scheer, A. Schindler, C. Gröger, A. V. Virovets, E. V. Peresypkina, *Angew. Chem. Int. Ed.* **2009**, *48*, 5046-5049; e) M. Scheer, A. Schindler, R. Merkle, B. P. Johnson, M. Linseis, R. Winter, C. E. Anson, A. V. Virovets, *J. Am. Chem. Soc.* **2007**, *129*, 13386-13387.

[8] a) M. Detzel, T. Mohr, O. J. Scherer, G. Wolmershäuser, *Angew. Chem.* **1994**, *106*, 1142-1144; b) O. J. Scherer, T. Mohr, G. Wolmershäuser, *J. Organomet. Chem.* **1997**, *529*, 379-385; c) B. Koch, O. J. Scherer, G. Wolmershäuser, *Z. Anorg. Allg. Chem.* **2000**, *626*, 1797-1802; d) O. J. Scherer, *Acc. Chem. Res.* **1999**, *32*, 751-762.

[9] a) M. V. Butovskiy, G. Balázs, M. Bodensteiner, E. V. Peresypkina, A. V. Virovets, J. Sutter, M. Scheer, *Angew. Chem. Int. Ed.* **2013**, *52*, 2972-2976; b) T. Li, J. Wiecko, N. A. Pushkarevsky, M. T. Gamer, R. Köppe, S. N. Konchenko, M. Scheer, P. W. Roesky, *Angew. Chem. Int. Ed.* **2011**, *50*, 9491-9495; c) T. Li, M. T. Gamer, M. Scheer, S. N. Konchenko, P. W. Roesky, *Chem. Commun.* **2013**, *49*, 2183-2185.

[10] E. Mädl, M. V. Butovskii, G. Balázs, E. V. Peresypkina, A. V. Virovets, M. Seidl, M. Scheer, *Angew. Chem. Int. Ed.* **2014**, *53*, 7643-7646.

[11] a) S. Heinl, G. Balazs, M. Bodensteiner, M. Scheer, *Dalton Trans.* **2016**, *45*, 1962-1966; b) O. J. Scherer, J. Schwalb, G. Wolmershäuser, W. Kaim, R. Gross, *Angew. Chem. Int. Ed.* **1986**, *25*, 363-364; c) L. Y. Goh, R. C. S. Wong, C. K. Chu, T. W. Hambley, *J. Chem. Soc., Dalton Trans.* **1990**, 977-982.

[12] a) Alexander R. Kudinov, Dmitry A. Loginov, Zoya A. Starikova, Pavel V. Petrovskii, M. Corsini, P. Zanello, *Eur. J. Inorg. Chem.* **2002**, *2002*, 3018-3027; b) D. A. Loginov, I. D. Baravi, O. I. Artyushin, Z. A. Starikova, P. V. Petrovskii, A. R. Kudinov, *Russ. Chem. Bull.* **2010**, *59*, 1312-1316.

[13] B. Rink, O. J. Scherer, G. Heckmann, G. Wolmershauser, *Chem. Ber.* **1992**, *125*, 1011-1016.

[14] cf. supplementary information.

[15] W. A. Herrmann, J. Rohrmann, E. Herdtweck, C. Hecht, M. L. Ziegler, O. Serhadli, *J. Organomet. Chem.* **1986**, *314*, 295-305.

[16] J. Heck, P. Maurice, J. A. Hermans, A. B. Scholten, W. P. J. H. Bosman, G. Meyer, T. Staffel, R. Stürmer, M. Wünsch, *Z. Anorg. Allg. Chem.* **1992**, *611*, 35-42.

[17] referenced against ferrocene.

[18] N. G. Connelly, W. E. Geiger, *Chem. Rev.* **1996**, *96*, 877-910.

[19] calculations regarding the spin density of **6** are performed at the moment, to investigate the unexpected paramagnetetism and were not yet completed by the end of this thesis.

[20] O. J. Scherer, T. Brück, G. Wolmershäuser, *Chem. Ber.* **1989**, *122*, 2049-2054.
[21] P-P bond lengths were taken from one of the five molecules of the asymmetric unit.

5.2 Supporting Information

Supporting information of the manuscript entitled:

Triple-decker sandwich complexes with a bent *cyclo*-P_5 middle deck

Contents

General Procedures: All manipulations were performed with rigorous exclusion of oxygen and moisture in Schlenk-type glassware on a dual manifold Schlenk line in argon atmosphere or in Ar filled glove box with a high-capacity recirculator (<0.1ppm O_2). THF, toluene, hexane, and DME were distilled from sodium benzophenoneketyl. Deuterated solvents were degassed, dried and distilled prior to use. The complex [Cp*Fe(η^5-P_5)] (**I**), [Li][**1a**] and [Li][**1b**] were prepared according to their published procedures.[1] NMR spectra were recorded on a Bruker Avance 300 MHz and Bruker Avance 400 MHz spectrometers. Chemical shifts were measured at ambient temperature and are given in ppm; they are referenced to TMS for ^{1}H and ^{13}C, and 85 % H_3PO_4 for ^{31}P as external standard. Elemental analyses (CHN) were determined using in-house facility. The X-Band EPR measurements were carried out with a MiniScope MS400 device with a frequency of 9.44 GHz and a rectangular resonator TE102 of the company Magnettech GmbH.

The magnetic susceptibility χ_M and the effective magnetic moment μ_{eff} for **2a** and **8** was determined on a Bruker Avance 400 MHz spectrometer (^{1}H: 400.130 MHz) by Evans method (equations (1) and (2)),[2] neglecting the diamagnetic contributions. Pure solvent was used as an internal reference.

Equation:

$$\chi_M = \frac{3 \cdot \Delta f}{1000 \cdot f \cdot c} \qquad (1)$$

$$\mu_{eff} = 798 \cdot \sqrt{T \cdot \chi_M} \qquad (2)$$

χ_M: molar susceptibility of the sample in $m^3 \cdot mol^{-1}$.

Δf: chemical shift difference between solvent in presence of paramagnetic solute and pure solvent in Hz.

f: operating frequency of NMR spectrometer in Hz.

c: concentration of the paramagnetic sample: 0.01 mol/L

T: absolute temperature in K.

μ_{eff}: effective magnetic moment in μ_B.

5.2.1 Experimental details: complex syntheses and characterization

All transition metal compounds [Cp'''MX]$_2$ (M = Cr, Fe, Co, Ni; X = Cl, Br) were prepared in situ in THF by mixing the MX_2 salt with NaCp''' in the right stoichiometrie and adding the solvent at room temperature. The suspension was stirred overnight, the solvent removed, the product solved in *n*-hexane, filtered through a well dried frit and used for subsequent reactions. As a side note: For the synthesis of [Cp'''CrCl]$_2$ it is important to use very fresh $CrCl_2$, otherwise the reaction is likely to fail.

Synthesis of [2a]: To 234 mg (0.4 mmol) of **1a**·2 Et_2O in 20 mL THF, 130 mg (0.2 mmol) of [Cp'''CoCl]$_2$ in 20 mL THF was added and the solution was stirred overnight. The solvent was removed and **2a** extracted with *n*-hexane, filtered and the solvent removed. **2a** is obtained in 35 % (103 mg) crystalline yield from a CH_2Cl_2 (5 mL) : MeCN (30 mL) mixture at 0 °C, and in 80 % yield (234 mg) as a powder. Single crystals suitable for X-ray measurements could be obtained from a saturated solution of **2a** in MeCN. $C_{31}H_{55}CoFeP_5Si$ (725.50): calcd. C 51.31, H 7.64; found C 51.39, H 7.19. X-band EPR (toluene, 77 K): g_{iso} = 2.069. Evans (C_6D_6, 300 K): μ_{eff} = 1.94 μ_B.

Synthesis of [2b]: To 170 mg (0.3 mmol) of **1b**·2 THF in 20 mL THF, 103 mg (0.15 mmol) of [Cp'''CoCl]$_2$ in 20 mL THF was added and the solution was stirred overnight. The solvent was removed, **2b** extracted with *n*-hexane, filtered and the solvent was concentrated to 5mL. If the last solvent is removed slowly over the course of two weeks **4b** is obtained in 15 % (31 mg) crystalline yield. Higher yields are obtained by isolating **4b** as a powder (64 %, 126 mg), analogue to **4a**. $C_{29}H_{50}CoFeP_5N$ (682.36): calcd. C 51.04, H 7.39, N 2.05; found C 51.12, H 7.32, N 2.16. X-band EPR (toluene, 77 K): g_{iso} = 2.076. Evans (C_6D_6, 300 K): μ_{eff} = 1.62 μ_B.

Synthesis of [3]: To 213 mg (0.3 mmol) of **1b**·3 THF in 20 mL THF, 129 mg (0.15 mmol) of [Cp'''NiBr]$_2$ in 20 mL THF was added and stirred overnight. The solvent was removed and **3** was extracted with *n*-hexane and filtered through a frit. The solution was concentrated to the first precipitation (5 mL) and stored over night at −30 °C. **3** is isolated in 50 % crystalline yield (118 mg). FD-MS: 681.1 (M^+, 100 %). $C_{29}H_{50}FeNiP_5N$ (682.12): calcd. C 51.06, H 7.39, N 2.05; found C 50.99, H 7.42, N 1.93.^{1}H NMR (400.13 MHz, C_6D_6): δ [ppm] = 1.45 (s, 9 H, Cp'''), 1.61 (s, 18 H, Cp'''), 1.68 (s, 15 H, Cp*), 2.107 (d, 6 H, NMe_2), 5.04 (s, 2 H, Cp'''). $^{13}C\{^1H\}$ NMR (100.62 MHz, C_6D_6): δ = 11.5 (s, $C_5(CH_3)_5$), 31.68 (s, $C(CH_3)_3$), 32.26 (s, $C(CH_3)_3$), 33.55 (s, $C(CH_3)_3$), 33.67 (s, $C(CH_3)_3$), 36.32 (t, NMe_2), 90.82 (s, CH), 91.69 (*s*, $C_5(CH_3)_5$), 116.69 (s, *C*-$C(CH_3)_3$), 118.06 (s, *C*-$C(CH_3)_3$). ^{31}P NMR (161.97 MHz, C_6D_6): δ = −53.87 (m, 2 P), −30.28 (m, 2 P), 40.63 (t, 1 P).

Synthesis of [4]: To 180 mg (0.33 mmol) of **1b**·2 THF in 20 mL THF, 245 mg (0.16 mmol) of [Cp'''FeBr]$_2$ in 20 mL THF was added and stirred overnight. The solvent was removed, **4** extracted with *n*-hexane, filtered and the solvent was concentrated to 5 mL and stored over night at −30 °C. **4** is isolated in 58 % crystalline yield (131 mg). $C_{29}H_{50}Fe_2P_5N$ (679.27): calcd. C 51.28, H 7.42, N 2.06; found C 51.34, H 7.47, N 2.36. ^{1}H NMR (400.13 MHz, THF-d_8): δ [ppm] = 1.19 (s, 9 H, Cp'''), 1.42 (s 18 H, Cp'''), 1.62 (s, 15 H, Cp*), 2.51 (d, 6 H, NMe_2), 3.78 (s, 2 H, Cp'''). $^{13}C\{^1H\}$ NMR (100.62 MHz, THF-d_8): δ = 10.74 (s, $C_5(CH_3)_5$), 31.61(s, $C(CH_3)_3$), 32.19 (s, $C(CH_3)_3$), 34.105 (s, $C(CH_3)_3$), 34.34(s, $C(CH_3)_3$), 40.73 (s, NMe_2), 74.76 (s, CH), 85.85 (*s*, $C_5(CH_3)_5$), 103.93(s, *C*-$C(CH_3)_3$), 106.07 (s, *C*-$C(CH_3)_3$). ^{31}P NMR (161.97 MHz, THF-d_8): δ = −151.5 (broad, 2 P), −131.2 (broad, 2 P), 73.75 (s, 1 P).

Synthesis of [5]: To 0.173 mg (0.3 mmol) of **1a**·2 Et_2O in 20 mL THF, 95 mg (0.15 mmol) of [Cp'''CrCl]$_2$ in 20 mL was added and stirred overnight. The solvent was removed, **5** extracted with *n*-hexane, filtered and the solvent was concentrated to 5mL and stored over night at −30 °C. **5** could be isolated in 94 % crystalline yield (100 mg). $C_{31}H_{55}CrFeP_5Si$ (718.56): calcd. C 51.82, H 7.71; found C 51.43, H 7.86. ^{1}H NMR (400.13 MHz, C_6D_6): δ [ppm] = 0.34 (s, 9 H, $SiMe_3$), 1.32 (s, 9 H, Cp'''), 1.49

(s, 18 H, Cp'''), 1.52 (s broad, 15 H, Cp*), 1.58 (s, 2 H, CH_2SiMe_3), 3.41 (s, 1 H, CH), 4.62 (s, 1 H, CH). ^{31}P NMR (161.97 MHz, C_6D_6): δ = −66.73 (tt, 1 P), 9.46 (d broad, 2 P), 281.16 (dd broad, 2 P).

Synthesis of [6][PF_6]: To 300 mg (0.48 mmol) of **1a**·2 Et_2O in THF 130 mg (0.4 mmol) of [Cp_2Fe][PF_6] was added at −50 °C. The mixture was stirred and warmed up to room temperature overnight. The solvent was removed and the residue washed five times with *n*-hexane. **6** is poorly soluble in Et_2O and after the repeatedly extraction with Et_2O, removing of solvent and washing with *n*-hexane, very few crystals of **6**, suitable for single crystal measurement, could be obtained (3 mg, 7 %).

Synthesis of [7]: To 0.112 mg (0.1 mmol) of [K_2(dme)$_3$][(Cp*Fe)$_2$(μ,$\eta^{4:4}$-P_{10})] in 10 mL DME, 73 mg (0.1 mmol) of [Cp'''CoCl]$_2$ in 10 mL DME was added at room temperature and stirred overnight. A color change to dark brown-violet was observed. The solvent was removed, **7** extracted with *n*-hexane, filtered and the solvent was concentrated to 5 mL and stored at −30 °C overnight. **7** could be isolated in 41 % (58 mg) crystalline yield.

Alternative Synthesis:

7 could be alternatively synthesized by adding a solution of 293 mg (0.434 mmol) of [(Cp'''Co)$_2$(μ,$\eta^{4:4}$-C_7H_8)] to a solution of 300 mg (0.876 mmol) of [Cp*Fe(η^5-P_5)] in toluene (10 mL) at room temperature. Traces of impurities were removed by a short column chromatography (8 x 3 cm) on silica, using hexane/toluene (3:1) as eluent. **7** could be obtained in 93 % (514 mg) yield. $C_{27}H_{44}CoFeP_5$ (638.29): calcd. C 50.81, H 6.95; found C 50.97, H 6.90. FD-MS: 638.2 (M^+, 100 %). ^{1}H NMR (400.13 MHz, C_6D_6, 300 K): δ [ppm] = 1.30 (s, 15 H, Cp*), 1.34 (s, 9 H, Cp'''), 1.41 (s, 18 H, Cp'''), 3.72 (s, 2 H, Cp'''). ^{31}P NMR (161.97 MHz, C_6D_6, 193 K): δ = −249.65 (m, 2 P), −206.50 (m, 2 P), 288.9 (m, 2 P).

Synthesis of [8]: To 0.2 mg (0.18 mmol) of [K_2(dme)$_4$][(Cp*Fe)$_2$(μ,$\eta^{4:4}$-P_{10})] in 10 mL DME 128 mg (0.18 mmol) of [Cp'''FeBr]$_2$ in 10 mL DME was added at room temperature and stirred overnight. The solvent was removed, **8** extracted with *n*-hexane, filtered and the solvent was concentrated to 5 mL. By removing the solvent slowly over the course of two weeks **8** could be isolated in 36 % (72 mg) crystalline yield. $C_{27}H_{44}Fe_2P_5$ (635.20): calcd. C 51.05, H 6.98; found C 51.78, H 7.34. FD-MS: 604.3 (**8** − P, 25 %), 635.1 (**8**, 100 %). X-band EPR (C_6D_6, 77 K): g_{iso} = 2.048. Evans (C_6D_6, 300 K): μ_{eff} = 1.0 μ_B.

5.2.2 Experimental and simulated NMR spectra

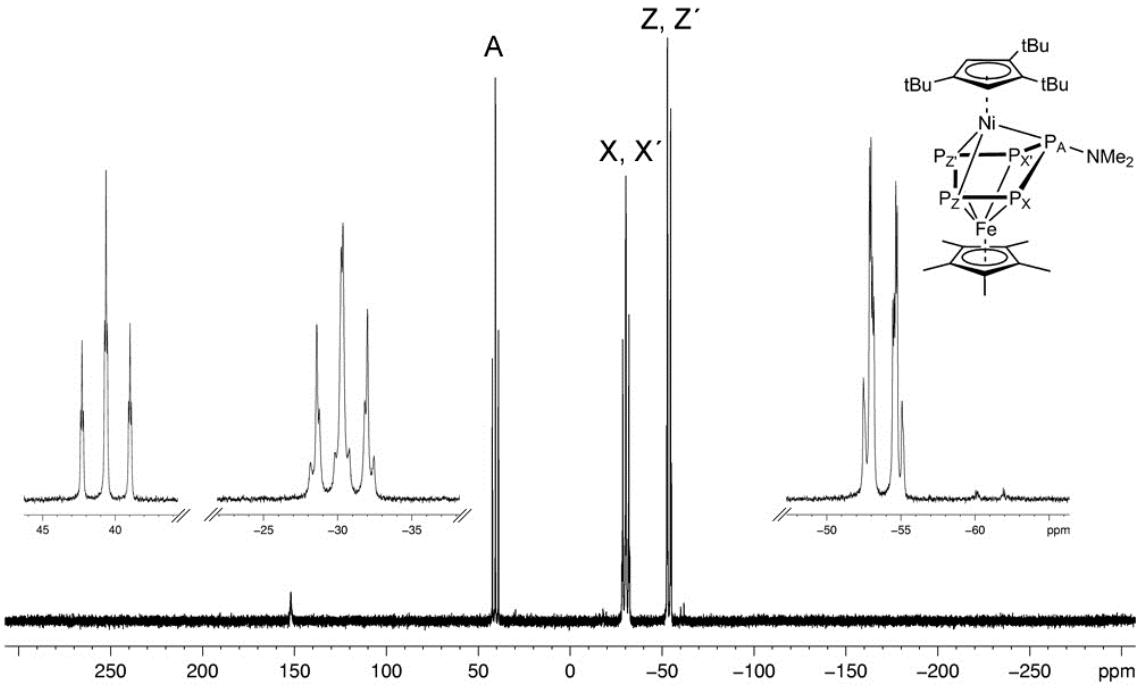

Figure S1. ^{31}P NMR (161.97 MHz, C_6D_6) spectrum of **3**.

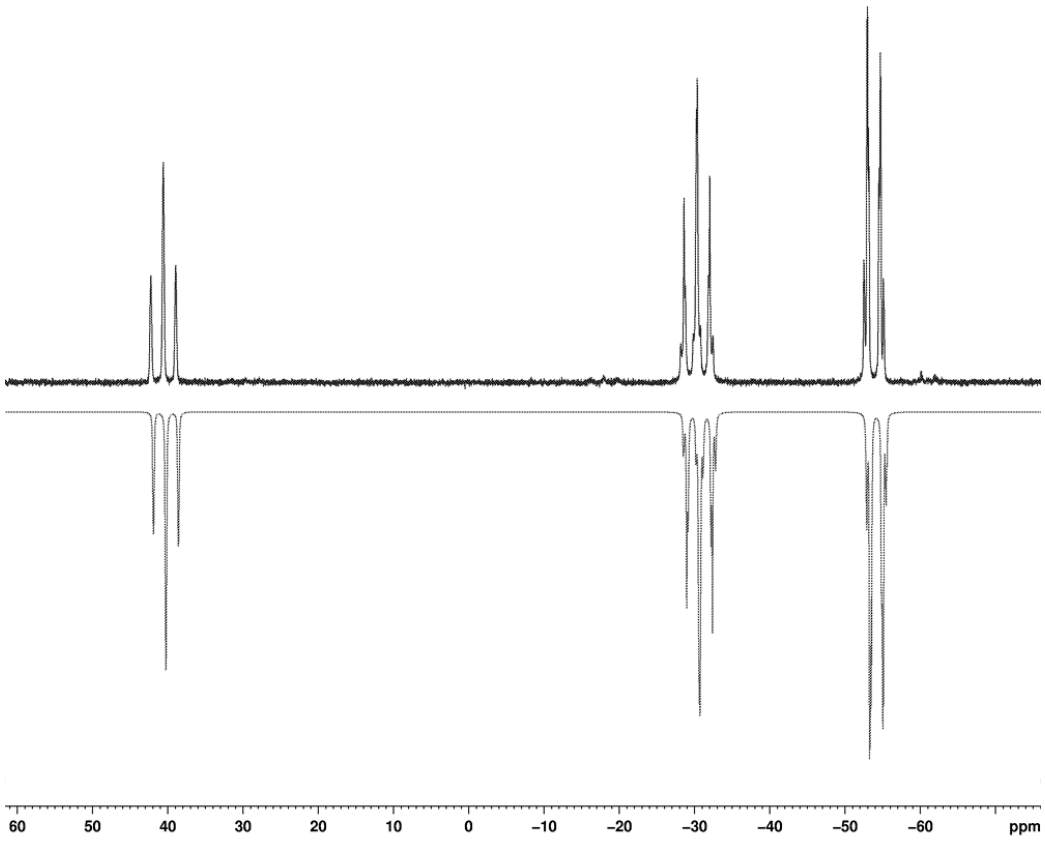

Figure S2. Experimental (top) and simulated (bottom) ^{31}P NMR (161.97 MHz, C_6D_6) spectrum of **3**.

Table S1. ^{31}P NMR chemical shifts and coupling constants for **3** obtained from the simulation.

	J (Hz)			δ (ppm)	
$^1J_{P_A\text{-}P_X}$	269.83	$^1J_{P_X\text{-}P_Z}$	290.36	A, A'	40.61
$^1J_{P_A\text{-}P_{X'}}$	267.89	$^2J_{P_X\text{-}P_{Z'}}$	−17.13	X, X'	30.37
$^2J_{P_A\text{-}P_Z}$	−14.13	$^2J_{P_{X'}\text{-}P_Z}$	−2.62	Z, Z'	−53.79
$^2J_{P_A\text{-}P_{Z'}}$	−17.22	$^1J_{P_{X'}\text{-}P_{Z'}}$	302.00		
$^1J_{P_X\text{-}P_{X'}}$	98.94	$^1J_{P_{Z'}\text{-}P_{Z'}}$	11.08		

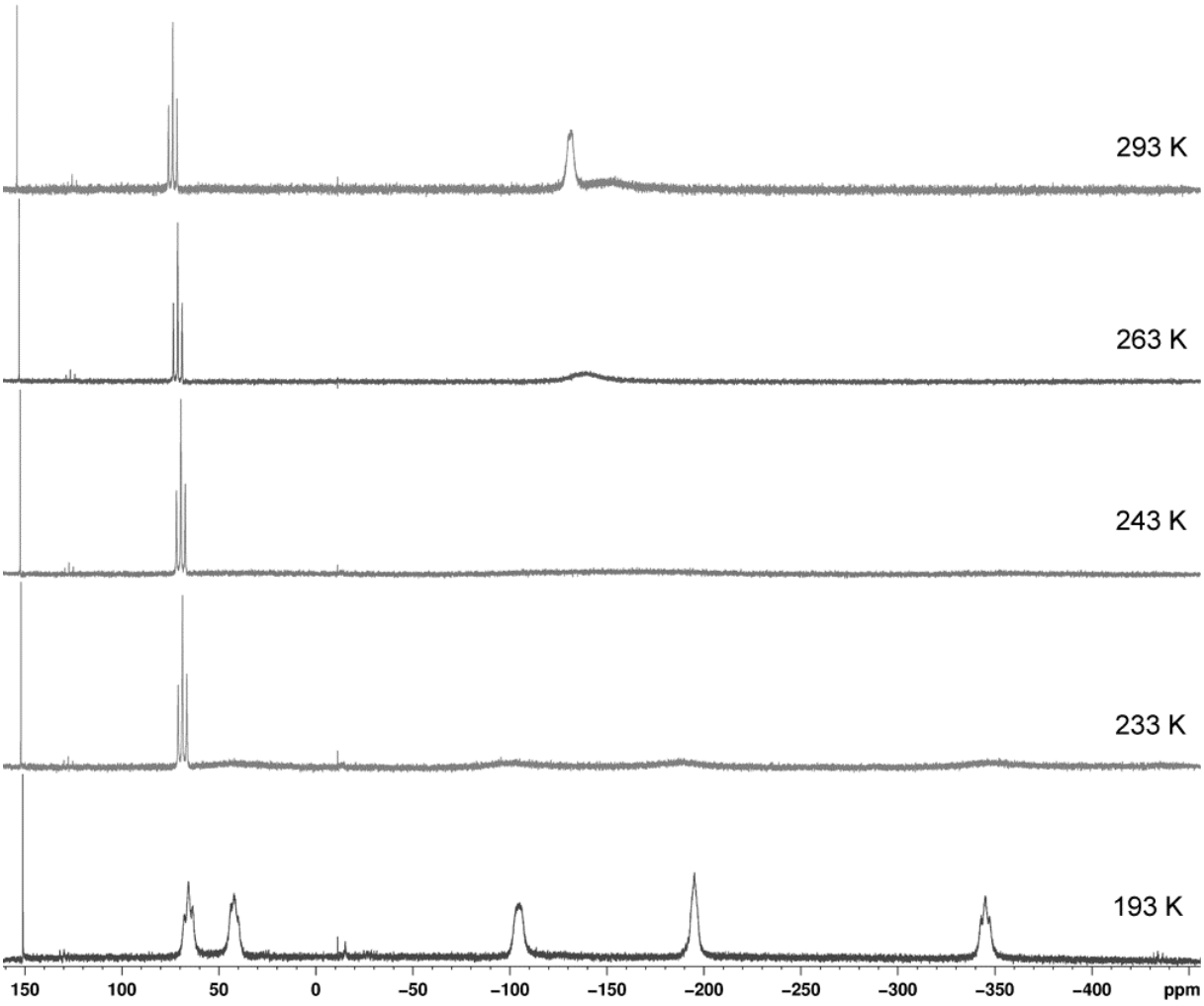

Figure S3. ^{31}P NMR (161.97 MHz, C_6D_6) spectrum of **4** at different temperatures.

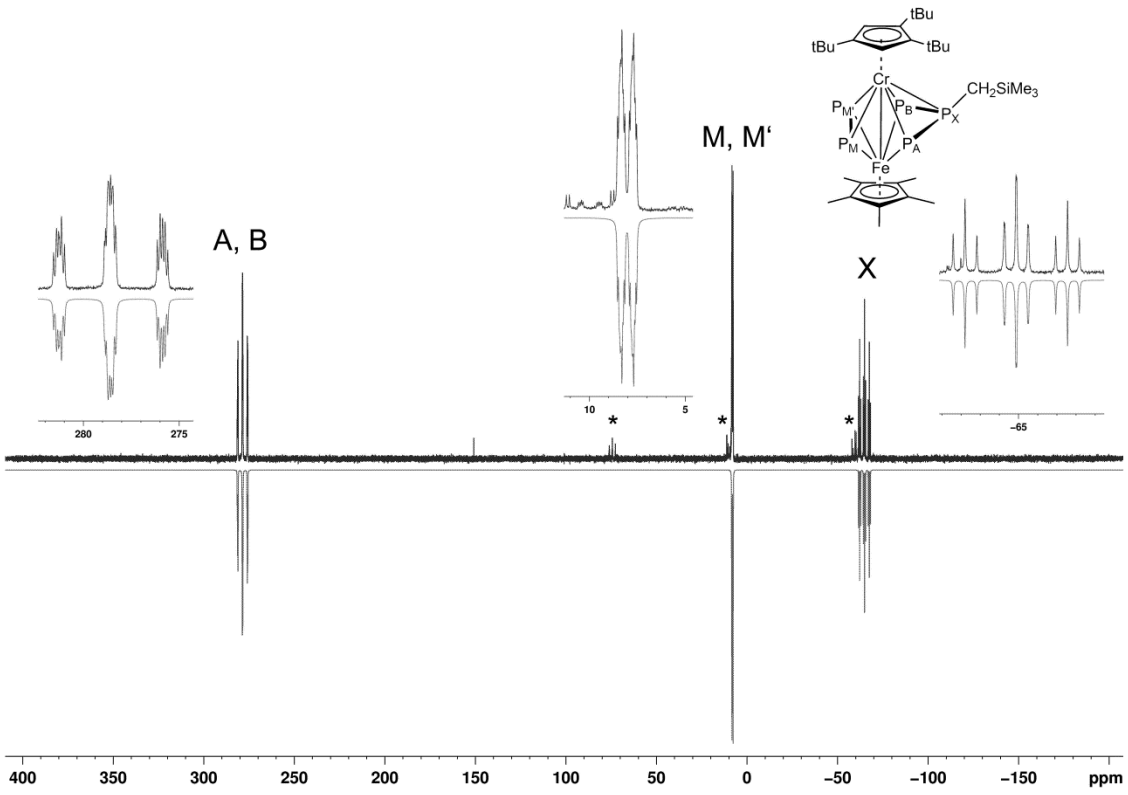

Figure S4. ^{31}P NMR (161.97 MHz, C_6D_6) spectrum of **5** at 253 K. Impurities are marked with *.

Table S2. ^{31}P NMR chemical shifts and coupling constants for **5** at 253 K obtained from the simulation

J (Hz)				δ (ppm)	
$^1J_{P_A\text{-}P_X}$	429.62	$^2J_{P_B\text{-}P_M}$	−25.62	A	279.93
$^1J_{P_B\text{-}P_X}$	437.11	$^2J_{P_X\text{-}P_M}$	99.70	B	277.22
$^1J_{P_A\text{-}P_M}$	22.66	$^2J_{P_X\text{-}P_{M'}}$	100.13	M	7.9928
$^1J_{P_B\text{-}P_{M'}}$	21.16	$^1J_{P_M\text{-}P_{M'}}$	3.36	M’	8.0736
$^2J_{P_A\text{-}P_{M'}}$	-27.48	$^2J_{P_A\text{-}P_B}$	42.20	X	−64.87

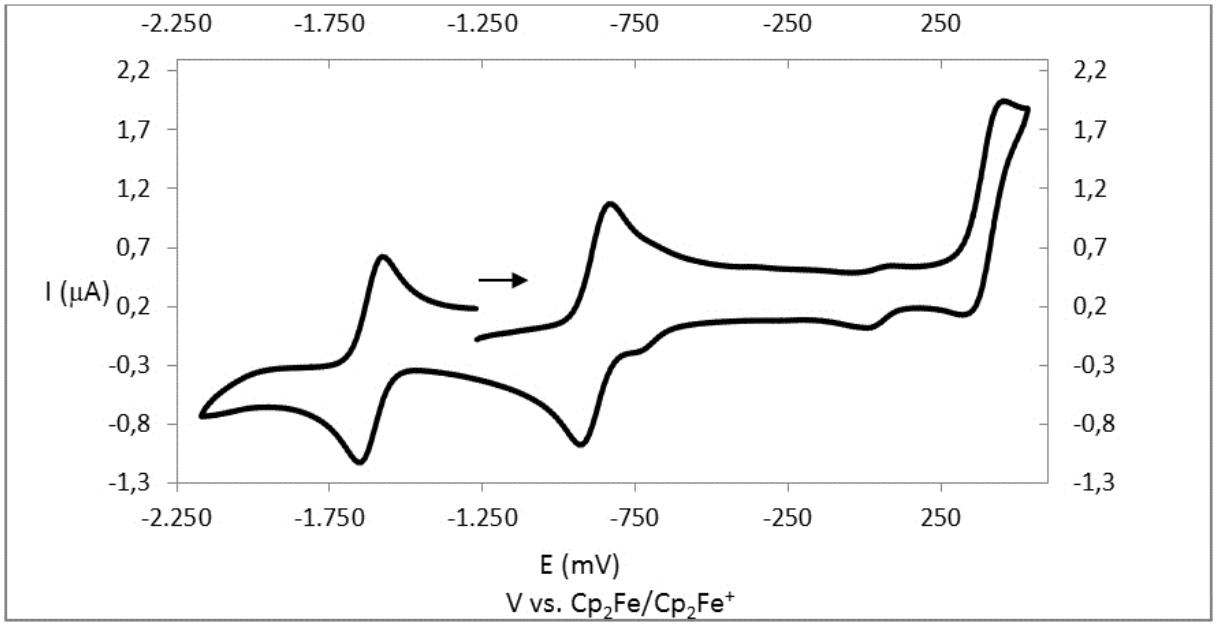

Figure S5. Cyclic voltammogram of **2b** recorded at a platinum disc electrode in 1,3-difluorobenzene at 100 mV/s and referenced against fc/fc+; supporting electrolyte $[Bu_4N][PF_6]$ (0.1 mol/L).

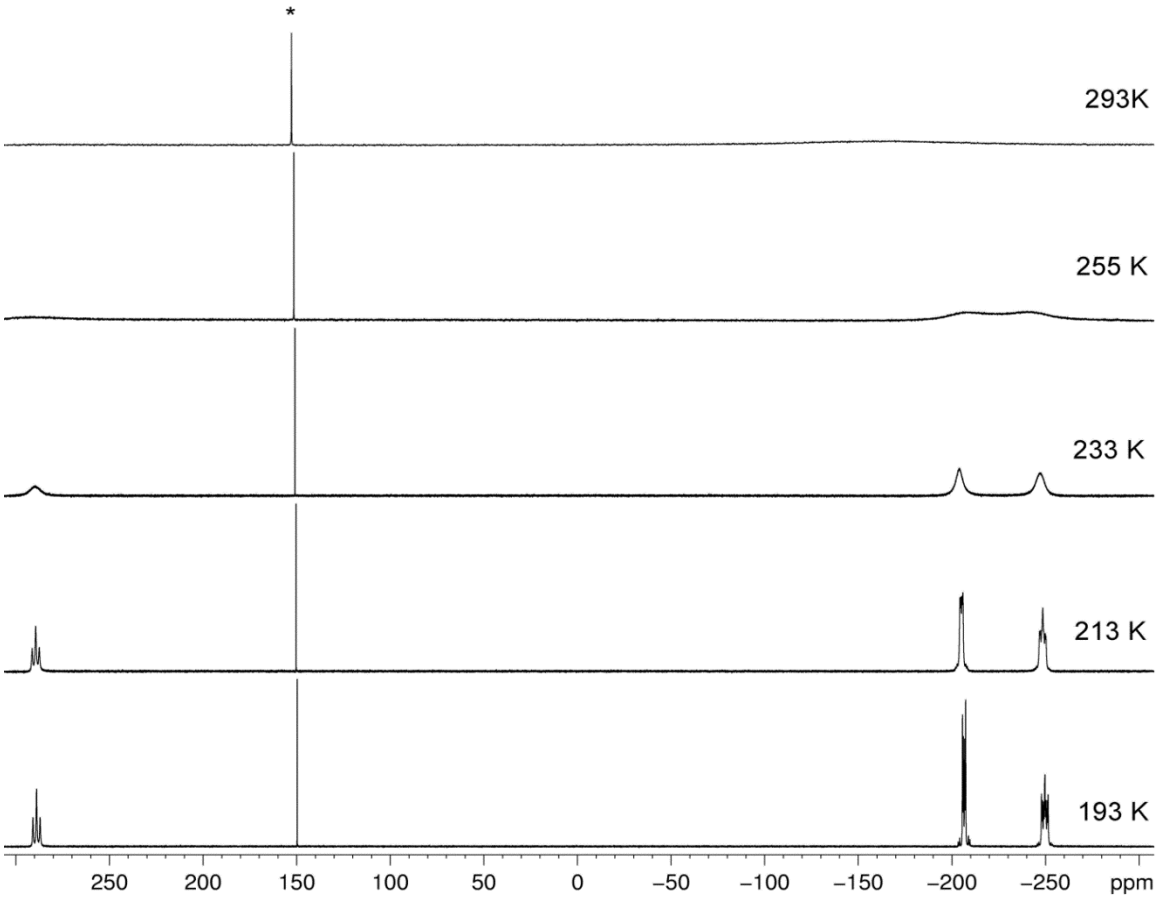

Figure S6. ^{31}P NMR (161.97 MHz, C_6D_6) spectrum of **7** at different temperatures. Traces of **1** are marked with *.

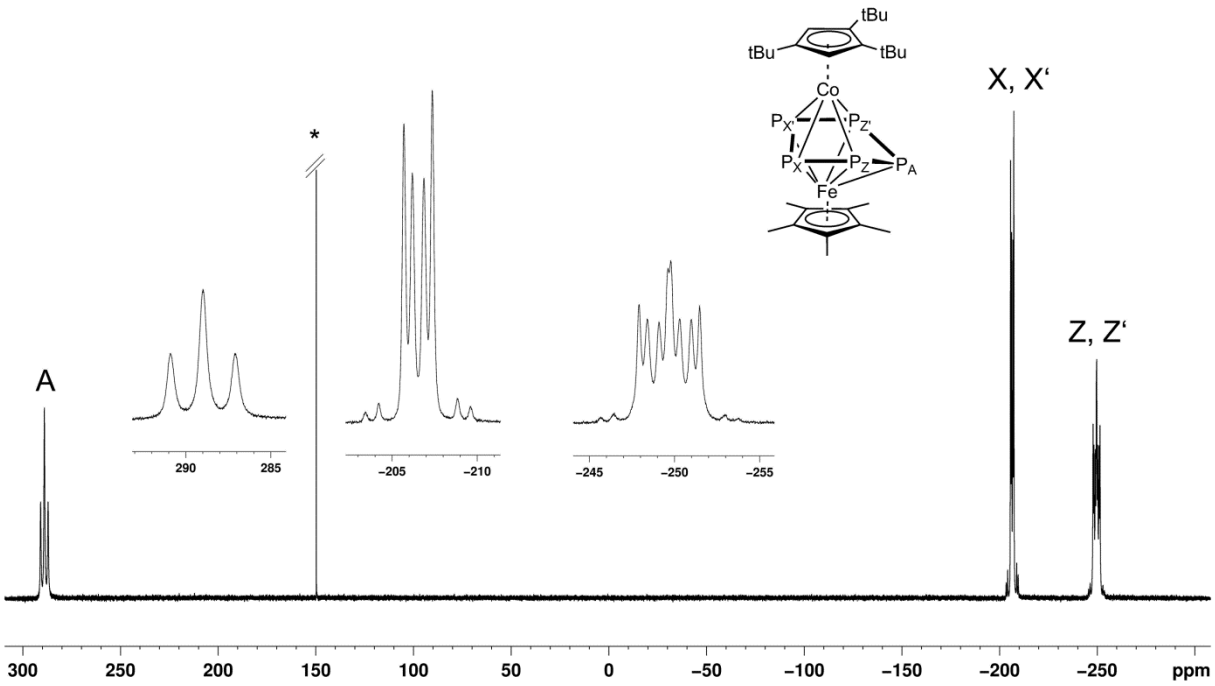

Figure S7. ^{31}P NMR (161.97 MHz, C_6D_6, 193K) spectrum of **7** at 193K. Traces of **1** are marked with *.

5.2.3 EPR spectra

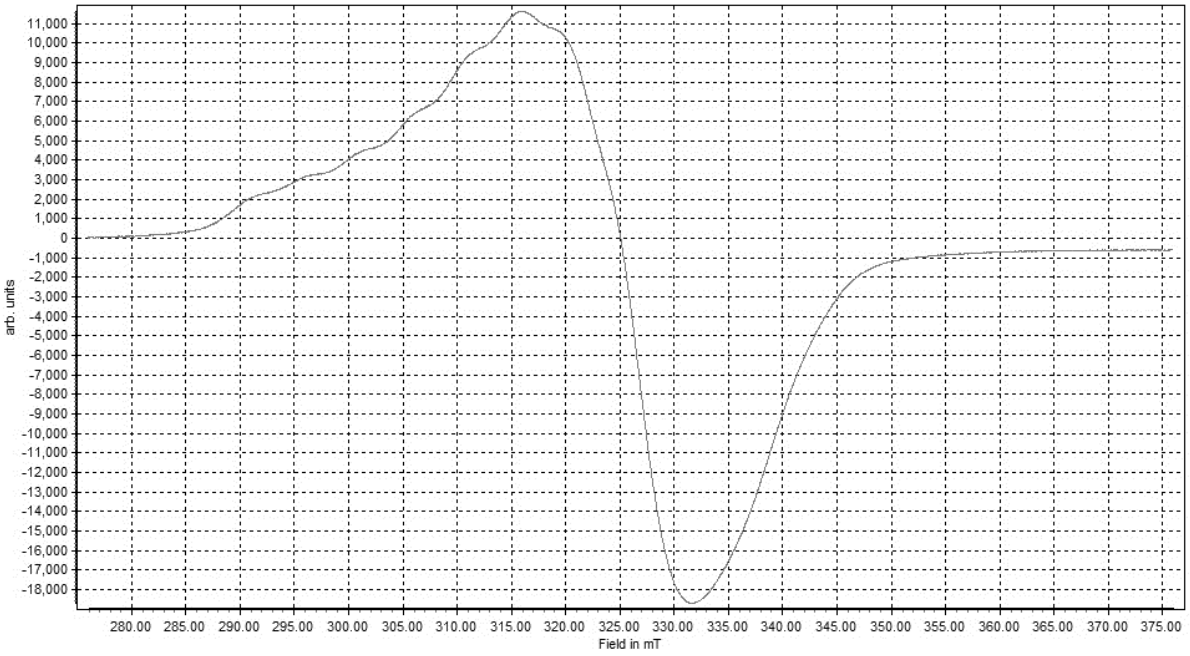

Figure S8. X-band EPR spectrum of **2a**, in toluene at 77 K.

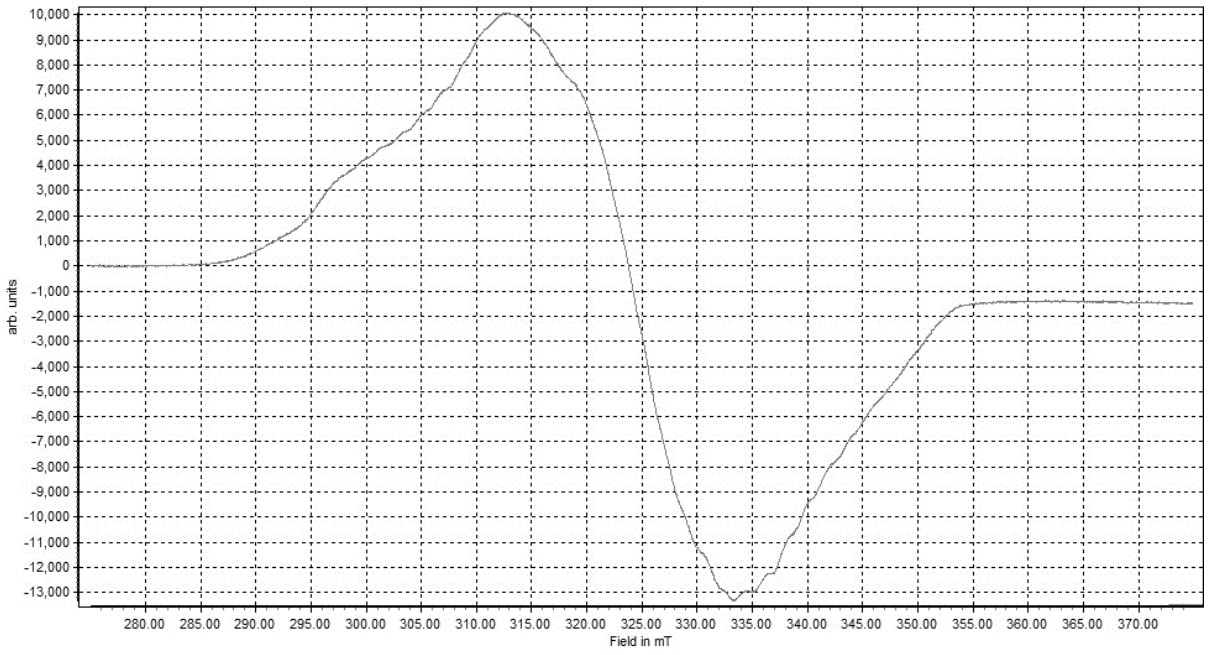

Figure S9. X-band EPR spectrum of **2b**, in toluene at 77 K.

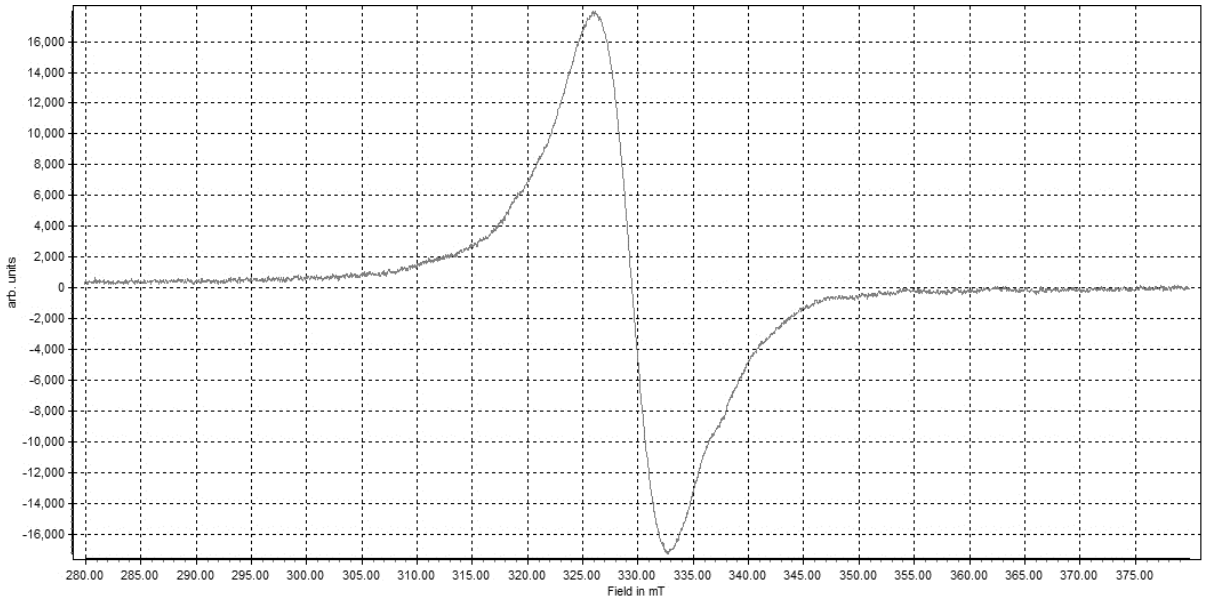

Figure S10. X-band EPR spectrum of **8**, in C_6D_6 at 77 K.

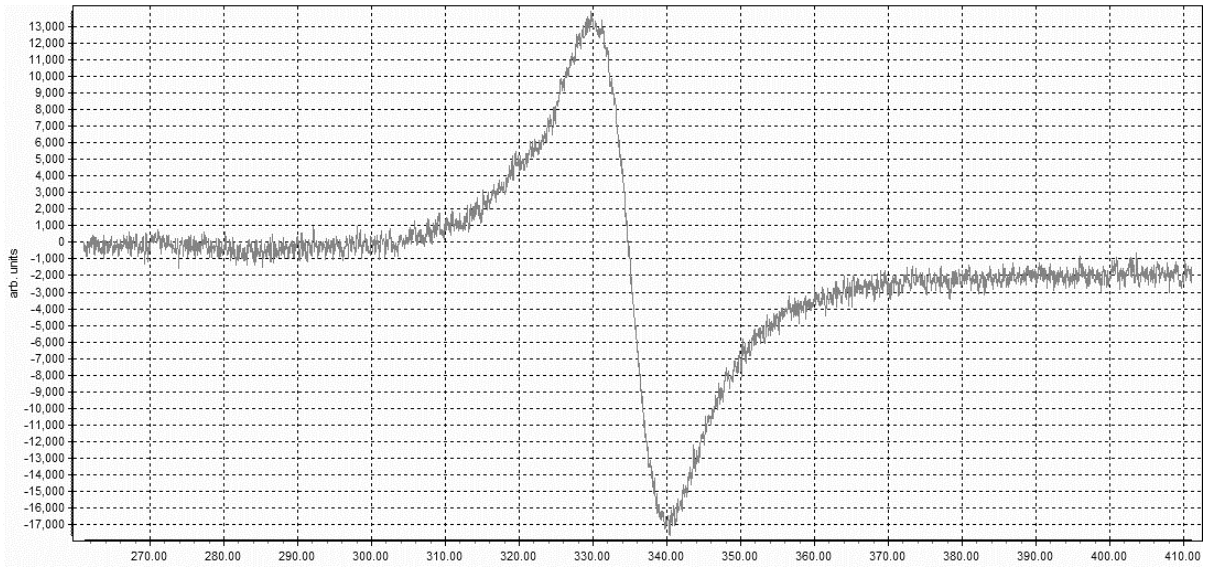

Figure S11. X-band EPR spectrum of **6**, in DME at 300 K.

5.2.4 Details on X-ray structure determinations and ortep-like plots

The diffraction data were collected on a Gemini R-Ultra diffractometer (**2a**, **2b**, **3**) equipped with Ruby detector or SuperNova diffractometers (Agilent Technologies) equipped with Atlas (**5**-**6**) or Titan^{S2} (**8**) CCD detectors, respectively, and micro-focus SuperNova sourse (CuK_α radiation, λ = 1.54178 Å) using ω scans of 1° (**5**, **6**, **8**), 0.5° (**2a**, **2b**, **3**, **7**) or 0.25° (**4**) frames. The diffraction experiment for **4** was performed on a SuperNova equipped with CCD detector Eos with Mo *K*α radiation (λ = 0.71073Å) using ω scans of 0.25° frames. All measurements were performed at 123 K. All structures were solved by direct methods with ShelXT[3] or Olex2[4] programs and refined by full-matrix least-squares method against $|F|^2$ in anisotropic approximation using SHELXTL or its multiprocessor version SHELX2013[3]. Absorption corrections were applied analytically using *CrysAlis PRO* Software (Table S3-4).[5] All non-hydrogen atoms were refined in anisotropic approximation. Hydrogen atoms were refined in calculated positions using riding on pivot atom model.

Compounds **2b**, **3** are isostructural. The crystal of **8** showed pseudo-monoclinic symmetry (R_{int}=0.119). The attempt to solve and refine the crystal structure in monoclinic unit cell setting (a=10.071, b=13.602, c=12.152 Å, β=114.26°, V=1517.75 Å^3) and $P2_1/m$ space group gives R_1=0.157 and wR_2 (all data) = 0.364 with molecular complex **8** lying on the *m* plane. The Cp* ligand and one of *i*Pr substituent of Cp''' as well as two phosphorous atoms of *cyclo*-P_5 ligand are disordered by a reflection over the mirror plane. The model cannot be refined in anisotropic approximation for P and C atoms. We supposed that the proper symmetry can be triclinic, and *m* plane could be a twinning element. The corresponding triclinic unit cell was found (Table S4) using transformation matrix (1 0 0 / 0 0 1 / 0 -1 0). The structure was solved by direct methods revealing the completely ordered molecular complex **8** occupying general position and refined to R_1 = 0.151. The residual density (2.8-4.8 e·Å^{-3}) could be assigned to minor positions of P atoms similarly to symmetrically related positions in the monoclinic model. However, the contribution of this positions was only 0.33, not 0.5 as would be dictated by m plane. Therefore, thinning element corresponding to the mirror plane in pseudo-monoclinic setting (twin law: 0 1 0/ 1 0 0/ 0 0 -1) was introduced into the refinement. The twin batches were refined to 0.663(2)/0.337(2) that lead to minor disordered positions of P atoms to disappear. The resulting R_1 = 0.059 and wR_2 (all data) = 0.1516 with the residual density not exceeding 1.5 e·Å^{-3}. Crystal structure **7** contains five crystallographically unique molecules, of which three possess different types of the disorder. The *cyclo*-P_5 ligand is disordered over two (in two molecules) or four close positions (in one molecule). Sometimes this reorientation of the ligand is accompanied of the disorder of the Fe and coordinated Cp* ligand. The occupancies for the disordered atoms were refined as 0.82/0.18 (P31-P35, positions A and B); 0.75/0.25 (P41-P45, Fe1, positions A and B) and 0.45/0.25/0.17/0.18 (P51-P55, Fe5, positions A, B, C and D). The disordered atoms were refined anisotropically if the occupancies exceeded 0.25 for phosphorus and 0.5 for carbon atoms.

None of these disordered positions can be neglected for the sake of simplicity of the structural model. In this case, the residual density increases to the magnitude of more than 2.5 e·Å^{-3}.

The supplementary crystallographic data for this publication (Tables S3-S4) can be obtained free of charge at www.ccdc.cam.ac.uk/conts/retrieving.html (or from the Cambridge Crystallographic Data Centre, 12 Union Road, Cambridge CB2 1EZ, UK; Fax: + 44-1223-336-033; e-mail: deposit@ccdc.cam.ac.uk). All drawings for **2a**, **2b** − **8** were made in Olex2[2].

Table S3. Crystal data, data collection parameters, and convergence results for **2a**, **2b** − **4**.

	2a	**2b**	**3**	**4**
CCDC Code	CCDC-XXXXX	CCDC-XXXXX	CCDC-XXXXX	CCDC-XXXXX
Crystal data				
Chemical formula	$C_{31}H_{55}CoFeP_5Si$	$C_{29}H_{50}CoFeNP_5$	$C_{29}H_{50}FeNNiP_5$	$C_{29}H_{50}Fe_2NP_5$
M_r	725.47	682.33	682.11	679.25
Crystal system, space group	Triclinic, $P\bar{1}$	Monoclinic, $P2_1/n$	Monoclinic, $P2_1/n$	Monoclinic, $P2_1/c$
Temperature (K)	123	123	123	123
a, b, c (Å)	10.1595 (3), 12.5137 (4), 15.7867 (5)	12.7300 (1), 15.5790 (1), 17.3044 (1)	12.7483 (1), 15.4746 (1), 17.3699 (2)	17.2557 (3), 12.4359 (2), 16.6796 (3)
α, β, γ (°)	100.375 (2), 100.066 (2), 108.045 (3)	90, 108.258 (1), 90	90, 107.710 (1), 90	90, 114.972 (2), 90
V (Å^3)	1819.16 (10)	3259.05 (4)	3264.25 (5)	3244.67 (11)
Z	2	4	4	4
F(000)	766	1436	1440	1432
D_x (Mg m^{-3})	1.324	1.391	1.388	1.390
Radiation type	Cu $K\alpha$	Cu $K\alpha$	Cu $K\alpha$	Mo $K\alpha$
μ (mm^{-1})	9.30	10.02	6.74	1.16
Crystal shape and colour	Black block	Black block	Brown plate	Dark green trapezoid
Crystal size (mm)	0.31 × 0.13 × 0.11	0.12 × 0.10 × 0.09	0.19 × 0.17 × 0.06	0.10 × 0.07 × 0.05
Data collection				
Diffractometer	Xcalibur, Ruby, Gemini ultra diffractometer	Xcalibur, Ruby, Gemini ultra diffractometer	Xcalibur, Ruby, Gemini ultra diffractometer	SuperNova, Single source at offset, Eos diffractometer
Absorption correction	Analytical	Analytical	Analytical	Analytical
T_{min}, T_{max}	0.179, 0.518	0.463, 0.555	0.434, 0.734	0.914, 0.958
No. of measured, independent and observed [> 2σ(I)] reflections	13401, 7013, 6204	17145, 5732, 4810	15331, 5591, 4600	20562, 10520, 6944
R_{int}	0.021	0.032	0.027	0.028
$(\sin\theta/\lambda)_{max}$ (Å^{-1})	0.624	0.595	0.594	0.754
Range of h, k, l	h = -12→8, k = -15→15, l = -18→19	h = -15→13, k = -17→18, l = -16→20	h = -15→15, k = -15→17, l = -20→18	h = -25→24, k = -17→14, l = -25→20
Refinement				
$R[F^2 > 2\sigma(F^2)]$, $wR(F^2)$, S	0.026, 0.080, 1.09	0.029, 0.068, 0.93	0.024, 0.056, 0.91	0.030, 0.061, 0.84
No. of reflections	7013	5732	5591	10520
No. of parameters	369	350	350	350
No. of restraints	0	0	0	0
H-atom treatment	H-atom parameters constrained	H-atom parameters constrained	H-atom parameters constrained	H-atom parameters constrained
$\Delta\rangle_{max}$, $\Delta\rangle_{min}$ (e Å^{-3})	0.32, -0.43	0.61, -0.40	0.32, -0.25	0.47, -0.29

Table S4. Crystal data, data collection parameters, and convergence results for **5** − **8**.

	5	**6**	**7**	**8**
CCDC Code	CCDC-XXXXX	CCDC-XXXXX	CCDC-XXXXX	CCDC-XXXXX
Crystal data				
Chemical formula	$C_{31}H_{55}CrFeP_5Si$	$C_{31}H_{55}CoFeP_5Si{\cdot}F_6P$	$C_{27}H_{44}CoFeP_5$	$C_{27}H_{44}Fe_2P_5$
M_r	718.54	870.44	638.25	635.17
Crystal system, space group	Monoclinic, $P2_1/c$	Monoclinic, $P2_1/n$	Triclinic, $P\bar{1}$	Triclinic, $P\bar{1}$
Temperature (K)	123	123	123	123
a, b, c (Å)	19.9256 (2), 11.6275 (1), 16.4157 (2)	14.9545 (1), 16.8539 (1), 15.7381 (1)	11.9075 (2), 22.7419 (5), 29.3326 (5)	10.0692 (6), 12.1581 (5), 13.5969 (4)
α, β, γ (°)	90, 106.491 (1), 90	90, 98.016 (1), 90	107.370 (2), 93.929 (2), 90.287 (2)	89.991 (3), 89.773 (4), 65.719 (5)
V (Å^3)	3646.82 (7)	3927.90 (4)	7560.5 (3)	1517.30 (13)
Z	4	4	10	2
F(000)	1520	1808	3340	666
D_x (Mg m^{-3})	1.309	1.472	1.402	1.390
Radiation type	Cu $K\alpha$	Cu $K\alpha$	Cu $K\alpha$	Cu $K\alpha$
μ (mm^{-1})	8.17	9.31	10.76	10.27
Crystal shape and colour	Dark green plate	Dark brown needle	Black plate	Black prism
Crystal size (mm)	0.16 × 0.12 × 0.06	0.30 × 0.25 × 0.12	0.18 × 0.09 × 0.07	0.13 × 0.05 × 0.04
Data collection				
Diffractometer	SuperNova, Single source at offset, Atlas diffractometer	SuperNova, Single source at offset, Atlas diffractometer	SuperNova, TitanS2 diffractometer	SuperNova, TitanS2 diffractometer
Absorption correction	Analytical	Analytical	Gaussian	Gaussian
T_{min}, T_{max}	0.422, 0.700	0.174, 0.517	0.352, 0.585	0.526, 0.751
No. of measured, independent and observed [> 2σ(I)] reflections	63463, 7334, 6576	129446, 7934, 7215	56759, 28906, 20199	13226, 5561, 4305
R_{int}	0.046	0.045	0.056	0.071
(sin θ/λ)$_{max}$ (Å^{-1})	0.625	0.623	0.626	0.623
Range of h, k, l	h = -24→24, k = -14→14, l = -20→19	h = -18→18, k = -20→20, l = -19→19	h = -8→14, k = -28→27, l = -36→36	h = -12→12, k = -14→14, l = -15→16
Refinement				
$R[F^2 > 2\sigma(F^2)]$, $wR(F^2)$, S	0.028, 0.078, 1.09	0.024, 0.066, 1.08	0.057, 0.154, 1.02	0.059, 0.152, 0.96
No. of reflections	7334	7934	28906	5561
No. of parameters	369	432	1918	322
No. of restraints	0	0	0	0
H-atom treatment	H-atom parameters constrained	H-atom parameters constrained	H-atom parameters constrained	H-atom parameters constrained
Δ⟩$_{max}$, Δ⟩$_{min}$ (e Å^{-3})	0.69, -0.41	0.41, -0.34	1.03, -1.17	1.41, -0.92

Computer programs: *CrysAlis PRO*, Agilent Technologies, Version 1.171.37.34 (release 22-05-2014 CrysAlis171 .NET) (compiled May 22 2014,16:03:01), *SHELXL97* (Sheldrick, 1997), *SHELXL2013* (Sheldrick, 2013).

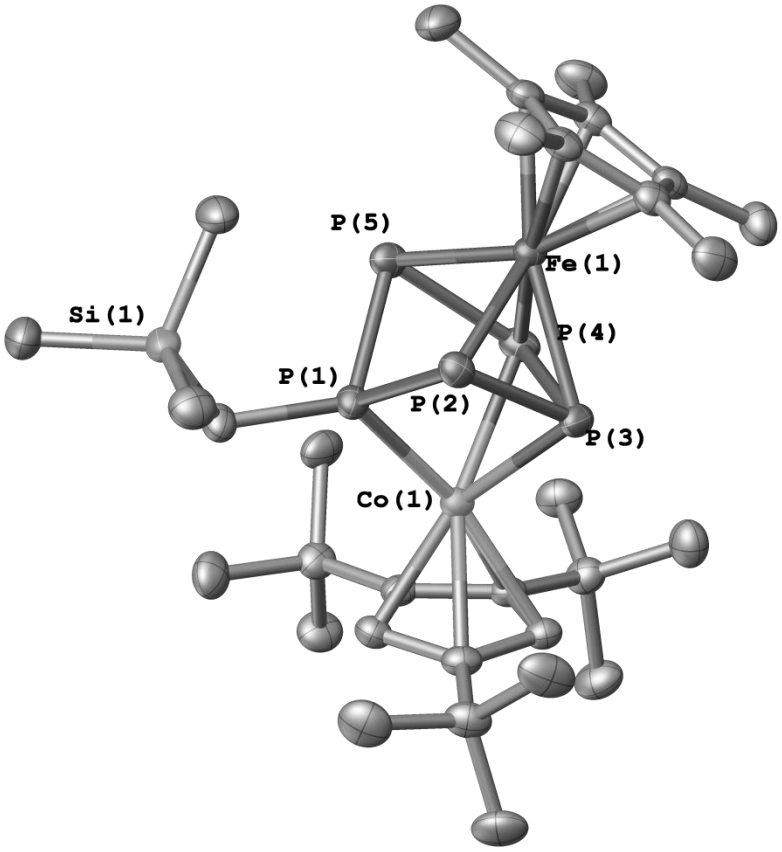

Figure S12. Molecular structure (ellipsoids at 50 % probability) and enumeration scheme for **2a**

Table S5. Selected geometric parameters (Å, º) for **2a**

Fe1—P4	2.3475 (5)	P4—P3	2.3530 (7)
Fe1—P2	2.2822 (6)	P2—P1	2.1928 (7)
Fe1—P5	2.2726 (6)	P2—P3	2.1911 (7)
Fe1—P3	2.3158 (6)	P5—P1	2.1771 (7)
Co1—P4	2.3555 (6)	Si1—C28	1.899 (2)
Co1—P1	2.1691 (6)	Si1—C31	1.861 (3)
Co1—P3	2.3136 (6)	Si1—C30	1.866 (2)
P4—P5	2.1790 (7)	Si1—C29	1.868 (2)

P5—P4—P3	101.38 (3)	P5—P1—P2	91.86 (3)
P3—P2—P1	86.00 (3)	P2—P3—P4	99.27 (3)
P1—P5—P4	83.17 (3)		

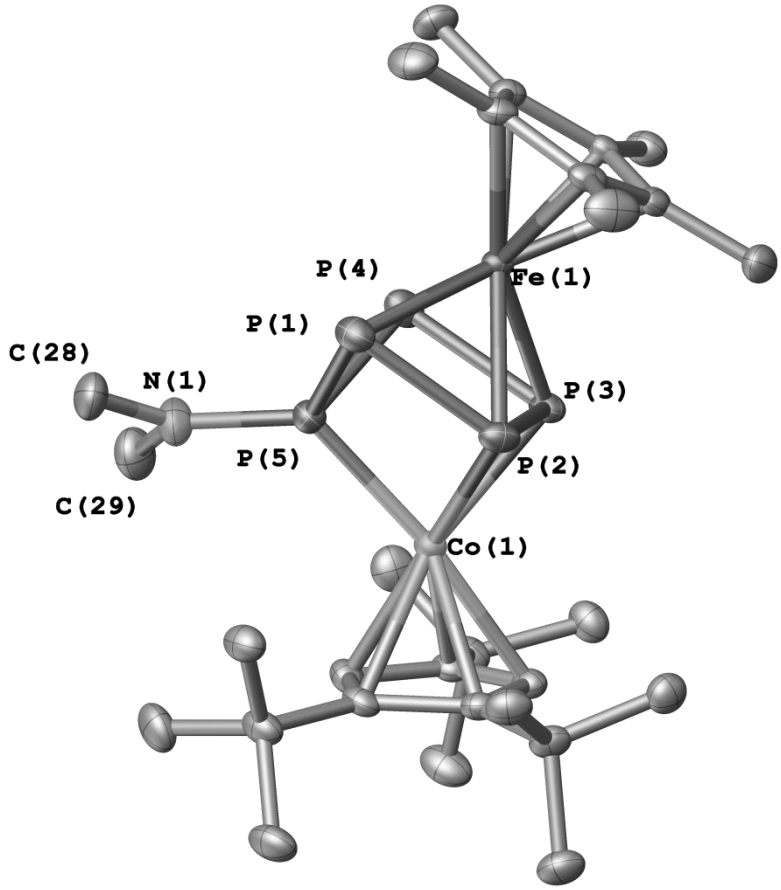

Figure S13. Molecular structure (ellipsoids at 50 % probability) and enumeration scheme for **2b**

Table S6. Selected geometric parameters (Å, º) for **2b**

P1—Fe1	2.3139 (6)	P4—P5	2.2004 (8)
P2—Fe1	2.3278 (6)	P3—Co1	2.2774 (6)
P3—Fe1	2.3048 (6)	P2—Co1	2.3596 (6)
P4—Fe1	2.2752 (6)	P5—Co1	2.1743 (6)
P1—P2	2.1854 (8)	N1—P5	1.6649 (19)
P1—P5	2.1569 (8)	C28—N1	1.452 (3)
P2—P3	2.4132 (8)	C29—N1	1.454 (3)
P3—P4	2.1855 (8)		

C28—N1—C29	115.41 (19)	P4—P3—P2	97.02 (3)
C28—N1—P5	124.47 (16)	P3—P4—P5	86.75 (3)
C29—N1—P5	120.11 (16)	N1—P5—P1	115.09 (8)
P5—P1—P2	79.71 (3)	N1—P5—P4	115.63 (8)
P1—P2—P3	103.96 (3)	P1—P5—P4	95.21 (3)

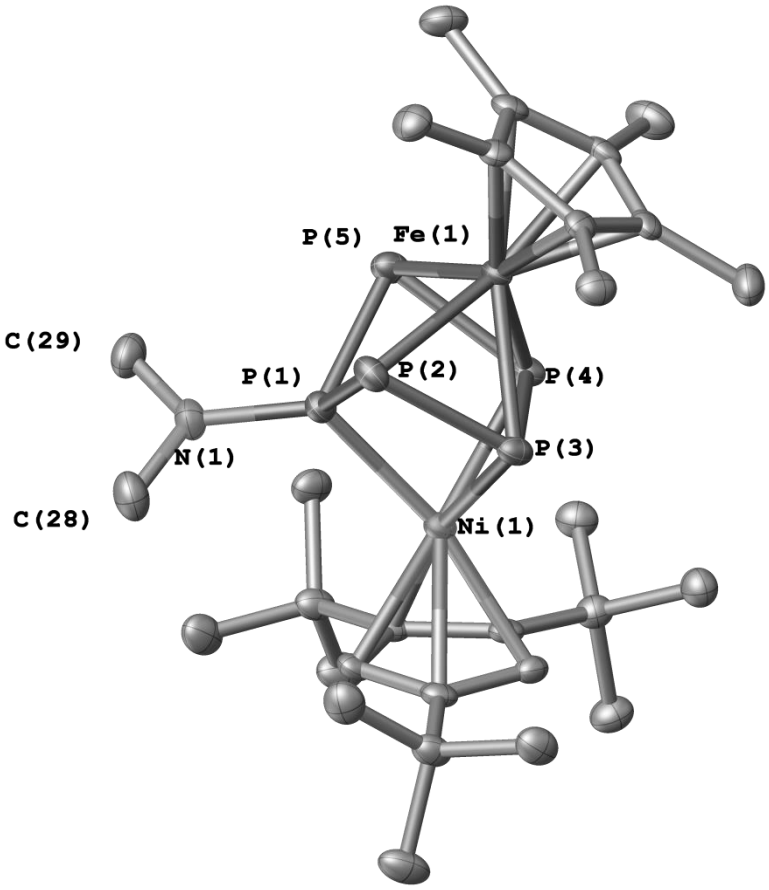

Figure S14. Molecular structure (ellipsoids at 50 % probability) and enumeration scheme for **3**

Table S7. Selected geometric parameters (Å, º) for **3**

P2—Fe1	2.2923 (5)	P5—P1	2.1620 (7)
P3—Fe1	2.2912 (5)	P1—Ni1	2.1998 (6)
P4—Fe1	2.2968 (5)	P3—Ni1	2.2846 (5)
P5—Fe1	2.3106 (6)	P4—Ni1	2.2972 (5)
P2—P1	2.1791 (7)	N1—P1	1.6706 (17)
P2—P3	2.1738 (7)	C28—N1	1.455 (3)
P3—P4	2.4739 (7)	C29—N1	1.451 (3)
P4—P5	2.1753 (7)		

P3—P2—P1	82.05 (2)	N1—P1—P2	116.15 (6)
P2—P3—P4	99.18 (2)	N1—P1—P5	114.89 (7)
P5—P4—P3	100.75 (2)	P5—P1—P2	96.03 (3)
P1—P5—P4	80.56 (2)		

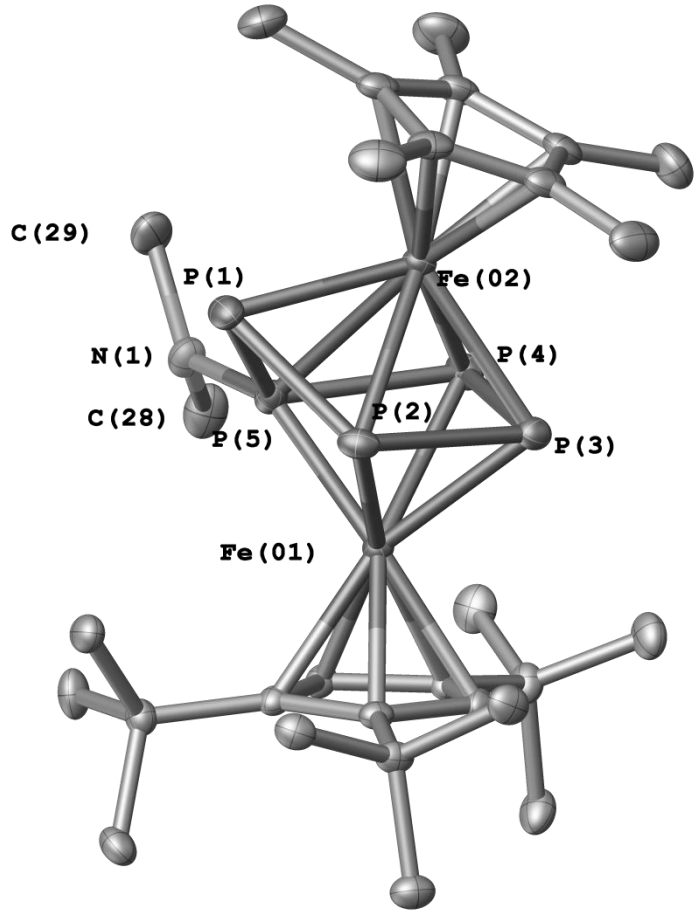

Figure S15. Molecular structure (ellipsoids at 50 % probability) and enumeration scheme for **4**

Table S8. Selected geometric parameters (Å, º) for **4**

Fe01—P5	2.1362 (5)	P5—P4	2.3187 (6)
Fe01—P3	2.3252 (5)	P5—P1	2.0952 (6)
Fe01—P4	2.4690 (5)	P3—P4	2.1054 (6)
Fe01—P2	2.3685 (5)	P3—P2	2.3587 (6)
Fe02—P5	2.6313 (5)	P2—P1	2.2063 (6)
Fe02—P3	2.3472 (5)	P5—N1	1.6804 (14)
Fe02—P4	2.4120 (5)	N1—C29	1.469 (2)
Fe02—P2	2.4323 (5)	N1—C28	1.460 (2)
Fe02—P1	2.3169 (5)	P5...P2	2.6552 (6)

P4—P5—P2	86.423 (19)	N1—P5—P1	113.58 (5)
P1—P5—P4	115.21 (2)	C29—N1—P5	117.52 (12)
P1—P5—P2	53.793 (18)	C28—N1—P5	119.79 (12)
N1—P5—P4	106.21 (5)	C28—N1—C29	112.81 (14)
N1—P5—P2	165.87 (5)		

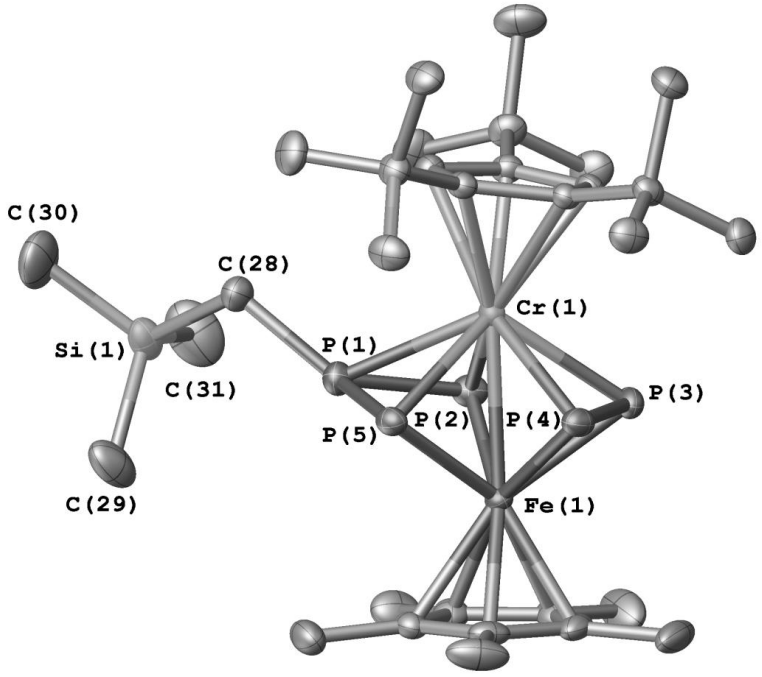

Figure S16. Molecular structure (ellipsoids at 50 % probability) and enumeration scheme for **5**

Table S9. Selected geometric parameters (Å, º) for **5**

Fe1—Cr1	2.6252 (4)	P5—P4	2.6258 (7)
Fe1—P5	2.2936 (5)	P5—P1	2.1549 (6)
Fe1—P2	2.2885 (5)	P2—P1	2.1558 (7)
Fe1—P4	2.2822 (5)	P2—P3	2.6328 (7)
Fe1—P3	2.2820 (5)	P4—P3	2.1040 (7)
Cr1—P5	2.3053 (5)	P1—C28	1.8574 (19)
Cr1—P2	2.2969 (5)	Si1—C28	1.878 (2)
Cr1—P4	2.3744 (5)	Si1—C29	1.856 (2)
Cr1—P1	2.5066 (5)	Si1—C30	1.865 (3)
Cr1—P3	2.3776 (5)	Si1—C31	1.851 (3)

P1—P2—P3	117.41 (2)	P3—P4—P5	102.78 (2)
P5—P1—P2	97.72 (2)	C28—P1—P5	125.15 (7)
P4—P3—P2	102.31 (2)	C28—P1—P2	128.44 (7)

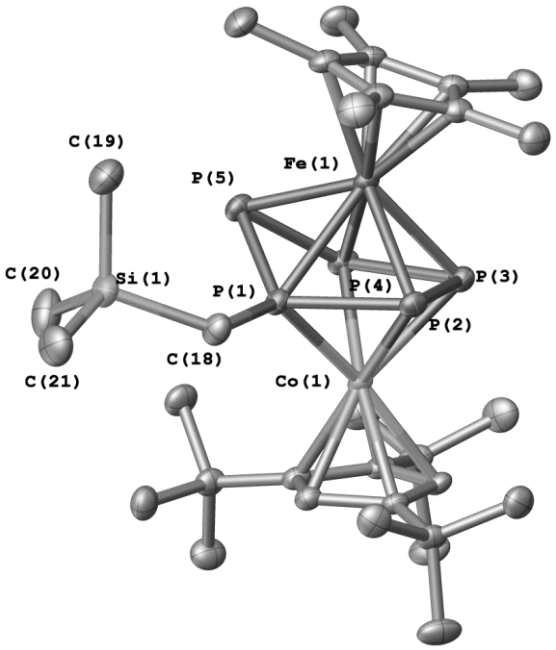

Figure S17. Cationic complex (ellipsoids at 50 % probability) and enumeration scheme for **6**

Table S10. Selected geometric parameters (Å, º) for **6**

C18—Si1	1.9046 (15)	P1—Fe1	2.4339 (4)
C18—P1	1.8233 (15)	P1—Co1	2.1924 (4)
C19—Si1	1.852 (2)	P2—P3	2.1045 (5)
C20—Si1	1.862 (2)	P2—Fe1	2.3647 (4)
C21—Si1	1.8564 (19)	P2—Co1	2.3842 (4)
F1—P6	1.5991 (13)	P3—P4	2.2715 (5)
F2—P6	1.6056 (13)	P3—Fe1	2.3547 (4)
F3—P6	1.5866 (15)	P3—Co1	2.3193 (4)
F4—P6	1.5894 (14)	P4—P5	2.1986 (5)
F5—P6	1.5969 (13)	P4—Fe1	2.4871 (4)
F6—P6	1.5964 (14)	P4—Co1	2.3447 (4)
P1—P2	2.2811 (5)	P5—Fe1	2.2918 (4)
P1—P5	2.1089 (5)		

P1—C18—Si1	118.83 (9)	C18—P1—P5	122.07 (5)
C19—Si1—C18	109.24 (8)	C18—P1—Fe1	129.16 (6)
C19—Si1—C20	110.87 (10)	C18—P1—Co1	127.73 (5)
C19—Si1—C21	109.83 (10)	P5—P1—P2	118.59 (2)
C20—Si1—C18	110.11 (8)	P3—P2—P1	94.402 (19)
C21—Si1—C18	107.37 (8)	P2—P3—P4	102.07 (2)
C21—Si1—C20	109.35 (10)	P5—P4—P3	113.80 (2)
C18—P1—P2	105.45 (5)	P1—P5—P4	79.579 (18)

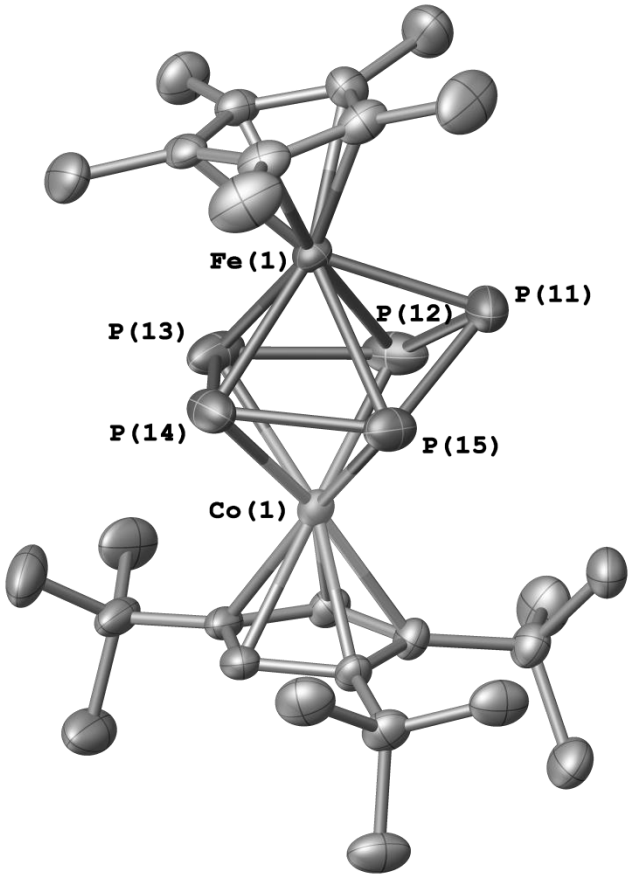

Figure S18. Molecular structure (ellipsoids at 50 % probability) and enumeration scheme for **7.** Other molecules are enumerated in the same way with 1st number denoting the molecule and the second the number of an atom. The A-D letters enumerate the positions of the disordered group.

Table S11. Selected geometric parameters (Å, º) for **7**

Fe1—P11	2.2670 (14)	Fe4A—P41A	2.294 (2)
Fe1—P13	2.3300 (12)	Fe4A—P43A	2.347 (2)
Fe1—P14	2.3424 (13)	Fe4A—P44A	2.360 (3)
Fe1—P15	2.5002 (13)	Fe4A—P45A	2.463 (2)
Fe1—P12	2.5142 (14)	Fe4A—P42A	2.499 (2)
Fe2—P21	2.2666 (14)	Co4A—P42A	2.291 (3)
Fe2—P24	2.3440 (12)	Co4A—P45A	2.294 (2)
Fe2—P23	2.3506 (12)	Co4A—P44A	2.311 (2)
Fe2—P25	2.5092 (13)	Co4A—P43A	2.340 (3)
Fe2—P22	2.5318 (14)	P41A—P42A	2.128 (2)
Fe3—P31A	2.2690 (16)	P41A—P45A	2.131 (3)
Fe3—P34B	2.271 (8)	P42A—P43A	2.248 (3)
Fe3—P33B	2.307 (9)	P43A—P44A	2.131 (3)
Fe3—P33A	2.3336 (14)	P44A—P45A	2.306 (2)
Fe3—P34	2.3661 (16)	Fe4B—P41B	2.294 (12)

Fe3—P31B	2.407 (10)	Fe4B—P44B	2.354 (9)
Fe3—P32A	2.4921 (15)	Fe4B—P43B	2.363 (7)
Co1—P12	2.3038 (14)	Fe4B—P45B	2.432 (10)
Co1—P15	2.3162 (13)	Fe4B—P42B	2.452 (10)
Co1—P14	2.3242 (13)	Co4B—P42B	2.303 (9)
Co1—P13	2.3304 (13)	Co4B—P45B	2.310 (11)
Co2—P22	2.3054 (13)	Co4B—P43B	2.321 (11)
Co2—P25	2.3119 (12)	Co4B—P44B	2.373 (11)
Co2—P24	2.3167 (13)	P41B—P42B	2.094 (12)
Co2—P23	2.3313 (13)	P41B—P45B	2.124 (13)
Co3—P34B	2.229 (8)	P42B—P43B	2.172 (10)
Co3—P35B	2.232 (7)	P43B—P44B	2.148 (10)
Co3—P33B	2.288 (9)	P44B—P45B	2.240 (11)
Co3—P32A	2.2973 (15)	Fe5A—P51A	2.292 (3)
Co3—P35	2.2999 (16)	Fe5A—P53A	2.297 (5)
Co3—P34	2.3292 (17)	Fe5A—P54A	2.351 (4)
Co3—P33A	2.3596 (14)	Fe5A—P52A	2.445 (4)
Co5—P55D	2.194 (9)	Fe5A—P55A	2.500 (5)
Co5—P52D	2.214 (14)	P51A—P52A	2.100 (5)
Co5—P52C	2.231 (7)	P51A—P55A	2.147 (6)
Co5—P53A	2.247 (3)	P52A—P53A	2.237 (6)
Co5—P55C	2.254 (11)	P53A—P54A	2.141 (6)
Co5—P55B	2.279 (7)	P54A—P55A	2.271 (6)
Co5—P54D	2.291 (9)	Fe5B—P54B	2.255 (10)
P11—P15	2.1418 (19)	Fe5B—P53B	2.320 (9)
P11—P12	2.148 (2)	Fe5B—P51B	2.355 (8)
P12—P13	2.236 (2)	Fe5B—P55B	2.506 (8)
P13—P14	2.121 (2)	Fe5B—P52B	2.542 (11)
P14—P15	2.2419 (18)	P51B—P55B	2.196 (12)
P22—P21	2.1555 (19)	P51B—P52B	2.206 (12)
P22—P23	2.2289 (19)	P52B—P53B	2.323 (15)
P21—P25	2.1530 (18)	P53B—P54B	2.055 (12)
P25—P24	2.2463 (18)	P54B—P55B	2.167 (12)
P24—P23	2.1307 (17)	P51C—P52C	2.013 (16)
P35—P31A	2.133 (2)	P51C—P55C	2.183 (16)
P35—P34	2.248 (3)	P52C—P53C	2.273 (15)
P34—P33A	2.146 (2)	P53C—P54C	2.057 (18)
P31A—P32A	2.161 (2)	P54C—P55C	2.348 (17)
P32A—P33A	2.242 (2)	P51D—P55D	2.062 (17)
P31B—P32B	2.079 (13)	P51D—P52D	2.184 (17)
P31B—P35B	2.160 (12)	P52D—P53D	2.230 (16)

P32B—P33B	2.131 (14)	P53D—P54D	2.193 (15)
P33B—P34B	2.109 (12)	P54D—P55D	2.262 (15)
P35B—P34B	2.323 (12)		

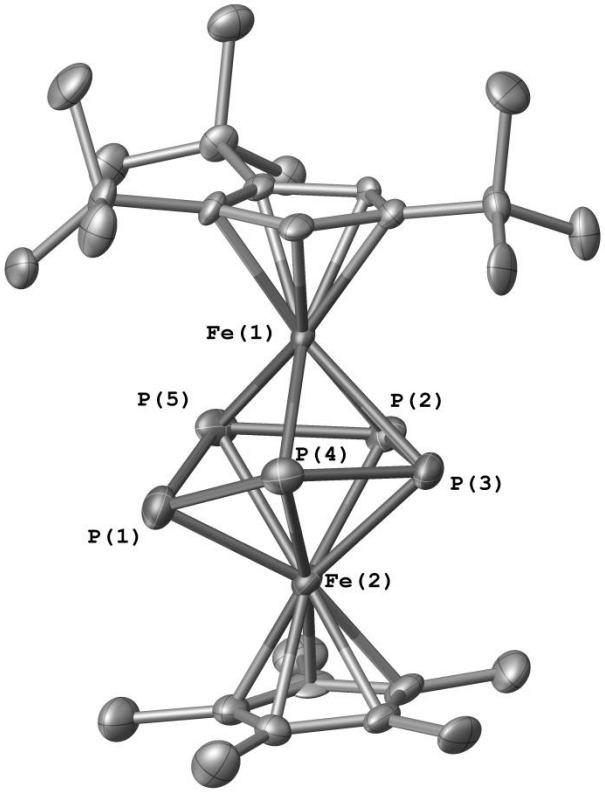

Figure S19. Molecular structure (ellipsoids at 50 % probability) and enumeration scheme for **8**

Table S12. Selected geometric parameters (Å, º) for **8**

Fe1—P5	2.3198 (17)	Fe2—P5	2.5111 (19)
Fe1—P4	2.324 (2)	Fe2—P4	2.536 (2)
Fe1—P2	2.3713 (19)	P1—P4	2.141 (3)
Fe1—P3	2.4112 (15)	P1—P5	2.153 (3)
Fe2—P1	2.2796 (19)	P2—P3	2.126 (3)
Fe2—P3	2.3529 (17)	P2—P5	2.203 (3)
Fe2—P2	2.386 (2)	P3—P4	2.193 (3)

P4—P1—P5	98.67 (11)	P1—P4—P3	109.50 (10)
P3—P2—P5	104.62 (11)	P1—P5—P2	109.89 (10)
P2—P3—P4	105.12 (8)		

5.2.5 Details on DFT calculations

The geometries of the compounds have been fully optimized with gradient-corrected density functional theory (DFT) in form of Becke's three-parameter hybrid method B3LYP[6] with def2-SVP all electron basis set.[7] Gaussian 03 program package[8] was used throughout. All structures correspond to minima on their respective potential energy surfaces.

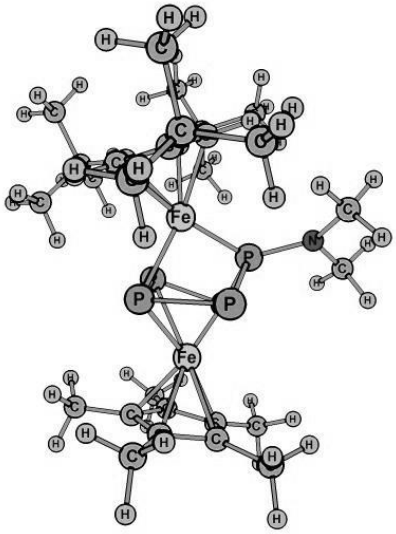

3fefe 0 kJ mol^{-1}

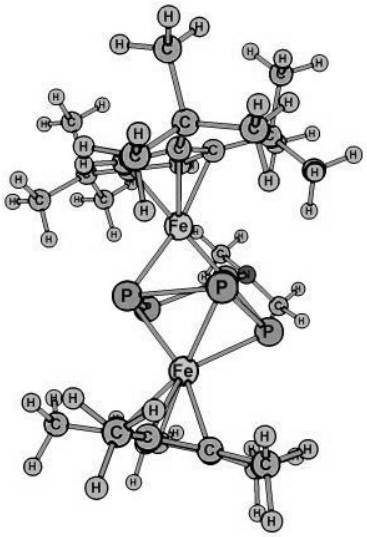

4 0 kJ mol^{-1}

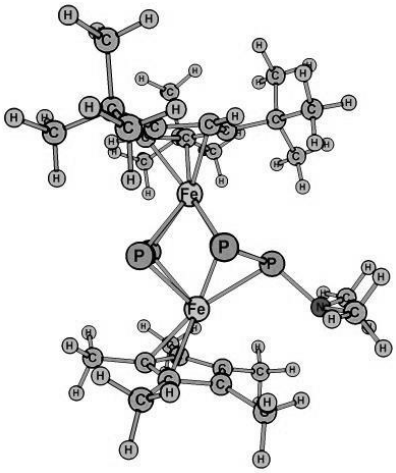

5fefe +55.9 kJ mol^{-1}

Figure S20. Optimized structures and relative energies of the compound **4** and its isomers **3**fefe and **5**fefe.

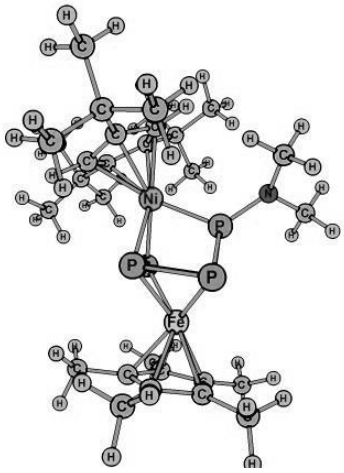

3 0 kJ mol^{-1}

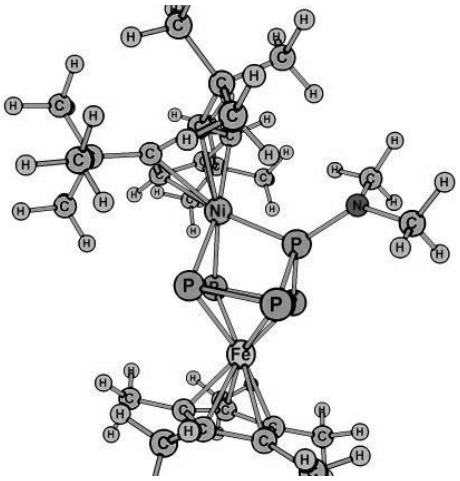

4nife 0 kJ mol^{-1}

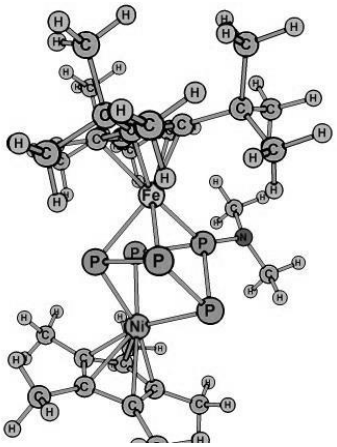

4feni 44.4 kJ mol^{-1}

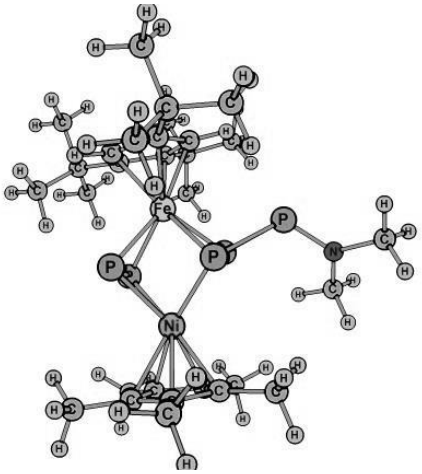

5nife 90.2 kJ mol^{-1}

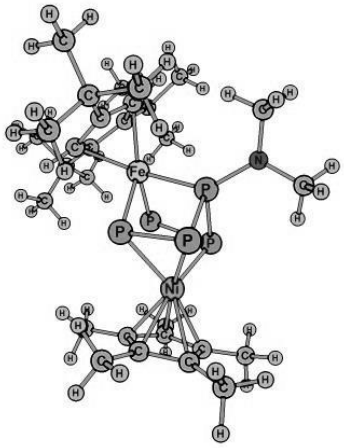

3feni 106.9 kJ mol^{-1}

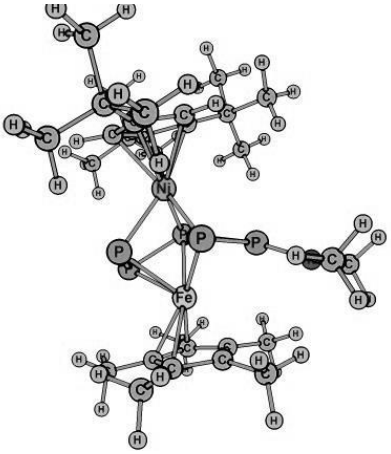

5feni 106.8 kJ mol^{-1}

Figure S21. Optimized structures and relative energies of the isomers.

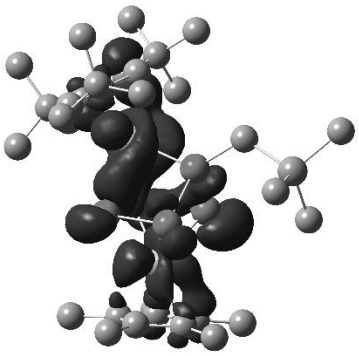

SOMO_**2a**

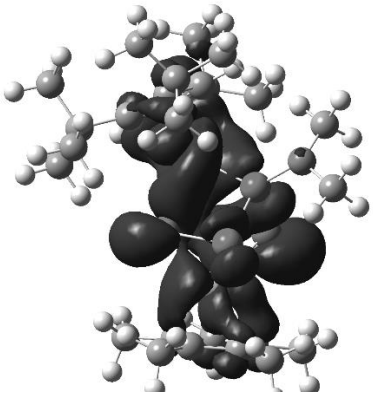

SOMO_**2b**

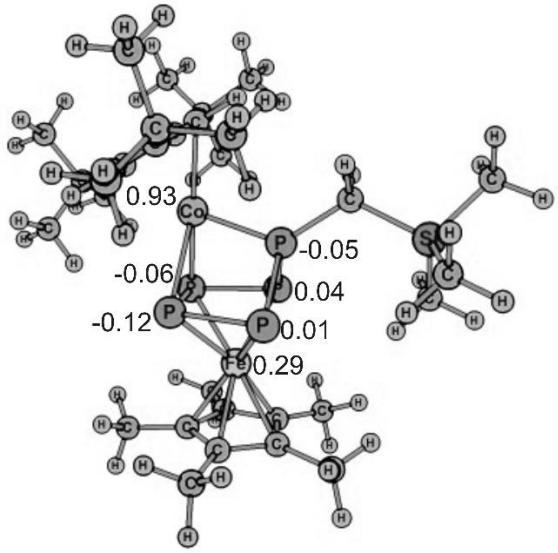

Atomic spin density for **2a**

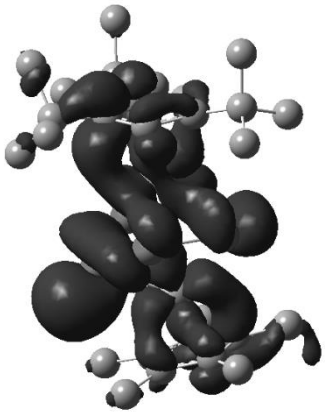

SOMO_**8**

Figure S22. Isosurface of the single-occupied molecular orbitals (SOMO) in **2a**, **2b** and **8**.

Table S13. Wiberg bond indexes (WBI): (numbering of atoms corresponds to the Figures 1, 2 and 5 in the manuscript).

		M-P1	M-P2	M-P3	M-P4	M-P5
2a	Co	0.75	0.06	0.53	0.48	0.06
	Fe	0.05	0.80	0.65	0.66	0.80
2b	Co	0.67	0.01	0.42	0.49	0.04
	Fe	0.03	0.59	0.54	0.55	0.60
7	Co	0.10	0.72	0.59	0.59	0.73
	Fe	0.71	0.38	0.56	0.57	0.38
8	Fe1	0.16	0.67	0.58	0.55	0.66
	Fe2	0.66	0.40	0.52	0.55	0.41

Table S14. Wiberg bond indexes (WBI): (numbering of atoms corresponds to the Figures 1, 2 and 5 in the manuscript).

	M-M	P1-P2	P2-P3	P3-P4	P4-P5	P5-P1	P2-P5
2a	0.12	0.93	1.00	0.70	0.98	0.92	0.07
2b	0.12	0.94	1.01	0.67	1.00	0.85	0.07
3	0.13	0.88	1.03	0.51	1.01	0.95	0.07
5	0.47	0.91	0.22	1.14	0.22	0.90	0.07
7	0.13	0.99	0.80	0.95	0.79	0.99	0.07
8	0.14	0.97	0.85	0.95	0.85	0.97	0.05

Table S15. Mulliken atomic charges and atomic spin densities (numbering of atoms corresponds to the Figures 1, 2 and 5 in the manuscript).

	Mulliken atomic charge				Atomic Spin density			
	2a	**2b**	**7**	**8**	**2a**	**2b**	**7**	**8**
Co/Fe1	-0.021	-0.029	-0.259	-0.205	0.930	0.926	0	0.897
Fe	-0.407	-0.414	-0.405	-0.396	0.295	0.278	0	0.106
P1	0.027	0.183	-0.022	-0.033	-0.055	-0.050	0	0.175
P2	-0.015	-0.015	-0.002	-0.011	0.005	0.0006	0	0.024
P3	-0.012	-0.048	0.033	0.011	-0.128	-0.122	0	-0.057
P4	-0.051	-0.029	0.024	-0.004	-0.060	-0.057	0	-0.060
P5	0.001	-0.005	0.013	0.003	0.041	0.048	0	0.024
N		-0.480				-0.003		
C	-0.303				-0.003			

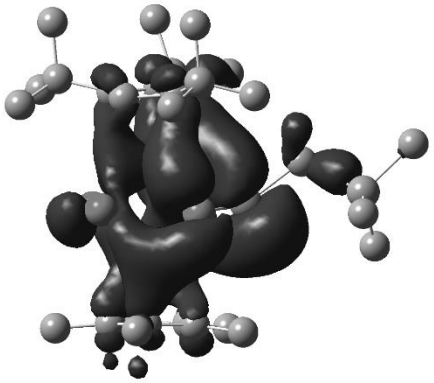

Figure S23. Isosurface of the HOMO-3 of **5**

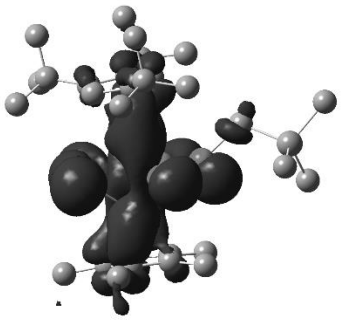

Figure S24. Isosurface of the HOMO of **5**

Table S16. Comparison of sum of valence angles around N and N-P bond distance.

Compound	Sum of angles on N atom	N-P, Å	WBI (N-P)
2b	351.29	1.712	0.813
3	351.68	1.715	
3fefe (converged to **4**)	355.45	1.706	
3feni	353.67	1.714	
4	355.44	1.706	0.818
4feni	351.44	1.713	
4nife	351.70	1.715	
5fefe	336.12	1.801	0.672
5feni	358.25	1.734	
5nife	359.93	1.708	

Table S17. Total energies E^o_0, sum of electronic and thermal enthalpies H^o_{298} (Hartree) and standard entropies S^o_{298} (cal $mol^{-1}K^{-1}$) for studied compounds. B3LYP/def2-SVP level of theory.

Compound	$E°_0$, Hartree	$H°_{298}$, Hartree	$S°_{298}$, cal mol^{-1} K^{-1}
2a	-5855.69586	-5854.851566	292.52
2b	-5541.765076	-5540.9811	268.41
3fefe	-5422.700466	-5421.916178	264.475
3feni	-5667.263255	-5666.479909	269.063
3	-5667.303973	-5666.519976	264.939
4feni	-5667.287074	-5666.503693	269.237
4nife	-5667.303973	-5666.519978	264.972
4	-5422.700467	-5421.916183	264.52
5fefe	-5422.679187	-5421.895554	263.898
5feni	-5667.263289	-5666.480117	269.542
5nife	-5667.269627	-5666.486312	273.926
5	-5517.379123	-5516.534161	284.233
7	-5407.2923478	-5406.595692	243.127
8	-5288.2392468	-5287.543040	248.362

5.2.6 References

[1] a) O. J. Scherer, T. Brück, *Angew. Chem.* **1987**, *99*, 59-59. b) E. Mädl, M. V. Butovskii, G. Balázs, E. V. Peresypkina, A. V. Virovets, M. Seidl, M. Scheer, *Angew. Chem. Int. Ed.* **2014**, *53*, 7643-7646.

[2] D. F. Evans, *J. Chem. Soc.* **1959**, 2003-2005.

[3] G. M. Sheldrick. *Acta Cryst.* **2015**, C71, 3-8.

[4] O.V. Dolomanov, L.J.Bourhis, R.J Gildea, , J.A.K. Howard, H. Puschmann, *J. Appl. Cryst*. **2009**, 42, 339-341.

[5] *CrysAlis PRO*, Agilent Technologies, Versions 1.171.36-38.

[6] a) A.D. Becke, *J. Chem. Phys.* **1993**, *98*, 5648. b) C. Lee, W. Yang, R.G. Parr, *Phys. Rev. B.* **1988**, *37*, 785.

[7] a) F. Weigend, R. Ahlrichs, *Phys.Chem.Chem.Phys.* **2005**, *7*, 3297-3305. b) D. Andrae, U. Haeussermann, M.Dolg, H.Stoll, H.Preuss, *Theor.Chim.Acta*, **1990**, *77*, 123-141.

[8] M. J. Frisch, G. W. Trucks, H. B. Schlegel, G. E. Scuseria, M. A. Robb, J. R. Cheeseman, J. A. Montgomery, Jr., T. Vreven, K. N. Kudin, J. C. Burant, J. M. Millam, S. S. Iyengar, J. Tomasi, V. Barone, B. Mennucci, M. Cossi, G. Scalmani, N. Rega, G. A. Petersson, H. Nakatsuji, M. Hada, M. Ehara, K. Toyota, R. Fukuda, J. Hasegawa, M. Ishida, T. Nakajima, Y. Honda, O. Kitao, H. Nakai, M. Klene, X. Li, J. E. Knox, H. P. Hratchian, J. B. Cross, V. Bakken, C. Adamo, J. Jaramillo, R. Gomperts, R. E. Stratmann, O. Yazyev, A. J. Austin, R. Cammi, C. Pomelli, J. W. Ochterski, P. Y. Ayala, K. Morokuma, G. A. Voth, P. Salvador, J. J. Dannenberg, V. G. Zakrzewski, S. Dapprich, A. D. Daniels, M. C. Strain, O. Farkas, D. K. Malick, A. D. Rabuck, K. Raghavachari, J. B. Foresman, J. V. Ortiz, Q. Cui, A. G. Baboul, S. Clifford, J. Cioslowski, B. B. Stefanov, G. Liu, A. Liashenko, P. Piskorz, I. Komaromi, R. L. Martin, D. J. Fox, T. Keith, M. A. Al-Laham, C. Y. Peng, A. Nanayakkara, M. Challacombe, P. M. W. Gill, B. Johnson, W. Chen, M. W. Wong, C. Gonzalez, and J. A. Pople, Gaussian03, revision B.05. Gaussian, Inc., Wallingford CT, 2004.

6. Chalcogen functionalized polyphosphorus complexes

David Konieczny, Eric Mädl, Michael Bodensteiner, Alexander V. Virovets and Manfred Scheer*

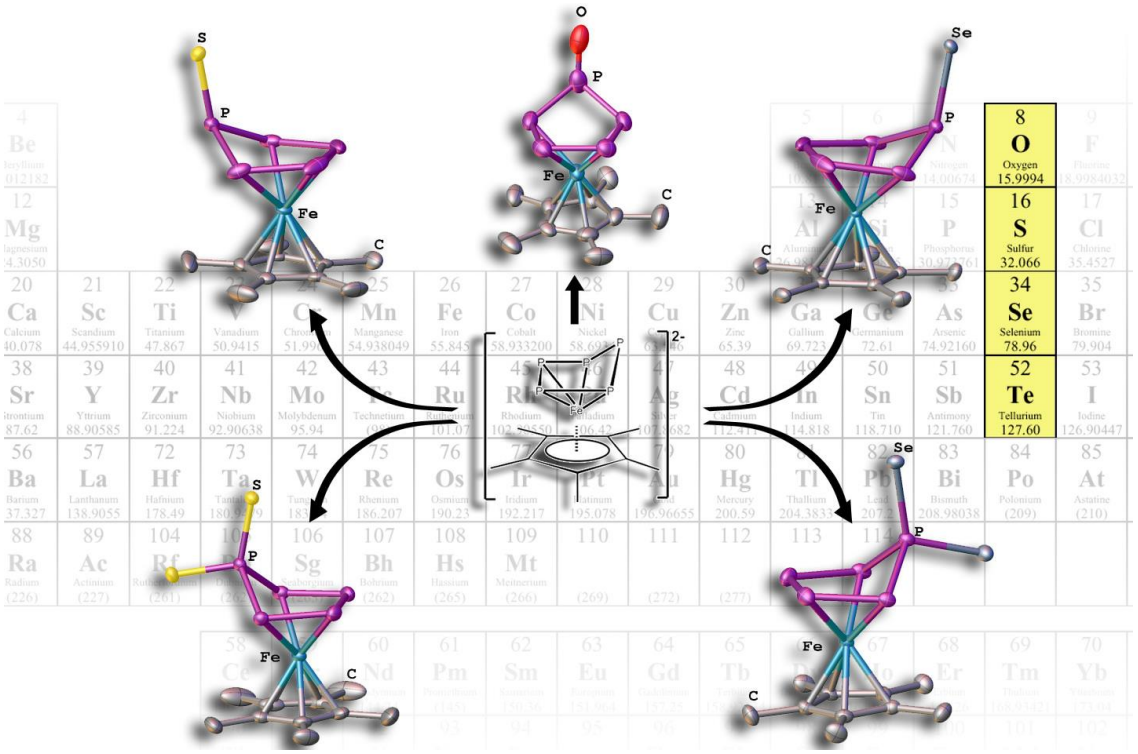

- Compound **8** is already described in Eric Mädl's master thesis. Compound **9** was synthesized by Eric Mädl. All remaining compounds were synthesized by David Konieczny in the scope of his master thesis.

- The discussion of the compounds **8** and **9** was written by Eric Mädl. The discussion of the remaining compounds was written by David Konieczny and edited by Eric Mädl. Details about X-ray structure analyses in the chapter "supporting information" were written by Michael Bodensteiner and Alexander Virovets.

- X-ray structure analyses and refinements were performed by Michael Bodensteiner, Eugenia V. Peresypkina and David Konieczny.

- All figures were made by Eric Mädl.

6.1 Discussion

David Konieczny, Eric Mädl, Michael Bodensteiner, Alexander V. Virovets and Manfred Scheer*

Abstract: *The reaction of [Cp*Fe(η^4-P_5)]$^{2-}$ (**2**) and [(Cp*Fe)$_2$(μ,$\eta^{4:4}$-P_{10})]$^{2-}$ (**3**) with the chalcogens sulfur and selenium gives, depending on the stoichiometry, novel functionalized pentaphosphaferrocene derivatives. By using one equivalent of S or Se, the dianionic products [Cp*Fe(η^4-P_5S)]$^{2-}$ (**4**) or [Cp*Fe(η^4-P_5Se)]$^{2-}$ (**5**) are obtained from **2**. The reaction of **2** and **3**, respectively, with two equivalents of chalcogen (S, Se) yield the disubstituted species [Cp*Fe(η^4-P_5S_2)]$^{2-}$ (**6**) and [Cp*Fe(η^4-P_5Se_2)]$^{2-}$ (**7**). The reaction of KOH with [Cp*Fe(η^5-P_5)] (**1**) gives [Cp*Fe(η^4-P_5OH)]$^-$ (**8**), which could subsequently be reduced with potassium to form [Cp*Fe(η^4-P_5O)]$^{2-}$ (**9**). All complexes are fully characterized by means of X-ray diffraction and NMR spectroscopy.*

Since its discovery in 1951[1] and the identification of its structure in 1952,[2] ferrocene has become a fundamental complex in organometallic synthesis with many applications.[3] By the isolobal relationship the *cyclo*-P_5 anion is related to the cyclopentadienyl ligand and therefore, complexes such as pentaphosphaferrocene [Cp*Fe(η^5-P_5)] (**1**), which is isolobal to ferrocene and exhibits an unsubstituted *cyclo*-P_5 unit,[4] are of special interest. The reactivity of pentaphosphaferrocene was extensively investigated towards organometallic compound moieties. Either a complete fragmentation of the P_5 ring is observed and only in few cases it stays intact,[5] or triple-decker complexes are formed.[6] On the other hand, due to the five accessible lone pairs of the *cyclo*-P_5 ligand, **1** is used as a building block in coordination chemistry.[7] Furthermore, the reaction of **1** with main group nucleophiles leads to functionalized anionic derivatives with a substituted, but intact *cyclo*-P_5 unit.[8] The redox properties of **1** were studied by cyclic voltammetry[9] and the products of the oxidation [(Cp*Fe)$_2$(μ,$\eta^{5:5}$-P_{10})]$^{2+}$ and reduction [(Cp*Fe)$_2$(μ,$\eta^{4:4}$-P_{10})]$^{2-}$ (**3**) could be isolated.[10] The reduction of **1** with an excess of potassium in DME leads to the unexpected and strongly nucleophilic dianion [Cp*Fe(η^4-P_5)]$^{2-}$ (**2**), which was not observed in CV studies. Both dianionic products **2** and **3** are strong nucleophiles and can activate white phosphorus, showing the potential of **2** and **3** for a subsequent chemistry und formation of new structural motifs. Therefore it is of great interest to investigate the potential of these nucleophilic reactions in terms of activation of other main group moieties, to access novel types of mixed main group element containing ligands. We report herein about the activation of the main-group elements sulfur and selenium by **2** and **3**, leading to unprecedented pentaphosphathio and -seleno ligands.

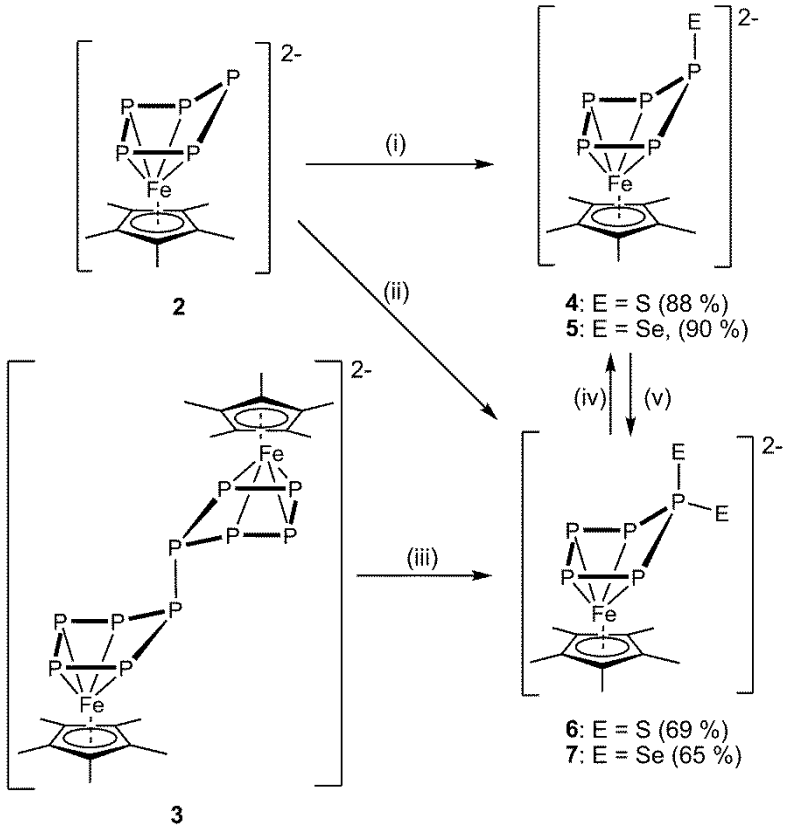

Scheme 1. Reactivity of the dianions **2** and **3** with sulfur and selenium in different stoichiometries. Reaction of **2**: (i) 1 eq. of S ($^1/_8$ S_8) or Se in DME, −60 °C → r.t.; (ii) 2 eq. of S or Se in DME, −60 °C → r.t.; reaction of **3**: (iii) 2 eq. of S/Se in DME, −60 °C → r.t.; reaction of **6**: (iv) 1 eq. of **2** in THF, −60 °C → r.t.; reaction of **4**: (v) 1 eq. S in DME, −60 °C → r.t.; yield are given in parenthesis.

The reaction of **2** with one equivalent of chalcogen (S, Se) in DME at low temperature leads to a color change from olive green to dark brown, while warming up to ambient temperature. After workup, $[Cp^*Fe(\eta^4\text{-}P_5S)]^{2-}$ (**4**) and $[Cp^*Fe(\eta^4\text{-}P_5Se)]^{2-}$ (**5**) are obtained in good yields and purity, respectively, as their potassium salts (Scheme 1). They are well soluble in THF and DME, slightly soluble in MeCN and insoluble in *n*-hexane. The ^{31}P NMR spectra show an AMM'XX' spin system, with three distinct multiplets centered at 14.6, 33.9 and 107.7 ppm and 14.4, 33.2 and 81.9 ppm for the anions **4** and **5**, respectively. The signals exhibit an intensity ratio of 2:2:1, which indicates an intact P_5 ring with envelope-like conformation, comparable to the starting material **2**. For the selenium containing compound **5** the signal at 81.9 ppm shows additional selenium satellites. The ^{77}Se NMR spectrum of **5** reveals a doublet at 352.0 ppm with a $^1J_{Se\text{-}P}$ coupling constant of 300 Hz. The central structural motif of **4** and **5**, obtained by X-ray structure analyses, is a η^4-P_5S and a η^4-P_5Se unit respectively, each with four phosphorus atoms in a plane, which are coordinating to the iron atom. The fifth P atom bears one chalcogen atom in an *endo*-position (Figure 1). In **4** the P-P bond lengths range from 2.129(4) to 2.166(2) Å (in **5**: 2.132(3) to 2.1648(8) Å) and thus exhibit double bond character.[11] The distances of the corresponding P atoms in the starting compound **2** are similar, although the bond lengths of the P2-P3 and P4-P5 bonds in **4** and **5** are significantly shorter compared to **2** (Figure 1). The Fe-P bond

lengths (**4**: 2.292(2) to 2.320(3) Å, **5**: 2.2925(5) Å to 2.3236(5) Å) are slightly elongated, whereas the $Cp^*_{centroid}$-Fe distances (**4**: 1.6708(8) Å, **5**: 1.7013(5) Å) are significantly shorter in comparison to **2**.[10] The P-S bond in **4**, with a bond length of 2.092(2) Å exhibits double bond character.[11] In contrast, the P-Se bond in **5**, with a bond length of 2.2518(4) Å is considered a P-Se single bond.[11]

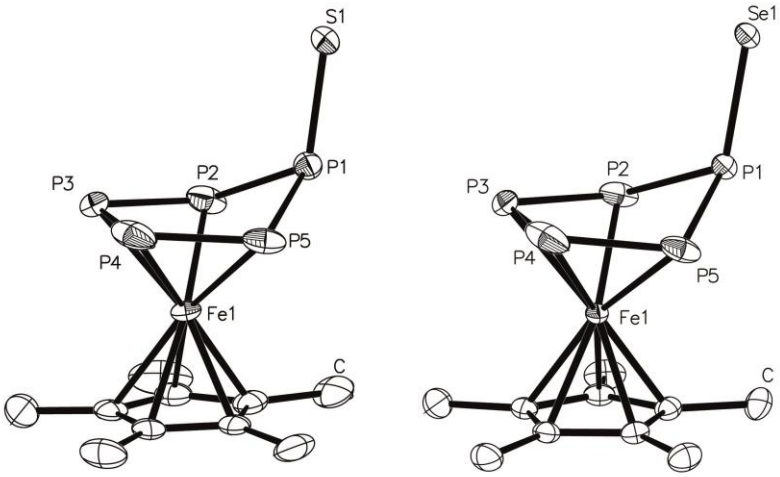

Figure 1. Molecular structures of the anionic part of $[K_2(dme)_2]$[**4**] (left) and $[K_2(dme)_2]$[**5**] (right). Ellipsoids are drawn at 50% probability level. Hydrogen atoms bonded to carbon are omitted for clarity. Selected bond lengths [Å] and angles [°]: **4**: P1-S1 2.092(2), P1-P2 2.156(2), P2-P3 2.159(3), P3-P4 2.129(4), P4-P5 2.157(3), P5-P1 2.166(2), Fe-P2 2.2916(19), Fe-P3 2.3204(25), Fe-P4 2.3102(21), Fe-P5 2.3077(18), P2-P1-S1 115.30(8), P5-P1-S1 121.14(8), P3-P4-P5 102.86(11), P1-P2-P3 111.52(11), P4-P3-P2 103.26(10), S1-P1-P2 115.38(9), S1-P1-P5 121.15(9), P2-P1-P5 91.82(8). **5**: Se1-P1 2.2518(4), Fe1-P2 2.3139(5), Fe1-P5 2.2925(5), Fe1-P4 2.3236(5), Fe1-P3 2.3116(5), P1-P2 2.1651(7), P1-P5 2.1520(7), P2-P3 2.1508(8), P5-P4 2.1648(8), P4-P3 2.1323(10), P3 P2-P1 111.71(3), P1-P5 P4 110.95(3), P3-P4-P5 102.99(3), P4-P3-P2 103.01(3), P5-P1-Se1 114.08(2).

Since in $[(Cp^*Fe)_2(\mu,\eta^{4:4}\text{-}P_{10})]^{2-}$ (**3**) two $[Cp^*Fe(\eta^4\text{-}P_5)]$ moieties are incorporated two equivalents of S or Se were added to **3**, yielding the twofold substituted compounds $[Cp^*Fe(\eta^4\text{-}P_5S_2)]^{2-}$ (**6**) and $[Cp^*Fe(\eta^4\text{-}P_5Se_2)]^{2-}$ (**7**), respectively (Scheme 1). The addition of only one equivalent of S or Se to **3** leads to the same product formation, but if an excess of chalcogen is used a decomposition of **3** to **1** is observed and no further products are determined by NMR spectroscopy. Furthermore, compounds **6** and **7** can also be synthesized by adding two equivalents of chalcogen to **2**, however **3** is easier to handle and excels in solubility. It is also noteworthy by adding one equivalent of **2** to the twofold substituted compound **6** the monosubstituted compound **4** is obtained. Vice versa, the addition of sulfur to **4** leads to the formation of **6** (Scheme 1).

The ^{31}P NMR spectra of the isolated compounds **6** and **7** show similar properties like the monosubstituted compounds **4** and **5**, with three multiplets centered at −8.8, 21.3 and 182.8 ppm and 0.7, 23.1 and 116.7 ppm, respectively, each with an intensity ratio of 2:2:1. For **7** the signal at 116.7 ppm exhibits additional satellites due to a $^1J_{Se\text{-}P}$ coupling. The ^{77}Se{^{1}H} NMR of **7** shows two doublets at −64.4 ppm ($^1J_{Se\text{-}P}$ = 471 Hz) and 560.1 ppm ($^1J_{Se\text{-}P}$ = 530 Hz). The assignment of these signals to the according selenium atoms is made by comparison of **7** with **5**. Since the *endo*-Se atom of **5** exhibits a chemical shift of 352.0 ppm, the low field shifted doublet in the ^{77}Se{^{1}H} NMR spectrum of **7** can be attributed to the *endo*-selenium atom in the anion **7**.[12] It is noteworthy, that the ^{31}P NMR spectra of the reaction solutions of **3** with two equivalents chalcogen show the formation of **1** as a byproduct in a 1:1 ratio. This indicates a heterolytic bond cleavage of the P-P bond in **3**, which is connecting the two [Cp*Fe(η^4-P$_5$)] moieties. **6** and **7** were recrystallized from THF to receive suitable single crystals of [K$_2$(thf)$_2$][**6**] and [K$_2$(thf)$_4$][**7**]. X-ray structure analyses show for both anions a central structural motif consisting of a P$_5$E$_2$ (E = S, Se) unit, which coordinates in a η^4-fashion to the Fe atom and exhibits an envelope conformation, similar to the mono substituted compounds **4** and **5** (Figure 2). Again, the chalcogen atoms are exclusively bonding to the non-coordinating P atom. The P-P bond lengths in **6**, the Fe-P distances and the Cp*$_{centroid}$–Fe distances are almost equal to those of the single substituted products. The P-S bonds (2.0258(7) and 2.0225(7) Å) in **6** show P-S double bond character. The P-Se bond lengths in **7** (2.1844(6) and 2.1938(7) Å) show partial double bond character.[11]

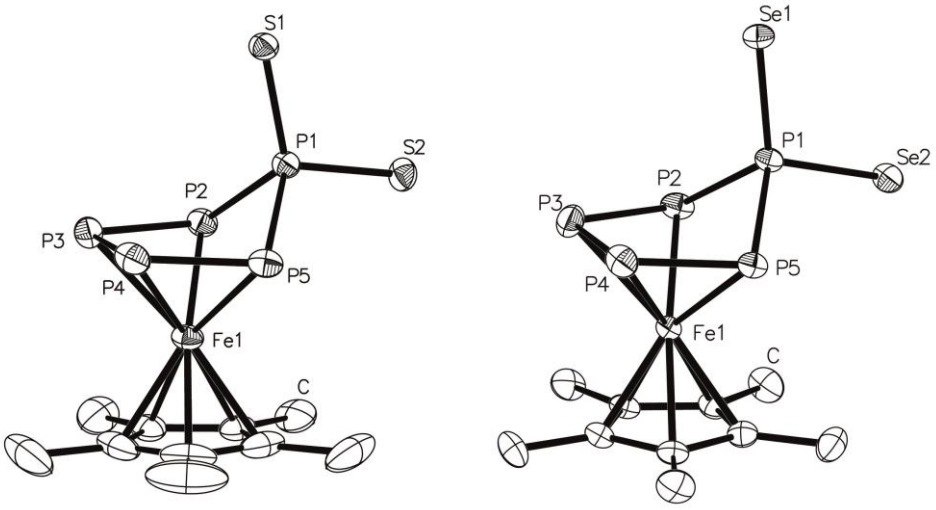

Figure 2. Molecular structures of anionic part of [K$_2$(thf)$_2$][**6**] (left) and [K$_2$(thf)$_4$][**7**] (right). Ellipsoids are drawn at 50% probability level. Hydrogen atoms bonded to carbon are omitted for clarity. Selected bond lengths [Å] and angles [°]: **6**: Fe1-P2 2.3119(6), Fe1-P5 2.3095(6), Fe1-P3 2.3275(7), Fe1-P4 2.3285(7), P1-P2 2.1834(7), P1-P5 2.1849(8), P2-P3 2.1361(8), P5-P4 2.1431(8), P3-P4 2.1737(9), S1-P1 2.0258(7), S2-P1 2.0225(7), S1-P1-P2 119.61(3), S1-P1-P5 116.28(3), S2-P1-P2 106.57(3), P2-P1-P5 92.37(3), P3-P2-P1 102.40(3), P4-P5-P1 100.96(3). **7**: Se1-P1 2.1844(6), Se2-P1 2.1938(7), Fe1-P5 2.2950(7), Fe1-P2 2.3087(8), Fe1-P4 2.3242(8), Fe1-P3 2.3458(8), P1-P5 2.1781(9), P1-P2

2.1786(9), P5-P4 2.1477(10), P2-P3 2.1276(11), Se1-P1-Se2 112.20(3), P5-P1-Se1 117.17(3), P5-P1-Se2 106.79(3), P5-P1-P2 92.63(3), P2-P1-Se1 121.33(4), P2-P1-Se2 104.26(3), P5-P4-P3 103.69(4), P2-P3-P4 102.84(4).

The P-P bond lengths in **6**, the Fe-P distances and the $Cp^*_{centroid}$–Fe distances are almost equal to those of the single substituted products. The P-S bonds (2.0258(7) and 2.0225(7) Å) in **6** show P-S double bond character. The P-Se bond lengths in **7** (2.1844(6) and 2.1938(7) Å) show partial double bond character.[11]

Unfortunately, the conversions of **2** and **3** with grey tellurium were not successful. In contrast to sulfur and selenium, which have almost the same redox potential (0.14 and −0.11 V), Te is a significantly stronger reducing agent (−1.143 V, in water).[13] This might prohibit the reduction and thus the reaction with Te. Instead, approaches with other tellurium sources, in which Te exhibits another oxidation state, might be successful.

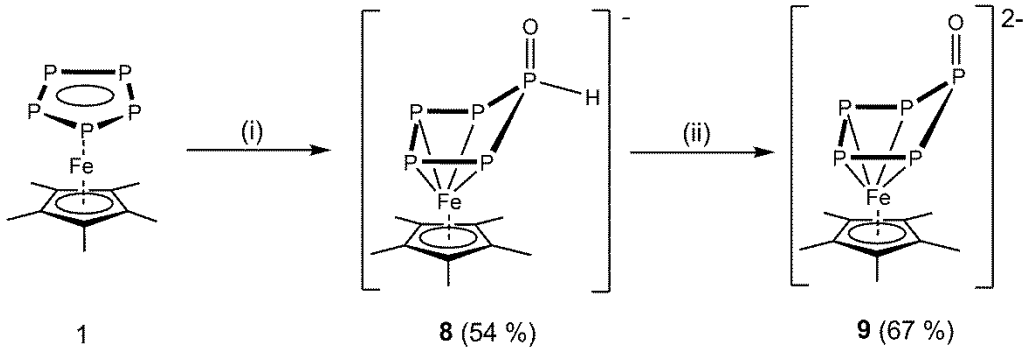

1 **8** (54 %) **9** (67 %)

Scheme 3. Formation of **8** and the subsequent reduction to the dianion **9**. Reaction of **1**: (i) KOH in DME, r.t.; reaction of **8**: (ii) excess K in DME, r.t.; yields are given in parenthesis.

To complement the series of $[Cp^*Fe(\eta^4\text{-}P_5E)]^{2-}$ (E = O, S, Se) also for oxygen a different synthetic approach had to be chosen (Scheme 3). Therefore, the nucleophile KOH was reacted with **1**, yielding the anionic compound $[Cp^*Fe(\eta^4\text{-}P_5OH)]^-$ (**8**). The ^{31}P NMR spectrum of the isolated compound **8** shows three signals centered at −17.5, 19.0 and 80.9 ppm. The signal at 80.9 ppm, which shows a $^1J_{P\text{-}H}$ coupling of 364.6 Hz, is assigned to the phosphorus atom that bears the hydroxide group. In the ^{1}H NMR spectrum a signal at 7.5 ppm is observed, with a multiplicity as a dublet of triplet of triplets. Therefore, based on the NMR spectra, a P-H bond can be assumed. Single crystals suitable for X-ray structure analysis were obtained from the lithium salt $[Li(thf)_2][\mathbf{8}]$, by reacting LiOH with **1**. The structural motif of **8** consists of an enveloped *cyclo*-P_5 ring, which coordinates to the iron fragment in a η^4-fashion (Figure 3), very similiar to already discussed compounds.[8] Noteworthy, the hydroxy group undergoes a tautomeric rearrangement and forms a P=O (1.528(2) Å) and a P-H bond, as shown by NMR spectroscopy. To yield the dianionic compound $[Cp^*Fe(\eta^4\text{-}P_5O)]^{2-}$ (**9**) potassium was used to remove the proton and reduce **8**. In the ^{31}P NMR of **9** no proton coupling is observed anymore, along

three multiplets centered at 20.9 and 35.6 and 165.4 ppm. Crystals suitable for X-ray structure analysis were obtained from a DME/pentane/toluene mixture, showing very similar structural features of **9**, compared to **4** and **5** (Figure 3). All P-P bonds exhibit double bond character (P-P bond lengths: 2.136(3) – 2.172(2) Å) and a P=O bond was determined, with 1.441(6) Å in average.

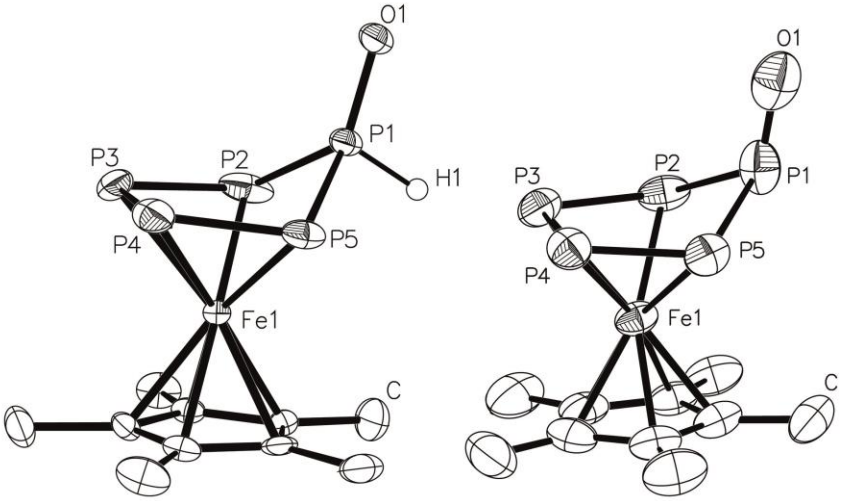

Figure 3: Molecular structures of the anionic part of $[Li(thf)_2]$[**8**] (left) and $[K_8(dme)_8]$[**9**]$_4$·2PhCH$_3$ (right). Hydrogen atoms bonded to carbon are omitted for clarity. Selected bond lengths [Å] and angles [°]: **8**: P1-O3 1.528(2), P1-P2 2.1353(11), P1-P5 2.1355(10), P2-P3 2.1406(15), P4-P3 2.1430(16), P5-P4 2.1269(13), Cp*$_{centroid}$-Fe 1.698; O3-P1-P2 123.58(10), O3-P1-P5 124.64(10), P2-P1-P5 98.54(4), P1-P2-P3 102.03(5), P2-P3-P4 105.00(5), P5-P4-P3 104.69(5), P4-P5-P1 102.63(5). **9**: P1-P5 2.136(3), P1-P2 2.144(3), P1-O1 1.441(6), P5-P4 2.172(2), P4-P3 2.131(2), P3-P2 2.167(3), Fe1-P5 2.2944(18), Fe1-P4 2.3178(18), Fe1-P3 2.3251(18), Fe1-P2 2.3071(19). O1-P1-P2 120.9(2), O1-P1-P5 117.7(2), P12-P1-P2 92.92(10), P3-P4-P5 103.21(10), P4-P3-P2 102.66(9).

In conclusion $[Cp^*Fe(\eta^4\text{-}P_5)]^{2-}$ (**2**) and $[(Cp^*Fe)_2(\mu,\eta^{4:4}\text{-}P_{10})]^{2-}$ (**3**) have been proven to be useful reagents for the activation of selenium and sulfur, leading to mono- or disubstituted dianionic pentaphosphaferrocene derivatives. For compound **2** a stoichiometry dependency was found, in contrast to **3**. The oxygen containing compound $[Cp^*Fe(\eta^4\text{-}P_5O)]^{2-}$ (**9**) could also be synthesized by the reduction of $[Cp^*Fe(\eta^4\text{-}P_5OH)]^{-}$ (**8**), which is obtained from the addition of hydroxide as nucleophile to pentaphosphaferrocene. All compounds described are stable, accessible in good yields, highly charged and thus interesting starting materials for further reactivity studies.

References

[1] T. J. Kealy, P. L. Pauson, *Nature* **1951**, *168*, 1039-1040.

[2] G. Wilkinson, M. Rosenblum, M. C. Whiting, R. B. Woodward, *J. Am. Chem. Soc.* **1952**, *74*, 2125-2126.

[3] a) H. Werner, *Angew. Chem. Int. Ed.* **2012**, *51*, 6052-6058; b) K. Heinze, H. Lang, *Organometallics* **2013**, *32*, 5623-5625; c) M. F. R. Fouda, M. M. Abd-Elzaher, R. A. Abdelsamaia, A. A. Labib, *Appl. Organomet. Chem.* **2007**, *21*, 613-625.

[4] O. J. Scherer, T. Brück, *Angew. Chem.* **1987**, *99*, 59-59.

[5] a) O. J. Scherer, S. Weigel, G. Wolmershäuser, *Chem. Eur. J.* **1998**, *4*, 1910-1916; b) B. Koch, O. J. Scherer, G. Wolmershäuser, *Z. Anorg. Allg. Chem.* **2000**, *626*, 1797-1802; c) O. J. Scherer, T. Mohr, G. Wolmershäuser, *J. Organomet. Chem.* **1997**, *529*, 379-385.

[6] a) O. J. Scherer, T. Brück, G. Wolmershäuser, *Chem. Ber.* **1989**, *122*, 2049-2054; b) B. Rink, O. J. Scherer, G. Heckmann, G. Wolmershauser, *Chem. Ber.* **1992**, *125*, 1011-1016; c) O. J. Scherer, *Angew. Chem. Int. Ed.* **1990**, *29*, 1104.

[7] a) J. Bai, A. V. Virovets, M. Scheer, *Angew. Chem. Int. Ed.* **2002**, *41*, 1737-1740; b) F. Dielmann, A. Schindler, S. Scheuermayer, J. Bai, R. Merkle, M. Zabel, A. V. Virovets, E. V. Peresypkina, G. Brunklaus , H. Eckert, M. Scheer, *Chem. Eur. J.* **2012**, *18*, 1168-1179; c) M. Scheer, L. J. Gregoriades, A. V. Virovets, W. Kunz, R. Neueder, I. Krossing, *Angew. Chem. Int. Ed.* **2006**, *45*, 5689-5693; d) J. Bai, A. V. Virovets, M. Scheer, *Science* **2003**, *300*, 781-783; e) B. P. Johnson, F. Dielmann, G. Balázs, M. Sierka, M. Scheer, *Angew. Chem. Int. Ed.* **2006**, *45*, 2473-2475; f) M. Scheer, J. Bai, B. P. Johnson, R. Merkle, A. V. Virovets, C. E. Anson, *Eur. J. Inorg. Chem.* **2005**, *2005*, 4023-4026; g) M. Scheer, A. Schindler, J. Bai, B. P. Johnson, R. Merkle, R. Winter, A. V. Virovets, E. V. Peresypkina, V. A. Blatov, M. Sierka, H. Eckert, *Chem. Eur. J.* **2010**, *16*, 2092-2107; h) M. Scheer, A. Schindler, C. Gröger, A. V. Virovets, E. V. Peresypkina, *Angew. Chem. Int. Ed.* **2009**, *48*, 5046-5049; i) M. Scheer, A. Schindler, R. Merkle, B. P. Johnson, M. Linseis, R. Winter, C. E. Anson, A. V. Virovets, *J. Am. Chem. Soc.* **2007**, *129*, 13386-13387; j) S. Welsch, C. Gröger, M. Sierka, M. Scheer, *Angew. Chem.* **2011**, *123*, 1471-1474.

[8] E. Mädl, M. V. Butovskii, G. Balázs, E. V. Peresypkina, A. V. Virovets, M. Seidl, M. Scheer, *Angew. Chem. Int. Ed.* **2014**, *53*, 7643-7646.

[9] R. F. Winter, W. E. Geiger, *Organometallics* **1999**, *18*, 1827-1833.

[10] M. V. Butovskiy, G. Balázs, M. Bodensteiner, E. V. Peresypkina, A. V. Virovets, J. Sutter, M. Scheer, *Angew. Chem. Int. Ed.* **2013**, *52*, 2972-2976.

[11] P. Pyykkö, M. Atsumi, *Chem. Eur. J.* **2009**, *15*, 12770-12779.

[12] Under the assumption that the compared Se atoms underlie a similar electronic shielding.

[13] A. J. Bard, R. Parsons, J. Jordan, *Standard Potentials in Aqueous Solutions*, M. Dekker, New York, **1985**.

6.2 Supporting Information

Supporting information of the manuscript entitled:

Chalcogen functionalized polyphosphorus complexes

David Konieczny, Eric Mädl, Michael Bodensteiner, Alexander Virovets and Manfred Scheer*

Contents

6.2.1 Experimental details: complex syntheses and characterization

General Procedures: All manipulations were performed with rigorous exclusion of oxygen and moisture in Schlenk-type glassware on a dual manifold Schlenk line in argon atmosphere or in Ar filled glove box with a high-capacity recirculator (<0.1ppm O_2). THF, *n*-hexane, CH_2Cl_2 and acetonitrile were taken from the MBRAUN solvent purification system SPS-800. DME was distilled from sodium benzophenoneketyl. Deuterated solvents were degassed, dried and distilled prior to use. Sulfur and selenium were available and the complexes $[Cp^*Fe(\eta^5\text{-}P_5)]$[1] (**1**), $[K_2(dme)_2][Cp^*Fe(\eta^4\text{-}P_5)]$ ($[K_2(dme)_2][\mathbf{2}]$) and $[K_2(dme)_3][(Cp^*Fe)_2(\eta^{4:4}\text{-}P_{10})]$[2] ($[K_2(dme)_3][\mathbf{3}]$) were prepared according to published procedures. NMR spectra were recorded on a BrukerAvance 300 MHz and BrukerAvance 400 MHz spectrometers. Chemical shifts were measured at ambient temperature and are given in ppm; they are referenced to TMS for ^1H and ^{13}C, 85% H_3PO_4 for ^{31}P as external standard and $Se(CH_3)_2$ for ^{77}Se as external standard. ES-MS spectra were measured on a ThermoQuest Finnigan TSG 7000 mass spectrometer. Elemental analyses (CHN) were determined using in-house facility.

Synthesis of $[K_2(dme)_2][4]$, [4] = $[Cp^*Fe(\eta^4\text{-}P_5S)]^{2-}$: To a solution of $[K_2(dme)_2][\mathbf{2}]$ (150 mg, 0.248 mmol) in DME (15 mL) at −60 °C a solution of sulfur (8.0 mg, 0.031 mmol) in DME (5 mL) was added. The reaction mixture turned from dark olive green to dark brown while slowly warming up to ambient temperature and was stirred for 18 h at room temperature. The volume of the solution was reduced to ca. 5 mL and layered with *n*-hexane (15 ml). After 2 days at 0 °C dark brown microcrystalline precipitate of $[K_2(dme)_2][\mathbf{4}]$ (0.140 g, 88%) has formed. $C_{10}H_{15}FeK_2P_5S \cdot 1.5\ C_4H_{10}O_2$ (590.92): calcd. C 32.50, H 5.11, S 5.42; found C 32.05, H 4.96, S 4.67. ^{1}H NMR (400.13 MHz, THF-d_8): δ [ppm] = 1.39 (s, 15 H, $C_5(CH_3)_5$), 3.28 (s, 12 H, CH_3, DME), 3.43 (s, 8 H, CH_2, DME). ^{13}C{^{1}H} NMR (100.62 MHz, THF-d_8): δ [ppm] = 11.4 (s, $C_5(CH_3)_5$), 58.7 (s, CH_3, DME), 72.6 (s, CH_2, DME), 86.1 (s, $C_5(CH_3)_5$). ^{31}P{^{1}H} NMR (161.97 MHz, THF-d_8): δ [ppm] = 14.6 (m, 2 P), 33.9 (m, 2 P), 107.7 (tt, 1 P). ^{31}P NMR (161.97 MHz, THF-d_8): δ [ppm] = 14.6 (m, 2 P), 33.9 (m, 2 P), 107.7 (tt, 1 P). For the assignment of the phosphorus atoms and coupling constants see Figure S7 and Table S4. ES-MS (m/z): 314.8 (20) $[Cp^*FeP_4H]^-$, 346.7 (37) $[Cp^*FeP_5H]^-$, 378.8 (5) $[Cp^*FeP_5SH]^- \triangleq [M^{2-}+H^+]^-$, 408.8 (100) $[C_{10}H_{14}FeP_5S_2]^-$, 417.8 (23) $[C_{10}H_{15}FeP_5SK]^-$.

Synthesis of $[K_2(dme)][5]$, [5] = $[Cp^*Fe(\eta^4\text{-}P_5Se)]^{2-}$: To a solution of $[K_2(dme)_2][\mathbf{2}]$ (90 mg, 0.149 mmol) in DME (20 mL) at −60 °C a suspension of red selenium (11.8 mg, 0.149 mmol) in DME (5 mL) was added. The reaction mixture turned from dark olive green to dark brown while slowly warming up to ambient temperature and was stirred for 18 h at room temperature. The volume of the solution was reduced to ca. 5 mL and layered with *n*-hexane (15 ml). After 2 days at 0 °C dark brown crystals of $[K_2(dme)_2][\mathbf{5}]$ (88 mg, 90%) have formed. $C_{10}H_{15}FeK_2P_5Se \cdot 1.3\ C_4H_{10}O_2$ (620.85): calcd. C 29.43, H 4.55; found C 29.62, H 4.13. ^{1}H NMR (400.13 MHz, THF-d_8): δ [ppm] = 1.38 (s, 15 H, $C_5(CH_3)_5$), 3.28 (s, 6 H, CH_3, DME), 3.43 (s, 4 H, CH_2, DME). ^{13}C{^{1}H} NMR (100.62 MHz, THF-d_8): δ [ppm] = 11.5 (s, $C_5(CH_3)_5$), 58.9 (s, CH_3, DME), 72.7 (s, CH_2, DME), 86.3 (s, $C_5(CH_3)_5$). ^{31}P{^{1}H} NMR (161.97 MHz, THF-d_8): δ [ppm] = 14.5 (m, 2 P), 33.1 (m, 2 P), 81.9 (tt, 1 P). ^{31}P NMR (161.97 MHz, THF-d_8): δ [ppm] = 14.5 (m, 2 P), 33.1 (m, 2 P), 81.9 (tt, 1 P). ^{77}Se NMR (76.27 MHz, THF-d_8): δ [ppm] = 352.0 (d, ^1J(Se,P) = 300 Hz, 1 Se, P*Se*). For the assignment of the phosphorus atoms and coupling constants see Figure S8 and Table S5. ES-MS (m/z): 508.0 (10) $[C_{10}H_{16}FeP_5Se_2]^- \triangleq [M^{2-}+Se+H^+]^-$.

Synthesis of $[K_2(dme)_2][6]$, [6] = $[Cp^*Fe(\eta^4\text{-}P_5S_2)]^{2-}$: To a solution of $[K_2(dme)_3][\mathbf{3}]$ (250 mg, 0.24 mmol) in DME (20 mL) at −60 °C a solution of sulfur (15.4 mg, 0.06 mmol) in DME (5 mL) was added. The reaction mixture turned from dark olive green to dark red brown at low temperature and then to dark brown green while slowly warming up to ambient temperature and was stirred for 18 h at room temperature. The solvent was removed und the product was washed with *n*-hexane. The product was dissolved in THF (10 mL) and the solution was layered with *n*-hexane (30 mL). After 4 days at 0 °C dark green needles of $[K_2(dme)_2][\mathbf{6}]$ (110 mg, 69%) have formed. $C_{10}H_{15}FeK_2P_5S_2 \cdot 1.3\ C_4H_{10}O_2$

(604.88): calcd. C 30.16, H 4.66, S 10.59; found C 30.32, H 4.78, S 12.31. ^{1}H NMR (400.13 MHz, THF-d_8): δ [ppm] = 1.63 (s, 15 H, $C_5(CH_3)_5$), 3.28 (s, 12 H, CH_3, DME), 3.44 (s, 8 H, CH_2, DME). ^{13}C{^{1}H} NMR (100.62 MHz, THF-d_8): δ [ppm] = 11.7 (s, $C_5(CH_3)_5$), 58.9 (s, CH_3, DME), 72.7 (s, CH_2, DME), 88.0 (s, $C_5(CH_3)_5$). ^{31}P{^{1}H} NMR (161.97 MHz, THF-d_8): δ [ppm] = −8.7 (m, 2 P), 21.2 (m, 2 P), 182.8 (t, 1 P). ^{31}P NMR (161.97 MHz, THF-d_8): δ [ppm] = −8.7 (m, 2 P), 21.2 (m, 2 P), 182.8 (t, 1 P). For the assignment of the phosphorus atoms and coupling constants see Figure S9 and Table S6. ES-MS (m/z): 314.8 (15) $[Cp^*FeP_4H]^-$, 346.7 (7) $[Cp^*FeP_5H]^-$, 408.8 (100) $[C_{10}H_{14}FeP_5S_2]^- \triangleq [M^{2-}\text{-}H^-]^-$.

Synthesis of $[K_2(dme)_2]$[6] from $[K_2(dme)_2]$[2] and sulfur: To a solution of $[K_2(dme)_2]$[**2**] (100 mg, 0.17 mmol) in DME (20 mL) at −60 °C a solution of sulfur (10.6 mg, 0.04 mmol) in DME (5 mL) was added. The reaction mixture turned from dark olive green to dark brown green while slowly warming up to ambient temperature and was stirred for 18 h at room temperature. For completion of the conversion of **2** additional sulfur (6.5 mg, 0.025 mmol) was added at −60 °C. The mixture was allowed to come to room temperature and stirred for another 18 h. After layering with *n*-hexane and storage at 0 °C for 4 d dark green crystalline precipitate of $[K_2(dme)_2]$[**6**] has formed (88 mg, 78%).

Synthesis of $[K_2(dme)_2]$[7], [7] = $[Cp^*Fe(\eta^4\text{-}P_5Se_2)]^{2-}$: To a solution of $[K_2(dme)_3]$[**3**] (250 mg, 0.24 mmol) in DME (20 mL) at −60 °C a suspension of selenium (38 mg, 0.48 mmol) in DME (10 mL) was added. The reaction mixture turned from dark olive green to dark red at low temperature and then to dark brown green while slowly warming up to ambient temperature. The mixture was stirred for 2 h at room temperature. The solvent was removed and the product was washed with *n*-hexane. The product was dissolved in THF (10 mL) and the solution was layered with *n*-hexane (30 mL). After 2 days at 0 °C brown blocks of $[K_2(dme)_2]$[**7**] (120 mg, 65%) have formed. $C_{10}H_{15}FeK_2P_5Se_2 \cdot 1.3\ C_4H_{10}O_2$ (700.77): calcd. C 26.11, H 4.04; found C 25.73, H 4.05. ^{1}H NMR (400.13 MHz, THF-d_8): δ [ppm] = 1.61 (s, 15 H, $C_5(CH_3)_5$), 3.28 (s, 12 H, CH_3, DME), 3.44 (s, 8 H, CH_2, DME). ^{13}C{^{1}H} NMR (100.62 MHz, THF-d_8): δ [ppm] = 11.6 (s, $C_5(CH_3)_5$), 58.9 (s, CH_3, DME), 72.7 (s, CH_2, DME), 88.1 (s, $C_5(CH_3)_5$). ^{31}P{^{1}H} NMR (161.97 MHz, THF-d_8): δ [ppm] = 0.7 (m, 2 P), 23.0 (m, 2 P), 116.6 (t, 1 P). ^{31}P NMR (161.97 MHz, THF-d_8): δ [ppm] = 0.7 (m, 2 P), 23.0 (m, 2 P), 116.6 (t, 1 P). ^{77}Se{^{1}H} NMR (76.27 MHz, THF-d_8): δ [ppm] = −64.4 (d, ^{1}J(Se,P) = 471 Hz, 1 Se, Se_B), 560.1 (d, ^{1}J(Se,P) = 530 Hz, 1 Se, Se_A). For the assignment of the phosphorus atoms and coupling constants see Figure S10 and Table S7.

Synthesis of $[K_2(dme)_2]$[7] from $[K_2(dme)_2]$[2] and selenium: To a solution of $[K_2(dme)]$[**2**] (70 mg, 0.14 mmol) in DME (20 mL) at −60 °C a suspension of selenium (22 mg, 0.28 mmol) in DME (5 mL) was added. The reaction mixture turned from dark olive green to dark brown while slowly warming up

to ambient temperature and was stirred for 30 min at room temperature. After removal of the solvent, $[K_2(dme)_2][\mathbf{6}]$ was obtained as dark brown powder (83 mg, 79%).

Synthesis of [K][8], [8] = $[Cp^*Fe(\eta^4\text{-}P_5OH)]^-$: To a mixture of KOH (117 mg, 2.1 mmol) and $[Cp^*Fe(\eta^5\text{-}P_5)]$ (800 mg, 2.3 mmol) 130 mL DME is added. The solution is stirred for three days. A color change from green to brown is observed. The solvent is removed, the precipitate washed with *n*-hexane, dried in vacuum for 3 hours and K[**8**] isolated (500 mg, 54 %). A crystal suitable for X-ray structure analysis was obtained from the analog reaction of $[Cp^*Fe(\eta^5\text{-}P_5)]$ with LiOH. $C_{10}H_{16}FeP_5OK$ (402.05): calcd. C 29.87, H 4.01; found C 30.14, H 3.99. ^{1}H NMR (400.13 MHz, THF-d_8): δ [ppm] = 1.5 (s, 15 H, $C_5(CH_3)_5$), 7.5 (dtt, $^1J_{H,P}$ = 364,6 Hz, ^2J(H,P) = 45.9 Hz, ^2J(H,P) = 5.6 Hz; 1 H, P-H). ^{31}P NMR (161.97 MHz, THF-d_8): δ [ppm] = −17.55 (m, 1 P), 19.0 (m, 2 P), 80.9 (m, 1 P). ^{13}C{^{1}H} NMR (100.62 MHz, THF-d_8): δ [ppm] = 11.6 (s, $C_5(CH_3)_5$), 87.3 (s, $C_5(CH_3)_5$). For the assignment of the phosphorus atoms and coupling constants see Figure S13.

Synthesis of $[K_2]$[9], [9] = $[Cp^*Fe(\eta^4\text{-}P_5O)]^{2-}$: To a mixture of K (13 mg, 0.33 mmol) and K[$Cp^*Fe(\eta^4\text{-}P_5OH)$] (80 mg, 0.23 mmol) 15 mL of DME is added. The solution is stirred for three days, resulting in a dark brown-greenish solution. The solution was filtered, the solvent removed, dried in vacuum for 3 hours and K_2[**9**] isolated (59 mg, 67 %). $C_{10}H_{15}FeP_5K_2$ (440.14): calcd. C 27.29 H 3.44; found C 27.30 H 3.70. ^{1}H NMR (400.13 MHz, THF-d_8): δ [ppm] = 1.3 (s, 15 H, $C_5(CH_3)_5$). ^{31}P NMR (161.97 MHz, THF-d_8): δ [ppm] = 20.83 (m, 2 P), 35.52 (m, 2 P), 165.28 (m, 2 P). ^{13}C{^{1}H} NMR (100.62 MHz, THF-d_8): δ [ppm] = 11.6 (s, $C_5(CH_3)_5$), 85.4 (s, $C_5(CH_3)_5$). For the assignment of the phosphorus atoms and coupling constants see Figure S14 and Table S8.

6.2.2 Details on X-ray structure determinations and ortep-like plots

The crystal structure analyses were performed on an Agilent Technologies (former Oxford Diffraction) Gemini R Ultra diffractometer with Cu-K_α-radiation (λ = 1.54178 Å) and a Ruby CCD detector ([K_2(dme)$_2$][**5**], [K_2(thf)$_2$][**6**], [K_2(thf)$_4$][**7**]) or on an Agilent Technologies (former Oxford Diffraction) GV-50 diffractometer with Cu-K_α-radiation and a TitanS2 CCD detector ([K_2(dme)$_2$][**4**]). The measurements were carried out at 123 K. CrysAlisPro was used for data reduction and an analytical absorption correction was carried out for all compounds.[3] The structures were solved by SHELXT employing direct methods and refined with the least square method on F^2 with the program SHELXL 2014-7[4] using anisotropic displacement parameters for all non-hydrogen atoms. Hydrogen atoms were located in idealized positions and refined isotopically according to the riding model. The figures of the molecular structures were prepared with the OLEX^2 software.[5]

The crystal of [K_2(dme)$_2$][**4**] was a racemic twin and the Cp* ring disorder was modelled at two positions with an occupancy of 79 % and 21 %, respectively. In [K_2(thf)$_2$][**6**], two THF molecules are partially disordered over two positions with occupancies of 60 % and 40 %.

CCDC-### (compound [K_2(dme)$_2$][**4**]), -### (compound [K_2(dme)$_2$][**5**]), -### (compound [K_2(thf)$_2$][**6**]), -### (compound [K_2(thf)$_4$][**7**]), -### (compound [Li_2(thf)$_4$][**8**]$_2$) and -### (compound [K_8(dme)$_8$][**9**]·2PhCH$_3$) contain the supplementary crystallographic data for this publication. These data can be obtained free of charge at www.ccdc.cam.ac.uk/conts/retrieving.html (or from the Cambridge Crystallographic Data Centre, 12 Union Road, Cambridge CB2 1EZ, UK; Fax: + 44-1223-336-033; e-mail: deposit@ccdc.cam.ac.uk).

Table S1. Crystal data, data collection parameters, and convergence results $[K_2(dme)_2][\mathbf{4}]$ and $[K_2(dme)_2][\mathbf{5}]$.

Compound	$[K_2(dme)_2][\mathbf{4}]$	$[K_2(dme)_2][\mathbf{5}]$
Crystal data		
Empirical Formula	$C_{18}H_{35}FeK_2O_4P_5S$	$C_{18}H_{35}FeK_2O_4P_5Se$
Formula Weight [g/mol]	636.42	683.32
Temperature [K]	123(2)	123(2)
Crystal System	orthorhombic	monoclinic
Space Group	$Pna2_1$	$P2_1/c$
a [Å]	25.9380(4)	13.97112(7)
b [Å]	13.81698(17)	8.23327(4)
c [Å]	8.24649(11)	25.98608(13)
α [°]	90	90
β [°]	90	95.6651(5)
γ [°]	90	90
Volume [$Å^3$]	2955.42(7)	2974.53(3)
Z	4	4
ρ_{calc} [g/cm^3]	1.430	1.526
μ [mm^{-1}]	10.019	10.698
F(000)	1320.0	1392.0
Crystal Shape, Colour	rod, dark black	block, dark brown
Crystal Size [mm^3]	0.3383 × 0.165 × 0.0924	0.1924 × 0.1193 × 0.098
Data Collection		
Diffractometer	GV1000, Single source at offset, Titan diffractometer	Xcalibur, Ruby, Gemini ultra diffractometer
Radiation	CuK_α (λ = 1.54184 Å)	CuK_α (λ = 1.54184 Å)
2Θ Range for Data Collection [°]	6.816 to 148.686	6.836 to 133.638
Index Ranges	$-32 \le h \le 28$; $-17 \le k \le 16$; $-10 \le l \le 10$	$-16 \le h \le 16$; $-9 \le k \le 9$; $-30 \le l \le 30$
Reflections Collected	25196	71326
Independent Reflections	5770 [R_{int} = 0.0955, R_{sigma} = 0.0600]	5279 [R_{int} = 0.0318, R_{sigma} = 0.0134]
Refinement		
Data/Restraints/Parameters	5770/271/373	5279/0/289
Goodness-of-Fit on F^2	1.023	1.030
Final *R* Indexes [I > 2σ (I)]	R_1 = 0.0452, wR_2 = 0.1065	R_1 = 0.0213, wR_2 = 0.0505
Final *R* Indexes [All Data]	R_1 = 0.0511, wR_2 = 0.1111	R_1 = 0.0220, wR_2 = 0.0510
H-atom treatment	H-atom parameters constrained	H-atom parameters constrained
Largest Diff. Peak/Hole / [$e \cdot Å^{-3}$]	0.40/-0.35	0.80/-0.67
Flack Parameter	0.076(9)	-

Table S2. Crystal data, data collection parameters, and convergence results for $[K_2(thf)_2]$[**6**] and $[K_2(thf)_4]$[**7**].

Compound	$[K_2(thf)_2]$[**6**]	$[K_2(thf)_4]$[**7**]
Crystal data		
Empirical Formula	$C_{36}H_{62}Fe_2K_4O_4P_{10}S_4$	$C_{26}H_{47}FeK_2O_4P_5Se_2$
Formula Weight [g/mol]	1264.89	870.45
Temperature [K]	126(6)	122.8(6)
Crystal System	triclinic	triclinic
Space Group	$P\bar{1}$	$P\bar{1}$
a [Å]	11.6217(3)	11.9313(6)
b [Å]	15.4648(4)	12.4517(4)
c [Å]	18.2721(5)	12.8425(6)
α [°]	67.695(2)	105.191(4)
β [°]	79.084(2)	90.312(4)
γ [°]	69.783(2)	94.241(4)
Volume [$Å^3$]	2844.69(15)	1835.63(14)
Z	2	2
ρ_{calc} [g/cm^3]	1.477	1.575
μ [mm^{-1}]	11.022	9.891
F(000)	1304.0	884.0
Crystal Shape, Colour	plate, green brown	block, dark brown
Crystal Size [mm^3]	0.3444 × 0.1284 × 0.0728	0.2632 × 0.1289 × 0.1206
Data Collection		
Diffractometer	Xcalibur, Ruby, Gemini ultra diffractometer	Xcalibur, Ruby, Gemini ultra diffractometer
Radiation	CuK_α (λ = 1.54184 Å)	CuK_α (λ = 1.54184 Å)
2Θ Range for Data Collection [°]	8.126 to 133.476	7.38 to 133.28
Index Ranges	$-13 \le h \le 13$; $-18 \le k \le 17$; $-21 \le l \le 21$	$-12 \le h \le 14$; $-11 \le k \le 14$; $-15 \le l \le 14$
Reflections Collected	48720	19061
Independent Reflections	10009 [R_{int} = 0.0451, R_{sigma} = 0.0308]	6423 [R_{int} = 0.0356, R_{sigma} = 0.0371]
Refinement		
Data/Restraints/Parameters	10009/48/593	6423/0/366
Goodness-of-Fit on F^2	1.016	1.037
Final *R* Indexes [I > 2σ (I)]	R_1 = 0.0293, wR_2 = 0.0720	R_1 = 0.0296, wR_2 = 0.0676
Final *R* Indexes [All Data]	R_1 = 0.0325, wR_2 = 0.0740	R_1 = 0.0353, wR_2 = 0.0705
H-atom treatment	H-atom parameters constrained	H-atom parameters constrained
Largest Diff. Peak/Hole / [$e \cdot Å^{-3}$]	0.50/-0.30	0.42/-0.51
Flack Parameter	-	-

Table S3. Crystal data, data collection parameters, and convergence results for $[Li_2(thf)_4][\mathbf{8}]_2$ and $[K_8(dme)_8][\mathbf{9}]\cdot 2PhCH_3$.

Compound	$[Li_2(thf)_4][\mathbf{8}]_2$	$[K_8(dme)_8][\mathbf{9}]_4\cdot 2PhCH_3$
Crystal data		
Empirical Formula	$C_{36}H_{64}Fe_2Li_2O_6P_{10}$	$C_{86}H_{156}Fe_4K_8O_{20}P_{20}$
Formula Weight [g/mol]	1028.15	2665.70
Temperature [K]	123(2)	123(2)
Crystal System	monoclinic	monoclinic
Space Group	$P2_1/c$	$C2/c$
a [Å]	15.0287(3)	36.044(4)
b [Å]	9.2847(2)	12.4098(7)
c [Å]	17.2637(3)	34.159(3)
α [°]	90	90
β [°]	91.157(2)	119.046(14)
γ [°]	90	90
Volume [$Å^3$]	2408.43(8)	13358(3)
Z	2	4
ρ_{calc} [g/cm^3]	1.418	1.326
μ [mm^{-1}]	8.297	8.35
F(000)	1072	5552
Crystal Shape, Colour	block, black	needle, black
Crystal Size [mm^3]	0.187 × 0.147 × 0.07	0.246 × 0.037 × 0.013
Data Collection		
Diffractometer	SuperNova, single SuperNova source at offset, Atlas detector	SuperNova, single SuperNova source at offset, Atlas detector
Radiation	CuK_α (λ = 1.54184 Å)	CuK_α (λ = 1.54184 Å)
2Θ Range for Data Collection [°]	5.88 to 145.72	5.92 to 145.99
Index Ranges	$-18 \le h \le 15$; $-6 \le k \le 11$; $-21 \le l \le 20$	$-39 \le h \le 43$; $-10 \le k \le 14$; $-41 \le l \le 41$
Reflections Collected	9281	20962
Independent Reflections	4674 [R_{int} = 0.0372, R_{sigma} = 0.0456]	12685 [R_{int} = 0.060, R_{sigma} = 0.101]
Refinement		
Data/Restraints/Parameters	4674/0/262	12685/6/643
Goodness-of-Fit on F^2	1.039	0.847
Final *R* Indexes [I > 2σ (I)]	R_1 = 0.0445, wR_2 = 0.1231	R_1 = 0.0675, wR_2 = 0.1733
Final *R* Indexes [All Data]	R_1 = 0.0502, wR_2 = 0.1165	R_1 = 0.1122, wR_2 = 0.1891
H-atom treatment	H-atom parameters constrained	H-atom parameters constrained
Largest Diff. Peak/Hole / [$e\cdot Å^{-3}$]	0.77/-0.65	1.24 / -0.73

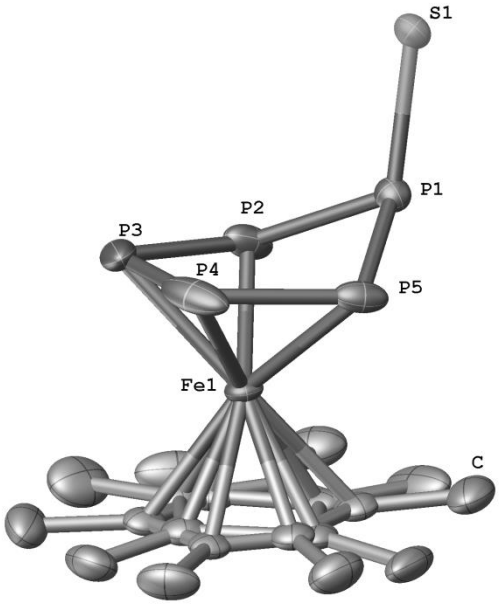

Figure S1. Molecular structure of the anionic part of $[K_2(dme)_2]$[**4**]. Ellipsoids are drawn at 50% probability level. Hydrogen atoms bonded to carbon are omitted for clarity. Selected bond lengths [Å] and angles [°]: P1-S1 2.092(2), P1-P2 2.156(2), P2-P3 2.159(3), P3-P4 2.129(4), P4-P5 2.157(3), P5-P1 2.166(2), Fe-P2 2.2916(19), Fe-P3 2.3204(25), Fe-P4 2.3102(21), Fe-P5 2.3077(18), P2-P1-S1 115.30(8), P5-P1-S1 121.14(8), P3-P4-P5 102.86(11), P1-P2-P3 111.52(11), P4-P3-P2 103.26(10), S1-P1-P2 115.38(9), S1-P1-P5 121.15(9), P2-P1-P5 91.82(8).

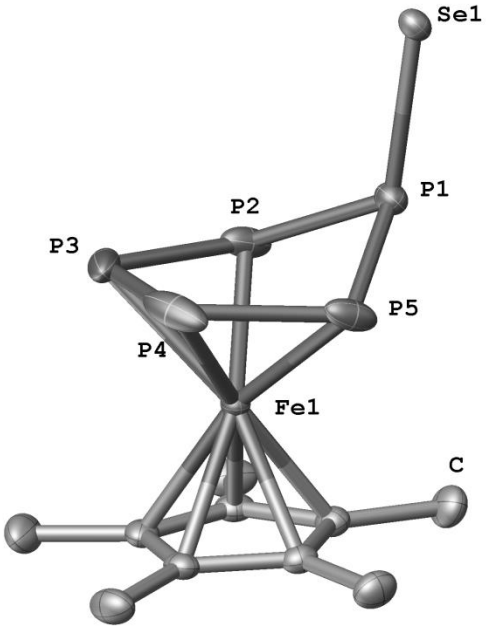

Figure S2. Molecular structure of the anionic part of $[K_2(dme)_2]$[**5**]. Ellipsoids are drawn at 50% probability level. Hydrogen atoms bonded to carbon are omitted for clarity. Selected bond lengths [Å] and angles [°]: Se1-P1 2.2518(4), Fe1-P2 2.3139(5), Fe1-P5 2.2925(5), Fe1-P4 2.3236(5), Fe1-P3 2.3116(5), P1-P2 2.1651(7), P1-P5 2.1520(7), P2-P3 2.1508(8), P5-P4 2.1648(8), P4-P3 2.1323(10),

P3 P2-P1 111.71(3), P1-P5 P4 110.95(3), P3-P4-P5 102.99(3), P4-P3-P2 103.01(3), P5-P1-Se1 114.08(2).

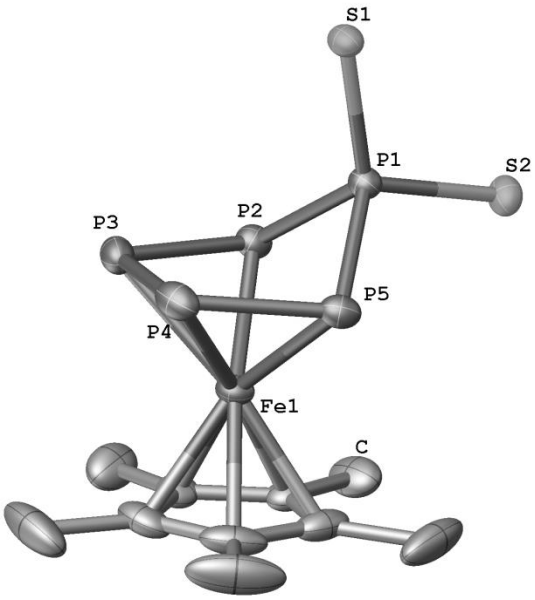

Figure S3. Molecular structure of the anionic part of $[K_2(thf)_2]$[**6**]. Ellipsoids are drawn at 50% probability level. Hydrogen atoms bonded to carbon are omitted for clarity. Selected bond lengths [Å] and angles [°]: Fe1-P2 2.3119(6), Fe1-P5 2.3095(6), Fe1-P3 2.3275(7), Fe1-P4 2.3285(7), P1-P2 2.1834(7), P1-P5 2.1849(8), P2-P3 2.1361(8), P5-P4 2.1431(8), P3-P4 2.1737(9), S1-P1 2.0258(7), S2-P1 2.0225(7), S1-P1-P2 119.61(3), S1-P1-P5 116.28(3), S2-P1-P2 106.57(3), P2-P1-P5 92.37(3), P3-P2-P1 102.40(3), P4-P5-P1 100.96(3).

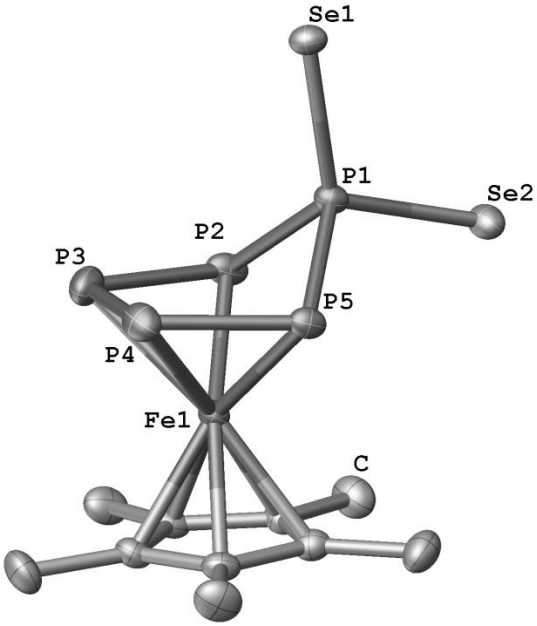

Figure S4. Molecular structure of anionic part of $[K_2(thf)_4]$[**7**]. Ellipsoids are drawn at 50% probability level. Hydrogen atoms bonded to carbon are omitted for clarity. Selected bond lengths [Å] and angles [°]: Se1-P1 2.1844(6), Se2-P1 2.1938(7), Fe1-P5 2.2950(7), Fe1-P2 2.3087(8), Fe1-P4

2.3242(8), Fe1-P3 2.3458(8), P1-P5 2.1781(9), P1-P2 2.1786(9), P5-P4 2.1477(10), P2-P3 2.1276(11), Se1-P1-Se2 112.20(3), P5-P1-Se1 117.17(3), P5-P1-Se2 106.79(3), P5-P1-P2 92.63(3), P2-P1-Se1 121.33(4), P2-P1-Se2 104.26(3), P5-P4-P3 103.69(4), P2-P3-P4 102.84(4).

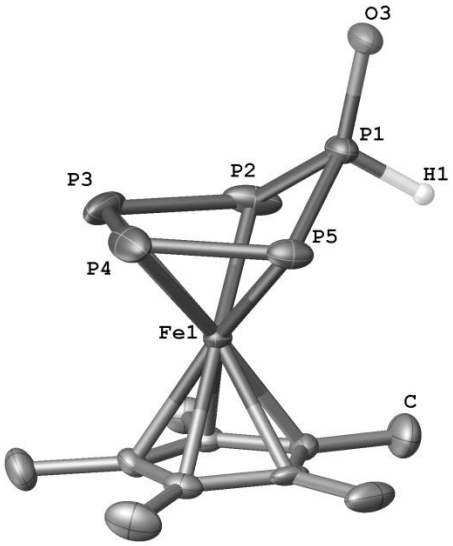

Figure S5. Molecular structure of anionic part of $[Li_2(thf)_4][\mathbf{8}]_2$. Ellipsoids are drawn at 50% probability level. Hydrogen atoms bonded to carbon are omitted for clarity. Selected bond lengths [Å] and angles [°]: P1-O3 1.528(2), P1-P2 2.1353(11), P1-P5 2.1355(10), P2-P3 2.1406(15), P4-P3 2.1430(16), P5-P4 2.1269(13), $Cp^*_{centroid}$-Fe 1.698; O3-P1-P2 123.58(10), O3-P1-P5 124.64(10), P2-P1-P5 98.54(4), P1-P2-P3 102.03(5), P2-P3-P4 105.00(5), P5-P4-P3 104.69(5), P4-P5-P1 102.63(5).

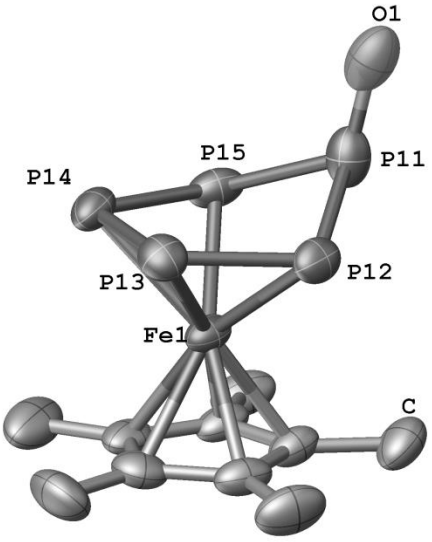

Figure S6. Molecular structure of anionic part of $[K_8(dme)_8][\mathbf{9}]_4 \cdot 2PhCH_3$. Ellipsoids are drawn at 50% probability level. Hydrogen atoms bonded to carbon are omitted for clarity. Selected bond lengths [Å] and angles [°]:P11-P12 2.136(3), P11-P15 2.144(3), P11-O1 1.441(6), P12-P13 2.172(2), P13-P14

2.131(2), P14-P15 2.167(3), Fe1-P12 2.2944(18), Fe1-P13 2.3178(18), Fe1-P14 2.3251(18), Fe1-P15 2.3071(19). O1-P11-P15 120.9(2), O1-P11-P12 117.7(2), P12-P11-P15 92.92(10), P14-P13-P12 103.21(10), P13-P14-P15 102.66(9).

6.2.3 Experimental and simulated NMR spectra

The ^{31}P NMR spectra of **4**, **5**, **6** and **7** are of higher order. To determine the coupling constants of the phosphorus atoms the ^{31}P NMR spectrum of each anion was simulated with the software TOPSPIN 3.0.

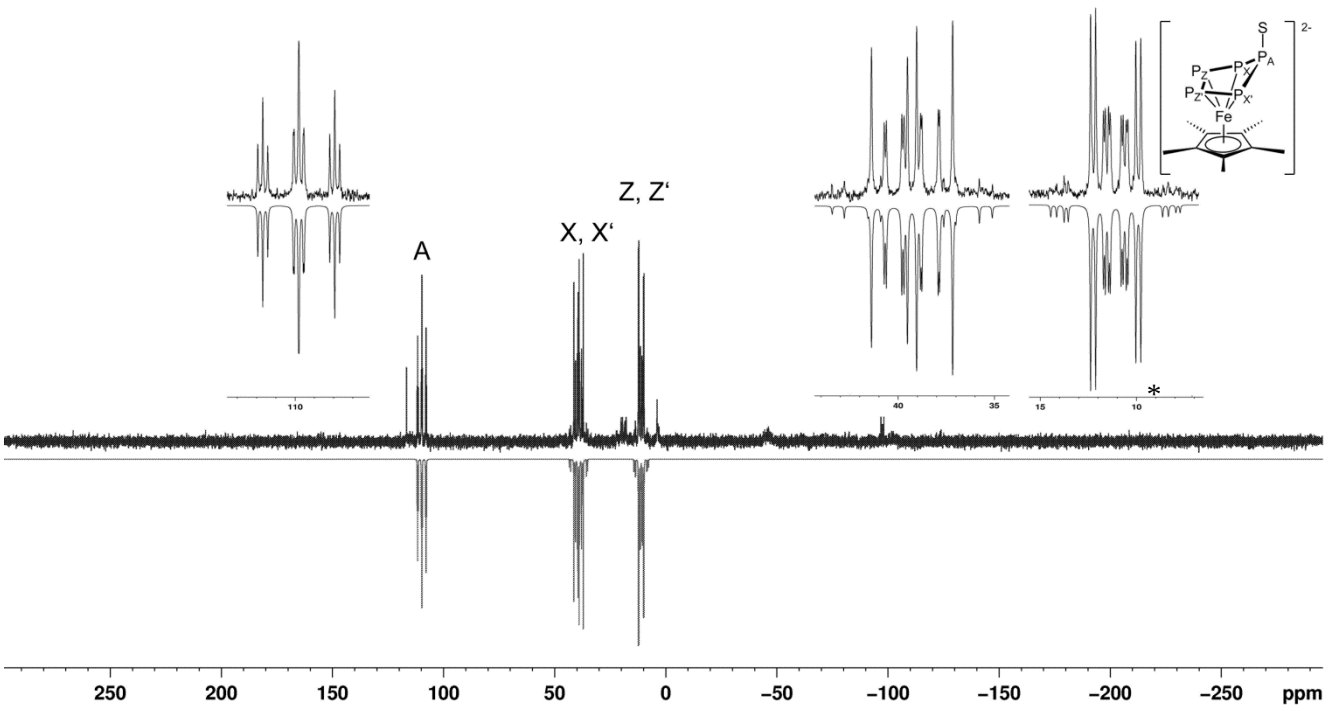

Figure S7. Experimental (top) and simulated (bottom) ^{31}P NMR (161.97 MHz, DME/DMSO-d_6) spectrum of $[K_2(dme)_2]$[**4**]. Impurities are marked with *.

Table S4. ^{31}P NMR chemical shifts and coupling constants for $[K_2(dme)_2][\mathbf{4}]$ obtained from the simulation of the ^{31}P NMR (161.97 MHz, DME/DMSO-d_6) spectrum.

J (Hz)		δ (ppm)	
$^1J_{P_A\text{-}P_X} = {}^1J_{P_A\text{-}P_{X'}}$	303.36	$P_{Z,Z'}$	11.1
$^2J_{P_A\text{-}P_Z} = {}^2J_{P_A\text{-}P_{Z'}}$	−42.62	$P_{X,X'}$	39.2
$^2J_{P_X\text{-}P_{X'}}$	−60.51	P_A	109.8
$^1J_{P_X\text{-}P_Z} = {}^1J_{P_{X'}\text{-}P_{Z'}}$	375.56		
$^2J_{P_X\text{-}P_{Z'}} = {}^2J_{P_{X'}\text{-}P_Z}$	4.35		
$^1J_{P_{Z'}\text{-}P_Z}$	396.55		

Table S5. ^{31}P NMR chemical shifts and coupling constants for $[K_2(dme)][\mathbf{5}]$ obtained from the simulation of the ^{31}P NMR (161.97 MHz, THF-d_8) spectrum.

J (Hz)				δ (ppm)	
$^1J_{P_A\text{-}P_X}$	284.21	$^1J_{P_X\text{-}P_Z}$	371.41	$P_{Z,Z'}$	14.5
$^1J_{P_A\text{-}P_{X'}}$	284.23	$^2J_{P_X\text{-}P_{Z'}}$	1.27	$P_{X,X'}$	33.1
$^2J_{P_A\text{-}P_Z}$	−39.79	$^2J_{P_{X'}\text{-}P_Z}$	1.19	P_A	81.9
$^2J_{P_A\text{-}P_{Z'}}$	−39.78	$^1J_{P_{X'}\text{-}P_{Z'}}$	371.46		
$^2J_{P_X\text{-}P_{X'}}$	−59.25	$^1J_{P_{Z'}\text{-}P_Z}$	399.46		
$^1J_{P_A\text{-}Se}$	300.02				

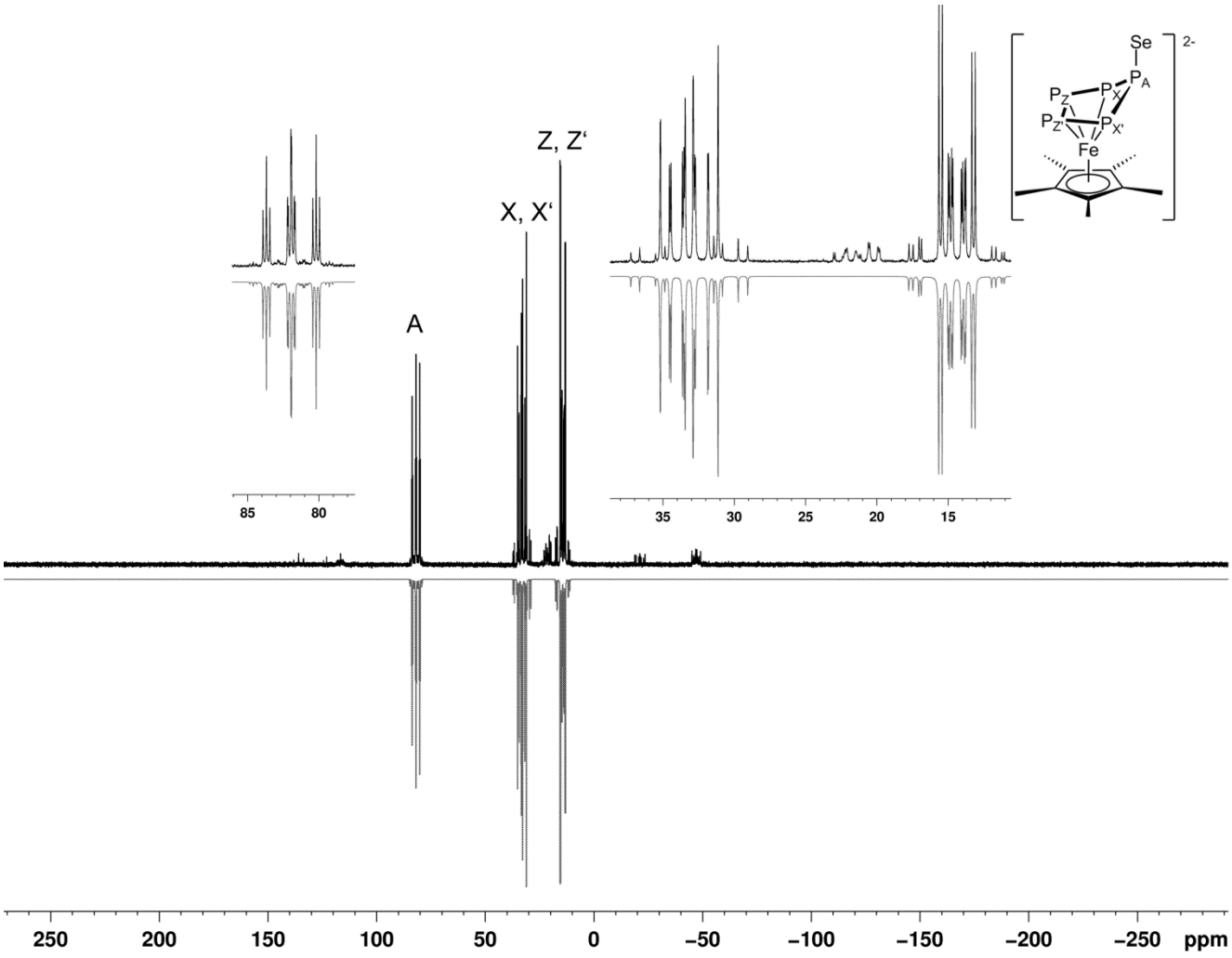

Figure S8. Experimental (top) and simulated (bottom) ^{31}P NMR (161.97 MHz, THF-d_8) spectrum of [K_2(dme)][**5**]. Impurities are marked with *.

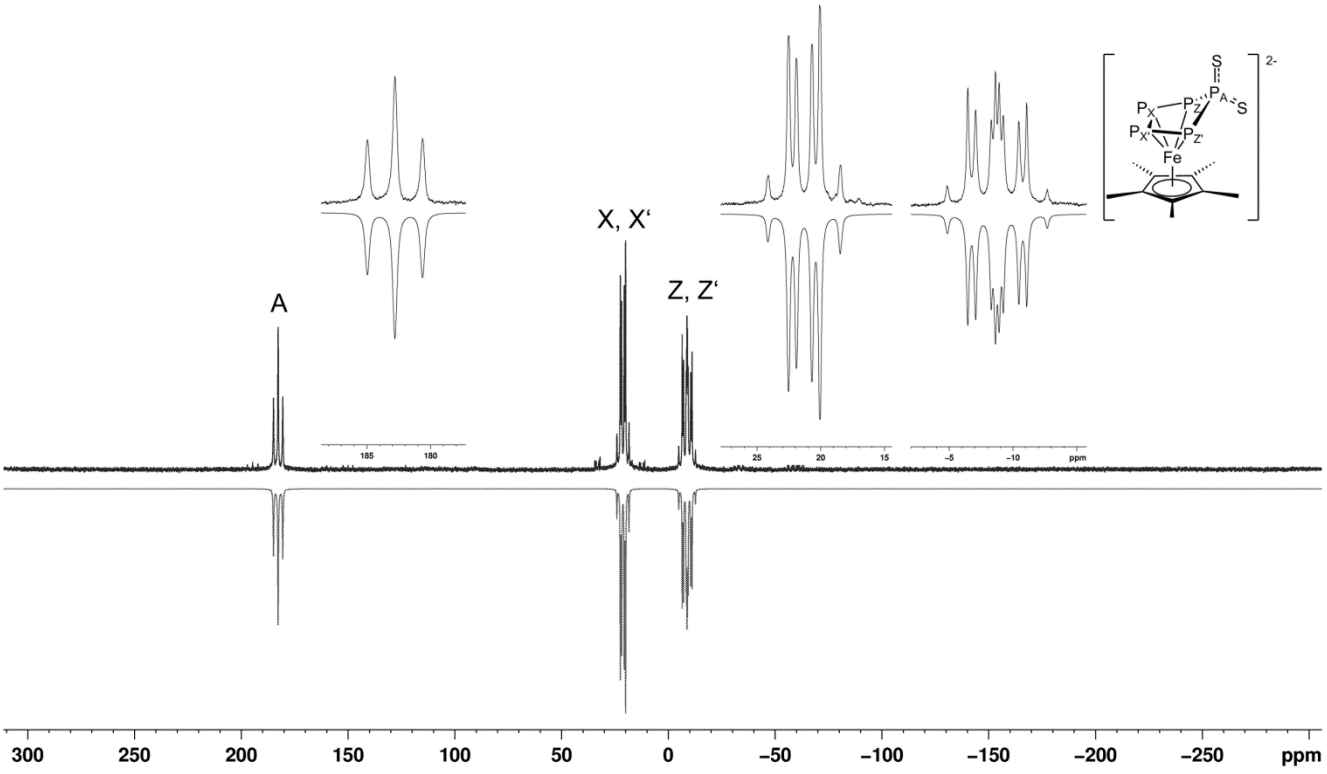

Figure S9. Experimental (top) and simulated (bottom) ^{31}P NMR (161.97 MHz, THF-d_8) spectrum of $[K_2(dme)_2]$[**6**].

Table S6. ^{31}P NMR chemical shifts and coupling constants for $[K_2(dme)_2]$[**6**] obtained from the simulation of the ^{31}P NMR (161.97 MHz, THF-d_8) spectrum.

J (Hz)		δ (ppm)	
$^2J_{P_A\text{-}P_X} = {}^2J_{P_A\text{-}P_{X'}}$	−17.16	$P_{Z,Z'}$	−8.7
$^1J_{P_A\text{-}P_Z} = {}^1J_{P_A\text{-}P_{Z'}}$	351.11	$P_{X,X'}$	21.2
$^1J_{P_X\text{-}P_{X'}}$	362.62	P_A	182.8
$^1J_{P_X\text{-}P_Z} = {}^1J_{P_{X'}\text{-}P_{Z'}}$	411.16		
$^2J_{P_X\text{-}P_{Z'}} = {}^2J_{P_{X'}\text{-}P_Z}$	−13.39		
$^2J_{P_{Z'}\text{-}P_Z}$	9.28		

Table S7. ^{31}P NMR chemical shifts and coupling constants for $[K_2(dme)_2][\mathbf{7}]$ obtained from the simulation of the ^{31}P NMR (161.97 MHz, THF-d_8) spectrum.

J (Hz)				δ (ppm)	
$^2J_{P_A\text{-}P_X}$	−16.89	$^1J_{P_X\text{-}P_Z}$	401.67	$P_{Z,Z'}$	0.7
$^2J_{P_A\text{-}P_{X'}}$	−16.92	$^2J_{P_X\text{-}P_{Z'}}$	−14.61	$P_{X,X'}$	23.0
$^1J_{P_A\text{-}P_Z}$	355.87	$^2J_{P_{X'}\text{-}P_Z}$	−14.49	P_A	116.6
$^1J_{P_A\text{-}P_{Z'}}$	355.86	$^1J_{P_{X'}\text{-}P_{Z'}}$	401.76		
$^1J_{P_X\text{-}P_{X'}}$	369.74	$^2J_{P_{Z'}\text{-}P_Z}$	0.91		
$^1J_{P_A\text{-}Se_A}$	530.15	$^1J_{P_A\text{-}Se_B}$	471.14		

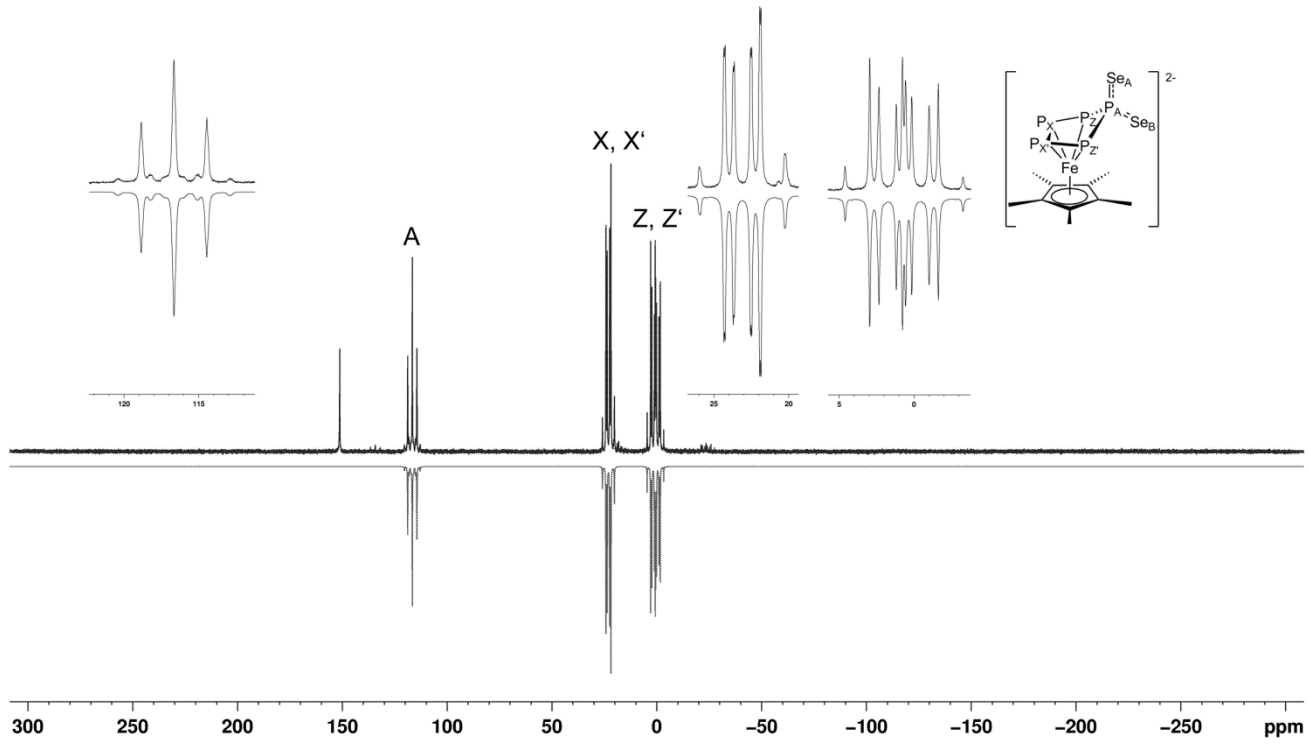

Figure S10. Experimental (top) and simulated (bottom) ^{31}P NMR (161.97 MHz, THF-d_8) spectrum of $[K_2(dme)_2][\mathbf{7}]$.

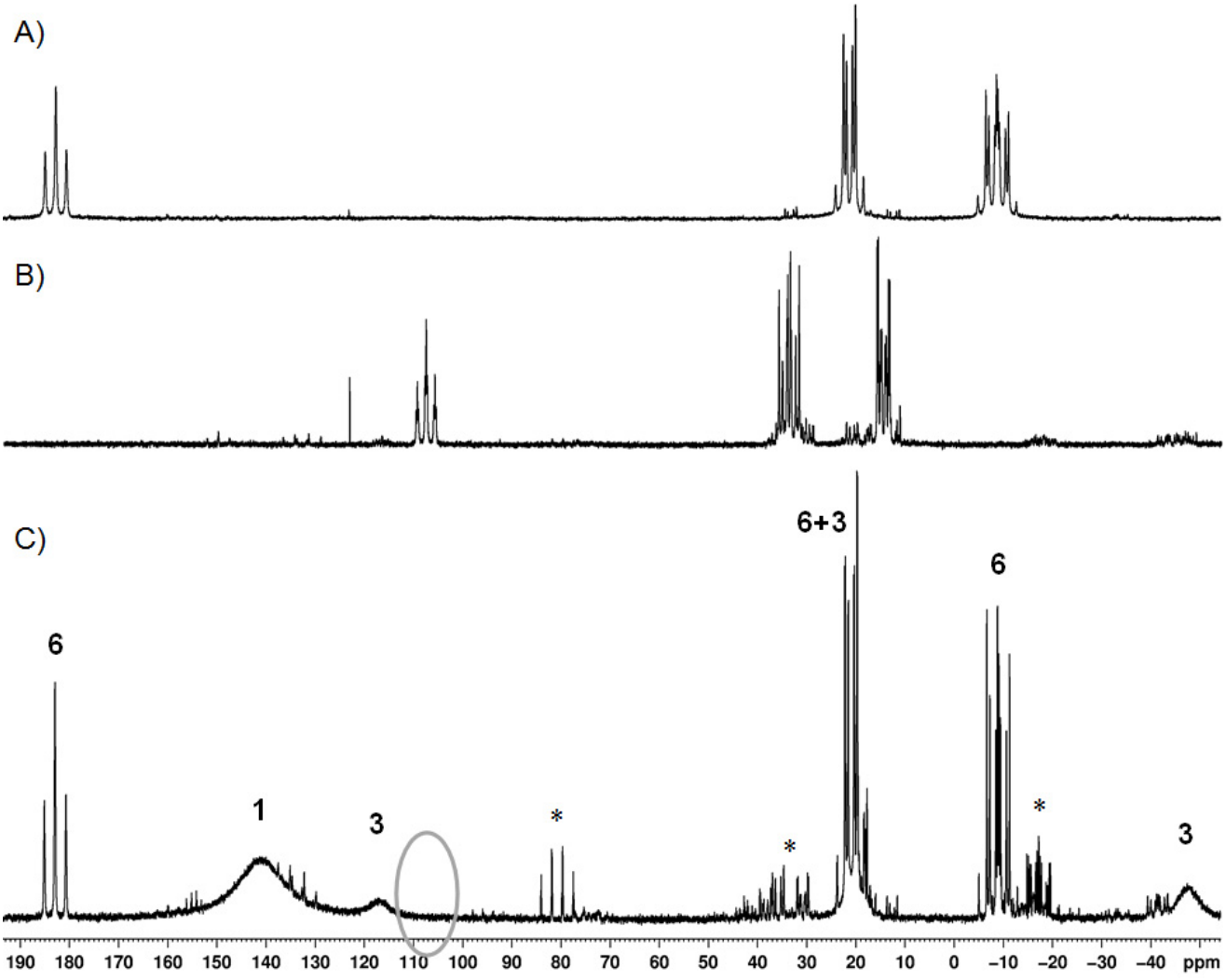

Figure S11. Experimental ^{31}P NMR (161.97 MHz, THF-d_8) spectrum of A) $[K_2(dme)_2]$[**6**], B) $[K_2(dme)_2]$[**4**] and C) the reaction of $[K_2(dme)_3]$[**3**] with one equivalent of sulfur. In C the signals are assigned to the corresponding anions. The characteristic signal of **4** is missing (region marked with grey circle). Impurities are marked with *.

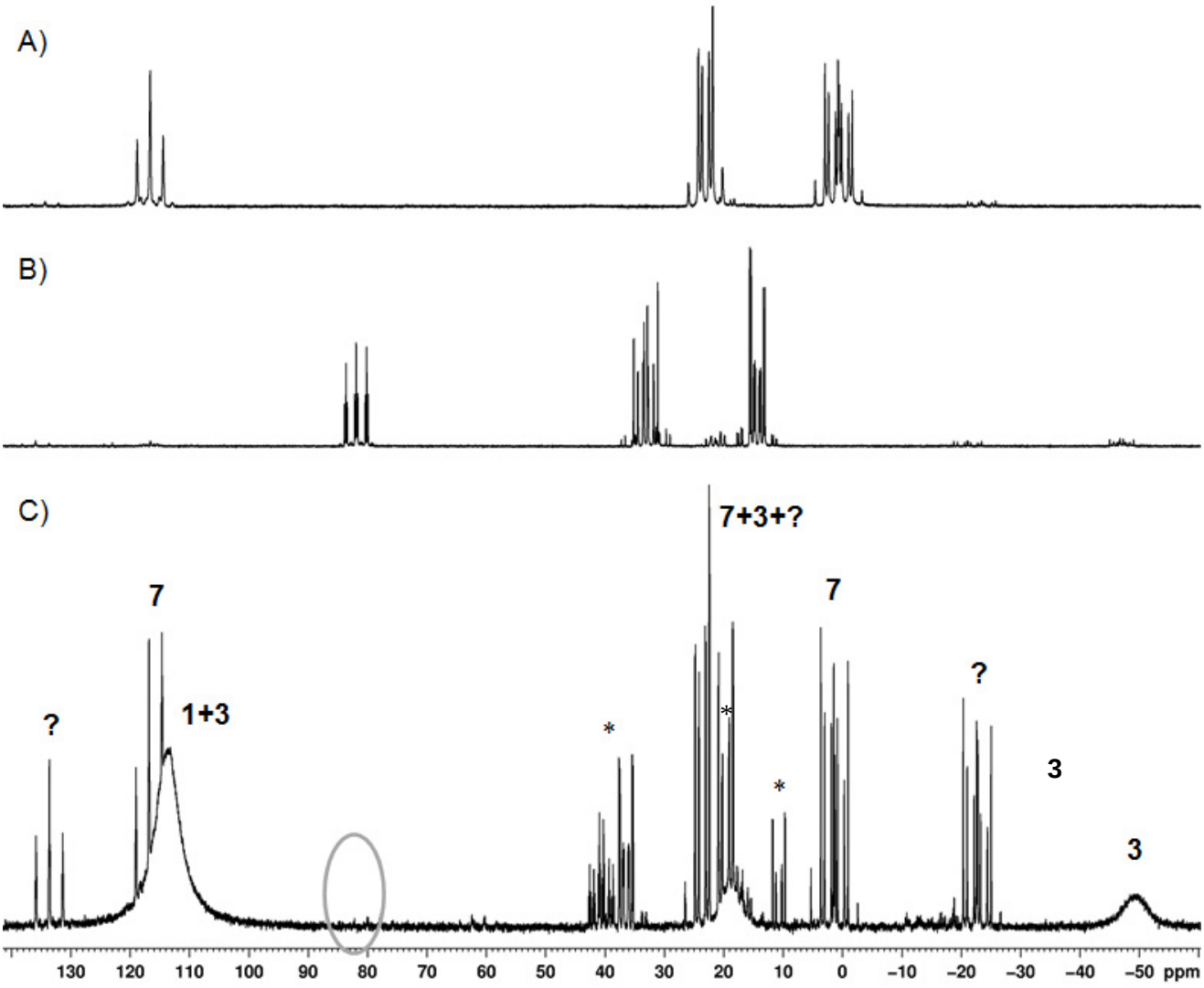

Figure S12. Experimental ^{31}P NMR (161.97 MHz, THF-d_8) spectrum of A) $[K_2(dme)_2][\mathbf{7}]$, B) $[K_2(dme)][\mathbf{5}]$ and C) the reaction of $[K_2(dme)_3][\mathbf{3}]$ with one equivalent of selenium. In C the signals are assigned to the corresponding anions. The characteristic signal of **5** is missing (region marked with grey circle). A not identified byproduct is marked with '?'. Impurities are marked with *.

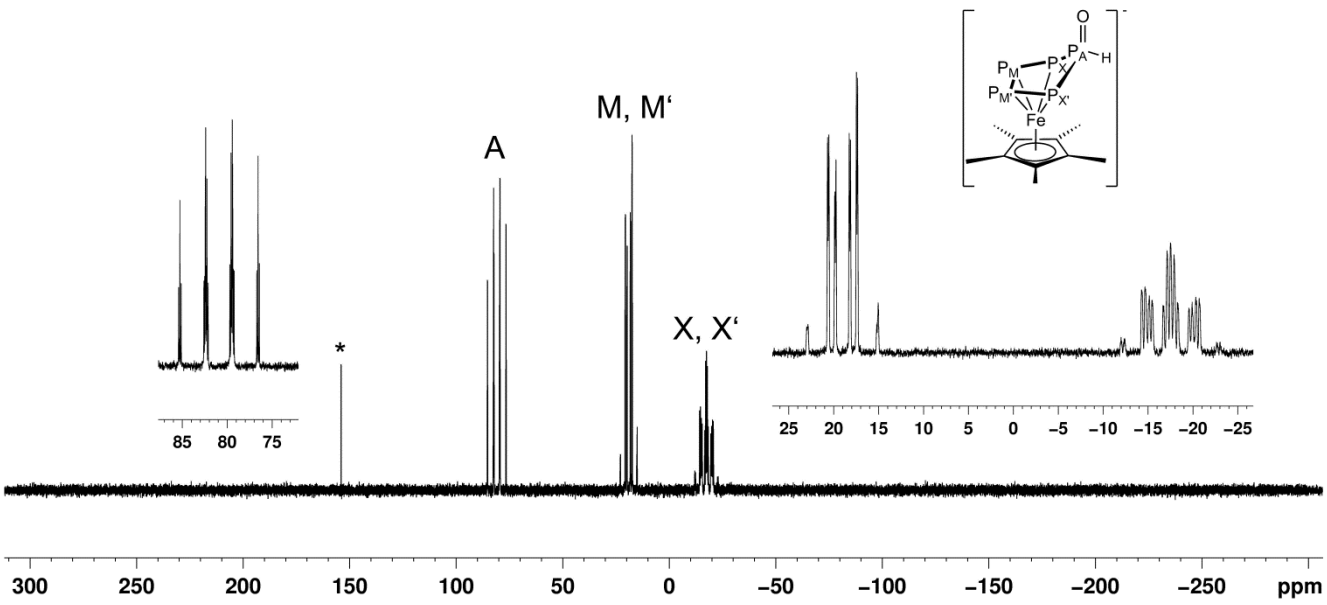

Figure S13. ^{31}P NMR (161.97 MHz, THF-d_8) spectrum of $[Li_2(thf)_2]$[**8**]. Impurities of **1** are marked with *.

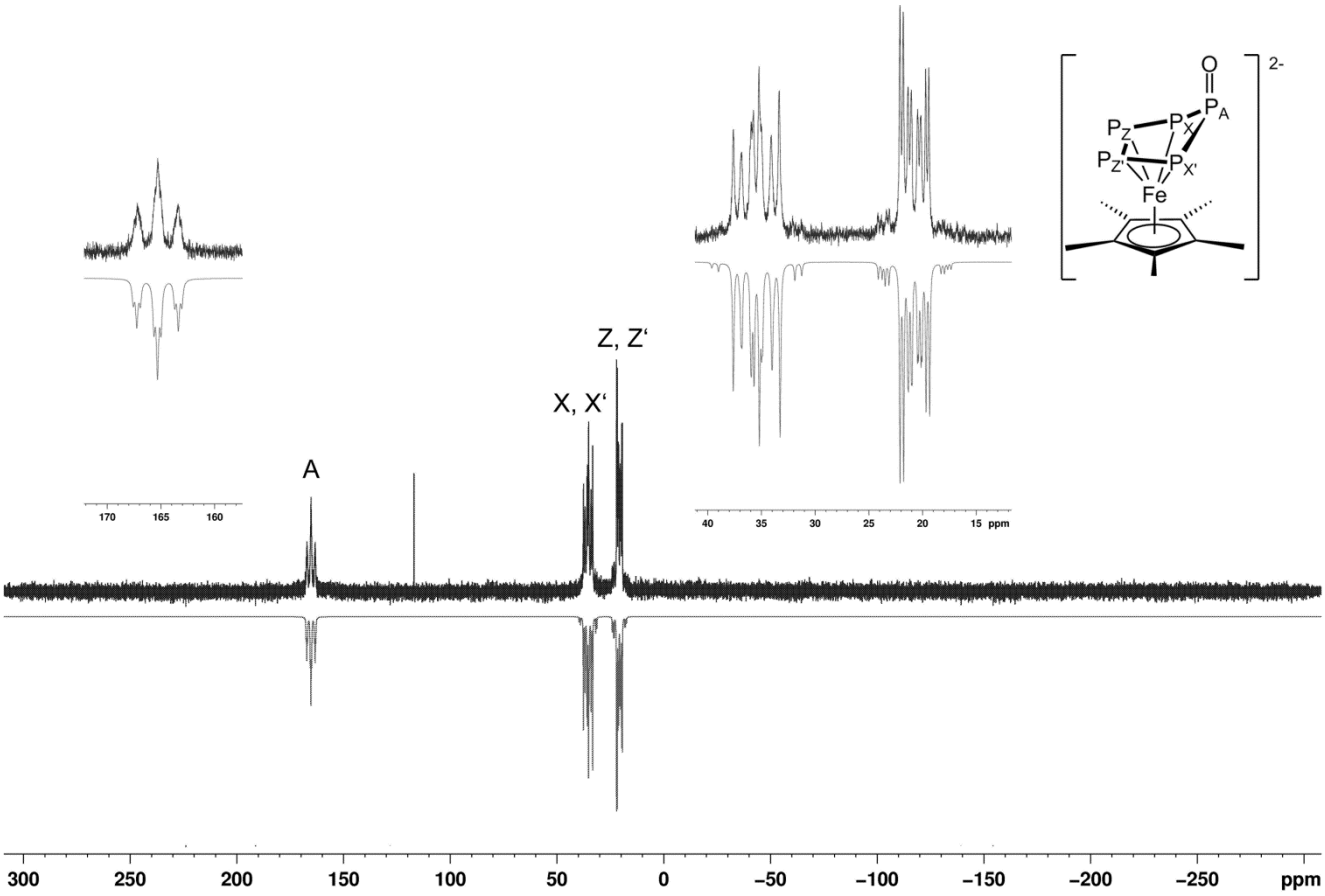

Figure S14. Experimental (top) and simulated (bottom) ^{31}P NMR (161.97 MHz, THF-d_8) spectrum of $[K_2(dme)_2][\mathbf{9}]\bullet 0.5\ C_7H_8$.

Table S8. Spectral parameters for an AXX'ZZ' spin system obtained from the simulation of the ^{31}P NMR (161.97 MHz, THF-d_8) spectrum of $[K_2(dme)_2][\mathbf{9}]$.

J (Hz)		δ (ppm)	
$^1J_{P_A\text{-}P_X} = {}^1J_{P_A\text{-}P_{X'}}$	315.37	$P_{Z,Z'}$	20.9
$^2J_{P_A\text{-}P_Z} = {}^2J_{P_A\text{-}P_{Z'}}$	−56.65	$P_{X,X'}$	35.4
$^1J_{P_Z\text{-}P_X} = {}^1J_{P_{Z'}\text{-}P_{X'}}$	379.52	P_A	165.3
$^2J_{P_X\text{-}P_{Z'}} = {}^2J_{P_{X'}\text{-}P_Z}$	15.32		
$^1J_{P_Z\text{-}P_{Z'}}$	59.25		

6.2.4 References

[1] O. J. Scherer, T. Brück, *Angew. Chem.* **1987**, *99*, 59-59.
[2] M. V. Butovskiy, G. Balázs, M. Bodensteiner, E. V. Peresypkina, A. V. Virovets, J. Sutter, M. Scheer, *Angew. Chem. Int. Ed.* **2013**, *52*, 2972-2976.
[3] Agilent Technologies Inc., *CrysAlisPro* **2015**, different versions, Oxford, UK.
[4] G. M. Sheldrick, *Acta Cryst.* **2008**, *A64*, 112–122.
[5] O. V. Dolomanov, L. J. Bourhis, R. J. Gildea, J. A. K. Howard, H. Puschmann, *J. Appl. Cryst.* **2009**, *42*, 339-341.

7. Unexpected reactivity of [Cp'''Ni(η^3-P_3)] towards main group nucleophiles and by reduction

Eric Mädl, Gábor Balázs, Eugenia Peresypkina and Manfred Scheer*

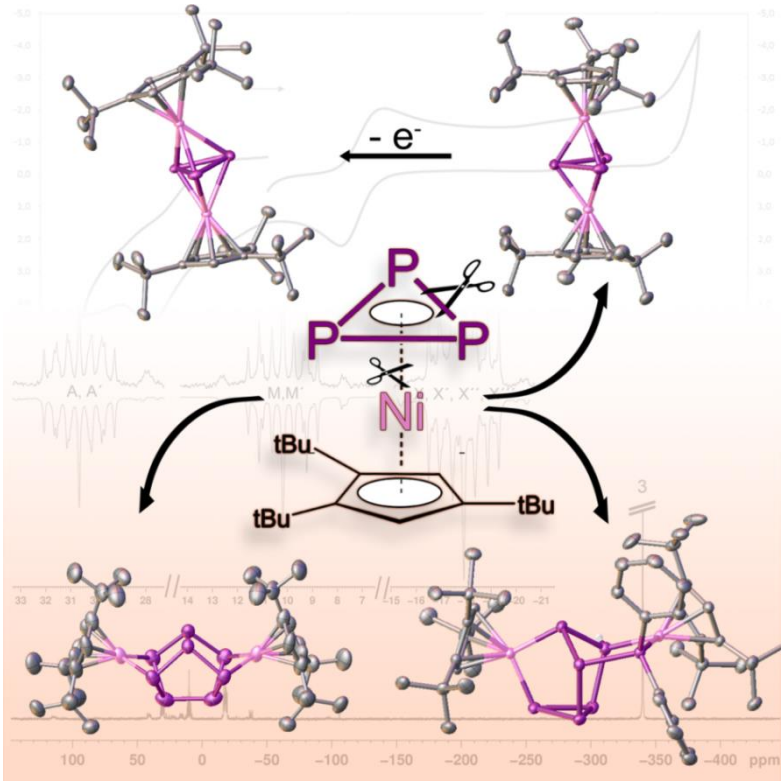

- All compounds were synthesized by Eric Mädl.
- The chapter "discussion" was written by Eric Mädl, except for parts regarding calculations, which were written by Gábor Balász. Details about X-ray structure analyses in the chapter "supporting information" were written by Eugenia V. Peresypkina.
- DFT calculations were performed by Gábor Balász. X-ray structure analyses and refinements were performed by Eric Mädl and Eugenia V. Peresypkina.
- Figures in the chapter "discussion" were made by Eric Mädl. Figures in the chapter "supporting information" regarding X-ray structure analyses were made by Eugenia V. Peresypkina. Figures regarding calculations were made by Gábor Balász.

7.1 Discussion

Abstract: *The reduction of [Cp'''Ni(η^3-P_3)] (**1**) with potassium leads to the formation of the anionic compound [(Cp'''Ni)$_2$(μ,$\eta^{2:2}$-P_8)]$^{2-}$ (**2**), containing a realgar-like P_8 unit. When **1** is reacted with $NaNH_2$ as nucleophile the anionic triple-decker sandwich complex [(Cp'''Ni)$_2$(μ,$\eta^{3:3}$-P_3)]$^-$ (**3**) with a* cyclo-P_3 *middle deck is obtained. Na[**3**] can subsequently be oxidized with AgOTf to the neutral triple-decker complex [(Cp'''Ni)$_2$(μ,$\eta^{3:3}$-P_3)] (**4**). In contrast, **1** reacts with $LiPPh_2$ to give the anionic compound [(Cp'''Ni)$_2$(μ,$\eta^{2:2}$-P_6PPh_2)]$^-$ (**5**), a complex containing a bicyclic P_7 fragment, being coordinated by two Cp'''Ni units. Protonation of Li[**5**] with HBF_4 leads to the neutral complex [(Cp'''Ni)$_2$(μ,$\eta^{2:2}$-(HP_6PPh_2)] (**6**). By adding $LiNMe_2$ to **1** [Cp'''Ni(η^2-P_3NMe_2)]$^-$ (**7**) is accessible, a complex being the first formed compound after the nucleophilic attack at the* cyclo-P_3 *ring of **1**. The complexes K_2[**2**], Na[**3**], **4**, **6** and Li[**7**] were fully characterized and their structures were determined by single crystal X-ray diffraction.*

The reactivity – inclusive catalysis – and transformations of organometallic compounds is one of the most active research topics in chemistry. The methine unit − CH − is related to a naked P moiety by the isolobal relationship. Therefore, mixed P and CR containing complexes have been attracted considerable attention concerning their reactivity[1] and novel approaches to phosphorus and arsenic rich aromatic starting materials[2] opened new avenues for the fine tuning of such mixed complexes. In comparison with the isolobal CH fragments, due to their useable lone pairs the ring P atoms are additionally able to coordinate to Lewis acidic moieties, turning them into valuable starting materials in coordination chemistry[3] and catalysis.[4] In this respect, the all phosphorus or all arsenic analoga of such ligands in organometallic complexes are of unique interest since they can form unprecedented coordination polymers,[5] which are able e.g. to encapsulate instable molecules.[6] However, by employing the fivefold symmetry e.g. in the case of pentaphosphaferrocene [Cp*Fe(η^5-P_5)], the formation of giant molecular nanoclusters with fullerene-like topology is possible.[7]

Recently, the redox behavior of [Cp*Fe(η^5-P_5)] was investigated, leading to the dianionic compounds [Cp*Fe(η^4-P_5)]$^{2-}$ and [(Cp*Fe)$_2$(μ,$\eta^{4:4}$-P_{10})]$^{2-}$, as well as to the dicationic compound [(Cp*Fe)$_2$($\eta^{5:5}$-P_{10})]$^{2+}$ containing a P_{10} unit.[8] This is contrary to the reactivity of its organometallic analogue and phosphorus free compound ferrocene.[9] Moreover, reacting main group nucleophiles with pentaphosphaferrocene a new direction of reactivity could be found and, thus, versatile functionalization and unexpected connectivity pattern could be realized.[10] The nucleophiles add on the *cyclo*-P_5 ligand, leading to an enveloped conformation of the ring. By using organic nucleophiles P-C bonds are formed hereby, a first step on the transformation to organophosphorus ligands. The

question arises, whether this reactivity is limited to pentaphosphaferrocene or, if extendable, which scope and perspectives will be opening up.

[Cp'''Ni(η^3-P_3)] (**1**) seems to be a promising starting material to investigate these topics. Due to the ring strain in the *cyclo*-P_3 unit an unusual reactivity towards main group nucleophiles or reducing agents is assumed. According to DFT calculations on **1** (Figure 1), the HOMO does not reflect any donor properties of the P atom, which goes in line with our unsuccessful attempts to use this compound for supramolecular aggregation. The LUMO, however, is located on the *cyclo*-P_3 unit similarly to the pentaphosphaferrocene [Cp*Fe(η^5-P_5)],[11] which indicates that a reduction or a nucleophilic attack should occur at the phosphorus ring.

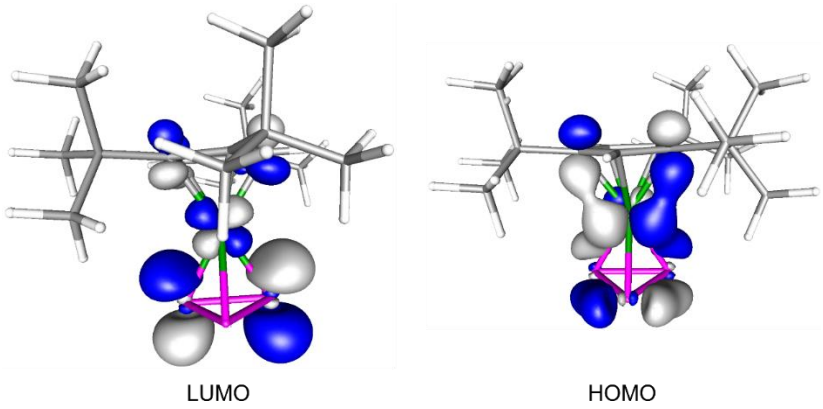

Figure 1. Selected molecular orbitals of **1** calculated at the BP86/def2-TZVP level of theory.

Herein we report on the reduction of **1** to give for the first time a complete structural rearrangement and reaggregation of a *cyclo*-P_n ligand complex, forming an unprecedented dianionic dinuclear complex with a P_8 realgar-type structural moiety. Furthermore, the reaction with nucleophiles leads also to a structural rearrangement to form either an anionic triple-decker sandwich complex, or – for PPh_2^- – after addition a ring expansion is observed, giving a novel P_7Ph_2 ligand which is coordinated by two Cp'''Ni moieties (Scheme 1). These unexpected results show the potential of the *cyclo*-P_3 ligand containing complex **1** to act as a building block with diverse structural reorganizations.

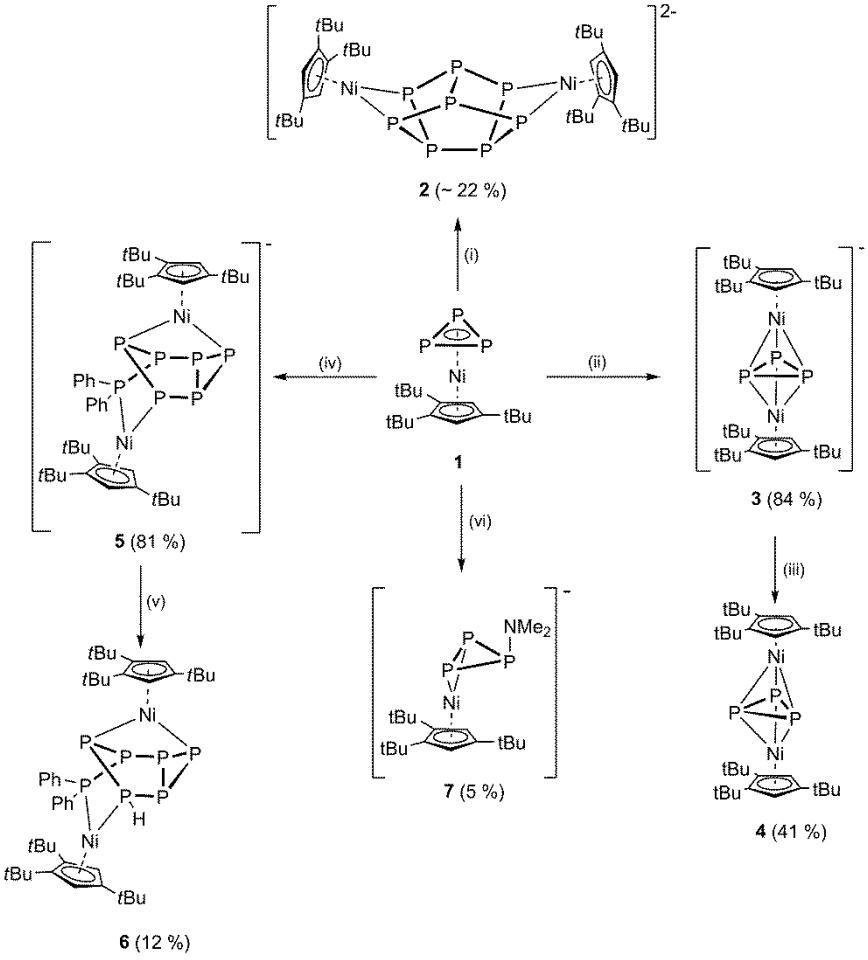

Scheme 1. Reaction of **1**: (i) excess K in DME, r.t.; (ii) $NaNH_2$ in DME, r.t.; (iii) AgOTf in DME, r.t.; (iv) $LiPPh_2$ in THF, −60 °C → r.t.; (v) HBF_4 in THF, r.t; (vi) $LiNMe_2$ in THF, r.t.; yields are given in parenthesis.

If **1** is reduced by potassium K_2[**2**] is formed, along with the triple-decker complex K[**3**] in a ratio of 1:5. Compound K_2[**2**] shows an AA'MM'XX'X"X''' spin system in the ^{31}P NMR spectrum due to its C_{2v} symmetry, with multiplets centered at 30.6, 10.1 and −17.9 ppm,. The assignment of the AA' and MM' signals was achieved by the simulation of the ^{31}P NMR spectrum.[12] Single crystals suitable for X-ray structure analysis are obtained by adding 18-crown-6 to a solution of K_2[**2**] in DME. The molecular structure of [K_2(18-c-6)$_2$(DME)][**2**] shows a P_8 realgar-like core coordinating to two 15 valence electron (VE) Cp'''Ni fragments (Figure 2). Although there are a few complexes known containing a P_8 structural motif, this is the first ionic compound with such a polyphosphorus cage.[13] All bond lengths in the P_8 core are in the range of P-P single bonds (2.191(3) − 2.243(4) Å) and are similar to the corresponding bond lengths in other related P_8 derivatives. The formation of **2** shows that by the reaction with strong reducing agents **1** can act as a phosphorus source, leading via rearrangements to larger phosphorus aggregates. Natural Population Analysis (NPA) on **2** reaveals that the phosphorus atoms, which are coordinating to Ni atoms are negatively charged (−0.26), while the Ni centers bear a

positive charge of 0.45. The non-coordinating phosphorus atoms are only slightly negatively charged (−0.14, −0.15).

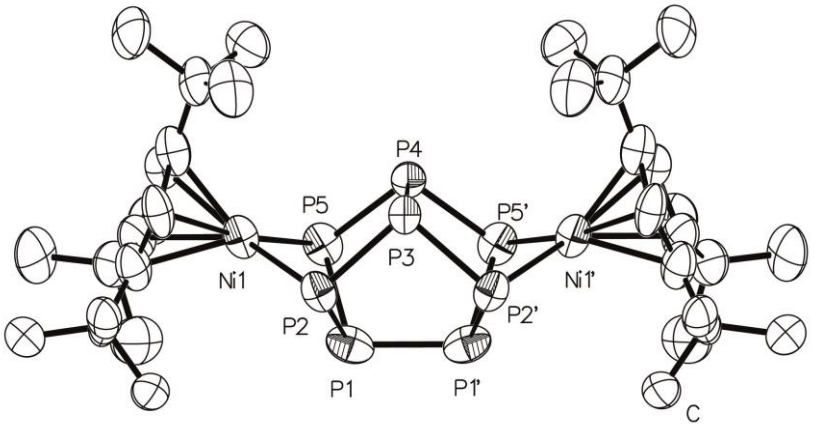

Figure 2. Molecular structure of the anionic part of [K_2(18-c-6)$_2$(DME)][**2**]. H atoms bonded to carbon are omitted for clarity. Ellipsoids are drawn at 50% probability level. Selected bond lengths [Å] and angles [°]: P1-P2 2.191(3), P1-P5 2.206(3), P1-P1´ 2.243(4), P2-P3 2.200(2), P3-P4 2.212(3), P4-P5 2.210(2), P4-P5 2.211(2), Ni1-P2 2.211(2), Ni1-P5 2.216(2), P2-P1-P5 84.87(9), P2-P1-P1´ 103.93(7), P5-P1-P1´ 104.35(8), P1-P2-P3 98.46(10), P1-P2-Ni1 85.26(9), P3-P2-Ni1 102.70(9), P2-P3-P2´ 97.12(14), P2-P3-P4 100.09(10), P5-P4-P5´ 98.02(15), P5-P4-P3 99.64(10), P1-P5-P4 98.06(10), P1-P5-Ni1 84.76(9), P4-P5-Ni1 102.77(10).

Since the reduction of **1** to form **2** is accompanied by the formation of the triple-decker complex **3** it is not possible to separate both in an analytically pure manner. However, we found that adding $NaNH_2$ to **1** appears to be a straightforward method to synthesize the triple-decker complex Na[**3**] in 84% isolated yield (Scheme 1). Note that in contrast, the reaction of pentaphosphaferrocene with $NaNH_2$ leads to a nucleophilic attack and a subsequent autometallation process product, yielding the trianionic compound [{Cp*Fe(η^4-P_5)}$_2$N]$^{3-}$.[10] Compound **3** was characterized by multinuclear NMR spectroscopy, showing a singlet in the ^{31}P NMR spectrum in THF-d_8 at −346.5 ppm, which is shifted strongly to higher field compared to **1** (−163.4 ppm) and is close to the chemical shift of the neutral compound [Cp'''Mo(CO)$_2$(η^3-P_3)] (−348.9 ppm).[14] Cyclic voltammetric studies of **3** in acetonitrile show one reversible oxidation with a half potential at −1.46 V.[15] In addition, an irreversible reduction at −2.13 V is observed. No further oxidations or reductions at higher or lower potentials occur. Based on these results an equimolar solution of AgOTf in DME was added to a solution of **3** in DME, leading to a color change to yellow-green and an immediate formation of a silver layer. After column chromatography the neutral triple-decker complex [(Cp'''Ni)$_2$($\eta^{3:3}$-P_3)] (**4**) is isolated in 41 % yield (Scheme 1). The 33 valence electron complex **4** was characterized by EPR spectroscopy and the magnetic moment was determined by the Evans method.[12] In the latter an effective magnetic moment of μ_{eff} = 1.92 μB is monitored, representing one unpaired electron. DFT calculations on **4** reveal that

the spin density is mainly localized on the two Ni atoms with minor contributions of the *cyclo*-P_3 phosphorus atoms and the Cp ligands. X-ray structure analysis of [Na(dme)$_4$][**3**] and **4**, respectively, show sandwich triple-decker complexes with a three-membered phosphorus ring as a middle deck: for **3** the anionic and for **4** the neutral compound (Figure 3). In contrast to the anion **3**, in which the P-P single bonds result in a non-distorted P_3 ring (P-P bonds: 2.1950(7) − 2.2408(7) Å), in **4** two P-P bond lengths are shortened (P1-P2: 2.1851(6) Å; P2-P3: 2.1817(5) Å) and one is elongated (P1-P3: 2.3976(6) Å) and reveals therefore an allylic distortion.

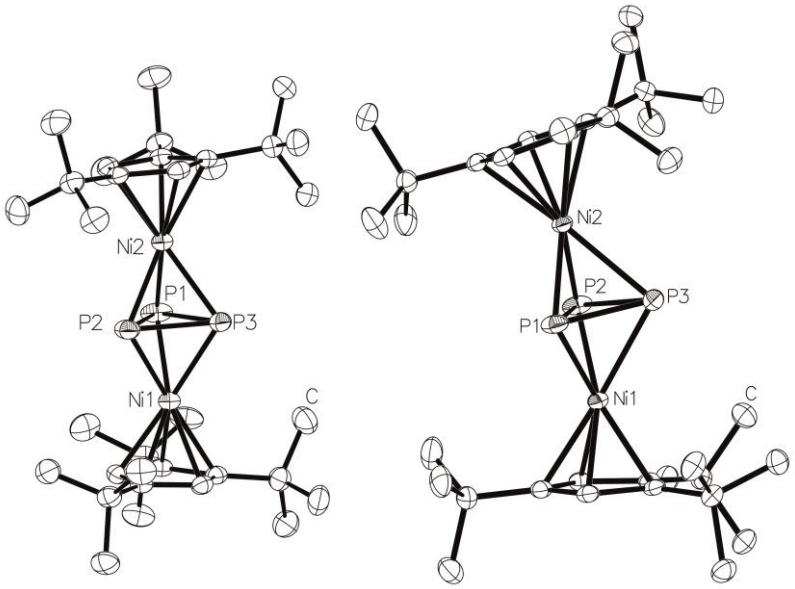

Figure 3. Molecular structure of the anionic part of [Na(dme)$_4$][**3**] (left) and the oxidized neutral compound **4** (right). H atoms bonded to carbon are omitted for clarity. Ellipsoids are drawn at 50% probability level. Selected bond lengths [Å] and angles [°]: [Na(dme)$_4$][**3**]: P1-P2: 2.2408(7), P1-P3 2.1950(7), P2-P3: 2.2094(6), Ni1-P1 2.2621(5), Ni1-P2: 2.2508(5), Ni1-P3: 2.2807(5), P2-P1-P3: 59.74(2), P1-P2-P3: 59.10(2), P1-P3-P2 61.16(2). **4**: P1-P2: 2.3976(6), P1-P3: 2.1851(6), P2-P3: 2.1817(5), Ni1-P1: 2.2077(4), Ni1-P2: 2.2086(4), Ni1-P3: 2.3778(4), P2-P1-P3: 56.63(2), P1-P2-P3: 56.77(2), P1-P3-P2: 66.60(2).

The three-membered ring in **3** is symmetrically coordinating in a $\eta^{3:3}$-fashion to both nickel atoms (P-Ni1: 2.2508(5) − 2.2807(5) Å; P-Ni2: 2.2519(5) − 2.2875(5) Å). A similar structural motif was reported for the dicationic compound [{Ni($CH_3C(CH_2PPh_2)_3)_2$}$_2$(μ,$\eta^{3:3}$-P_3)][BPh_4]$_2$.[16] In **4** the Ni-P bonds differ (P1-Ni1: 2.2077(4) Å, P2-Ni1 2.2086(4) Å, P3-Ni1 2.3778(4) Å) and as a result the P_3 ring is shifted out of the center of the complex, resulting in a nonlinear conformation (Ni1-$P_{3center}$-Ni2: 176.89(1)° in **3**; Ni1-$P_{3center}$-Ni2: 160.67(1)° in **4**). DFT calculations on the model compounds [(CpNi)$_2$(μ,$\eta^{3:3}$-P_3)]$^{+/0/-}$ (Figure 4) show that the distortion of the P_3 unit from the allylic to the symmetrical *cyclo*-P_3 unit is caused by the stepwise population of a P-P bonding molecular orbital, by

going from the cation $[(CpNi)_2(\mu,\eta^{3:3}\text{-}P_3)]^+$ to the anion $[(CpNi)_2(\mu,\eta^{3:3}\text{-}P_3)]^-$. This MO represents the lowest unoccupied orbital (LUMO) in $[(CpNi)_2(\mu,\eta^{3:3}\text{-}P_3)]^+$ and the highest occupied MO (HOMO) in the anion $[(CpNi)_2(\mu,\eta^{3:3}\text{-}P_3)]^-$. The increase in the strength of the P-P bond by going from $[(CpNi)_2(\mu,\eta^{3:3}\text{-}P_3)]^+$ to $[(CpNi)_2(\mu,\eta^{3:3}\text{-}P_3)]^-$ is confirmed by the Wiberg bond index (WBI), which vary from 0.35 over 0.69 to 0.94, respectively.

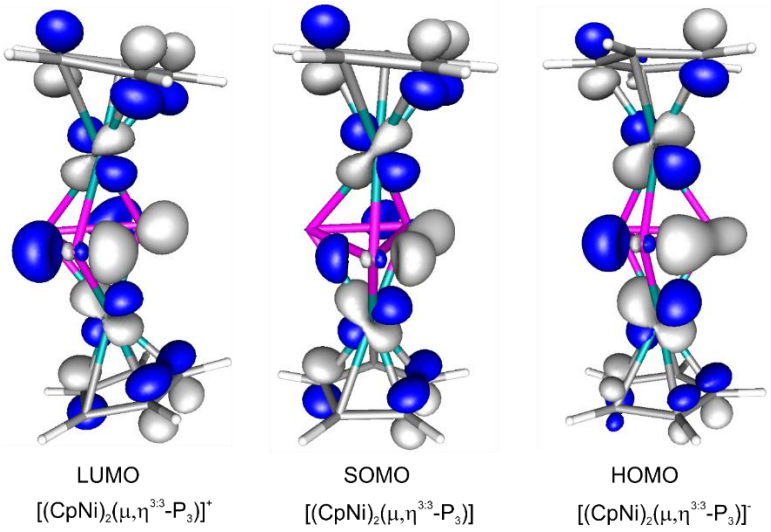

Figure 4. Frontier molecular orbitals for $[(CpNi)_2(\mu,\eta^{3:3}\text{-}P_3)]^{+/0/-}$, calculated at the BP86/def2-TZVP level of theory.

Regardless of several attempts, no further information about the pathway of the reaction (ii) (Scheme 1) for the formation of **3** could be obtained. Neither any insoluble polyphosphorus compounds are formed, nor any soluble phosphorus containing byproducts could be detected in the ^{31}P NMR spectrum.[17] To our knowledge complex **3** and **4** are the first anionic and neutral nickel/nickel triple-decker sandwich complexes exhibiting a $\eta^{3:3}$-P_3 middle deck with cyclopentadienyl ligands so far.[16,18]

When **1** is reacted with $LiPPh_2$ at room temperature complex $[(Cp'''Ni)_2(\mu,\eta^{2:2}\text{-}P_7Ph_2)]^-$ (**5**) is formed (Scheme 1). The ^{31}P NMR spectrum of the crude reaction mixture shows seven multiplets, centered at 212.1, 135.8, 106.7, 74.0, −48.50, −119.6 and −133.8 ppm, which are attributed to **5**, as proven by a ^{31}P, ^{31}P COSY experiment.[12,19] Additionally two unassigned signals at 7.4 and −14.2 ppm were observed. All coupling constants obtained from the simulation of the ^{31}P NMR spectrum of **5** lie in the expected ranges.[12] Due to the high sensitivity of **5** all attempts to crystalize and purify **5** failed. Therefore, **5** was reacted with an equimolar amount of HBF_4, to give the protonated species $[(Cp'''Ni)_2(\mu,\eta^{2:2}\text{-}HP_7Ph_2)]$ (**6**), which could be isolated after column chromatographic work up. The ^{31}P NMR spectrum of **6** shows seven multiplets centered at 140.2, 105.0, 35.4, −35.15, −132.5 and −211.05 ppm.[12] Single crystals, suitable for X-ray diffraction measurements, could be obtained from a pentane solution. The molecular structure of **6** reveals a bicyclic P_6 ligand, containing an exocyclic PPh_2 unit, which coordinates to two Cp'''Ni fragments (Figure 5). The position of the hydrogen atom

bonded to the P2 atom could be localized from the difference electron density map and was proven as well by ^{31}P NMR spectroscopy in solution. All P-P bonds are in the range of single bonds (2.1778(9) Å - 2.2241(8) Å). The NPA of **6** shows a positive charge concentration on the Ni and P7 atoms (Ni1: 0.46, Ni2: 0.49 and P7: 0.69); the P1 and P4 atoms bear negative charges (−0.20 and −0.13, respectively). The other phosphorus atoms are basically neutral.

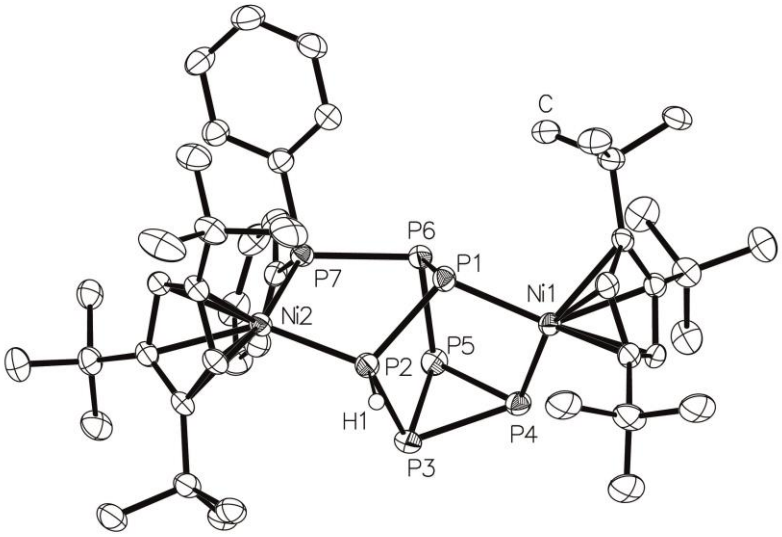

Figure 5. Molecular structure of **6**·C_5H_{12}. H atoms bonded to carbon and the solvated pentane molecules are omitted for clarity. Ellipsoids are drawn at 50% probability level. Selected bond lengths [Å] and angles [°]: P1-Ni1 2.1711(5), P1-P2 2.1789(6), P1-P6 2.1840(6), P2-Ni2 2.1663(5), P2-P3 2.2003(6), P2-H1 1.26(2), P3-P4 2.2012(6), P3-P5 2.2154(6), P4-Ni1 2.1864(5), P4-P5 2.2199(6), P5-P6 2.2241(6), P6-P7 2.2244(6), P7-Ni2 2.1759(5), P2-P1-P6 88.61(2), P1-P2-P3 105.67(2), P2-P3-P4 100.28(2), P2-P3-P5 96.44(2), P4-P3-P5 60.348(19), P3-P4-P5 60.14(2), P3-P5-P4 59.51(2), P3-P5-P6 104.78(2), P4-P5-P6 96.99(2), P1-P6-P5 103.94(2), P1-P6-P7 98.36(2), P5-P6-P7 99.42(2).

For the formation of the P_7 ligand in **5** a reaction pathway is proposed, in which an intermediate **A** is passed (Scheme 2). In order to gain further insight, an excess of three equivalents of $LiPPh_2$ was added to **1**, to prevent the subsequent reaction of **A** with another equivalent of **1**. Of such reaction mixture, the ^{31}P NMR spectrum at 193 K shows three signals centered at 16.3 (dt, $^1J_{P\text{-}P}$ = 291.7 Hz; $^2J_{P\text{-}P}$ = 54.5Hz), −142.6 (dd, $^1J_{P\text{-}P}$ = 195.7, $^2J_{P\text{-}P}$ = 54.5) and −187.3 (dt, $^1J_{P\text{-}P}$ = 291.7, $^1J_{P\text{-}P}$ = 196.8 Hz) ppm, which confirms the intermediate **A**. Furthermore, two unassigned signals centered at −139.8 (d, $^1J_{P\text{-}P}$ = 197.2) and −171.5 (t, $^1J_{P\text{-}P}$ = 197.2) are recorded, in addition with one sharp singlet at −21.5 ppm for $LiPPh_2$. When the sample is warmed up to room temperature the signals for **A** decrease in intensity and finally disappear. In return the signal for $LiPPh_2$ broadens and a very broad signal at −158.9 ppm becomes visible, which is close to the chemical shift of the starting material **1** (−163.4 ppm).[12,20] This broad signal together with the previous observations are explained by a fluctional process for **A** in

solution. This is also in line with corresponding DFT calculations. According to them, **A** possess elongated P-PPh_2 (P–P 2.367 Å) as well as Ni–P(PPh_2) (2.804 Å) bonds, with Wiberg bond orders (WBI) of 0.81 and 0.28, respectively. The WBIs of the other two Ni–P bonds are 0.81 and 0.79. The reaction of **1** with $LiPPh_2$ to **A** is favored by −39.2 kJ·mol^{-1} in solution, whereas the reaction of **A** with **1** is considerably more exothermic (−84.2 kJ·mol^{-1}; Figure 6). The weakening of one Ni–P bond leads obviously to an increased reactivity of **A** towards **1**, giving after rearrangements the bicyclic complex **5**.[21]

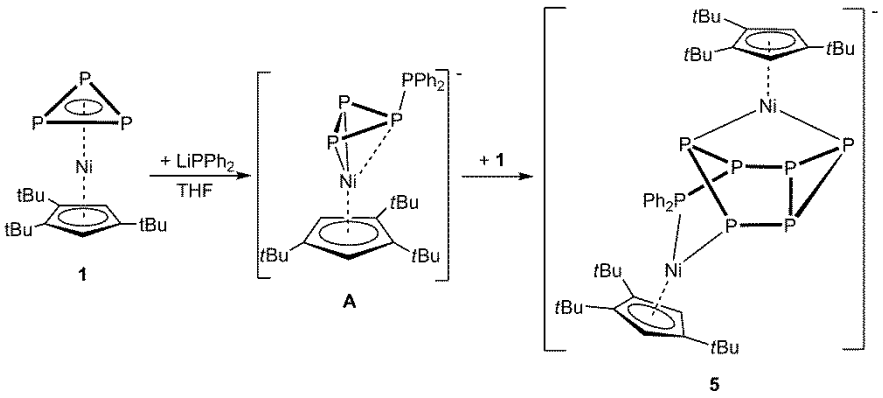

Scheme 2. Proposed reaction pathway for the formation of **5**.

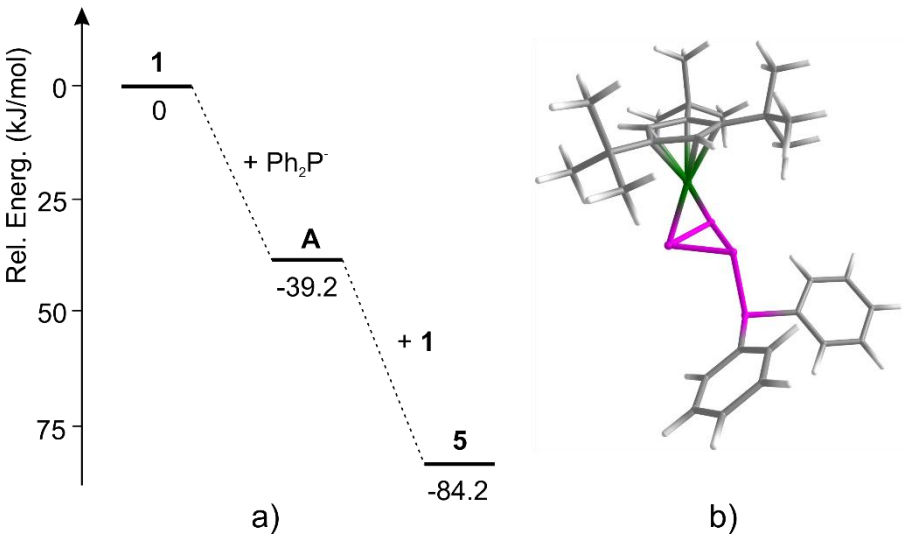

Figure 6. a) Energy profile of the reaction of **1** with Ph_2P^- and b) Optimized geometry of **A**; calculated at the BP86/def2-TZVP level of theory.

To the best of our knowledge there is no other example reported in the literature for such bicyclic phosphorus ligand in **5** coordinating to a transition metal. The organic substituted, neutral and uncoordinated 2,3,4,6-tetra-tert-butylbicyclo[3.1.0]hexaphosphane is known[22] and the compound $[P_7Cy_6][OTf]$ was synthesized recently.[23]

If $LiNMe_2$ (not $NaNH_2$, as used above) is reacted with **1** in THF the formation of the sandwich triple-decker complex **3** cannot be observed.[24] Instead, by adding 1.5 equivalents of $LiNMe_2$, the ^{31}P NMR spectrum shows the formation of two products in a ratio of 1:5. The minor product exhibits 6 multiplets centered at 180.1, 162.0, 65.3, 10.5, −109.9 and −117.4 ppm with an integral ratio of 1:1:1:1:1:1, indicating the formation of a bicyclic analog of **5**, which could not be isolated. The main product, $[Cp'''Ni(\eta^2\text{-}P_3NMe_2)]^-$ (**7**), consists of one triplet at −104.6 ppm ($^1J_{P\text{-}P}$ = 246.9 Hz) and one doublet at −168.0 ppm ($^1J_{P\text{-}P}$ = 247.1 Hz). This finding is in contrast to the reaction of **1** with $LiPPh_2$, which leads to the bicyclus **5** as the main product, but it confirms the first reaction product **A** (Scheme 2). By layering the solution with *n*-hexane few crystals of $[Li(thf)_3]$[**7**] were obtained. The X-ray structure analysis reveals a structural motif similar to **A** (Figure 7). In **7** the *cyclo*-P_3 ligand is coordinating in a η^2-fashion and the non-coordinating phosphorus atom bears the NMe_2 unit. The P-P bond between the coordinating P atoms is shortened in comparison to the remaining P-P bonds (P-P bond lengths: 2.1337(7), 2.1736(6), 2.1940(5) Å). Note, if an excess of two equivalents $LiNMe_2$ is used **7** is formed exclusively, as proven by ^{31}P NMR spectroscopy. However, during the work up process **7** decomposes due to its high sensitivity.

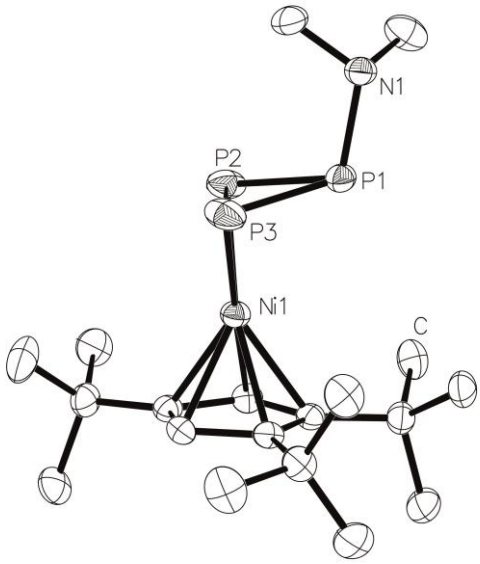

Figure 7. Molecular structure of the anionic part of $[Li(thf)_3]$[**7**]. H atoms bonded to carbon are omitted for clarity. Ellipsoids are drawn at 50% probability level. Selected bond lengths [Å] and

angles [°]: P1-P2 2.1940(5), P1-P3 2.1736(6), P2-P3 2.1337(7), P1-N1 1.8196(13), Ni1-P2 2.2049(5), Ni1-P3 2.1979(5), P1-P2-P3 60.28(2), P1-P3-P2 61.24(2), P2-P1-P3 58.48(2).

In summary, we have shown that the reduction of [Cp'''Ni(η^3-P_3)] (**1**) by potassium leads for P_n ligand complexes for the first time to a reaggregation process, forming the unprecedented compound [(Cp'''Ni)$_2$(μ,$\eta^{2:2}$-P_8)]$^{2-}$ (**2**), which contains a realgar-like P_8 core. Furthermore, the reaction of **1** with $NaNH_2$ does not lead to substituted *cyclo*-P_3 compounds, however, the anionic triple-decker complex [(Cp'''Ni)$_2$(μ,$\eta^{3:3}$-P_3)]$^-$ (**3**) is formed instead. Na[**3**] can be oxidized to its neutral derivative **4**, containing a distorted P_3 middle deck. The reaction of Ph_2P^- as a nucleophile with **1** leads to a nucleophilic addition. But the product **A** reacts further with **1** to form [(Cp'''Ni)$_2$(μ,$\eta^{2:2}$-(P_6PPh_2)]$^-$ (**5**), which can be trapped by protonation with HBF_4, yielding [(Cp'''Ni)$_2$(μ,$\eta^{2:2}$-(P_6HPPh_2)] (**6**). By changing the nucleophile to $LiNMe_2$ the substituted compound [Cp'''Ni(η^2-P_3NMe_2)]$^-$ (**7**) could be synthesized, which confirms the first found product [Cp'''Ni(η^2-P_3PPh_2)]$^-$ (**A**), in the reaction process for the formation of **5**.

Moreover, we were not only able to synthesize and characterize the mentioned products, revealing the manifold reactivity of **1** towards potassium and main group nucleophiles. But also does the formation of **2** and **3** indicate, that **1** may serve as an easy accessible phosphorous source, by separating the P_3 unit from its Cp'''Ni fragment, which has to be investigated further.

Acknowledgements

The authors thank the Deutsche Forschungsgemeinschaft (DFG) for financial support and Dr. I. G. Shenderovich for the measurement of ^{1}H HSQC NMR spectra.

References:

[1] a) J. F. Nixon, *Chem. Rev.* **1988**, *88*, 1327-1362; b) J. F. Nixon, *Coord. Chem. Rev.* **1995**, *145*, 201-258.

[2] a) C. Heindl, E. V. Peresypkina, A. V. Virovets, G. Balázs, M. Scheer, *Chem. Eur. J.* **2016**, *22*, 1944-1948; b) R. S. P. Turbervill, J. M. Goicoechea, *Chem. Rev.* **2014**, *114*, 10807-10828; c) R. S. P. Turbervill, J. M. Goicoechea, *Chem. Commun.* **2012**, *48*, 6100-6102; d) A. S. Ionkin, W. J. Marshall, B. M. Fish, A. A. Marchione, L. A. Howe, F. Davidson, C. N. McEwen, *Eur. J. Inorg. Chem.* **2008**, *2008*, 2386-2390.

[3] a) M. Scheer, E. Herrmann, *Z. Chem.* **1990**, *29*, 41; b) O. J. Scherer, *Angew. Chem. Int. Ed.* **1990**, *29*, 1104.

[4] a) B. Breit, R. Winde, T. Mackewitz, R. Paciello, K. Harms, *Chem. Eur. J.* **2001**, *7*, 3106-3121; b) L. E. E. Broeckx, A. Bucci, C. Zuccaccia, M. Lutz, A. Macchioni, C. Müller, *Organometallics* **2015**, *34*, 2943-2952.

[5] a) B. Attenberger, E. V. Peresypkina, M. Scheer, *Inorg. Chem.* **2015**, *54*, 7021-7029; b) J. Bai, A. V. Virovets, M. Scheer, *Angew. Chem. Int. Ed.* **2002**, *41*, 1737-1740; c) M. Scheer, L. J. Gregoriades, A. V. Virovets, W. Kunz, R. Neueder, I. Krossing, *Angew. Chem. Int. Ed.* **2006**, *45*, 5689-5693; d) F. Dielmann, A. Schindler, S. Scheuermayer, J. Bai, R. Merkle, M. Zabel, A. V. Virovets, E. V. Peresypkina, G. Brunklaus , H. Eckert, M. Scheer, *Chem. Eur. J.* **2012**, *18*, 1168-1179.

[6] C. Schwarzmaier, A. Schindler, C. Heindl, S. Scheuermayer, E. V. Peresypkina, A. V. Virovets, M. Neumeier, R. Gschwind, M. Scheer, *Angew. Chem. Int. Ed.* **2013**, *52*, 10896-10899.

[7] a) J. Bai, A. V. Virovets, M. Scheer, *Science* **2003**, *300*, 781-783; b) M. Scheer, A. Schindler, J. Bai, B. P. Johnson, R. Merkle, R. Winter, A. V. Virovets, E. V. Peresypkina, V. A. Blatov, M. Sierka, H. Eckert, *Chem. Eur. J.* **2010**, *16*, 2092-2107; c) M. Scheer, J. Bai, B. P. Johnson, R. Merkle, A. V. Virovets, C. E. Anson, *Eur. J. Inorg. Chem.* **2005**, *2005*, 4023-4026; d) M. Scheer, A. Schindler, C. Gröger, A. V. Virovets, E. V. Peresypkina, *Angew. Chem. Int. Ed.* **2009**, *48*, 5046-5049; e) M. Scheer, A. Schindler, R. Merkle, B. P. Johnson, M. Linseis, R. Winter, C. E. Anson, A. V. Virovets, *J. Am. Chem. Soc.* **2007**, *129*, 13386-13387; f) S. Welsch, C. Gröger, M. Sierka, M. Scheer, *Angew. Chem. Int. Ed.* **2011**, *50*, 1435-1438.

[8] a) R. F. Winter, W. E. Geiger, *Organometallics* **1999**, *18*, 1827-1833; b) M. V. Butovskiy, G. Balázs, M. Bodensteiner, E. V. Peresypkina, A. V. Virovets, J. Sutter, M. Scheer, *Angew. Chem. Int. Ed.* **2013**, *52*, 2972-2976.

[9] a) M. D. Rausch, D. J. Ciappenelli, *J. Organomet. Chem.* **1967**, *10*, 127; b) A. G. Osborne, R. H. Whiteley, *J. Organomet. Chem.* **1978**, *162*, 79-81; c) M. Rausch, M. Vogel, H. Rosenberg, *J. Org. Chem.* **1957**, *22*, 900-903.

[10] E. Mädl, M. V. Butovskii, G. Balázs, E. V. Peresypkina, A. V. Virovets, M. Seidl, M. Scheer, *Angew. Chem. Int. Ed.* **2014**, *53*, 7643-7646.

[11] a) H. Krauss, G. Balazs, M. Bodensteiner, M. Scheer, *Chem. Sci.* **2010**, *1*, 337-342; b) E. J. P. Malar, *Eur. J. Inorg. Chem.* **2004**, 2723–2732.

[12] cf. supplementary information.

[13] a) M. E. Barr, B. R. Adams, R. R. Weller, L. F. Dahl, *J. Am. Chem. Soc.* **1991**, *113*, 3052-3060; b) S. N. Konchenko, N. A. Pushkarevsky, M. T. Gamer, R. Köppe, H. Schnöckel, P. W. Roesky, *J. Am. Chem. Soc.* **2009**, *131*, 5740-5741; c) C. P. Butts, M. Green, T. N. Hooper, R. J. Kilby, J. E. McGrady, D. A. Pantazis, C. A. Russell, *Chem. Commun.* **2008**, 856-858; d) M. Scheer, U. Becker, E. Matern, *Chem. Ber.* **1996**, *129*, 721-724; e) W. Huang, P. L. Diaconescu, *Chem. Commun.* **2012**, *48*, 2216-2218.

[14] M. Scheer, G. Friedrich, K. Schuster, *Angew. Chem.* **1993**, *105*, 641-643.

[15] referenced against ferrocene.

[16] M. Di Vaira, S. Midollini, L. Sacconi, *J. Am. Chem. Soc.* **1979**, *101*, 1757-1763.

[17] Only traces of **2** were observed.

[18] a) M. Di Vaira, C. A. Ghilardi, S. Midollini, L. Sacconi, *J. Am. Chem. Soc.* **1978**, *100*, 2550-2551; b) M. Caporali, L. Gonsalvi, A. Rossin, M. Peruzzini, *Chem. Rev.* **2010**, *110*, 4178-4235.

[19] According to the integral intensity of **5** in comparison to minor products, **5** is formed in about 81% conversion.

[20] This process is reversible, as the same signals for **A** are observed again, if the probe is cooled back down.
[21] Although the reaction pathway indicates a ratio for $LiPPh_2$:**1** of 1:2, best experimental yields could be achieved by using a 1:1 molar ratio. Probably, the higher ratio of $LiPPh_2$ shifts the equilibrium between **1** and **A** in favor of **A**.
[22] M. Baudler, Y. Aktalay, K.-F. Tebbe, T. Heinlein, *Angew. Chem. Int. Ed.* **1981**, *20*, 967-969.
[23] a) K.-O. Feldmann, J. J. Weigand, *Angew. Chem. Int. Ed.* **2012**, *51*, 7545-7549; b) M. H. Holthausen, J. J. Weigand, *Chem. Soc. Rev.* **2014**, *43*, 6639-6657.
[24] If one equivalent of $LiNMe_2$ is used a large product distribution is observed in the ^{31}P NMR spectrum and no signals can be assigned.

7.2 Supporting Information

Supporting information of the manuscript entitled:

Unexpected reactivity of [Cp'''Ni(η^3-P_3)] towards main group nucleophiles and by reduction

Eric Mädl, Gábor Balázs, Eugenia Peresypkina and Manfred Scheer*

Contents

7.2.1 Experimental details: complex syntheses and characterization

General Procedures: All manipulations were performed with rigorous exclusion of oxygen and moisture in Schlenk-type glassware on a dual manifold Schlenk line in argon atmosphere or in Ar filled glove box with a high-capacity recirculator (<0.1ppm O_2). THF, hexane and DME were distilled from sodium benzophenoneketyl. Deuterated solvents were degassed, dried and distilled prior to use. NMR spectra were recorded on a Bruker Avance 300 MHz and Bruker Avance 400 MHz spectrometers. Chemical shifts were measured at ambient temperature and are given in ppm; they are referenced to TMS for ^{1}H and ^{13}C, and 85% H_3PO_4 for ^{31}P as external standard. Elemental analyses (CHN) were determined using in-house facility. Spectrum simulations were performed with the simulation module "daisy", embedded in the software *Bruker Topspin (V. 3.0)*. **1** was synthesized according to the reported synthesis of [Cp''Ni(η^3-P_3)].[1]

The magnetic susceptibility χ_M for **4** and the effective magnetic moment μ_{eff} was determined on a Bruker Avance 400 MHz spectrometer (^{1}H: 400.130 MHz) by Evans method (equations (1) and (2)),[2] neglecting the diamagnetic contributions. Pure solvent was used an internal reference.

Equation:

$$\chi_M = \frac{3 \cdot \Delta f}{1000 \cdot f \cdot c} \quad (1)$$

$$\mu_{eff} = 798 \cdot \sqrt{T \cdot \chi_M} \quad (2)$$

χ_M: molar susceptibility of the sample in $m^3 \cdot mol^{-1}$.

Δf: chemical shift difference between solvent in presence of paramagnetic solute and pure solvent in Hz.

f: operating frequency of NMR spectrometer in Hz.

c: concentration of the paramagnetic sample: 0.01 mol/L

T: absolute temperature in K.

μ_{eff}: effective magnetic moment in μ_B.

Synthesis of [K_2(18-K-6)$_2$(dme)][2]: To a thin piece of potassium (25 mg, 0.64 mmol) a solution of **1** (200 mg, 0.51 mmol) in 30 mL DME is added and the reaction mixture is stirred overnight. After a few minutes a color change to burgundy is observed, which changes over night to dark violet. A solution of 18-crown-6 ether (137.3 mg, 0.51 mmol) in DME is added, the reaction mixture is reduced to 7 mL and layered with three times the amount of *n*-hexane. After 4 days at 4 °C few crystals of **2** (violet needles) and **3** (red plates) are obtained. The yield of **2**, as given in scheme 1 of the manuscript, has been determined by ^{31}P NMR spectroscopy. ES-MS: 675.3 (**3**$^-$, 10%), 831.2 (MH^-, 100%). ^{1}H NMR (400.13 MHz, THF-d_8): δ [ppm] = 1.21 (s, 9H, *t*Bu), 1.37 (s, 18H, *t*Bu), 5.58 (s, 2H, CH). ^{31}P{^{1}H} NMR (161.97 MHz, THF-d_8): δ [ppm] = 30.6 (m, 2P, P^A/ $P^{A'}$), 10.1 (m, 2P, P^M/ $P^{M'}$), −17.9 (m, 4P, P^X/ $P^{X'}$). For the assignments of the P atoms check Figure S2.

Synthesis of [Na(dme)$_3$][3]: To a mixture of **1** (260 mg, 0.67 mmol) and $NaNH_2$ (26 mg, 0.67 mmol) 25 mL DME is added and the suspension is stirred for two days. The reaction mixture turns slowly to burgundy red during the reaction. The solvent is concentrated to 5 mL and layered with double the amount of *n*-hexane, at 0 °C. After 3 days red crystals of [Na(dme)$_4$][**3**] are obtained. After drying [Na(dme)$_2$][**3**] is isolated in 84 % yield (200 mg). ES-MS: 675.3 (M^-, 100%). ^{1}H NMR (400.13 MHz, THF-d_8): δ [ppm] = 1.16 (s, 9H, *t*Bu), 1.35 (s, 18H, *t*Bu), 4.80 (s, 2H, CH). ^{13}C{^{1}H} NMR (100.62 MHz, THF-d_8): δ [ppm] = 31.74 (s, *C*(CH$_3$)$_3$), 32.77 (s, C(*C*H$_3$)$_3$), 33.52 (s, *C*(CH$_3$)$_3$), 35.09 (s, C(*C*H$_3$)$_3$), 86.74 (s, *C*H), 111.42 (s, *C*-C(CH$_3$)$_3$), 111.79 (s, *C*-C(CH$_3$)$_3$). ^{31}P{^{1}H} NMR (161.97 MHz, THF-d_8): δ[ppm] = −346.07 (s, 3P).

Synthesis of [4]: To a solution of [Na(dme)$_4$][**3**] (200 mg, 0.123 mmol) in 10 mL DME a solution of AgOTf (49.5 mg, 0.123 mmol) in 10 mL DME is slowly added, under strong stirring. An immediate silver layer is observed. The solution is stirred for another 2 hours, the solvent removed, the precipitate dissolved in a small amount of *n*-hexane and subsequently purified by column chromatography (Silica, 2.5 x 22 cm, *n*-hexane). Two bands are observed, a very light yellow one, which comes first and is discarded, and a second blackish-yellow one, which is collected. The solvent is strongly reduced and by removing remaining solvent slowly over a course of 2 weeks crystals of **4** (53 mg, 40.6 %) could be isolated. $C_{34}H_{58}Ni_2P_3$ (677.13): calcd. C 60.31, H 8.63; found C 60.26, H 8.35. FD-MS: 644.3 (M^+ – P, 10%), 675.2 (M^+, 100%). Evans (C_6D_6, 300 K): μ_{eff} = 1.68 μ_B.

Synthesis of [6]: To a solution of **1** (150 mg, 0.390 mmol) in 10 mL THF a solution of $LiPPh_2$ (70 mg, 0.364 mmol) in 20 mL THF is added at −60 °C. The solution is stirred over night at room temperature, forming **5**, which is used in situ for the synthesis of **6**. For the ^{31}P NMR spectroscopic data of **5** check Table S2 and Figure S6. 0.03 mL HBF_4 (0.478 mmol) are added and stirred overnight. The solvent is removed and 0.5 mL of THF is added. The dark red solution is purified via column chromatography (Al_2O_3, 1.0 x 5.0 cm, *n*-hexane). As a side note: **6** decomposes on the column, thus a short and quick dropping column should be used. The column is flushed with *n*-hexane until the dropping solution is clear (impurities of **1**). An eluent of *n*-hexane/THF of 20:1 is used and a red fraction is discarded. After the dropping solution is clear **6** is obtained by using pure THF as an eluent. The solvent is removed and **6** is isolated (23 mg, 12.4 %). FD-MS: 954.0 (M^+, 100%). ^{1}H NMR (400.13 MHz, THF-d_8): δ [ppm] = 1.05 (s, 9H, CpC(C*H$_3$*)), 1.14 (s, 9H, CpC(C*H$_3$*)), 1.16 (s, 9H, CpC(C*H$_3$*)), 1.35 s, 9H (s, 9H, CpC(C*H$_3$*)), 1.36 (s, 9H, CpC(C*H$_3$*)), 1.36 (s, 9H, CpC(C*H$_3$*)), 4.73 (broad d, 1H, C$_5$*H$_2$*), 4.84 (broad s, 1H, C$_5$*H$_2$*), 4.85 (broad s, 1H, C$_5$*H$_2$*), 5.48 (broad m, 1H, C$_5$*H$_2$*), 7.22 (dm, 1H, *H*P$_7$). ^{31}P{^{1}H} NMR (161.97 MHz, THF-d_8): δ = −208.3 − (−213.8) (m, 1P, P^Z), −130.0 − (−135.0) (m, 1P P^X), 33.4 − (−36.9) (m, 1P, P^Q), 40.0 − 30.8 (m, 1P, P^M/P^N), 106.2 − 103.7 (m, 1P, P^D), 143.2 − 137.2 (m, 1P, P^A). For the assignments of the P atoms check Figure S9.

Synthesis of Li[7]: 0.1 g (0.25 mmol) [Cp'''Ni(η^3-P_3)] in THF (10 mL) are added slowly to a suspension of 26 mg (0.5 mmol) $LiNMe_2$ in THF (30 mL) at room temperature and the solution is stirred for 24 h, resulting in a color change to orange-red. A few crystals suitable for X-ray structure analysis was obtained by reducing the solvent to 8 mL THF and layer the red solution with *n*-hexane (25 mL). If the solvent is removed a sticky residue is obtained. Due to its high sensitivity **7** could not be worked up further. A decomposition of **7** is observed during extraction and filtration with toluene. Thus only the crystalline yield of $[Li(thf)_3][\mathbf{7}]$ (5 mg, 3 %) is given. ES-MS: 428.2 (M^-, 80 %), 552.1 ([M^- + 4 P], 100 %), 799.2 ([$\{C_{17}H_{29}Ni\}_2P_7$], 20 %). ^{1}H NMR (400.13 MHz, DME with C_6D_6 capillary): δ [ppm] = 1.75 (s, 9 H), 1.94 (s, 18 H), 2.59 (d, 6 H), 5.31 (d, 2 H). ^{31}P NMR (161.97 MHz, DME with C_6D_6 capillary): δ = −160.8 (d, 2 P), −95.84 (t, 1 P).

7.2.2 Experimental and simulated NMR spectra and ortep-like plots

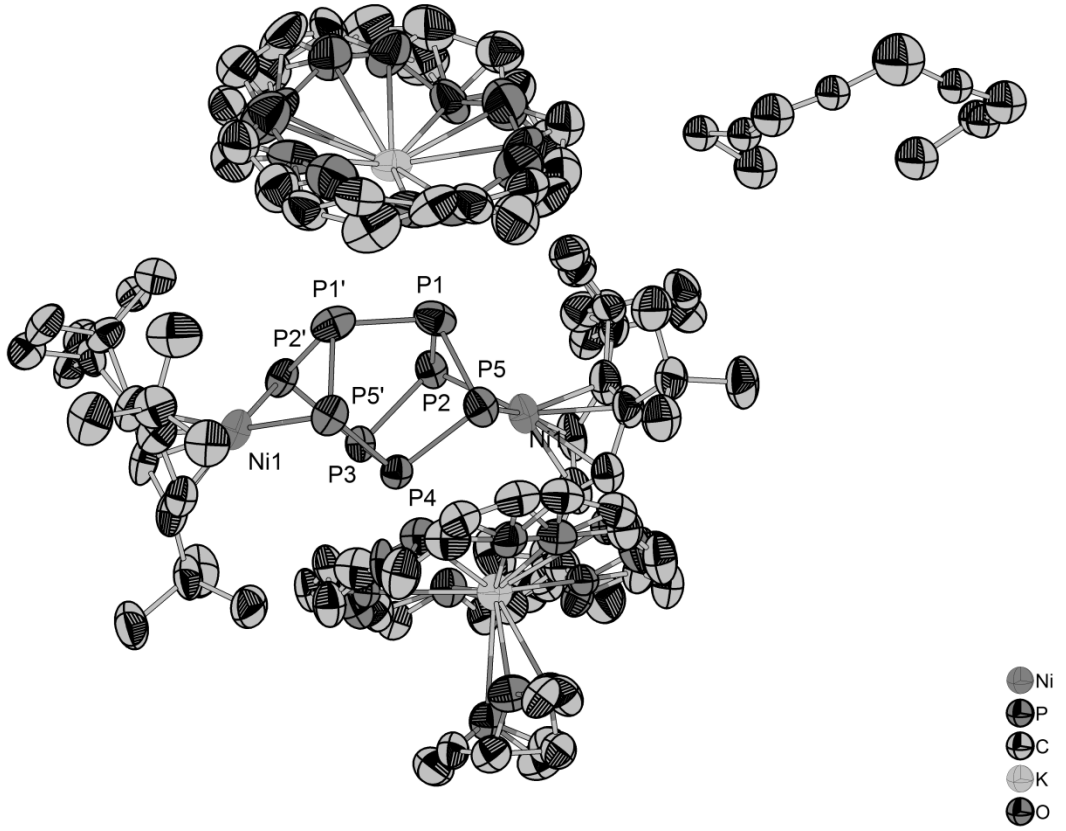

Figure S1. Molecular structure of $[K_2(18\text{-c-}6)_2(dme)]$[**2**]. H atoms bonded to carbon are omitted for clarity. The 18-crown-6 molecule and the coordinated DME are disordered over two positions with 50 % occupancy. Selected bond lengths [Å] and angles [°]: P1-P2 2.191(3), P1-P5 2.206(3), P1-P1´ 2.243(4), P2-P3 2.200(2), P3-P4 2.212(3), P4-P5 2.210(2), P4-P5 2.211(2), Ni1-P2 2.211(2), Ni1-P5 2.216(2), P2-P1-P5 84.87(9), P2-P1-P1´ 103.93(7), P5-P1-P1´ 104.35(8), P1-P2-P3 98.46(10), P1-P2-Ni1 85.26(9), P3-P2-Ni1 102.70(9), P2-P3-P2´ 97.12(14), P2-P3-P4 100.09(10), P5-P4-P5´ 98.02(15), P5-P4-P3 99.64(10), P1-P5-P4 98.06(10), P1-P5-Ni1 84.76(9), P4-P5-Ni1 102.77(10).

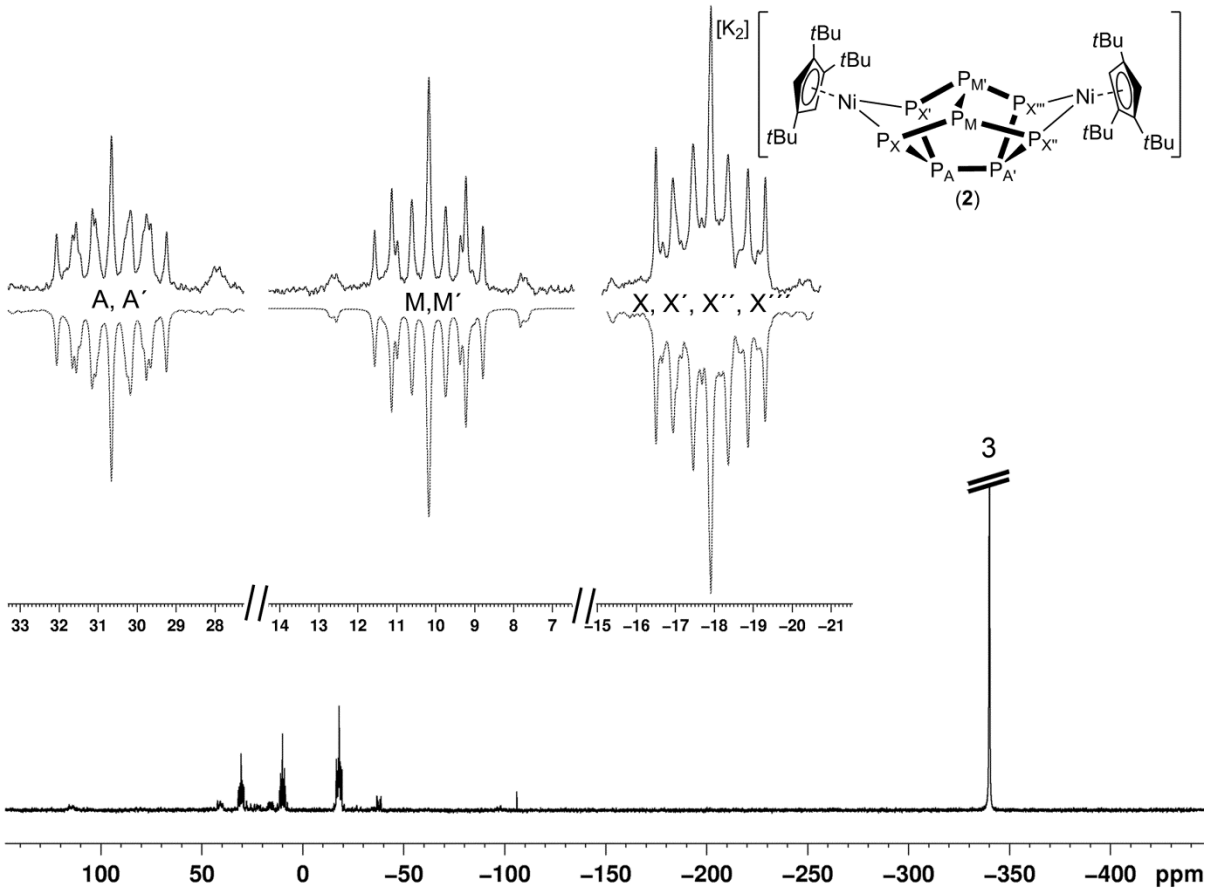

Figure S2. Experimental (top) and simulated (bottom) ^{31}P NMR (161.97 MHz, DME with C_6D_6 capillary) spectrum of the raw solution of K_2[**2**]. To determine A,A' and M,M' two simulations were performed, with both atom groups being swapped. The calculations as depicted in Table S1 and in the spectrum above showed the best fit of the simulated and experimental spectrum.

Table S1. ^{31}P NMR chemical shifts and coupling constants for K_2[**2**] obtained from the simulation.

	J (Hz)			δ (ppm)	
$^1J_{P_A\text{-}P_{A'}}$	338.65	$^3J_{P_X\text{-}P_{X'}} = {}^3J_{P_{X''}\text{-}P_{X'''}}$	−0.13	A, A'	30.63
$^1J_{P_A\text{-}P_X} = {}^1J_{P_A\text{-}P_{X'}} = {}^1J_{P_{A'}\text{-}P_{X''}} = {}^1J_{P_{A'}\text{-}P_{X'''}}$	234.97	$^2J_{P_X\text{-}P_{X''}} = {}^2J_{P_{X'}\text{-}P_{X'''}}$	−89.70	M, M'	10.14
$^2J_{P_A\text{-}P_{X''}} = {}^2J_{P_A\text{-}P_{X'''}} = {}^2J_{P_{A'}\text{-}P_X} = {}^2J_{P_{A'}\text{-}P_{X'}}$	−6.99	$^3J_{P_X\text{-}P_{X'''}} = {}^3J_{P_{X'}\text{-}P_{X''}}$	−7.41	X, X', X'', X'''	−17.88
$^2J_{P_A\text{-}P_M} = {}^2J_{P_A\text{-}P_{M'}} = {}^2J_{P_{A'}\text{-}P_M} = {}^2J_{P_{A'}\text{-}P_{M'}}$	3.56	$^1J_{P_X\text{-}P_M} = {}^1J_{P_{X'}\text{-}P_{M'}} = {}^1J_{P_{X''}\text{-}P_M} = {}^1J_{P_{X'''}\text{-}P_{M'}}$	224.38		
$^2J_{P_X\text{-}P_{M'}} = {}^2J_{P_{X'}\text{-}P_M} = {}^2J_{P_{X''}\text{-}P_{M'}} = {}^2J_{P_{X'''}\text{-}P_M}$	0.91	$^1J_{P_M\text{-}P_{M'}}$	252.39		

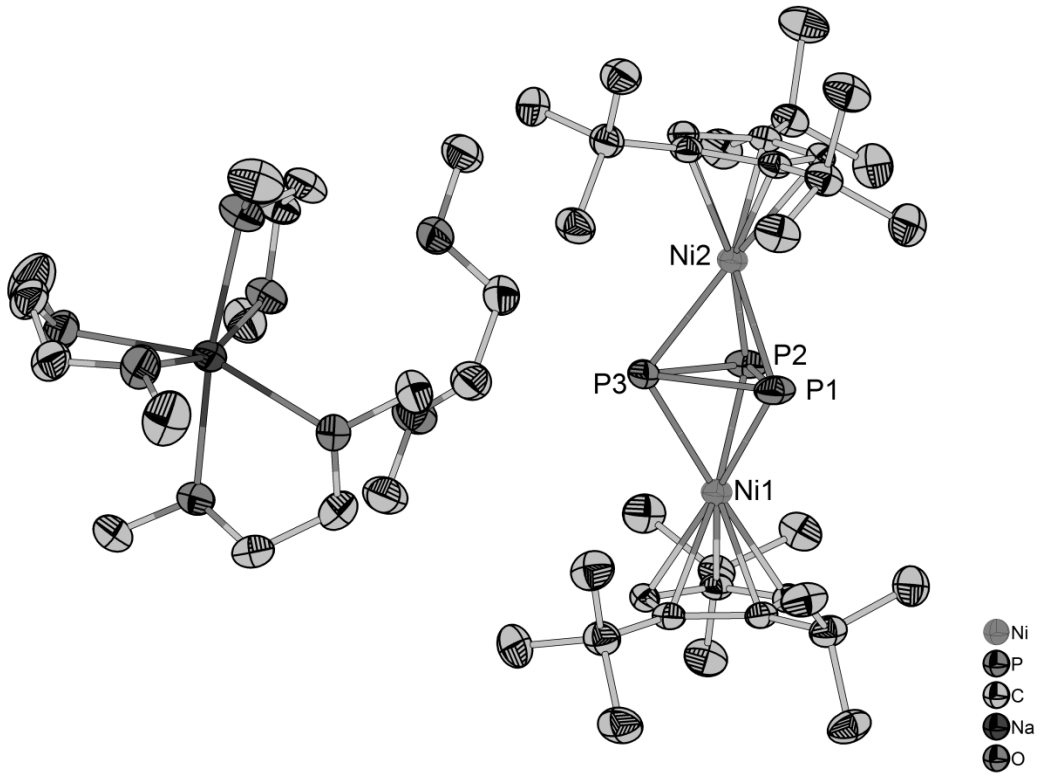

Figure S3. Molecular structure of [Na(dme)$_3$][**3**]·dme. H atoms bonded to carbon are omitted for clarity. Selected bond lengths [Å] and angles [°]: P1-P2: 2.2408(7), P1-P3 2.1950(7), P2-P3: 2.2094(6), Ni1-P1 2.2621(5), Ni1-P2: 2.2508(5), Ni1-P3: 2.2807(5), P2-P1-P3: 59.74(2), P1-P2-P3: 59.10(2), P1-P3-P2 61.16(2).

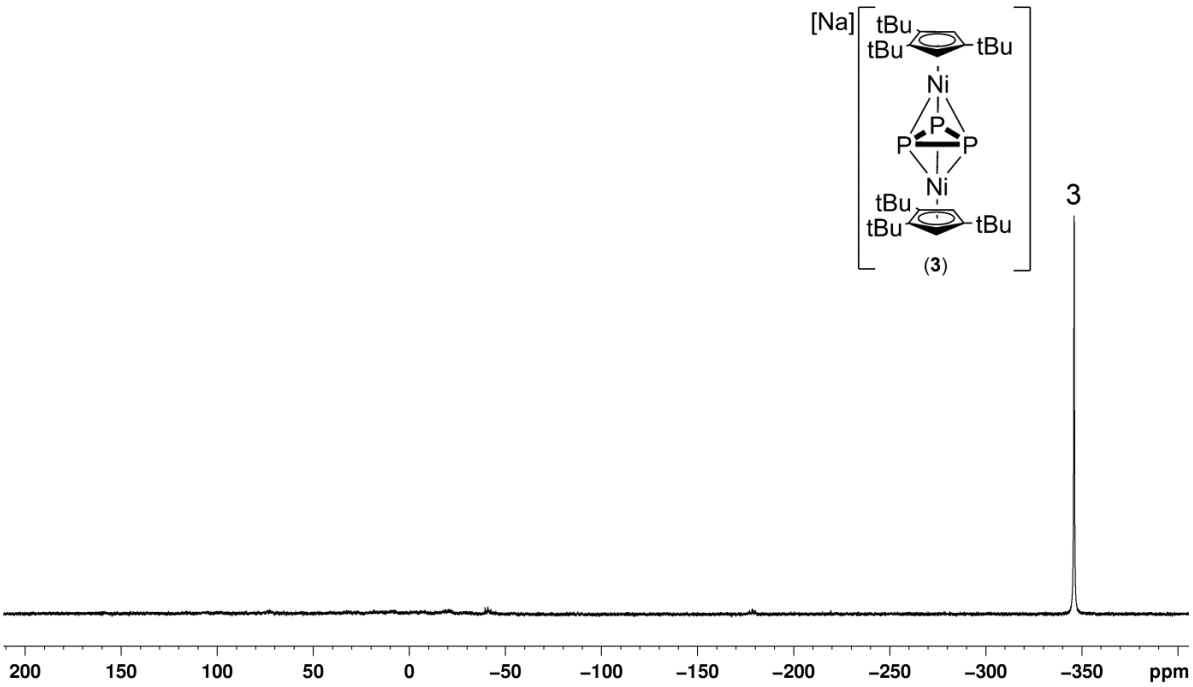

Figure S4. Experimental ^{31}P NMR (161.97 MHz, DME with C_6D_6 capillary) spectrum of Na[**3**].

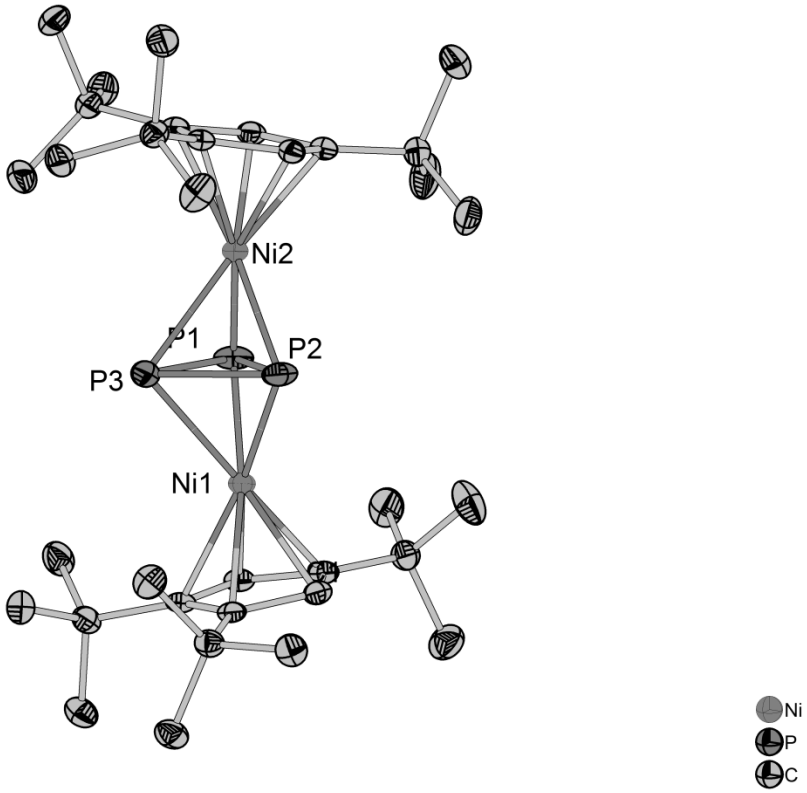

Figure S5. Molecular structure of **4**. H atoms bonded to carbon are omitted for clarity. Selected bond lengths [Å] and angles [°]: P1-P2: 2.3976(6), P1-P3: 2.1851(6), P2-P3 2.1817(5), Ni1-P1: 2.2077(4), Ni1-P2: 2.2086(4), Ni1-P3: 2.3778(4), P2-P1-P3: 56.63(2), P1-P2-P3 56.77(2), P1-P3-P2: 66.60(2).

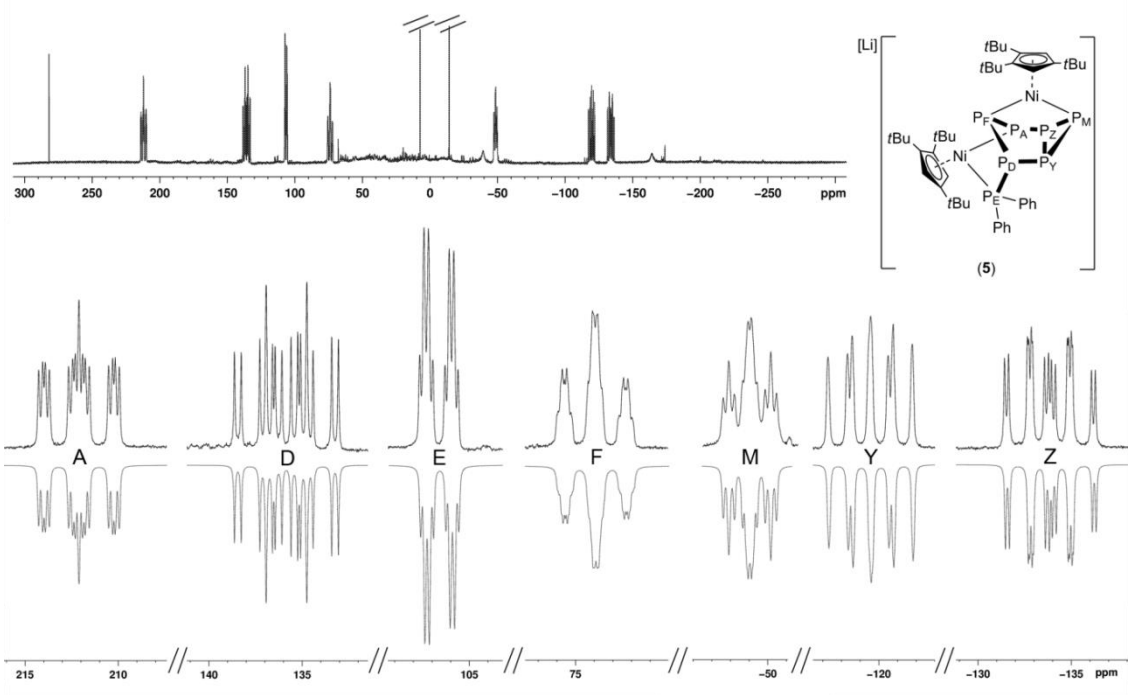

Figure S6. Experimental (top) and simulated (bottom) ^{31}P NMR (161.97 MHz, THF with C_6D_6 capillary) spectrum of the raw solution of Li[**5**].

Table S2. ^{31}P NMR chemical shifts and coupling constants for Li[**5**] obtained from the simulation.

J (Hz)				δ (ppm)	
$^2J_{P_A\text{-}P_D}$	58.00	$^2J_{P_E\text{-}P_F}$	−35.07	P_A	212.10
$^3J_{P_A\text{-}P_E}$	34.80	$^3J_{P_E\text{-}P_M}$	−43.43	P_D	135.81
$^1J_{P_A\text{-}P_F}$	260.48	$^2J_{P_E\text{-}P_Y}$	8.03	P_E	106.65
$^2J_{P_A\text{-}P_M}$	9.06	$^3J_{P_E\text{-}P_Z}$	5.36	P_F	73.98
$^2J_{P_A\text{-}P_Y}$	−6.07	$^3J_{P_F\text{-}P_M}$	54.66	P_M	−48.50
$^1J_{P_A\text{-}P_Z}$	347.77	$^2J_{P_F\text{-}P_Y}$	14.32	P_Y	−119.56
$^1J_{P_D\text{-}P_E}$	219.70	$^2J_{P_F\text{-}P_Z}$	−34.12	P_Z	−133.82
$^1J_{P_D\text{-}P_F}$	271.54	$^1J_{P_M\text{-}P_Y}$	167.75		
$^2J_{P_D\text{-}P_M}$	2.51	$^1J_{P_M\text{-}P_Z}$	196.98		
$^1J_{P_D\text{-}P_Y}$	354.51	$^1J_{P_Y\text{-}P_Z}$	210.52		
$^2J_{P_D\text{-}P_Z}$	−0.64				

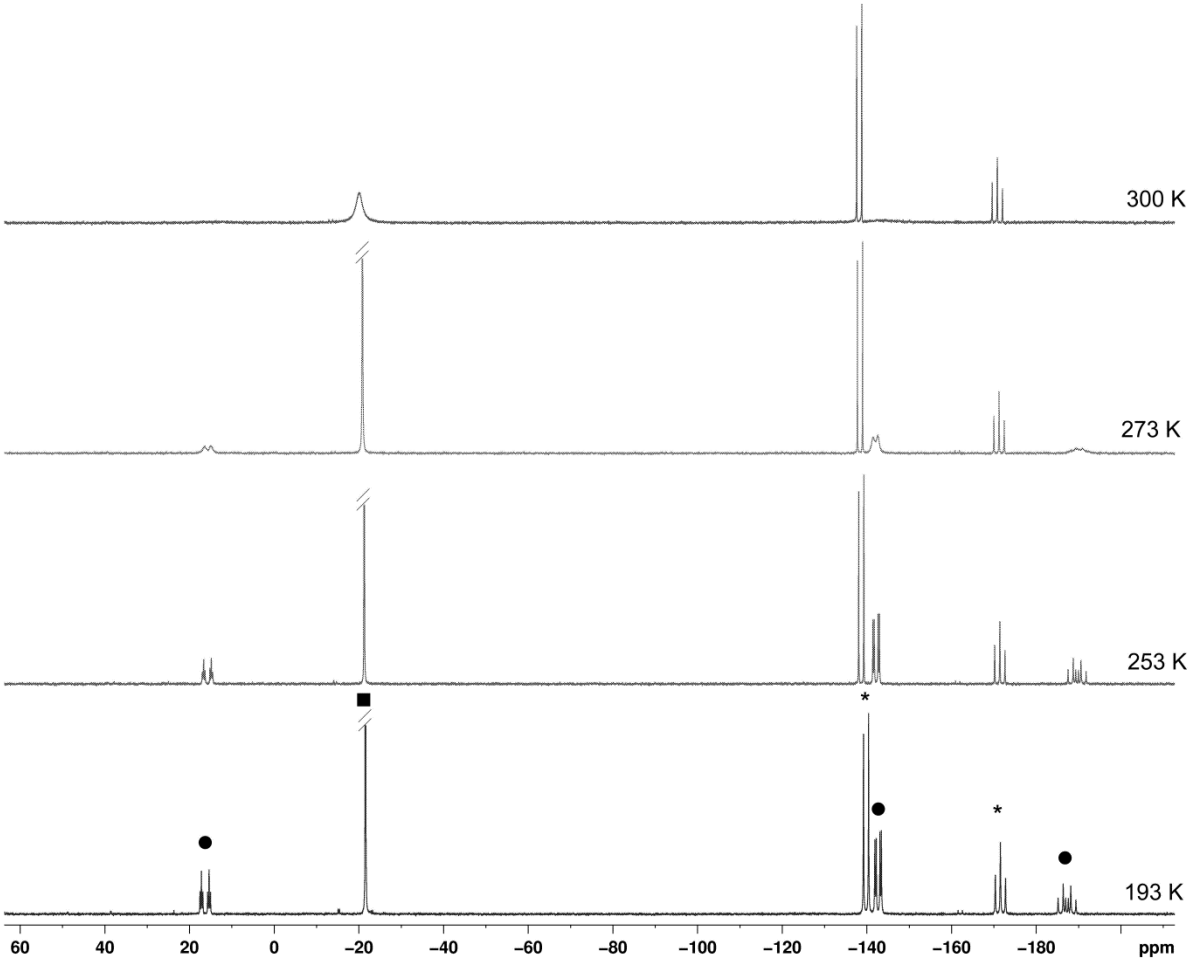

Figure S7. ^{31}P NMR spectrum (161.97 MHz, THF-d_8) at different temperatures of the reaction of **1** with 3 equivalents of $LiPPh_2$. **A** (labeling according to the manuscript) is marked with ●. $LiPPh_2$ is marked with ■. Impurities are marked with *.

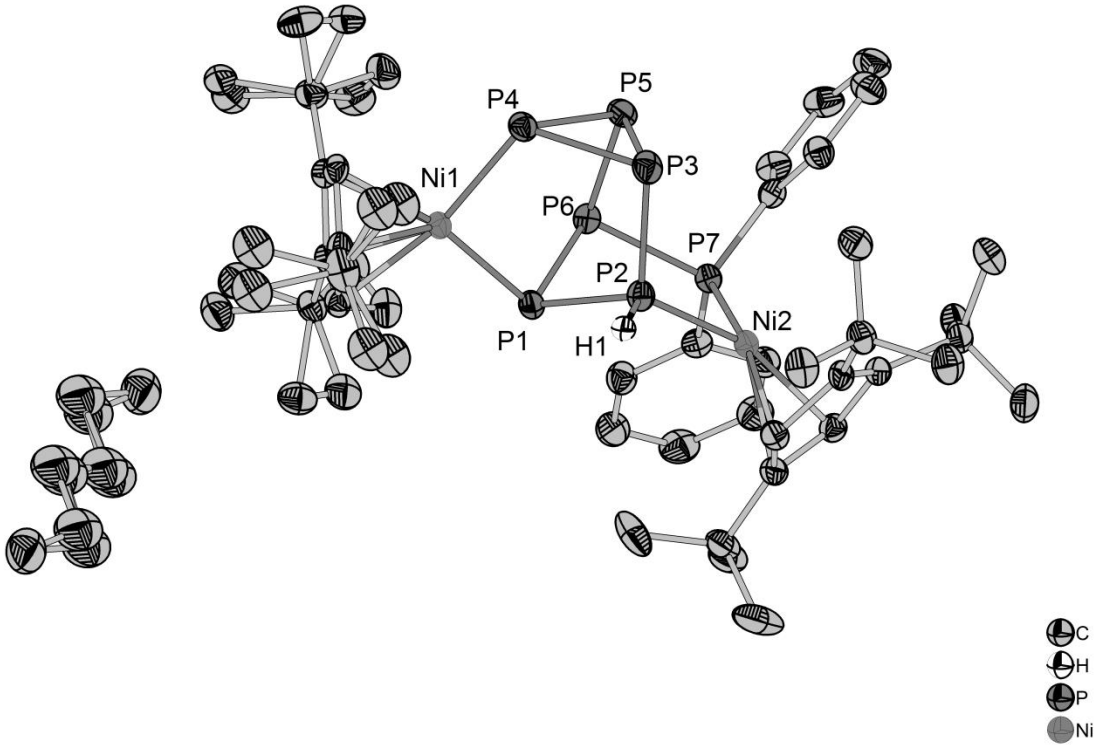

Figure S8. Molecular structure of [**6**]·0.5C_5H_{12}. H atoms bonded to carbon are omitted for clarity. Selected bond lengths [Å] and angles [°]: P1-Ni1 2.1711(5), P1-P2 2.1789(6), P1-P6 2.1840(6), P2-Ni2 2.1663(5), P2-P3 2.2003(6), P2-H1 1.26(2), P3-P4 2.2012(6), P3-P5 2.2154(6), P4-Ni1 2.1864(5), P4-P5 2.2199(6), P5-P6 2.2241(6), P6-P7 2.2244(6), P7-Ni2 2.1759(5), P2-P1-P6 88.61(2), P1-P2-P3 105.67(2), P2-P3-P4 100.28(2), P2-P3-P5 96.44(2), P4-P3-P5 60.348(19), P3-P4-P5 60.14(2), P3-P5-P4 59.51(2), P3-P5-P6 104.78(2), P4-P5-P6 96.99(2), P1-P6-P5 103.94(2), P1-P6-P7 98.36(2), P5-P6-P7 99.42(2).

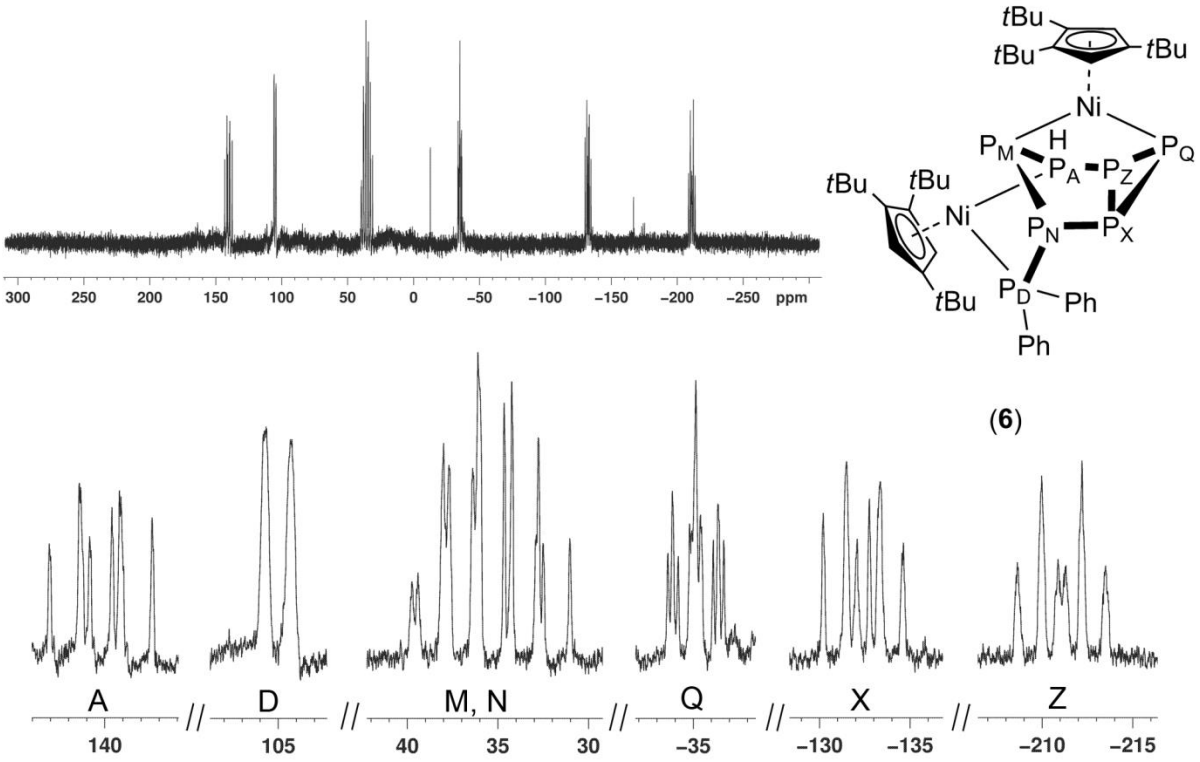

Figure S9. ^{31}P NMR (161.97 MHz, THF-d_8) spectrum of **6** after column chromatography.

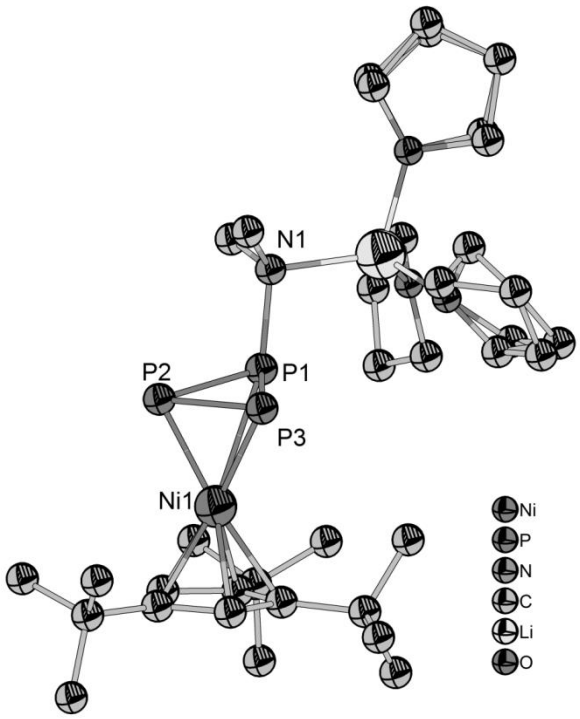

Figure S10. Molecular structure of $[Li(thf)_3][\mathbf{7}]$. H atoms bonded to carbon are omitted for clarity. Selected bond lengths [Å] and angles [°]: P1-N1 1.820(1), P1-P3 2.1736(6), P1-P2 2.1940(5), P2-P3 2.1337(7), Ni1-P1-P3 108.18(5), Ni1-P1-P2 108.65(4) P3-P1-P2 58.48(2), P2-P3-P1 61.24(2), P2-P3-Ni1 61.18(2), P1-P3-Ni1 81.51(2), P3-P2-P1 60.28(2).

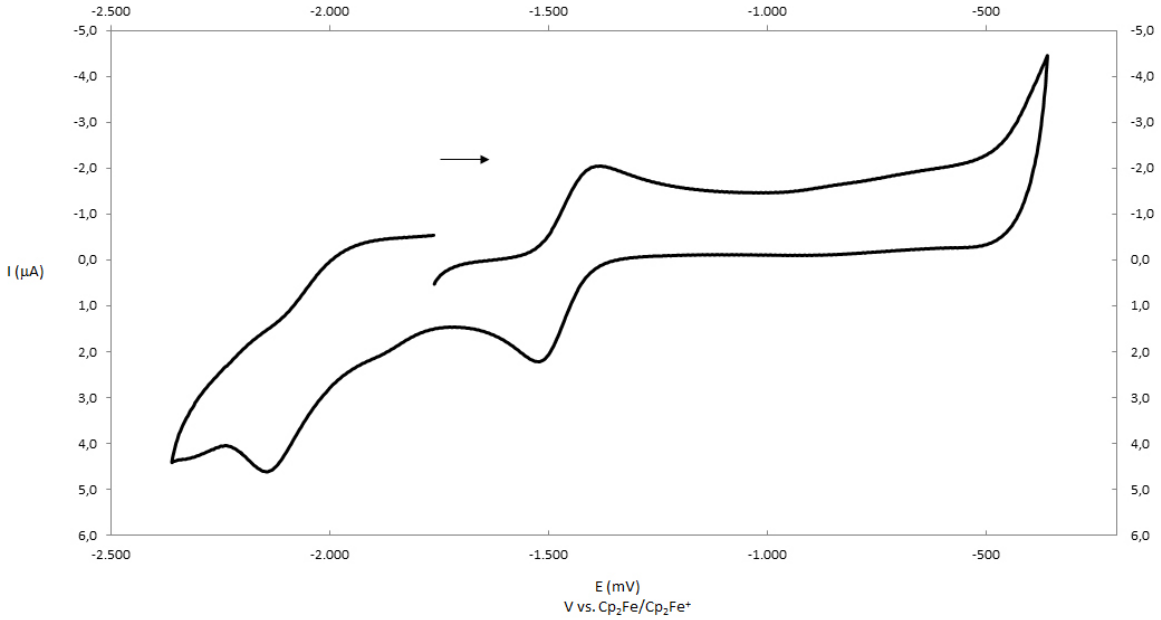

Figure S11. Cyclic voltammogram of [Na][**3**] recorded at a platinum disc electrode in MeCN at 100 mV/s and referenced against fc/fc^+; supporting electrolyte $[Bu_4N][PF_6]$ (0.1 mol/L).

7.2.3 Details on X-ray structure determinations

The diffraction data were collected on a Gemini R-Ultra or SuperNova CCD diffractometers (Agilent Technologies) with CuK_α radiation (λ = 1.54178 Å) using ω scans of 0.5 or 1° frames at 123 K. The structures $[(Cp'''Ni)_2P_3]$ and $[Na(dme)_3][(Cp'''Ni)_2P_3]\cdot$dme were solved by direct methods with SIR-97[3] and $[(Cp'''Ni)_2P_7Ph_2H]\cdot0.5C_5H_{12}$, $[K_2(18\text{-K-}6)_2(dme)][(Cp'''Ni)_2P_8]$ and $[Li(thf)_3][(Cp'''Ni)P_3NMe_2]$ with SHELXS[4] programs and refined by full-matrix least-squares method against $|F|^2$ in anisotropic approximation using SHELXTL or its multiprocessor version SHELX2013[5]. Absorption corrections were applied analytically using *CrysAlis PRO* Software (Table S1). All non-hydrogen atoms were refined in anisotropic approximation if their occupancy factors were > 0.5. Hydrogen atoms were refined in calculated positions using riding on pivot atom model. Pictures were made using Diamond 3.0.[5]

In $[(Cp'''Ni)_2P_7Ph_2H]\cdot0.5C_5H_{12}$ the t-Bu groups of one of the Cp''' ligand are disordered over two close positions by rotation about C-C$(CH_3)_3$ bond. The occupancies for all t-Bu groups were refined to give 0.53/0.47 ratio. During the refinement the atomic displacement parameters of one t-Bu group (containing C11, C12 and C13 atoms) had to be equated. The hydrogen atom of PH group was located from difference Fourier map and refined unconstrained. The solvent pentane molecule is disordered over the centre of symmetry so that the terminal positions of 6-atomic chain are half-occupied.

The crystal of $[K_2(18\text{-crown-}6)_2(dme)][(Cp'''Ni)_2P_8]\cdot0.2C_6H_{14}$ proved to be an inversion twin with the twin law (0 1 0/ 1 0 0/ 0 0 -1) and twin batches refined to 0.86(3)/0.14(3). The 18-crown-6 molecule belonging to $[K(18\text{-crown-}6)]^+$ cation and dme molecule coordinated to the outer-sphere cation $[K(18\text{-crown-}6)(dme)]^+$ are both disordered over a mirror plane giving two very close positions. For this reason some bond C-O and C-C distances of these molecules were restrained. The displacement parameters of two oxygen atoms and of all carbon atoms had to be treated with ISOR instruction in SHELX. The disordered solvent hexane molecule was refined in isotropic approximation and equated C-C distances due to its low molecular occupancy refined to 0.2.

In $[Li(thf)_3][(Cp'''Ni)P_3NMe_2]$ two of three THF molecules coordinated to lithium cation are disordered over two close positions. The refined molecular occupancies gave 0.43/0.57 and 0.34/0.66 ratios for the two molecules.

CCDC-### (compound…), -### (compound…), -### (compound ...) contain the supplementary crystallographic data for this publication. These data can be obtained free of charge at www.ccdc.cam.ac.uk/conts/retrieving.html (or from the Cambridge Crystallographic Data Centre, 12 Union Road, Cambridge CB2 1EZ, UK; Fax: + 44-1223-336-033; e-mail: deposit@ccdc.cam.ac.uk).

Table S3. Crystal data, data collection parameters and convergence results for K_2[**2**] and Na[**3**].

	$[K_2(18\text{-K-}6)_2(dme)]$[**2**]	$[Na(dme)_3]$[**3**]·dme
Crystal data		
Chemical formula	$C_{34}H_{58}Ni_2P_8^{2+}\cdot C_{16}H_{34}KO_8^{+}\cdot C_{12}H_{24}KO_6^{+}\cdot 0.2(C_6H_{14})$	$C_{34}H_{58}Ni_2P_3\cdot C_{12}H_{30}NaO_6\cdot C_4H_{10}O_2$
M_r	1546.16	1060.56
Crystal system, space group	Orthorhombic, $Cmc2_1$	Monoclinic, $P2_1/n$
Temperature (K)	123	123
a, b, c (Å)	23.6894(2), 26.0606(3), 14.7930(1)	13.1897(1), 17.5307(2), 26.0891(3)
α, β, γ (°)	90, 90, 90	90, 102.612(1), 90
V (Å^3)	9132.61 (14)	5886.89 (11)
Z	4	4
D_x (Mg m^{-3})	1.125	1.197
F(000)	3296	2296
Radiation type	Cu $K\alpha$	Cu $K\alpha$
μ (mm^{-1})	3.04	1.99
Crystal shape and colour	Black lath	Orange block
Crystal size (mm)	0.43 × 0.11 × 0.09	0.33 × 0.25 × 0.19
Data collection		
Diffractometer	Xcalibur, AtlasS2, Gemini ultra diffractometer	Xcalibur, Ruby, Gemini ultra diffractometer
Absorption correction	Gaussian	Analytical
T_{min}, T_{max}	0.422, 0.796	0.663, 0.763
No. of measured, independent and observed [> 2σ(I)] reflections	45392, 8156, 7532	19876, 10067, 8690
R_{int}	0.033	0.020
$(\sin\theta/\lambda)_{max}$ (Å^{-1})	0.596	0.595
Range of h, k, l	h = -27→28, k = -30→31, l = -17→17	h = -14→15, k = -20→14, l = -30→28
Refinement		
$R[F^2 > 2\sigma(F^2)]$, $wR(F^2)$, S	0.061, 0.191, 1.15	0.031, 0.083, 1.04
No. of reflections	8156	10067
No. of parameters	651	603
No. of restraints	321	0
H-atom treatment	H-atom parameters constrained	H-atom parameters constrained
$\Delta\rangle_{max}$, $\Delta\rangle_{min}$ (e Å^{-3})	0.83, -0.36	0.51, -0.28
Weighting scheme	$w=1/[\sigma^2(F_o^2)+(0.1428P)^2+1.0137P]$, where $P=(F_o^2+2F_c^2)/3$	$w=1/[\sigma^2(F_o^2)+(0.0398P)^2+1.6661P]$, where $P=(F_o^2+2F_c^2)/3$

Table S4. Crystal data, data collection parameters and convergence results for **4** and **6**.

	[**4**]	[**6**]·0.5C_5H_{12}
Crystal data		
Chemical formula	$C_{34}H_{58}Ni_2P_3$	$C_{46}H_{69}Ni_2P_7$·0.5(C_5H_{12})
M_r	677.09	992.29
Crystal system, space group	Triclinic, $P\bar{1}$	Triclinic, $P\bar{1}$
Temperature (K)	123	123
a, b, c (Å)	12.2126(2), 12.8731(2), 13.3174(2)	10.0939(3), 15.4520(4), 18.0030(4)
α, β, γ (°)	66.991(1), 71.635(1), 71.454(1)	71.553(2), 78.517(2), 73.418(2)
V (Å^3)	1782.86 (5)	2534.55 (11)
Z	2	2
D_x (Mg m^{-3})	1.261	1.300
F(000)	726	1054
Radiation type	Cu $K\alpha$	Cu $K\alpha$
μ (mm^{-1})	2.72	3.24
Crystal shape and colour	Brown block	Dark red needle
Crystal size (mm)	0.32 × 0.22 × 0.12	0.23 × 0.08 × 0.03
Data collection		
Diffractometer	Xcalibur, Ruby, Gemini ultra diffractometer	SuperNova, Single source at offset, Atlas diffractometer
Absorption correction	Analytical	Gaussian
T_{min}, T_{max}	0.613, 0.810	0.656, 0.931
No. of measured, independent and observed [> 2σ(I)] reflections	20865, 6283, 5718	21191, 9861, 7642
R_{int}	0.022	0.028
$(\sin\theta/\lambda)_{max}$ (Å^{-1})	0.595	0.624
Range of h, k, l	h = -14→13, k = -14→15, l = -14→15	h = -10→12, k = -19→18, l = -22→22
Refinement		
$R[F^2 > 2\sigma(F^2)]$, $wR(F^2)$, S	0.025, 0.068, 0.87	0.029, 0.071, 0.91
No. of reflections	6283	9861
No. of parameters	370	607
No. of restraints	0	414
H-atom treatment	H-atom parameters constrained	H atoms treated by a mixture of independent and constrained refinement
$\Delta\rangle_{max}$, $\Delta\rangle_{min}$ (e Å^{-3})	0.27, -0.30	0.61, -0.33
Weighting scheme	w=1/[$\sigma^2(F_o^2)$+(0.0521P)^2+0.5009P], where P=(F_o^2+2F_c^2)/3	w=1/[$\sigma^2(F_o^2)$+(0.0440P)^2], where P=(F_o^2+2F_c^2)/3

Table S5. Crystal data, data collection parameters and convergence results for **7**.

	[Li(thf)$_3$][**7**]
Crystal data	
Chemical formula	$C_{19}H_{35}NNiP_3 \cdot LiC_{12}H_{24}O_3$
M_r	652.35
Crystal system, space group	Orthorhombic, *Pbca*
Temperature (K)	123
a, *b*, *c* (Å)	16.7710 (2), 17.6947 (2), 24.3284 (2)
α, β, γ (°)	90, 90, 90
V (Å^3)	7219.64 (13)
Z	8
D_x (Mg m^{-3})	1.200
F(000)	2816
Radiation type	Cu $K\alpha$
μ (mm^{-1})	2.25
Crystal shape and colour	Light brown plate
Crystal size (mm)	0.74 × 0.33 × 0.05
Data collection	
Diffractometer	Xcalibur, Ruby, Gemini ultra diffractometer
Absorption correction	Analytical
T_{min}, T_{max}	0.471, 0.897
No. of measured, independent and observed [> 2σ(I)] reflections	23126, 6320, 5258
R_{int}	0.029
$(\sin \theta/\lambda)_{max}$ (Å^{-1})	0.595
Range of *h*, *k*, *l*	h = -19→18, k = -15→21, l = -28→20
Refinement	
$R[F^2 > 2\sigma(F^2)]$, $wR(F^2)$, S	0.030, 0.081, 1.03
No. of reflections	6320
No. of parameters	411
No. of restraints	0
H-atom treatment	H-atom parameters constrained
$\Delta\rangle_{max}$, $\Delta\rangle_{min}$ (e Å^{-3})	0.34, -0.29
Weighting scheme	$w = 1/[\sigma^2(F_o^2) + (0.0522P)^2]$ where $P = (F_o^2 + 2F_c^2)/3$

Computer programs: *CrysAlis PRO*, Agilent Technologies, Version 1.171.37.31d (release 11-02-2014 CrysAlis171 .NET) (compiled Feb 11 2014, 18:09:27), *SHELXL2014* (Sheldrick, 2014).

Table S6. Selected geometric parameters (Å, º) for [K_2(18-K-6)$_2$(dme)][**2**]

Ni1—C15	2.126 (8)	C12—C13	1.455 (13)
Ni1—C12	2.145 (8)	C13—C14	1.460 (11)
Ni1—C14	2.171 (8)	C13—C131	1.48 (2)
Ni1—C11	2.177 (8)	C13—C135	1.65 (2)
Ni1—C13	2.184 (9)	C14—C15	1.433 (12)
Ni1—P2	2.211 (2)	C14—C141	1.530 (12)
Ni1—P5	2.216 (2)	C111—C112	1.517 (12)
P1—P2	2.191 (3)	C111—C114	1.520 (15)
P1—P5	2.206 (3)	C111—C113	1.557 (12)
P1—P1^{i}	2.243 (4)	C131—C132	1.52 (3)
P2—P3	2.200 (2)	C131—C133	1.57 (3)
P3—P2^{i}	2.200 (2)	C131—C134	1.58 (2)
P3—P4	2.212 (3)	C135—C136	1.54 (3)
P4—P5	2.210 (2)	C135—C138	1.57 (3)
P4—P5^{i}	2.211 (2)	C135—C137	1.60 (3)
C11—C12	1.384 (11)	C141—C144	1.515 (14)
C11—C15	1.391 (10)	C141—C142	1.546 (15)
C11—C111	1.517 (12)	C141—C143	1.581 (14)

P2—P1—P5	84.87 (9)	P5—P4—P3	99.64 (10)
P2—P1—P1^{i}	103.93 (7)	P5^{i}—P4—P3	99.64 (10)
P5—P1—P1^{i}	104.35 (8)	P1—P5—P4	98.06 (10)
P1—P2—P3	98.46 (10)	P1—P2—Ni1	85.26 (9)
P2^{i}—P3—P2	97.12 (14)	P3—P2—Ni1	102.70 (9)
P2^{i}—P3—P4	100.09 (10)	P1—P5—Ni1	84.76 (9)
P2—P3—P4	100.09 (10)	P4—P5—Ni1	102.77 (10)
P5—P4—P5^{i}	98.02 (15)		

Table S7. Selected geometric parameters (Å, º) for [Na(dme)$_3$][**3**]·dme

Ni1—P1	2.2621 (5)	O8—C55	1.408 (2)
Ni1—P2	2.2508 (5)	C1—C2	1.415 (2)
Ni1—P3	2.2807 (5)	C1—C5	1.432 (2)
Ni1—C1	2.1548 (15)	C2—C6	1.519 (2)
Ni1—C2	2.1678 (16)	C2—C3	1.414 (2)
Ni1—C3	2.1424 (16)	C3—C4	1.434 (2)
Ni1—C4	2.1574 (16)	C4—C5	1.461 (2)
Ni1—C5	2.1802 (15)	C4—C10	1.538 (2)
Ni2—P1	2.2584 (5)	C5—C17	1.538 (2)

Ni2—P2	2.2519 (5)	C6—C7	1.541 (3)
Ni2—P3	2.2875 (5)	C6—C8	1.534 (3)
Ni2—C20	2.1536 (15)	C6—C9	1.530 (3)
Ni2—C21	2.1774 (15)	C10—C13	1.538 (3)
Ni2—C22	2.1578 (16)	C10—C12	1.544 (3)
Ni2—C23	2.1522 (15)	C10—C14	1.532 (3)
Ni2—C25	2.1775 (15)	C16—C17	1.539 (3)
P1—P2	2.2408 (7)	C17—C18	1.536 (3)
P1—P3	2.1950 (7)	C17—C19	1.537 (3)
P2—P3	2.2094 (6)	C20—C21	1.433 (2)
Na1—O3	2.3684 (16)	C20—C25	1.416 (2)
Na1—O4	2.3405 (14)	C21—C22	1.452 (2)
Na1—O5	2.4164 (15)	C21—C26	1.543 (2)
Na1—O6	2.3631 (14)	C22—C23	1.430 (2)
Na1—O1	2.4135 (15)	C22—C30	1.544 (2)
Na1—O2	2.3438 (16)	C23—C25	1.419 (2)
O1—C40	1.419 (3)	C25—C34	1.518 (2)
O1—C41	1.429 (2)	C26—C28	1.537 (3)
O2—C42	1.422 (3)	C26—C27	1.543 (3)
O2—C43	1.425 (3)	C26—C29	1.539 (3)
O3—C45	1.422 (2)	C30—C33	1.536 (3)
O3—C44	1.428 (3)	C30—C31	1.528 (3)
O4—C46	1.426 (2)	C30—C32	1.543 (3)
O4—C47	1.431 (3)	C34—C37	1.534 (3)
O5—C49	1.425 (2)	C34—C39	1.538 (3)
O5—C48	1.432 (3)	C34—C38	1.529 (2)
O6—C51	1.424 (2)	C41—C42	1.491 (3)
O6—C50	1.427 (2)	C45—C46	1.498 (3)
O7—C53	1.411 (2)	C49—C50	1.494 (3)
O7—C52	1.417 (2)	C53—C54	1.504 (3)
O8—C54	1.417 (2)		

P1—Ni1—P2	59.54 (2)	Ni1—P2—Ni2	112.23 (2)
P1—Ni1—P3	57.79 (2)	Ni1—P2—P1	60.48 (2)
P2—Ni1—P3	58.36 (2)	Ni1—P2—P3	61.50 (2)
P1—Ni2—P2	59.58 (2)	Ni2—P2—P1	60.35 (2)
P1—Ni2—P3	57.74 (2)	Ni2—P2—P3	61.69 (2)
P2—Ni2—P3	58.24 (2)	P1—P2—P3	59.10 (2)
Ni1—P1—Ni2	111.57 (2)	Ni1—P3—Ni2	109.83 (2)
Ni1—P1—P2	59.98 (2)	Ni1—P3—P1	60.68 (2)
Ni1—P1—P3	61.53 (2)	Ni1—P3—P2	60.15 (2)

Ni2—P1—P2	60.07 (2)	Ni2—P3—P1	60.46 (2)
Ni2—P1—P3	61.80 (2)	Ni2—P3—P2	60.07 (2)
P2—P1—P3	59.74 (2)	P1—P3—P2	61.16 (2)

Table S8. Selected geometric parameters (Å, º) for **4**

Ni1—P1	2.2077 (4)	C6—C7	1.528 (2)
Ni1—P2	2.2086 (4)	C6—C8	1.531 (2)
Ni1—P3	2.3778 (4)	C6—C9	1.535 (2)
Ni1—C1	2.1204 (13)	C10—C11	1.538 (2)
Ni1—C2	2.1152 (12)	C10—C12	1.536 (2)
Ni1—C3	2.1573 (13)	C10—C13	1.539 (2)
Ni1—C4	2.1317 (14)	C14—C15	1.540 (2)
Ni1—C5	2.1108 (14)	C14—C16	1.529 (2)
Ni2—P1	2.2019 (4)	C14—C17	1.538 (2)
Ni2—P2	2.2113 (4)	C18—C19	1.421 (2)
Ni2—P3	2.3898 (5)	C18—C22	1.4247 (19)
Ni2—C18	2.1229 (14)	C18—C23	1.517 (2)
Ni2—C19	2.1096 (14)	C19—C20	1.4284 (19)
Ni2—C20	2.1360 (13)	C20—C21	1.466 (2)
Ni2—C21	2.1553 (12)	C20—C31	1.535 (2)
Ni2—C22	2.1241 (13)	C21—C22	1.421 (2)
P1—P2	2.3976 (6)	C21—C27	1.5442 (19)
P1—P3	2.1851 (6)	C23—C24	1.531 (2)
P2—P3	2.1817 (5)	C23—C25	1.525 (2)
C1—C2	1.426 (2)	C23—C26	1.537 (2)
C1—C5	1.4201 (19)	C27—C28	1.538 (2)
C1—C6	1.517 (2)	C27—C29	1.537 (2)
C2—C3	1.421 (2)	C27—C30	1.542 (2)
C3—C4	1.465 (2)	C31—C32	1.538 (2)
C3—C10	1.542 (2)	C31—C33	1.528 (2)
C4—C5	1.429 (2)	C31—C34	1.540 (2)
C4—C14	1.540 (2)		

Ni1—P1—Ni2	112.16 (2)	Ni2—P2—P1	56.90 (1)
Ni1—P1—P2	57.14 (1)	Ni2—P2—P3	65.91 (2)
Ni1—P1—P3	65.54 (2)	P1—P2—P3	56.77 (2)
Ni2—P1—P2	57.28 (1)	Ni1—P3—Ni2	100.26 (2)
Ni2—P1—P3	66.01 (2)	Ni1—P3—P1	57.69 (1)
P2—P1—P3	56.63 (2)	Ni1—P3—P2	57.75 (1)

Ni1—P2—Ni2	111.76 (2)	Ni2—P3—P1	57.33 (1)
Ni1—P2—P1	57.10 (1)	Ni2—P3—P2	57.64 (1)
Ni1—P2—P3	65.58 (2)	P1—P3—P2	66.60 (2)

Table S9. Selected geometric parameters (Å, º) for [**6**]·0.5C_5H_{12}

C1—C5	1.437 (2)	C22—C31	1.543 (2)
C1—C2	1.454 (2)	C22—Ni2	2.2112 (16)
C1—C6	1.538 (2)	C23—C25	1.523 (3)
C1—Ni1	2.1576 (15)	C23—C26	1.529 (2)
C2—C3	1.397 (2)	C23—C24	1.533 (3)
C2—Ni1	2.1023 (16)	C27—C29	1.537 (3)
C3—C4	1.415 (2)	C27—C30	1.542 (2)
C3—C10	1.515 (2)	C27—C28	1.545 (2)
C3—Ni1	2.1407 (16)	C31—C33	1.534 (2)
C4—C5	1.443 (2)	C31—C34	1.541 (2)
C4—Ni1	2.0724 (16)	C31—C32	1.544 (2)
C5—C14	1.540 (2)	C35—C40	1.391 (2)
C5—Ni1	2.1569 (15)	C35—C36	1.400 (2)
C6—C7A	1.485 (4)	C35—P7	1.8322 (16)
C6—C9B	1.492 (4)	C36—C37	1.390 (2)
C6—C8B	1.535 (4)	C37—C38	1.389 (3)
C6—C7B	1.569 (4)	C38—C39	1.384 (3)
C6—C8A	1.572 (4)	C39—C40	1.387 (2)
C6—C9A	1.573 (5)	C41—C46	1.390 (2)
C10—C13B	1.411 (6)	C41—C42	1.395 (2)
C10—C11A	1.455 (5)	C41—P7	1.8266 (16)
C10—C12A	1.575 (5)	C42—C43	1.383 (2)
C10—C11B	1.597 (6)	C43—C44	1.385 (3)
C10—C12B	1.598 (5)	C44—C45	1.383 (3)
C10—C13A	1.611 (5)	C45—C46	1.387 (3)
C15A—C14	1.502 (4)	P1—Ni1	2.1711 (5)
C16A—C14	1.606 (4)	P1—P2	2.1789 (6)
C17A—C14	1.526 (5)	P1—P6	2.1840 (6)
C15B—C14	1.611 (5)	P2—Ni2	2.1663 (5)
C16B—C14	1.477 (4)	P2—P3	2.2003 (6)
C17B—C14	1.523 (6)	P3—P4	2.2012 (6)
C18—C19	1.406 (2)	P3—P5	2.2154 (6)
C18—C22	1.465 (2)	P4—Ni1	2.1864 (5)
C18—Ni2	2.0941 (16)	P4—P5	2.2199 (6)
C19—C20	1.414 (2)	P5—P6	2.2241 (6)

C19—C23	1.527 (2)	P6—P7	2.2244 (6)
C19—Ni2	2.1337 (15)	P7—Ni2	2.1759 (5)
C20—C21	1.469 (2)	C47—C47A	1.504 (7)
C20—Ni2	2.0591 (15)	C47—C48	1.562 (10)
C21—C22	1.417 (2)	C48—C49	1.598 (10)
C21—C27	1.535 (2)	C47A—C48A	1.458 (10)
C21—Ni2	2.1893 (15)	P2—H1	1.26 (2)

Ni1—P1—P2	108.20 (2)	P3—P4—P5	60.14 (2)
Ni1—P1—P6	98.724 (19)	P3—P5—P4	59.51 (2)
P2—P1—P6	88.61 (2)	P3—P5—P6	104.78 (2)
Ni2—P2—P1	110.83 (2)	P4—P5—P6	96.99 (2)
Ni2—P2—P3	116.77 (2)	P1—P6—P5	103.94 (2)
P1—P2—P3	105.67 (2)	P1—P6—P7	98.36 (2)
P2—P3—P4	100.28 (2)	P5—P6—P7	99.42 (2)
P2—P3—P5	96.44 (2)	Ni2—P7—P6	113.34 (2)
P4—P3—P5	60.348 (19)	P1—Ni1—P4	95.686 (18)
Ni1—P4—P3	114.46 (2)	P2—Ni2—P7	89.418 (18)
Ni1—P4—P5	111.65 (2)		

Table S10. Selected geometric parameters (Å, º) for $[Li(thf)_3]$[**7**]

Ni1—C3	2.0813 (14)	C1—C5	1.449 (2)
Ni1—C1	2.1130 (14)	C2—C3	1.424 (2)
Ni1—C5	2.1292 (14)	C2—C6	1.519 (2)
Ni1—C2	2.1323 (14)	C3—C4	1.430 (2)
Ni1—C4	2.1478 (14)	C4—C5	1.443 (2)
Ni1—P3	2.1979 (5)	C4—C10	1.542 (2)
Ni1—P2	2.2049 (5)	C5—C14	1.545 (2)
P1—N1	1.8196 (13)	C6—C7	1.530 (2)
P1—P3	2.1736 (6)	C6—C8	1.531 (2)
P1—P2	2.1940 (5)	C6—C9	1.533 (2)
P1—Li1	3.036 (3)	C10—C13	1.531 (2)
P3—P2	2.1337 (7)	C10—C11	1.537 (2)
N1—C26	1.464 (2)	C10—C12	1.538 (2)
N1—C27	1.469 (2)	C14—C16	1.535 (2)
N1—Li1	2.066 (3)	C14—C17	1.536 (3)
C1—C2	1.405 (2)	C14—C15	1.536 (2)
N1—P1—P3	108.18 (5)	C26—N1—C27	109.98 (14)
N1—P1—P2	108.65 (4)	C26—N1—P1	117.30 (10)
P3—P1—P2	58.48 (2)	C27—N1—P1	108.48 (11)
N1—P1—Li1	41.62 (6)	C26—N1—Li1	112.26 (13)
P3—P1—Li1	110.02 (5)	C27—N1—Li1	105.39 (12)
P2—P1—Li1	146.86 (5)	P1—N1—Li1	102.58 (9)
P2—P3—P1	61.24 (2)	C2—C1—C5	110.40 (12)
P2—P3—Ni1	61.178 (18)	C2—C1—Ni1	71.42 (8)
P1—P3—Ni1	81.510 (18)	C5—C1—Ni1	70.63 (8)
P3—P2—P1	60.28 (2)	C1—C2—C3	105.61 (12)
P3—P2—Ni1	60.847 (18)	C1—C2—C6	127.09 (12)
P1—P2—Ni1	80.896 (18)		

Symmetry code(s): (i) -*x*+1, *y*, *z*.

7.2.4 Details of DFT calculations.

All DFT calculations have been performed with the TURBOMOLE program package[7] at the RI[8]-BP86[9]/def2-TZVP[10] level of theory, followed by single point calculations without the RI approximation. For the determination of relative energies, single point calculation have been performed on the geometries optimized in the gas phase, in which the solvent effects were incorporated via the Conductor-like Screening Model (COSMO),[11] using THF ($\varepsilon = 7.580$) as solvent. The Multipole Accelerated Resolution of Identity (MARI-J)[12] approximation was used in the geometry optimization steps. The Natural Population Analysis (NPA) has been performed on the gas phase optimized geometries. The energy of some occupied molecular orbitals in **2** were positive, however incorporation of the solvent effects via the COSMO formalism leads to negative energies of all occupied MOs. The NPA analysis for **2** has been performed on the wave function corrected by solvent effects, but do not shows noticeable differences compared to the results of the NPA analysis of the non-corrected wave function.

Table S11. Reaction energies for selected transformations calculated at the BP86/def2-TZVP level of theory.

Transformation	Reaction Energy (kJ/mol)
[Cp'''Ni(η^3-P_3)] + Ph_2P^- = [Cp'''Ni(η^2-P_3PPh_2)]$^-$	−39.23
[Cp'''Ni(η^2-P_3PPh_2)]$^-$ + [Cp'''Ni(η^3-P_3)] = [(Cp'''Ni)$_2$(P_6PPh_2)]$^-$	−44.95
2 [Cp'''Ni(η^3-P_3)] + Ph_2P^- = [(Cp'''Ni)$_2$(P_6PPh_2)]$^-$	−84.18

Table S12. Mulliken spin distribution in [(Cp'''Ni)$_2$(μ,$\eta^{3:3}$-P_3)] (**4**) calculated at the BP86/def2-TZVP level of theory.

Atom	Spin density
1ni	0.27
2ni	0.27
3p	0.06
4p	0.06
5p	-0.06
6c	0.09
7c	0.02
8c	0.02
9c	0.08
10c	-0.02
23c	0.09
24c	-0.02
25c	0.08
26c	0.02
27c	0.02

Tables regarding the cartesian coordinates of all performed calculations can be found on the DVD-Rom, which is attached in the back of this work.

7.2.5 References

[1] a) O. J. Scherer, T. Dave, J. Braun, G. Wolmershäuser, *J. Organomet. Chem.* **1988**, *350*, C20-C24; b) Miriam D. Eberl, Dissertation, *University of Regensburg* **2011**.

[2] D. F. Evans, *J. Chem. Soc*. **1959**, 2003-2005.

[3] A. Altomare, M. C. Burla, M. Camalli, G. L. Cascarano, A. G. C. Giacovazzo, A. G. G. Moliterni, G. Polidori, R. Spagna, *J. Appl. Cryst*. **1999**, *32*, 115-119.

[4] Bruker, in *SHELXTL. Version 6.22*. (Ed.: W. Bruker AXS Inc. Madison, USA), **2003**.

[5] G. Scheldrick, *Acta Cryst. ser. A.* **2008**, *64*, 112-122.

[6] Diamond, Crystal and Molecular Structure Visualization Crystal Impact, Dr. H. Putz & Dr. K. Brandenburg GbR, Kreuzherrenstr. 102, 53227 Bonn, Germany. http://www.crystalimpact.com/diamond

[7] a) F. Furche, R. Ahlrichs, C. Hättig, W. Klopper, M. Sierka, F. Weigend, *WIREs Comput. Mol. Sci.* **2014**, *4*, 91-100. b) R. Ahlrichs, M. Bär, M. Häser, H. Horn, C. Kölmel, *Chem. Phys. Lett.***1989**, *162*, 165–169; c) O. Treutler, R. Ahlrichs, *J. Chem. Phys.***1995**, *102*, 346–354.

[8] a) K. Eichkorn, O. Treutler, H. Oehm, M. Häser, R. Ahlrichs, *Chem. Phys. Lett.***1995**, *242*, 652–660; b) K. Eichkorn, F. Weigend, O. Treutler, R. Ahlrichs, *Theor. Chem. Acc.***1997**, *97*, 119.

[9] a) P. A. M. Dirac, *Proc. Royal Soc. A*, 1929, **123**, 714-733. b) J. C. Slater, *Phys. Rev.***1951**, *81*, 385-390. c) S. H. Vosko, L. Wilk, M. Nusair, *Can. J. Phys.* **1980**, *58*, 1200-1211. d). A. D. Becke, *Phys. Rev. A*, 1988, **38**, 3098. e) J. P. Perdew, *Phys. Rev. B* **1986**, *33*, 8822-8824.

[10] a) F. Weigend, M. Häser, H. Patzelt, R. Ahlrichs, *Chem. Phys. Letters* **1998**, *294*, 143. b) F. Weigend, R. Ahlrichs, *Phys. Chem. Chem. Phys.* **2005**, *7*, 3297.

[11] A. Klamt, G. Schüürmann, *J. Chem. Soc. Perkin Trans.2*, **1993**, *5*, 799–805. b) A. Klamt, V. Jonas, *J. Chem. Phys.*, **1996**, *105*, 9972–9981.

[12] M. Sierka, A. Hogekamp, R. Ahlrichs, *J. Chem. Phys.***2003**, *118*, 9136.

7.3 Reactivity of $[(Cp'''Ni)_2(\mu,\eta^{3:3}\text{-}P_3)]^-$ towards MeI

The following NMR studies should be neglected for the publication of the previous chapter titled "Unexpected reactivity of [Cp'''Ni(η^3-P_3)] towards main group nucleophiles and by reduction". Therefore, this chapter is excluded and added at the end of the previous one.

First reactivity studies were performed with the anionic triple-decker complex $[(Cp'''Ni)_2(\mu,\eta^{3:3}\text{-}P_3)]^-$ (**3**) towards salt elimination. By adding an equimolar amount of MeI at room temperature to **3** an immediate color change from burgundy red to yellow-brown is observed. In the ^{31}P NMR spectrum the formation of a major product, with a singlet at 283.5 ppm, a minor product with a singlet at 68.2 ppm and a broad signal, ranging from 25 to −53 ppm are monitored. The peak at 283.5 ppm is identified as the compound $[(Cp'''Ni)_2(\mu,\eta^{2:2}\text{-}P_2)]$, which is already known and was characterized by F. Dielmann from our group.[1] In the EI mass spectrum of the raw reaction mixture a signal at m/z = 644.2 (10%) is determined for the compound $[(Cp'''Ni)_2(\mu,\eta^{2:2}\text{-}P_2)]$, along the peak for the starting material $[Cp'''Ni(\eta^3\text{-}P_3)]$ (384.0; 15 %). No other transition metal containing products are observed. Thus, during the salt elimination process one phosphorus atom is split off the *cyclo*-P_3 ring of **3**, which in return might form polyphosphorus compounds, indicated by the broad signal in the ^{31}P NMR spectrum. However, if the reaction is performed at lower temperature (213 K) no immediate color change is observed. By warming up the solution to ambient room temperature overnight, again a yellow-brown color occurs, but the compound $[(Cp'''Ni)_2(\mu,\eta^{2:2}\text{-}P_2)]$ has formed in less than 50 % yield, as monitored by ^{31}P{H} NMR spectroscopy. The main product $[(Cp'''Ni)_2(\mu,\eta^{3:3}\text{-}P_3Me]$ (**8**) consists of three doublet of doublets at 81.8, 65.9 and −91.3 ppm, each with an integral ratio of 1:1:1. By using an excess of MeI at low temperature the formation of **8** is achieved nearly exclusively (besides the formation of a small amount of **1**; Figure 2). The coupling constants obtained from the ^{31}P{H} NMR spectrum (Table 1) of **8** indicate that the *cyclo*-P_3 ring has been opened into an allylic P_3 unit. Otherwise the small coupling constant of 40.74 Hz, which is reasonable for a $^2J_{P\text{-}P}$ coupling, cannot be explained.

Table 1. Coupling constants and chemical shifts of the proposed compound **8**.

J (Hz)		δ (ppm)	
$^1J_{P_A\text{-}P_B}$	386.26	P_A	81.8
$^2J_{P_A\text{-}P_X}$	40.74	P_B	65.9
$^1J_{P_B\text{-}P_X}$	118.06	P_X	−91.3
$^2J_{P_X}$-H	12.06		

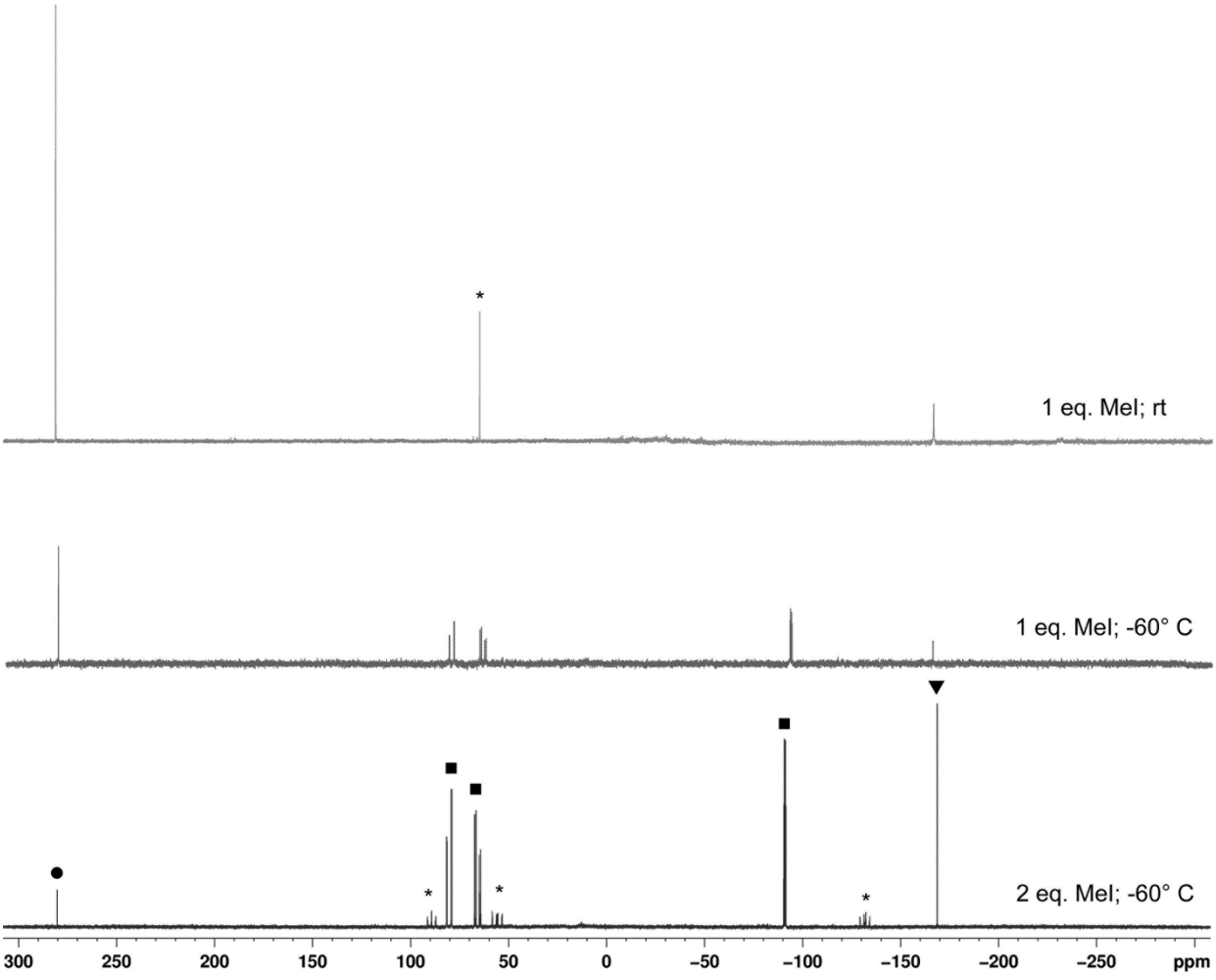

Figure 2. $^{31}P\{H\}$ NMR spectrum of the reaction mixture under different reaction conditions. Impurities are marked with *, compound $[(Cp'''Ni)_2(\mu,\eta^{2:2}\text{-}P_2)]$ is marked with ●, compound **8** is marked with ■ and **1** is marked with ▼.

Due to the occurrence of three signals in the ^{31}P NMR spectrum the methyl group has to be attached at the terminal position of the P_3 allylic chain. The ^{31}P NMR spectrum shows only for the P_X phosphorus atom (labeling according to Table 1) a P-H coupling, resulting in a doublet of doublet of quartets with a $^2J_{P\text{-}H}$ coupling of 12.06 Hz. In the ^1H NMR spectrum signals for two Cp'''-ligands are monitored, with six signals in total for each tert-butyl group. Based on these NMR studies the structural motif of the neutral and methylated triple-decker **8** can be suggested, exhibiting an allylic P_3 ligand, which bears a methyl group in terminal position and is coordinated by two Cp'''Ni fragments. Unfortunately no crystals of **8** for further analysis could be obtained.

Experimental Part:

Synthesis of $[(Cp'''Ni)_2(\mu,\eta^{3:3}\text{-}P_3Me)]$: To 70 mg of $[Na(thf)_2][(Cp'''Ni)_2(\mu,\eta^{3:3}\text{-}P_3)]$ (0.08 mmol) in THF (25 mL) 15 mL of MeI in Et_2O (0.16 mmol; 1.11 mol/L) are added at −80 °C. The solution is stirred and warmed up to ambient temperature overnight. ^{1}H NMR (400.13 MHz, C_6D_6): δ [ppm] = 1.38 (s, 9 H), 1.40 (s, 9 H), 1.43 (broad, 36 H), 5.05 (s, 2 H), 5.20 (s, 2 H). ^{31}P NMR (161.97 MHz, C_6D_6): δ = −91.01 (dd, 1 P), 65.78 (dd, 1 P), 80.31 (dd, 1 P).

References:

[1] Dielmann, Fabian Herbert. *Novel Phosphorus Rich Complexes And Their Use In Supramolecular Chemistry*. München: Verl. Dr. Hut, 2011. Print, 133.

8. Conclusion

First investigations of the reactivity of [Cp*Fe(η^5-P_5)] (**1**) towards nucleophiles were performed in the scope of my master thesis, by reacting **1** with $LiNMe_2$, $NaNH_2$ and KOH, respectively. In the reaction with $LiNMe_2$ the anionic compound [Cp*Fe(η^4-P_5NMe_2)]$^-$ (**2a**) was isolated. At the same time [Cp*Fe(η^4-$P_5CH_2SiMe_3$)]$^-$ (**2b**) was synthesized by the reaction of **1** with $LiCH_2SiMe_3$, by M. V. Butovskii from our group. If $NaNH_2$ is used instead, the trianionic, nitrogen bridged compound [{Cp*Fe(η^4-P_5)}$_2$N]$^{3-}$ (**3**) is formed by an autometalation process.

Within the thesis present two objectives were targeted. The first objective was to gain further insight into the reactivity of **1** towards different C, N and P donating nucleophiles, as well as the reactivity of the nucleophilic transformed anionic pentaphosphaferrocene derivatives towards electrophiles. The second part of this thesis is devoted to the reactivity of the complex [Cp'''Ni(η^3-P_3)] (**4**) towards reducing agents, as well as nucleophiles. Compound **4** was chosen because of the assumption, that the ring strain of the P_3 ligand might lead to a rearrangement of the P_3 unit and thus to the formation of larger, phosphorus containing complexes.

8.1 Reactivity of pentaphosphaferrocene towards nucleophiles

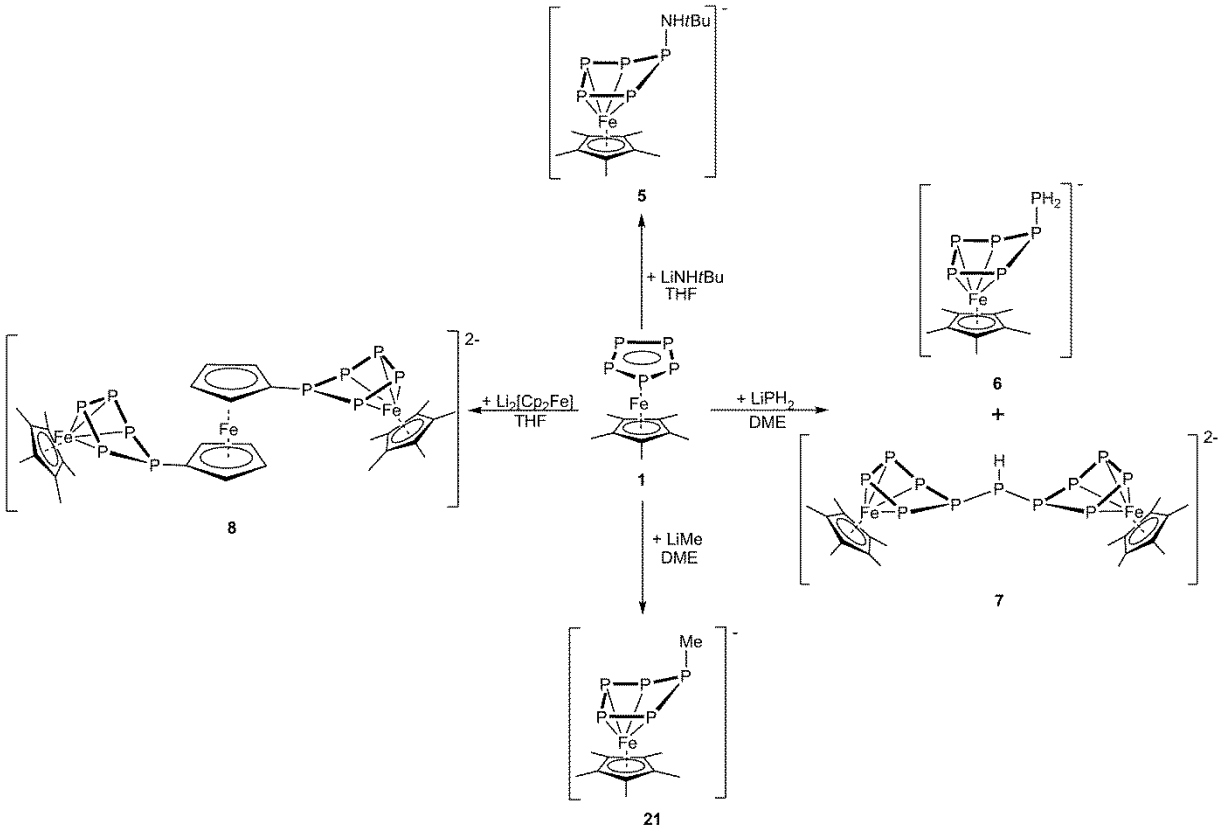

Scheme 1. Reactivity of **1** towards different nucleophiles.

In contrast to the reaction of **1** with $NaNH_2$, by using a primary amide, like LiNH*t*Bu, no autometalation occurs. The anionic compound $[Cp^*Fe(\eta^4\text{-}P_5NHtBu)]^-$ (**5**, Scheme 1) is formed instead, even in the presence of proton abstracting compounds like DBU or LDA. The reaction of $LiPH_2$ with **1** yields the anionic compound $[Cp^*Fe(\eta^4\text{-}P_5PH_2)]^-$ (**6**) as the main product. In addition, the dianionic compound $[(Cp^*Fe)_2(\mu,\eta^{4:4}\text{-}P_{11}H)]^{2-}$ (**7**), which exhibits a $P_{11}H$ ligand, was observed in traces. The different reactivity of **1** with $NaNH_2$ and $LiPH_2$ was explained by DFT calculations (Figure 1). All steps of the autometalation process to generate the nitrogen derivative $[\{Cp^*Fe(\eta^4\text{-}P_5)\}_2N]^{3-}$ (**3**) are exothermic, in contrast to the formation of the phosphorus derivatives **6** and **7**, which contains energetically disfavored reaction steps. To link two pentaphosphaferrocene units without an autometalation process, **1** was reacted with a dianionic nucleophile. By adding $Li_2[Cp_2Fe]$ to a solution of **1** the dianionic compound $[\{Cp^*Fe(\eta^4\text{-}P_5)\}_2Cp_2Fe]^{2-}$ (**8**) was isolated and the X-ray structure analysis shows, that two P_5 moieties are successfully bridged by one ferrocene unit. In all products the P_5 ring remains intact but loses its planarity, by exhibiting an enveloped-like conformation. Noteworthy, not many examples are known in the literature bearing such a structural motif.

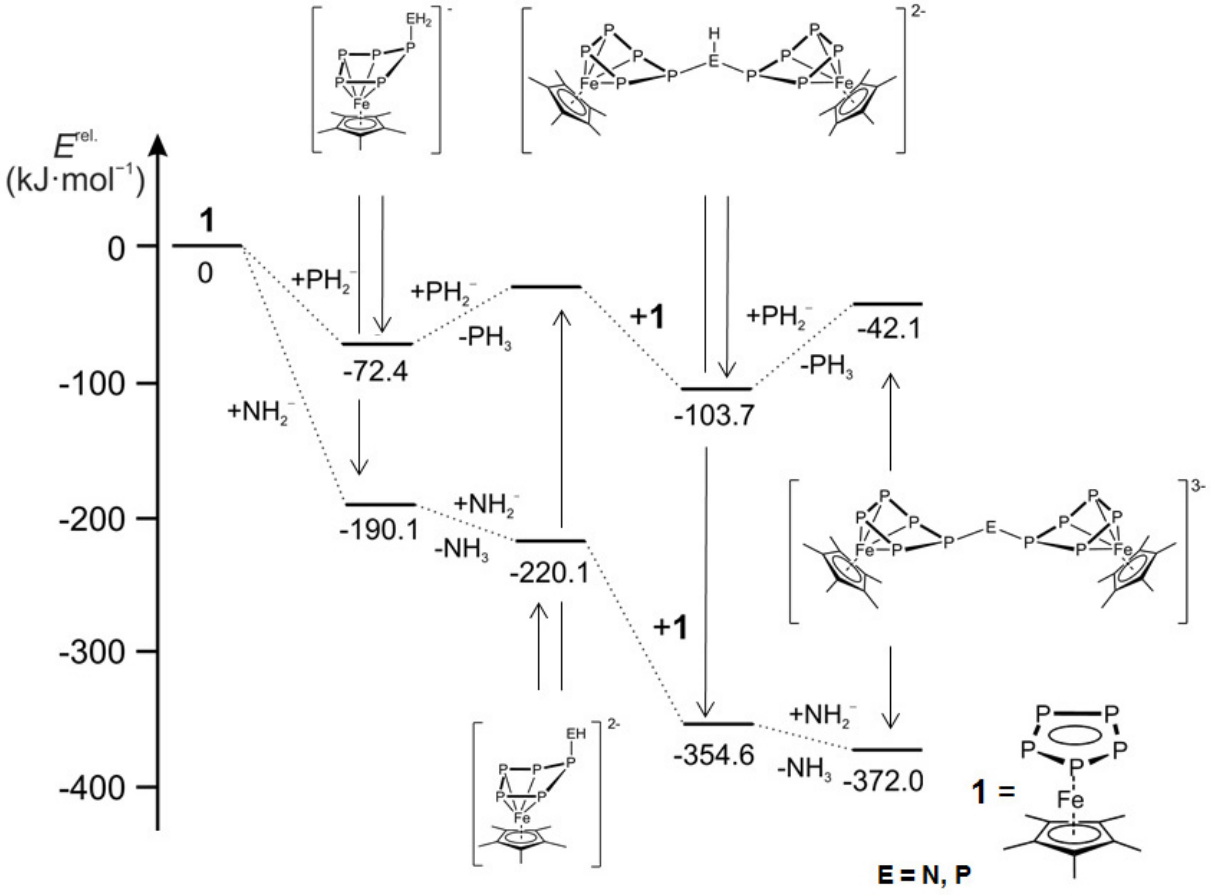

Figure 1. Energy profile of the reaction of **1** with NH_2^- and PH_2^-, respectively.

8.2 Reactivity of anionic pentaphosphaferrocene derivatives with organohalides and transition metal halides

All products described so far exhibit anionic character. Thus it was of special interest whether a reactivity of these anionic pentaphosphaferrocene derivatives towards electrophiles can be observed, in particular salt elimination processes were targeted for subsequent reactions. By adding organohalides such as MeI to $[Cp^*Fe(\eta^4\text{-}P_5R)]^-$ (**2a**: R = NMe_2; **2b**: R = CH_2SiMe_3; Scheme 2) the P_5 ring is functionalized further in a clean reaction, yielding the neutral compounds $[Cp^*Fe(\eta^4\text{-}P_5(Me)CH_2SiMe_3)]$ (**9**) and $[Cp^*Fe(\eta^4\text{-}P_5(Me)NMe_2)]$ (**10**), respectively. The methyl group is selectively bound to the phosphorus atom, which already exhibits one organic rest. An analogous reactivity is observed when 2-iodopropane is used as organohalide, as proven by NMR spectroscopic studies. These products show that it is now possible to synthesize highly functionalized, neutral pentaphosphaferrocene derivatives, which might play an important role as new building blocks in supramolecular chemistry.

In addition, the reactivity towards transition metal halides was investigated, by reacting **2a** and **2b** with $[Cp'''MX]_2$ (M = Cr, Fe, Co , Ni; X = Cl, Br; Scheme 2). As a result, a variety of triple-decker sandwich complexes were isolated and characterized and containing unprecedentedly functionalized P_5 units as middle decks. The nickel/iron and cobalt/iron triple-decker sandwich complexes $[(Cp^*Fe)(Cp'''M)(\mu,\eta^{4:3}\text{-}P_5R)]$ (**11**: M = Co, R = CH_2SiMe_3; **12**: M = Co, R = NMe_2; **13**: M = Ni, R = NMe_2) show similar structural features, in the iron/iron triple-decker sandwich complex $[(Cp^*Fe)(Cp'''Fe)(\mu,\eta^{4:4}\text{-}P_5NMe_2)]$ (**14**) a conformational change is observed. In **14** the phosphorus atom, which bears the organic rest, changes the position with a phosphorus atom from the $\eta^4\text{-}P_4$ plane, in comparison to **11**-**13**. The same conformational change is observed when **11** is oxidized by $[Cp_2Fe][PF_6]$, to give $[(Cp^*Fe)(Cp'''Co)(\mu,\eta^{5:4}\text{-}P_5CH_2SiMe_3)][PF_6]$ (**15**). The reaction of $[Cp'''CrCl]_2$ with **2b** yields the triple-decker sandwich complex $[(Cp^*Fe)(Cp'''Cr)(\mu,\eta^{4:5}\text{-}P_5CH_2SiMe_3)]$ (**16**; Scheme 2). Compound **16** exhibits for the first time no intact P_5 ring anymore. Instead the P_5 ligand is split into a P_3 allyl and a P_2 dumbbell moiety and a single bond between both metal centers is formed.

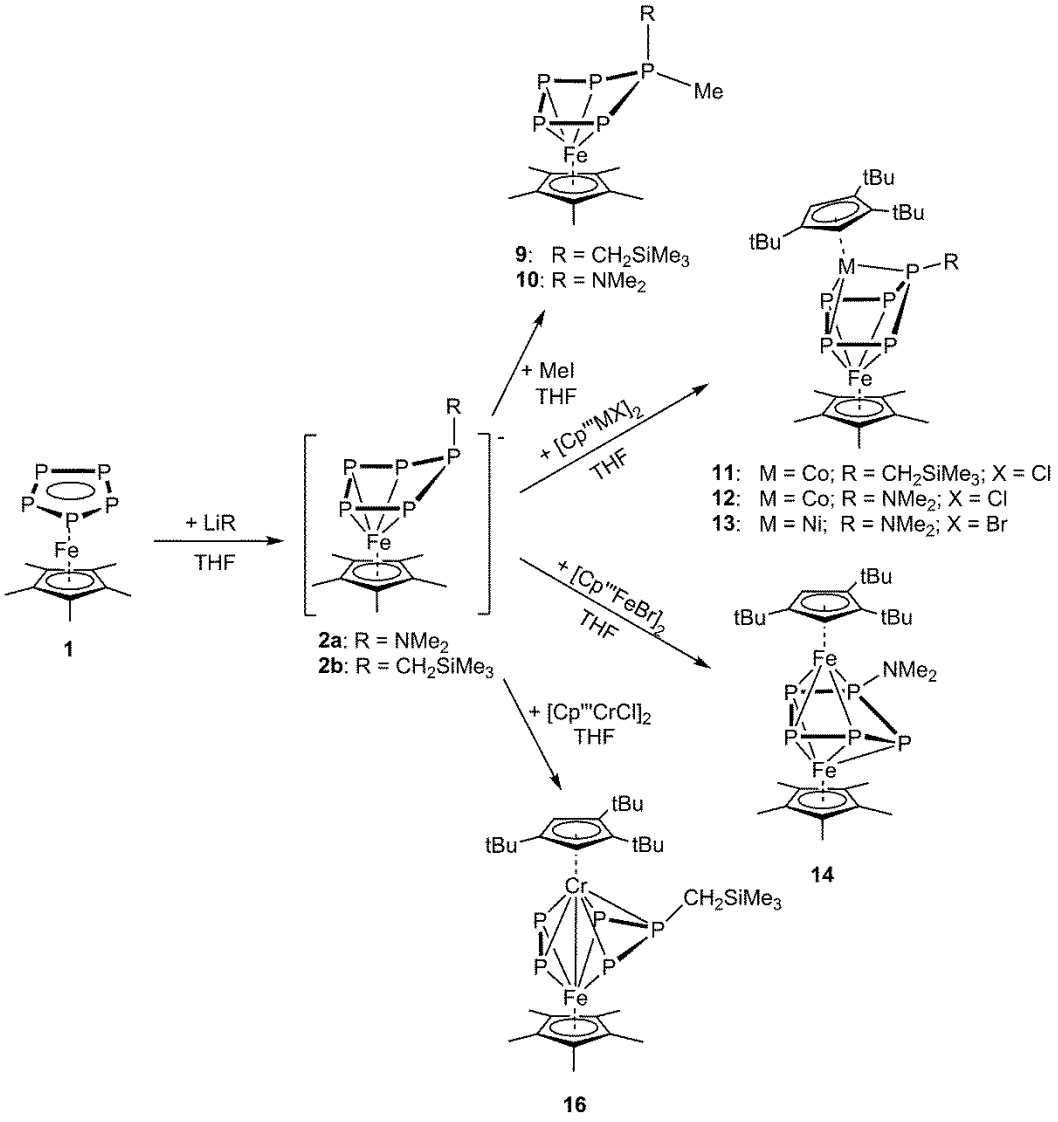

Scheme 2. Reactivity of the anionic pentaphosphaferrocene derivatives **2a**/**2b** towards MeI and transition metal halides.

Furthermore, the neutral triple-decker complexes [(Cp*Fe)(Cp'''M)(μ,$\eta^{5:4}$-P_5)] (**17**: M = Fe; **18**: M = Co), containing an unsubstituted P_5 ligand, were synthesized by reacting [(Cp*Fe)$_2$(μ,$\eta^{4:4}$-P_{10})]$^{2-}$ (**19**) with [Cp'''MX]$_2$ (M = Fe, Co; X = Cl, Br; Scheme 3). If **19** is reacted with two equivalents of MeI the P_{10} ligand breaks apart and the neutral twofold methylated compound [Cp*Fe(η^4-P_5Me_2)] (**20**) is obtained. Although **20** could not be crystalized, its formation could be proven by the stepwise reaction of **1** with MeLi − forming [Cp*Fe(η^4-P_5Me)]$^-$ (**21**) − and a subsequent salt elimination with MeI in a second reaction step, analog to the formation of **9** and **10**.

In addition, in the scope of this thesis the compound $[Cp^*Fe(\eta^4\text{-}P_5OH)]^-$ (**22**) was reduced to the dianionic compound $[Cp^*Fe(\eta^4\text{-}P_5O)]^{2-}$ (**23**). Based on this result further studies, regarding the reactivity of $[(Cp^*Fe)_2(\mu,\eta^{4:4}\text{-}P_{10})]^{2-}$ (**19**) and the highly reduced compound $[Cp^*Fe(\eta^4\text{-}P_5)]^{2-}$ (**24**) towards sulfur and selenium were performed by David Konieczny of our group.

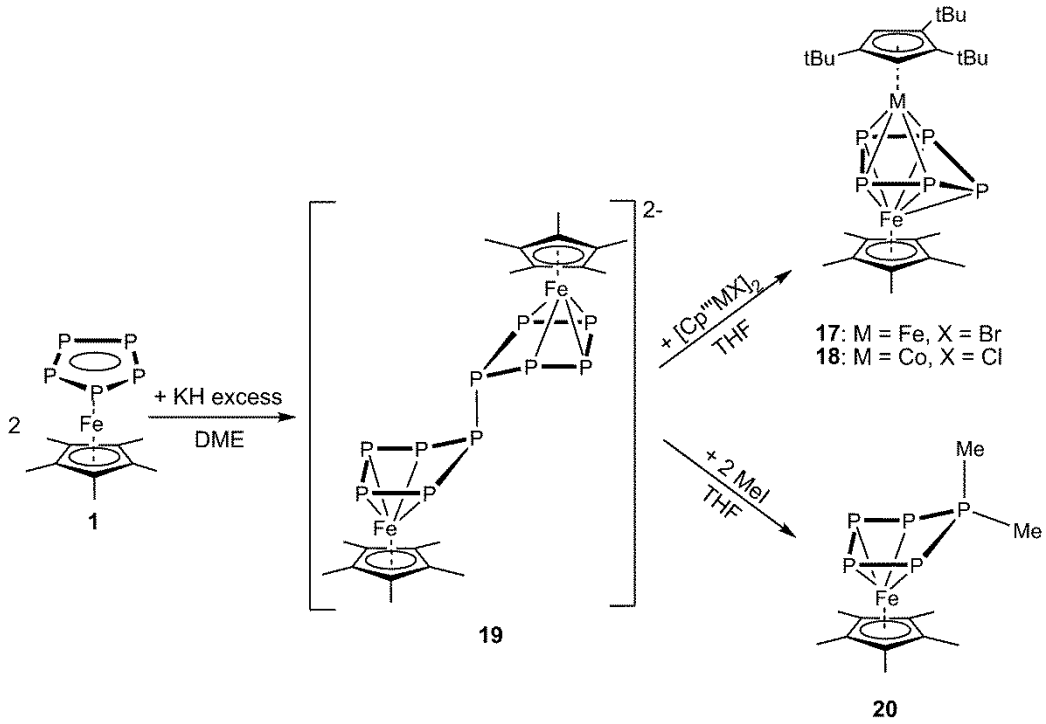

Scheme 3. Reactivity of **19** towards towards MeI and transition metal halides.

.

8.3 Reactivity of [Cp'''Ni(η^3-P_3)] towards nucleophiles and reducing agents

Besides the studies of pentaphosphaferrocene [Cp*Fe(η^5-P_5)] (**1**) as a starting material, the reactivity of the *cyclo*-P_3 ligand complex [Cp'''Ni(η^3-P_3)] (**4**) towards nucleophiles, as well as reducing agents was examined. The P_3 ring in **4** seemed to be a promising ligand due to its ring strain, to form bigger phosphorus-containing aggregates. In analogy to the reactivity of **1** towards nucleophiles (*vide supra*), in the reaction of **4** with nucleophiles an addition to the P_3 ligand was expected. Surprisingly, the reaction of **4** with $NaNH_2$ did not lead to an addition product. Instead the anionic triple-decker sandwich complex [(Cp'''Ni)$_2$(μ,$\eta^{3:3}$-P_3)]$^-$ (**25**), exhibiting a P_3 middle deck, was isolated (Scheme 4). So far, only positively charged nickel/nickel triple-decker complexes containing a P_3 middle deck are known. The anionic triple-decker complex **25** could subsequently be oxidized with AgOTf to the neutral compound [(Cp'''Ni)$_2$(μ,$\eta^{3:3}$-P_3)] (**26**). The P_3 ligand in **26** exhibits allylic character, which was well explained by means of DFT calculations.

If $LiPPh_2$ is used instead of $NaNH_2$, the reaction with **4** leads to the formation of the anionic compound [(Cp'''Ni)$_2$(μ,$\eta^{2:2}$-P_7Ph_2)]$^-$ (**27**). In this process a bicyclic P_6 unit is formed, which exhibits a five- and three-membered ring bearing one exocyclic PPh_2 group (Scheme 4). Although the structural motif of the bicyclic P_6 ligand is known it is unprecedented to be coordinated by transition metals. The reaction pathway was investigated by NMR spectroscopy and DFT calculations: In a first step the compound [Cp'''Ni(η^2-P_3PPh_2)]$^-$ (**28**) is formed by an addition of the PPh_2^- nucleophile to the *cyclo*-P_3 ring. Noteworthy, the P_3 ring is still intact but adopts a η^2-coordination mode. In a second step compound **28** reacts with another equivalent of **4** to form **27**. As shown by DFT calculations every step of the reaction is exothermic. After protonating **27** with HBF_4 compound [(Cp'''Ni)$_2$(μ,$\eta^{2:2}$-P_7HPh_2)] (**29**) was obtained and isolated after column chromatographic workup (Scheme 4). In contrast, [Cp'''Ni(η^2-P_3NMe_2)]$^-$ (**30**) was accessible and characterized in the reaction of $LiNMe_2$ with **4**.

Besides the reactivity of **4** towards nucleophiles, also the reactivity towards reducing agents was investigated. The reaction with potassium yields compound [(Cp'''Ni)$_2$(μ,$\eta^{2:2}$-P_8)]$^{2-}$ (**31**), featuring a P_8 ligand with a realgar-like structural motif, which is coordinating to two Cp'''Ni fragments (Scheme 4). As a byproduct, the triple-decker sandwich complex **25** is observed. This is reasonable, if the formation of the P_8 ligand in **31** is considered to be deriving from three equivalents of **4**.

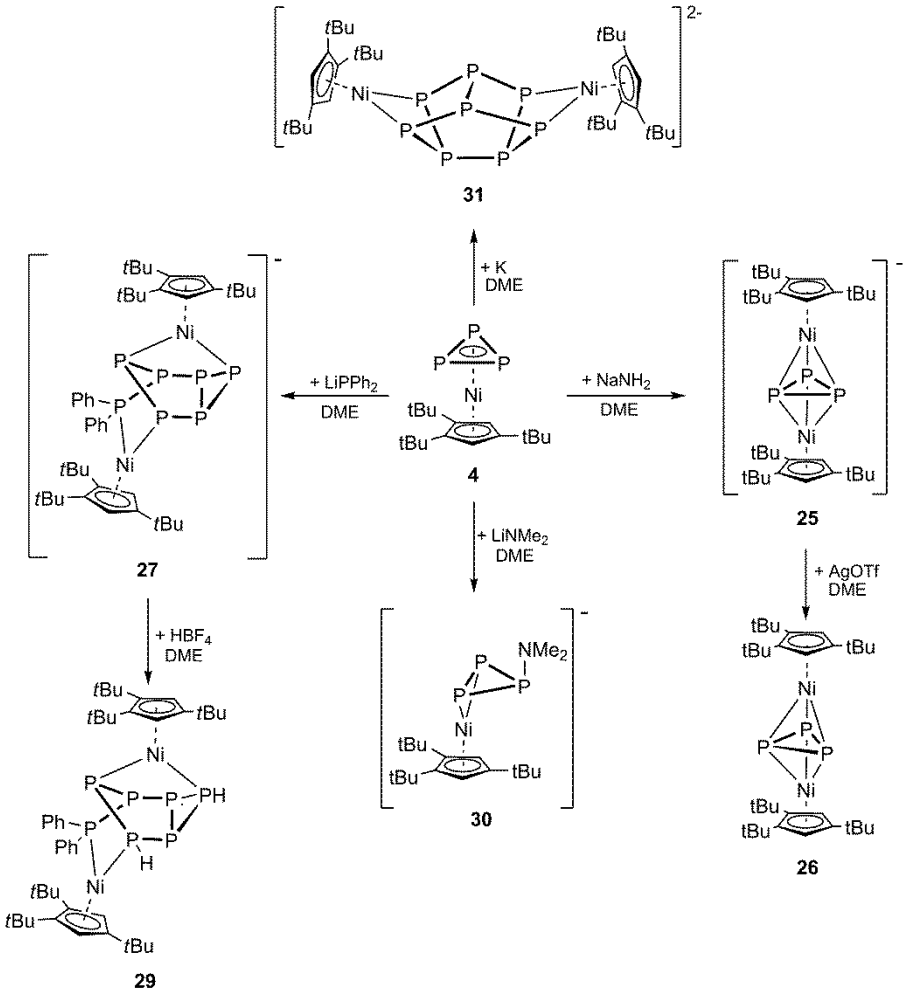

Scheme 4. Reactivity of **4** towards different nucleophiles and potassium.

Furthermore, first NMR spectroscopic studies regarding the reactivity of the triple-decker sandwich complex $[(Cp'''Ni)_2(\mu,\eta^{3:3}\text{-}P_3)]^-$ **25** were performed. When **25** is reacted with an equimolar amount of MeI at room temperature one phosphorus atom is separated from the former P_3 ligand and the neutral compound $[(Cp'''Ni)_2(\mu,\eta^{2:2}\text{-}P_2)]$ (**32**) is formed, featuring a P_2 unit (Scheme 5). However, if the reaction is performed at low temperature and an excess of MeI is used the P_3 ligand remains intact and a methylation of the *cyclo*-P_3 ligand in **25** occurs, forming $[(Cp'''Ni)_2(\mu,\eta^{3:3}\text{-}P_3Me)]$ (**33**). The coupling constants obtained from the ^{31}P NMR spectrum suggest an allylic-like P_3 unit, bearing the methyl group in terminal position (Scheme 5).

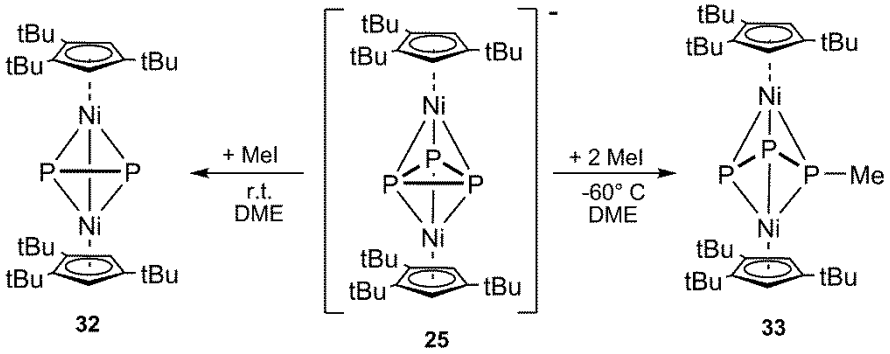

Scheme 5. Reactivity of **25** towards MeI.

These reactivity studies demonstrate the ability of the P_3 ligand complex [Cp'''Ni(η^3-P_3)] (**4**) to form higher aggregates and its use as a phosphorus source. Depending on the used nucleophiles **4** shows a diverse reactivity, yielding unique P_n ligand complexes.

In conclusion it can be stated, that this work contributed to the better understanding of the reactivity of the P_n ligand complexes [Cp*Fe(η^5-P_5)] (**1**) and [Cp'''Ni(η^3-P_3)] (**4**) towards reducing agents, nucleophiles and subsequent salt elimination reactions, which has been neglected so far and therefore established novel routes for the synthesis of phosphorus containing complexes.

9. Appendix

9.1 List of used abbreviations

Me	Methyl, -CH_3
Et	Ethyl, -C_2H_5
Ph	Phenyl, -C_6H_5
*t*Bu	*tert*-butyl, -CMe_3
OTf	Trifluormethanesulfonate
Cp	Cyclopentadienyl, C_5H_5
Cp*	Pentamethylcyclopentadienyl, C_5Me_5
Cp'	*Tert*-butylcyclopentadienyl, $C_5H_4(CMe_3)$
Cp"	1,3-di(*tert*-butyl)cyclopentadienyl, $C_5H_3(CMe_3)_2$
Cp"'	1,2,4-di(*tert*-butyl)cyclopentadienyl, $C_5H_2(CMe_3)_3$
Cp^+	Ethyltetramethylcyclopentadienyl, C_5EtMe_4
NMR	Nuclear magnetic resonance
δ	Chemical shift (ppm)
ppm	Parts per million
s (NMR)	Singlet
d (NMR)	Dublet
t (NMR)	Triplet
m (NMR)	Multiplet
J	coupling constant (Hz)
°C	Degree Celsius
EPR	Electron paramagnetic resonance
μ_B	Bohr magneton
μ_{eff}	Effective magnetic moment
Å	Angström (1 Å = 10^{-10} m)
EI	Electron ionization
ESI	Electropspray ionization
FD	Field desorption
LIFDI	Liquid injection field desorption
r.t.	Room temperature
THF	Tetrahydrofuran
DME	Dimethoxyethane
Tol	Toluene
NPA	Natural Population Analysis

DFT	Density functional theory
WBI	Wiberg bond index
CV	Cyclic voltammetry
SOMO	Singly occupied molecular orbital
HOMO	Highest occupied molecular orbital
LUMO	Lowest occupied molecular orbital

9.2 Acknowledgement

At this point I want to express my gratitude to:

- My family for the constant support in all those years.
- Prof. Dr. Manfred Scheer for giving me the opportunity to create this work under such excellent working conditions and to be given the possibility to develop my "own" chemistry.
- Dr. Gábor Balázs (Gobbi) for his time, answering questions of all sort and his input if needed. I also thank him for performing various DFT calculations for me.
- The crystallographic triumvirate Dr. Eugenia V. Peresypkina, Dr. Alexander V. Virovets and Dr. Michael Bodensteiner for answering and solving all my crystallographic problems.
- The team from the NMR department (Dr. Ilya Shenderovich, Annette Schramm, Georgine Stühler und Fritz Kastner) and the team of the elemental analysis (Helmut Schüller, Barbara Baumann und Wilhelmine Krutina).
- Dr. Alexey Y. Timoshkin for performing DFT calculations for me and our table tennis duels.
- Also I want to thank my girlfriend Helen, for making me laugh and sharing great years with me.
- The whole working group for the awesome working atmosphere. In detail and no specific order: Jens Brease and Moritz Modl for the constant motivation to pump the iron. My former working colleague Dr. Christian Graßl for the many hours of Django 3000. Felix Riedlberger and Michael Weinhart for "Wie soll ein Mensch das ertragen" and "Friday". I am not considering any of you to be a "ventilator". Eva-Maria Rummel for proof reading some parts of my work and her latest news from Imgur/Reddit. Monika Schmidt for her weird bavarian sayings. Hias and Moartl for being worthy opponents during tabletop soccer. Olli and his diet/training plans and becoming the hulk himself. I also want to thank: Karin Kilgert, Helena Brake, Luis Dütsch (thank you for the ESI-MS), Matthias Hautmann, Walter Meyer and Elisabeth Ederer (thank you for the fresh liquid nitrogen), Claudia Heindl (thank you for proof reading), Dr. Sebastian Heinl, Tobias Kahoun, Barbara Krämer, Dr. Kretschmer Robert (flavor flav), Petra Lugauer, Daniela Meyer, Dr. Mehdi Elsoyed Moussa, Julian Müller, Reinhard Rund, Thomas Schottenhammer (thank you for cheap board games in good condition), Andrea Schreiner, Dr. Michael Seidl, Andreas Seitz, Fabian Spitzer, Dr. Andreas Stauber, Barbara Treittinger, Valentin Vaas, Rudolf Weinzierl.